JPLCAT

Vol. 8, Part A-1, No. 4, April 1970

Journal of Polymer Science

Part A-1: Polymer Chemistry

Contents

Published by INTERSCIENCE PUBLISHERS a division of John Wiley & Sons, Inc.

Journal of Polymer Science: **Part A-1: Polymer Chemistry**

The Journal of Polymer Science is published in four sections as follows: Part A-1, Polymer Chemistry, monthly; Part A-2, Polymer Physics, monthly; Part B, Polymer Letters, monthly; Part C, Polymer Symposia, irregular.

Published monthly by Interscience Publishers, a Division of John Wiley & Sons, Inc., covering one volume annually. Publication Office at 20th and Northampton Sts., Easton, Pa. 18042. Executive, Editorial, and Circulation Offices at 605 Third Avenue, New York, N. Y. 10016. Second-class postage paid at Easton, Pa. Subscription price, $325.00 per volume (including Parts A-2, B, and C). Foreign postage $15.00 per volume (including Parts A-2, B, and C).

JOURNAL OF POLYMER SCIENCE: PART A-1 VOL. 8, 801–812 (1970)

NMR Study of Poly(vinyl Chloride)-β,β-d_2

L. CAVALLI, G. C. BORSINI, G. CARRARO, and G. CONFALONIERI, *Montecatini Edison S.p.A., Centro Ricerche Bollate, Milan, Italy*

Synopsis

The high-resolution NMR spectra at 60 and 100 Mcps of poly(vinyl chloride)-β,β-d_2 in *o*-dichlorobenzene, pyridine, and C_2HCl_5 solutions are reported. The use of low molecular weight samples and of $\{D\}$ spin-decoupling experiments, which yield higher resolution spectra, results in the observation of a number of additional resonances for the α-proton. These can be interpreted in terms of pentad configurational sequences of monomer units. It is found that, whereas the *S* syndiotactic pentads cannot be resolved, two components of the *H* heterotactic and all of the possible *I* isotactic pentads are clearly discernible. From the tacticity values of polymers prepared at +40, 0, and −40°C, enthalpy and entropy of activation for isotactic and syndiotactic monomer placement are found to be 630 cal/mole and 1.5 eu, respectively.

INTRODUCTION

The interpretation of the NMR spectrum of PVC, in particular of the CH_2-β band, has received considerable attention during the last years.[1–6] It was shown that the interpretation of the methylene proton signals by diads had to be revised. The equivalence of "isotactic" methylene protons, assumed originally by Johnsen[7] and supported afterwards by means of α-decoupled spectra,[8] was shown to be only an useful approximation. Several β-signals, due to different configurations, were in fact experimentally observed by Yoshino in his investigation on PVC α-*cis*-β-d_2.[9] Tetrad configurational sequences of monomer units were invoked, and a good interpretation of spectra was obtained. Following Yoshino's assignments in terms of tetrads, Bovey et al. recently reinterpreted the spectrum of PVCα-d_1.[6] Calculations of β-proton chemical shifts for the six different possible tetrad configurations[10] and detailed analyses of model compounds, such as 2,4-dichloropentanes[11–14] and 2,4,6-trichloroheptanes,[15,16] in various conditions of solvent and temperature have also been done.

In contrast to the CH_2-β band, the CH-α absorption has attracted little attention. The reason derives from the complexity of the CH-α signal, due to spin–spin coupling with vicinal methylene protons, which makes it difficult to obtain reliable tacticity values. On the other hand, investigation of the CH-α proton resonance would be more convenient, for more information on the local regularity of the chain can be achieved.[17] The CH-α proton was shown to be stereosensitive; three main signals were observed in the

β-decoupled spectrum and interpreted in terms of triad configurations of monomer units.[8]

On this basis the normal undecoupled α-absorption must be complicated by three overlapping quintets. Recently it was suggested that some pentad configurations must also be taken into account for the interpretation of CH-α absorption.[10] Some experimental support to such an idea could come from the 100 Mcpsα-proton resonance of undecoupled PVC, which is more complex than that at 60 Mcps.[5] In order to clarify this point and possibly to give an adequate interpretation of the CH-α signal of PVC we have chosen to investigate the α-proton resonance of PVC-β,β-d_2. In addition, samples of PVCβ,β-d_2, polymerized at different temperatures, were analyzed to get more accurate tacticity values.

EXPERIMENTAL

Vinyl chloride-β,β-d_2 was prepared as follows.[18] Tetradeutero-acetic acid (Merck, 99% purity) was reduced by lithium aluminum hydride to trideuteroethyl alcohol. Then the deuterated ethanol was converted into trideuteroethyl chloride from which CD_3CHCl_2 was obtained. By dehydrochlorination using nickel chloride supported on alumina, vinyl chloride-β,β-d_2 was synthesized. After fractionation, NMR measurement indicated a purity not less than 98% (Fig. 1).

Polymerizations were carried out in bulk, initiated by triethylboron and cumyl hydroperoxide at -40, 0 and $+40°$. Sealed Pyrex tubes equipped with breakseals were used: both monomer and catalyst systems were thermostatted before initiating polymerization in order to allow a better temperature control of the reaction. The polymerization was stopped after a few minutes by freezing in liquid nitrogen. Polymers were purified by dissolution in cyclohexanone and precipitation in methanol and then dried on the vacuum line.

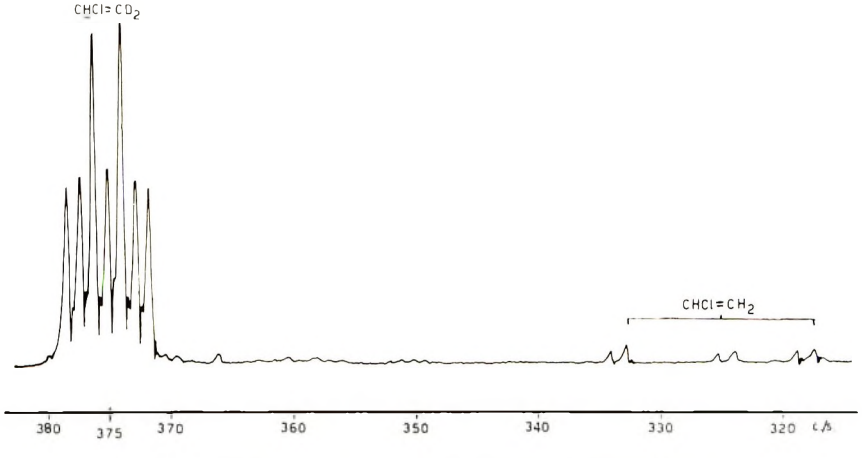

Fig. 1. NMR spectrum of vinyl chloride-β,β-d_2 (60 Mcps).

Molecular weights were estimated with a Mechrolab vapor-pressure osmometer model 301 A, with the use of tetrahydrofuran as solvent. Values found were in the range of 2500–3500. In order to test the possible influence of end groups, higher molecular weight (~10,000) samples were prepared with the same initiator and longer polymerization times. NMR spectra were obtained with Models A 56/60 and HA-100 Varian spectrometers at 120°C. The polymer solutions contained 15% (w/v) polymer and 2–3% of hexamethyldisiloxane (9.94 τ) as internal reference. The 60 Meps spectra were calibrated against side bands produced by audiofrequency modulation of the magnetic field. The $\{D\}$ spin-decoupling experiments were performed with a modified[19] HA-100 spectrometer in conjunction with a NMR Specialties heteronuclear spin decoupler, Model SD-60 B, externally locked by a Hewlett-Packard frequency generator 4204 A.

Intensity measurements of NMR signals were carried out by weighing the peaks after they were reproduced on thick paper. At each polymerization temperature at least ten independent spectra were selected and each of them was reproduced several times. The peaks of interest were then cut out, and their weights were measured and averaged.

RESULTS

NMR spectra of high molecular weight PVC-β,β-d_2 have been already reported.[20] The three main signals were ascribed, beginning from high

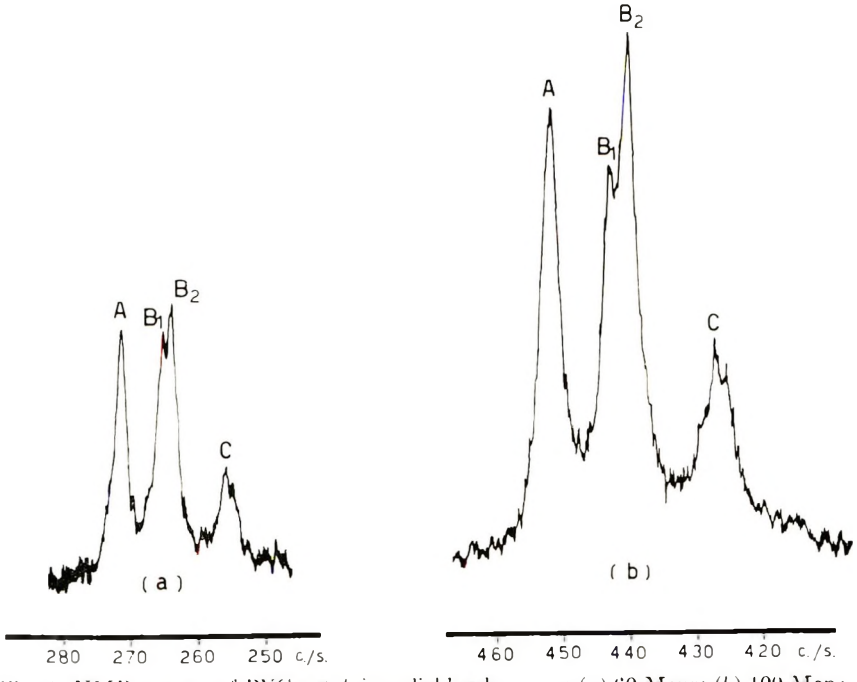

Fig. 2. NMR spectra of PVC-β,β-d_2 in *o*-dichlorobenzene: (*a*) 60 Meps; (*b*) 100 Meps.

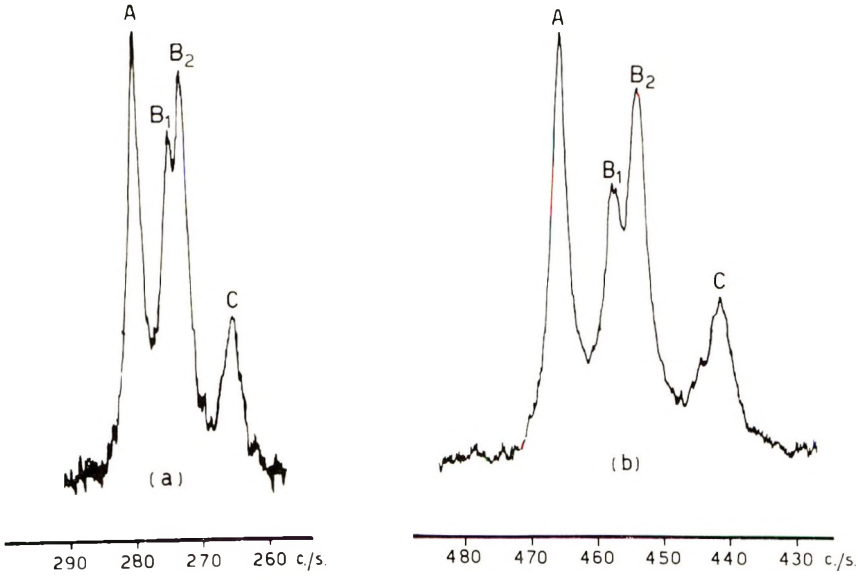

Fig. 3. NMR spectra of PVC-β,β-d_2 in pyridine: (*a*) 60 Mcps; (*b*) 100 Mcps.

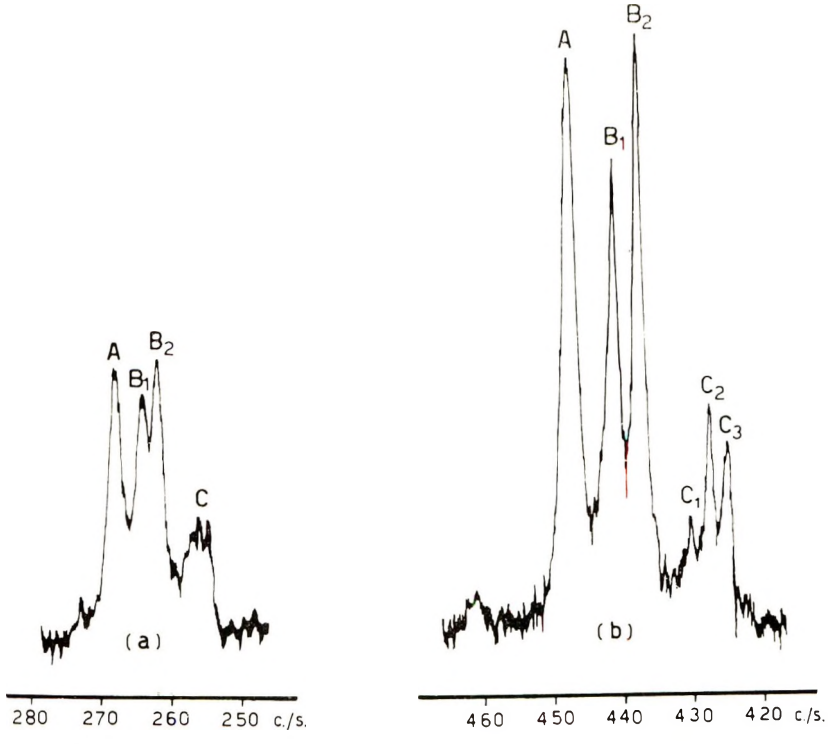

Fig. 4. NMR spectra of PVC-β,β-d_2 in C_2HCl_3: (*a*) 60 Mcps; (*b*) 100 Mcps.

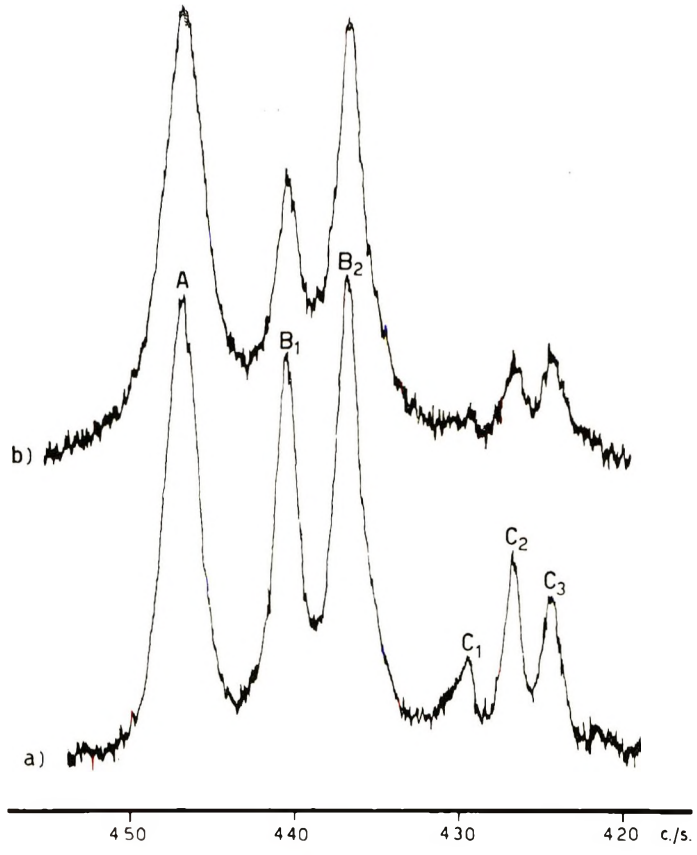

Fig. 5. The 100 [D] Mcps spectra in C_2HCl_5 for PVC-β,β-d_2 samples prepared at (a) +40° C and (b) −40° C.

field, to α-protons in the isotactic, heterotactic, and syndiotactic configurations, respectively. They do not show much difference from those of β-decoupled spectra.[1,4,8] In our case, the low molecular weight allowed several solvents and concentrated solutions to be employed. Well-resolved spectra could be obtained at both 60 and 100 Mcps as shown in Figures 2–5. The heterodecoupled $\{D\}$ NMR spectra at 100 Mcps are shown for the C_2HCl_5 solution in Figures 4b and in 5.

The signals observed can be divided into three groups, A, B, and C; A, includes the single signal at low field, B, comprises a splitted central band, B_1 and B_2, and C includes a broad band at high field, which in some of the best spectra is resolved into three signals, C_1, C_2, and C_3 (Fig. 4b and 5). The main feature of all spectra is the splitting of the central band, B.

Pyridine and C_2HCl_5 proved to be the best solvents for resolving the two signals B_1 and B_2, as they allow separation up to about 3.5 cps at 100 Mcps. Chemical shifts of all lines, observed in different solvents, are reported in Table I.

TABLE I
Chemical Shifts of PVC-β,β-d_2

Polymerization temperature, °C	Solvent	Chemical shift (τ), ppm					
		A	B_1	B_2	C_1	C_2	C_3
+40	*o*-Dichlorobenzene	5.47_7	5.58_0	5.59_8	5.72_6	5.74_4	5.76_2
0	"	5.47_3	5.57_7	5.59_5		5.74	
−40	"	5.47_3	5.57_6	5.59_4		5.73	
+40	Pyridine	5.34_5	5.43_2	5.46_2	5.56_6	5.58_7	5.60_4
0	"	5.34_2	5.43_3	5.46_0	5.56_3	5.58_3	5.60_0
−40	"	5.35_0	5.44_2	5.46_7		5.59	
+40	C_2HCl_5	5.52_9	5.59_1	5.62_6	5.69_4	5.72_4	5.74_9
0	"	5.53_0	5.59_4	5.63_3		5.73	
−40	"	5.52_5	5.58_8	5.62_5	5.69_8	5.72_7	5.74_9

Tacticity values, S, H, and I of samples polymerized at three different temperatures are summarized in Table II. These were obtained by calculating the ratios of peak areas (see Experimental), on the ground of the following assignments: the single signal, A, at low field, is ascribed to syndiotactic configurations, S; the central splitted band, B, and the com-

TABLE II
Tacticity Data for PVC

Polymerization temperature, °C	I, %	H, %	S, %	σ	η
40[a]	19.1	48.7	32.2	0.434	0.991
0[a]	16.4	47.0	36.6	0.399	0.980
−40[a]	12.0	46.3	41.7	0.351	1.015
58[b]	17	48	35	0.41	0.992
−30[b]	10	44	46	0.32	1.011
55[c]	16	49	35	0.405	1.017
−30[c]	9	44	47	0.31	1.029
52.5[d]	19	52	29	0.45	1.050
10[d]	18	50	32	0.43	1.020
0[d]	22	50	28	0.47	1.004
−15[d]	19	53	28	0.455	1.069
−25[d]	18	52	30	0.44	1.055
−35[d]	16	46	38	0.39	0.966
50[e]	36	28	36	0.40	0.583
−20[e]	31	31	38	0.465	0.623
−50[e]	27	35	38	0.445	0.709
−75[e]	27	26	47	0.40	0.542
Aldehyde[e]	36	23	41	0.475	0.461

[a] This work.
[b] Data of Enemoto et al.[18]
[c] Data of Satoh.[1]
[d] Data of Bargon et al.[4]
[e] Data of Tincher.[2]

plex pattern, C, at high field, are ascribed to heterotactic H and isotactic (I) sequences, respectively. Such an assignment makes the treatment of tacticity values, S, H, and I, analogous to that employed when triad configurations are considered.

In Table II, following Miller's treatment,[21] the calculated probability σ of isotactic monomer placement and the so-called "heterotactic index" η which represents the block character of polymer

$$\eta = H/2\sigma(1 - \sigma)$$

are also reported. For comparison, values from the literature have also been tabulated.

DISCUSSION

Interpretation of Spectrum

The most probable explanation for signal widths and fine structure of the CH-α absorption of PVC-β,β-d_2, is the existence of pentads of monomer units. Other possibilities, such as irregularities of polymer (chain branching) or effect of terminal groups must be ruled out, for example, on the ground of the intensities of the two central and prominent signals B_1 and B_2. The degree of chain branching for example, is too low,[22] even for samples prepared at +40°C, to explain the intensity of the observed signals.

The influence of endgroups must also be excluded, as the same characteristic pattern, even though less resolved, is displayed by samples of PVC-β,β-d_2 of higher molecular weight. In addition, the observed spectrum cannot be interpreted by conventional triad configurations of monomer units for which three signals are expected. Evidence of pentads of monomer units for PVC, on the other hand, have been recently obtained by using improved spin-decoupling experiments.[23] The $\{D\}$ 100 Mcps spectrum (Figs. 4*b* and 5), on the contrary, displays a set of six signals. Ten signals are expected if we consider the ten possible pentads of monomer units. Species of these pentads are listed in Table III. Notations have been already introduced by Ramey,[5] Schneider et al.,[10] and Frisch et al.[23] The first two have been adopted.

The pentads can be classified into three groups: (S) syndio, (H) hetero, and (I) iso. There are three pentads of syndio and iso type respectively, whereas four are possible for the hetero type. In our deuterated polymer, each can give only one signal of intensity equal to the probability calculated on the assumption that chain propagation is controlled only by one σ value of probability (simple Markov's mechanism). A first assignment which can be confidently done is to ascribe the three groups of experimental bands A, B, and C to syndio, hetero, and iso pentads, respectively. Subsequently the observed single signals can be tentatively assigned.

Whereas the three syndiotactic pentad configurations give a single signal at low field, the heterotactic ones clearly display two absorptions, B_1 and

TABLE III
Species and Probabilities of Pentads in PVC

Type	Designation: Ramey[5]	Designation: Schneider[10]	Structure	Probability
S	*sss*	*s.ss.s*	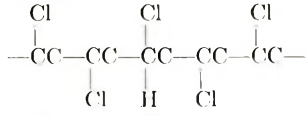	$(1 - \sigma)^4$
	ssh	*s.ss.i*	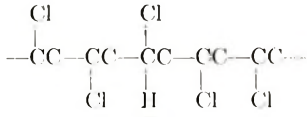	$2\sigma(1 - \sigma)^3$
	hsh	*i.ss.i*	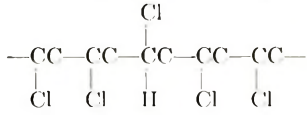	$\sigma^2(1 - \sigma)^2$
H	*shh*	*s.si.s*	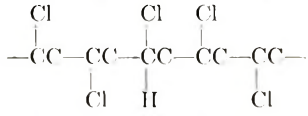	$2\sigma(1 - \sigma)^2$
	shi	*s.si.i.*	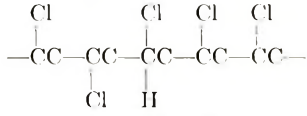	$2\sigma^2(1 - \sigma)^2$
	hhh	*i.si.i.*	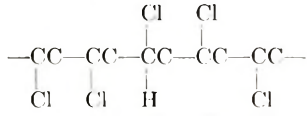	$2\sigma^2(1 - \sigma)^2$
	hhi	*i.si.i*	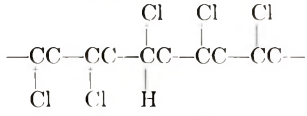	$2\sigma^3(1 - \sigma)$
I	*hih*	*s.ii.s*	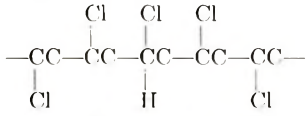	$\sigma^2(1 - \sigma)^2$
	hii	*s.ii.i*	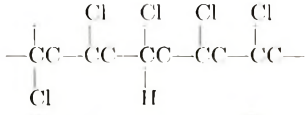	$2\sigma^3(1 - \sigma)$
	iii	*i.ii.i*	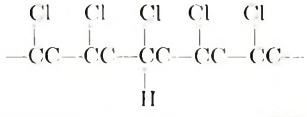	σ^4

B_2. If we consider signals, B_1 and B_2, it can be noticed that B_2 is always stronger than B_1 and that the intensity ratio B_2/B_1 increases markedly with decreasing polymerization temperature (Fig. 5). Since the probability of syndiotactic monomer placement is higher than that of isotactic placement ($\sigma < 0.5$), even at +40°C, we can conclude, according to pentad probability

calculations (Fig. 6), that the *hhi* pentad takes part in B_1 absorption, whereas *shh* should contribute to B_2. The other two pentads, *shi* and *hhh*, which have the same probability, must absorb separately, one in the region corresponding to B_1 and the other under B_2. The most probable conformations of heterotactic pentads must satisfy the following condi-

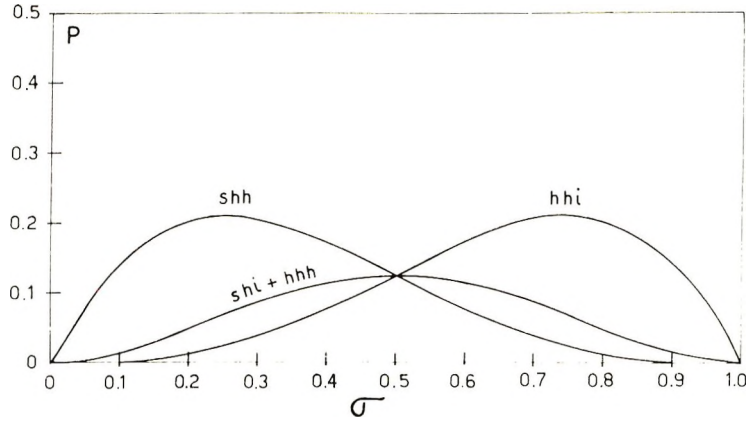

Fig. 6. Heterotactic pentad probabilities for Bernoulli trial PVC chains.

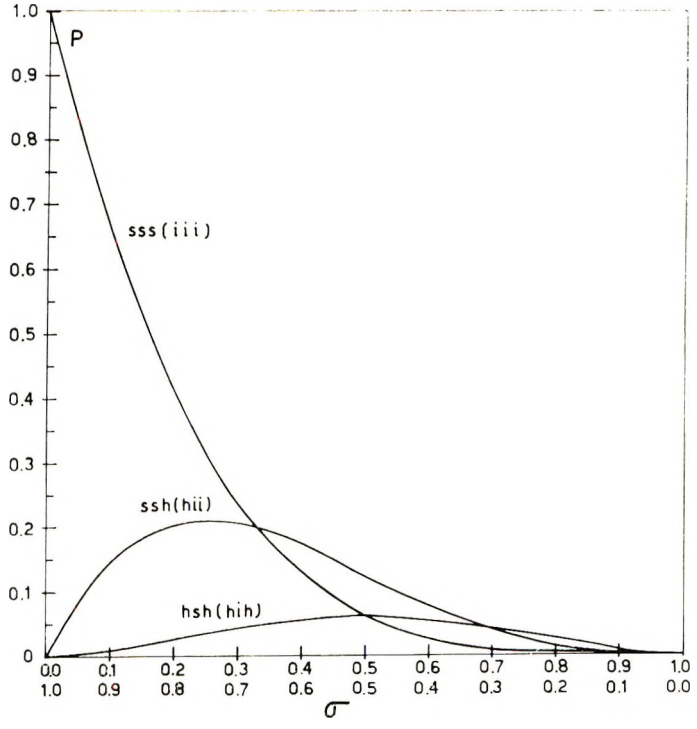

Fig. 7. Syndiotactic and isotactic pentad probabilities for Bernoulli trail PVC chains. For *sss*, *ssh*, and *hsh* the upper scale is used; for *iii*, *hii*, and *hih* the lower scale is used.

tions:[3] (*1*) conformation around C-C band should be staggered, (*2*) the pairs CH_2....Cl and Cl....Cl should not be close together. We can observe further that the spatial arrangement of chlorine atoms with respect to the central CH-α proton for the four heterotactic pentads is quite similar in the pair *shh–hhh* and *hhi–shi*. On this basis, *shi* and *hhh* can be tentatively assumed to absorb under B_1 and B_2, respectively. As far as the C group absorption is concerned, all spectra show a rather large band. Only in the 100 Mcps $\{D\}$ spectra was it possible to distinguish three signals.

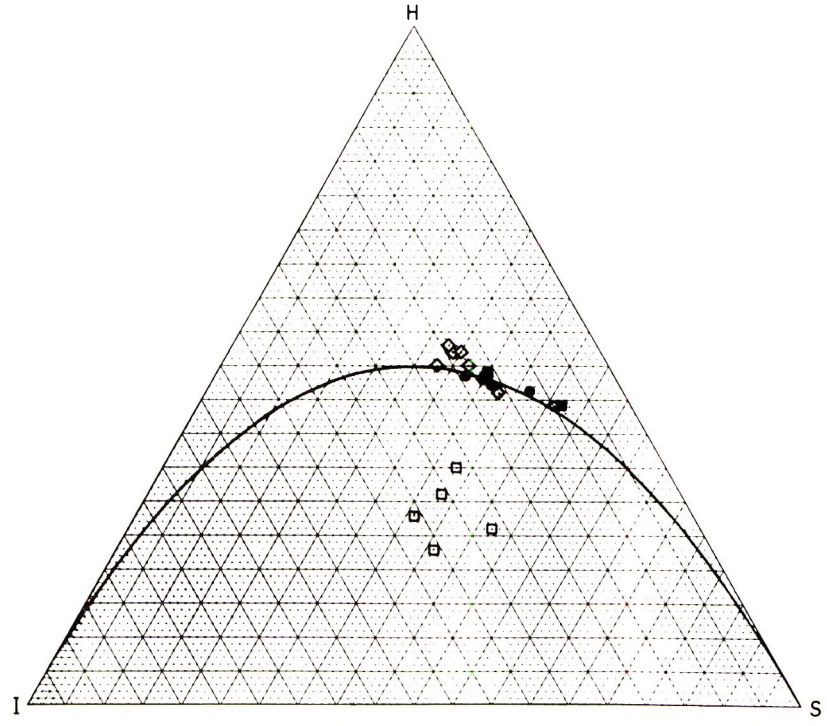

Fig. 8. Miller triangular diagram with results of trial measurements on samples of PVC: (●) this work; (◇) data of Bargon;[4] (■) data of Satoh;[1] (○) data of Enemoto et al.;[20] □ data of Tincher.[2]

Calculations of the chemical shifts of isotactic pentads have already been done, and they are expected to decrease in the order, *hih*, *hii*, and *iii*.[10] Agreement between experimental and calculated intensities of C_1, C_2, and C_3 seems to confirm such assignments. In fact, for $\sigma = 0.43$ (PVC polymerized at +40°C) the calculated intensities (Fig. 7) decrease from *hii* (C_2 signal) down to *hih* (C_3) and *iii* (C_1). According to this assignment, the suggested[10] partial overlap of isotactic pentads with those of heterotactic type is excluded, and tacticity values in PVC-β,β-d_2 can thus be determined in a straight-forward manner without any correction.

Interpretation of Tacticity Data

The tacticity values listed in Table II can be represented in a triangular diagram (Fig. 8) as suggested by Miller.[21] All points, with exception of the values given by Tincher, fall near the line representing random polymer: this fact gives further evidence of a random structure for the free-radical-initiated poly(vinyl chloride). As regards the discrepancies found with Tincher's data, it must be noted that they were obtained by decomposing the CH-α proton signal into the contributions of three quintets; such a treatment can be considered as approximation.

From the results of our measurements, values of 630 ± 30 cal/mole for Δ $(\Delta H_p)^*$ and 1.5 eu for $\Delta(\Delta S_p)^*$ were found: the Arrhenius plot is shown in Figure 9.

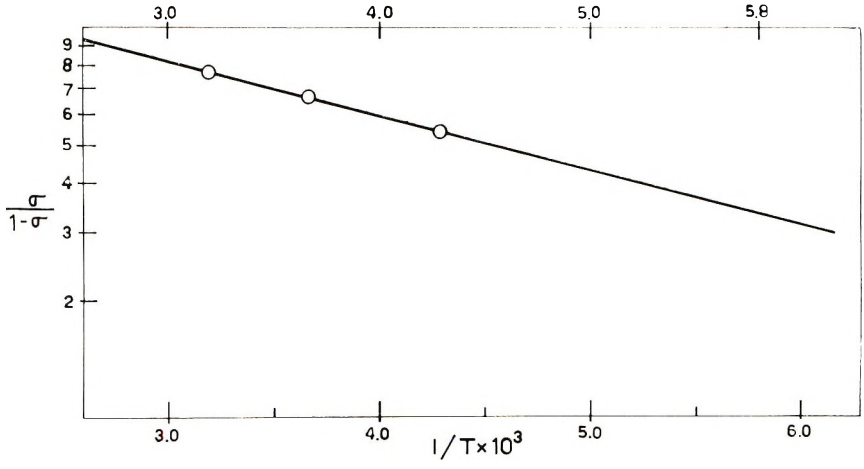

Fig. 9. Dependence of $\sigma/1\text{-}\sigma$ on 1/T for the polymerization of PVC-β,β-d_2, where T is the polymerization temperature (°K) and σ the probability of isotactic monomer placement.

The value of 630 cal/mole for the difference in enthalpy of activation for isotactic and syndiotactic monomer placement is in good agreement with that (600 cal/mole) previously estimated by Fordham et al.[24] Lower values, close to 300 cal/mole, have been recently reported by Bargon et al.[4] and Bovey et al.[6] In spite of these discrepancies, it is certain that there is an increase in poly(vinyl chloride) syndiotacticity with decreasing polymerization temperature. This dependence on temperature, however, cannot explain, by itself, the increase in crystallinity and the large difference found in the thermomechanical behavior of poly(vinyl chloride) obtained at low temperature. Other factors have been suggested to contribute to this improvement, particularly reduced branching caused by decreasing temperatures.[22]

The help of Dr. A. Segre (Istituto Chimica Industriale, Politecnico di Milano), in obtaining the 100 Mcps heterodecoupling $\{D\}$ spectra is kindly acknowledged.

References

1. S. Satoh, *J. Polym. Sci. A*, **2**, 5221 (1964).
2. W. C. Tincher, *Makromol. Chem.*, **85**, 20 (1965).
3. T. Simanouchi, M. Tasumi, and Y. Abe, *Makromol. Chem.*, **86**, 43 (1965).
4. J. Bargon, K. H. Hellwege, and U. Johnsen, *Makromol. Chem.*, **95**, 187 (1966).
5. K. C. Ramey, *J. Phys. Chem.*, **70**, 2525 (1966).
6. F. A. Bovey, F. P. Hood, E. W. Anderson, and R. L. Kornegay, *J. Phys. Chem.*, **71**, 312 (1967).
7. U. Johnsen, *J. Polym. Sci.*, **54**, S6 (1961).
8. F. A. Bovey, E. W. Anderson, and D. C. Douglas, *J. Chem. Phys.*, **39**, 1199 (1963).
9. T. Yoshino and J. Komyama, *J. Polym. Sci. B*, **3**, 311 (1965).
10. B. Schneider, J. Stokr, D. Doskocilova, M. Kolinsky, S. Sykora, D. Lim, paper presented at International Symposium Macromolecular Chemistry, Prague, 1965; preprint P 599.
11. D. Doskocilova and B. Schneider, *Coll. Czechoslov. Chem. Commun.*, **29**, 2299 (1964).
12. P. E. McMahon and W. C. Tincher, *J. Mol. Spectry.*, **15**, 180 (1965).
13. P. E. McMahon, *J. Mol. Spectry.*, **15**, 221 (1965).
14. B. C. Schneider, J. Stokr, D. Doskocilova, S. Sykora, J. Jakes, and M. Kolinsky, paper presented at International Symposium on Macromolecular Chemistry, Bruxelles, 1967; preprint 9.
15. D. Doskocilova, J. Stokr, E. Votavova, B. Schneider, and D. Lim, in *Macromolecular Chemistry Prague 1965*, (*J. Polym. Sci. C*, **16**), O. Wichterle and B. Sedláček, Eds., Interscience, New York, 1967, p. 215.
16. Y. Abe, M. Tasumi, T. Shimanouchi, S. Satoh, and R. Chujo, *J. Polym. Sci. A-1*, **4**, 1413 (1966).
17. F. A. Bovey and G. V. D. Tiers, *Fortschr. Hochpolym. Forsch.*, **3**, 139 (1963).
18. G. Confalonieri, G. Borsini, and L. Cavalli, to be published.
19. A. Segre, *Macromolecules*, **1**, 93 (1968).
20. S. Enemoto, M. Asahina, and S. Satoh, *J. Polym. Sci. A-1*, **4**, 1373 (1966).
21. R. L. Miller, *SPE Trans.*, 123 (April 1963).
22. G. Boccato, A. Rigo, G. Talamini, and F. Zilio-Grandi, *Makromol. Chem.*, **108**, 218 (1967).
23. U. Johnsen, K. Kolbe, *Zolloid Z.*, **221**, 64 (1967).
24. H. L. Frisch, C. L. Mallows, and F. A. Bovey, *J. Chem. Phys.*, **45**, 1565 (1966).
25. J. W. L. Fordham, P. H. Burleigh, and C. L. Sturm, *J. Polym. Sci.*, **41**, 73 (1959).

Received May 23, 1968

JOURNAL OF POLYMER SCIENCE: PART A-1 VOL. 8, 813–833 (1970)

Crosslinking, Filler, or Transition Constraint of Polymer Networks. I

A. F. BLANCHARD, *Dunlop Research Centre, Birmingham, England*

Synopsis

The basic theory of modulus/swelling is developed to allow for limited extensibility, filler reinforcement or transition effects, and steric hindrance of aligned segments by extended chains or filler particles.

Filler forms an effective hard fraction C_h per cubic centimeter of compound with v_c a new (compound) index of swelling. For $1/M_c + \sigma$ fix points having ratio ϕ to gum values $1/F_0(v_r)$ and with $F(v_c)$ replacing the Flory function $F(v_r)$:

$$\frac{1}{M_c} + \sigma = \frac{\phi}{F_0(v_r)} = \frac{1 - C_h}{1 + C_h}\frac{1}{F(v_c)}$$

where σ denotes entanglement. Linkage reinforcement ϕ does not vary with sulfur crosslinking of SBR. Vacuoles invalidate ϕ from mass-increment $F_0(v_r)/F(v_r)$ for inert fillers. Then, or for Graphon, with negligible $\phi \approx 1$:

$$C_h = \frac{1 - (v_{r0}/v_c)}{1 - v_{r0}} \qquad \phi\left(\frac{1 + C_h}{1 - C_h}\right) = \frac{F_0(v_r)}{F(v_c)}$$

The effective C_h includes rubber stretched hard on Graphon by swelling or trapped inside hard aggregates. Only the right-hand equation fits normal blacks. In theory, C_h can always be obtained from swollen moduli G by linear slopes $(1 + 1.4C_h)$ relating $F(v_c)$ and $(1 - C)\rho RT/G$. For filler fractions $C \geq 0$ cm^{-3} and low strains $\alpha = 1.5$–2.0 below prestretch the modulus G is given a new basic definition:

$$\ln \frac{F v_r^{1/3}}{\alpha - (1/\alpha^2)} - \frac{C_2^*(v_r)^{4/3}}{\alpha} = \ln G$$

Here $C_2^* \approx 0.7$ corresponds to Mooney-Rivlin C_2, and the effective crosslinking $1/[M_c] = (\rho RT)^{-1}G$ is equal to $(1 - C)(1/M_c + \sigma)$ for unswollen prestretched rubber ($v_r = 1$). For higher strains a hypothesis of strain hardening is proposed. This is distinct and opposite in character to the initial prestretch softening (Mullins effect). Nonlinear effects of crosslinks are expressed by a fractional stress-upturn Ω $(1/M_c + \sigma)$, effective mesh weight $(1/M_c + \sigma)^{-1} - \Omega$, and hard fraction $\Omega(1/M_c + \sigma)$. For μ_h characterizing strain hardening up to the prestretch $(\alpha_b - 1)$ their contribution is:

$$\Delta \ln F = \mu_h(\alpha - 1)^4 + J\left(\frac{\alpha - 1}{\alpha_b - 1}\right)^6$$

The sixth-power refinement has $J = j(\alpha_b - 1)^{1/2}$ with $j \approx 0.4$. The hard phase is augmented by filler and grows with increasing strain up to the prestretch.

INTRODUCTION

For a polymer network at equilibrium in solvent, Flory and Rehner[1] related the polymer fraction v_r of the swollen volume to the molecular weight M_c of the chains between crosslinks. Their equation is represented below by the function $F(v_r)$ with $[M_c]$ denoting the effective mesh weight, i.e., that obtained by physical measurements. Hence the effective crosslinking $1/[M_c]_s$ from swelling measurements v_r is given by $1/F(v_r)$. If we take Flory's refinement for tetrafunctional crosslinks,[2] we have

$$[M_c]_s = \frac{-\rho V_1(v_r^{1/3} - v_r/2)}{\mu v_r^2 + \ln(1 - v_r) + v_r} = F(v_r) \tag{1}$$

Here V_1 is the molar volume of the solvent, ρ is the density of the polymer, and μ is the interaction constant between polymer and solvent. For the modulus of elasticity G Flory and Rehner[1] also derived a simple equation whereby, with the present writer's notation $1/[M_c]$ for physically effective crosslinking:

$$G = \frac{f v_r^{1/3}}{A[\alpha - (1/\alpha^2)]} = \frac{\rho RT}{[M_c]} \tag{2}$$

Here A is the cross section before swelling, f the force of retraction on stretching, α the extension ratio of the swollen rubber, and RT is the product of the gas constant and absolute temperature. Gee[3] has shown that swollen vulcanizates obey the theoretical eq. (2) quite closely, in contrast to dry rubber; and Mullins et al.[4] confirmed this for various solvents and polymers.

Some chemical crosslinks are ineffective because macromolecules having finite primary weight before crosslinking will have free-end chains that do not contribute to equilibrium elasticity. On the other hand, chain entanglements contribute to the effective crosslinking from eq. (1) so that it may exceed actual $1/M_c$ values, as Moore and Watson showed by chemical analysis.[5] Hence with Mullins they estimated the effective entanglement,[5,6] and Blanchard and Wootton[7] and Mullins[8] published entanglement corrections which increase the influence of primary molecular weight.

Being concerned with effective crosslinking the present paper neglects primary weight, though finite (low) weights must be considered when estimating the actual (chemical) crosslinking at low cure states. Part I develops and refines the basic theory to allow for the limited extensibility of short network chains, steric hindrances due to alignment and interaction with short chains, or junction with reinforcing particles or other hard inclusions. Experimental details and discussion of the results will follow in Part II.[9]

THEORETICAL

Trapped entanglements are here distinguished from the actual number of chain snags and defined as the crosslink contribution σ to which they are

effectively equivalent at a specified strain. If the initial molecular weight and crosslinking are high enough to neglect the effect of free chain ends we can then write:

$$G = \rho RT[(1/M_c) + \sigma] \tag{3}$$

At this stage in defining entanglements the above reference to a specific strain is advisable, because σ may not be a constant fraction of the chain snags if with increasing strain they become more nearly equal to crosslinks. Notwithstanding this theoretical reservation the above working definition has proved satisfactory[10] for elongations of 30–250%. It may be incorporated in a more general correction Γ as follows:

$$G = \Gamma\rho RT/M_c \tag{4}$$

Then $\Gamma = 1 + \sigma M_c$ represents entanglements alone, but as a multiple of M_c plus a constant it could be adjusted to include for a given strain all deviations from ideal behavior having zero or first-order dependence on crosslinking. Of such low-order effects, those due to free-end chains are outside the scope of the present paper, and best taken into account by a separate factor.[8–11] For equilibrium swelling of imperfect networks, eq. 1 may be adjusted similarly by a factor γ corresponding to Γ for modulus:

$$M_c = \gamma F(v_r) \tag{5}$$

For gum networks Blanchard and Wootton[7] have shown that $\gamma = 1 + \sigma M_c$ with σ constant to fit the chemical data of Moore and Watson.[5] Evidence that $\Gamma = \gamma$ over a range of gum elongations[7,10] has shown that such corrections do not cover non-Gaussian distribution of chain displacements, because that would increase with elongation.

Free ends being regarded separately, the low-order deviation from basic theory is defined here by Γ or γ to represent all other network imperfections that change the effective crosslinking by a constant amount, or linearly in first-order proportion to the true crosslinking $1/M_c$. As first-order effects are appreciable with a volume fraction C of filler, it is convenient to express them by the subscript C as a separate factor Γ_C. From the definition of entanglements by their equivalent crosslinks σ, the gum factor for $C = 0$ is $1 + \sigma M_c$; and by combination with Γ_C:

$$\Gamma = \Gamma_C(1 + \sigma M_c) \tag{6}$$

Thus Γ is resolved by product into component factors Γ_C and $1 + \sigma M_c$, the effective crosslinking being $\Gamma/M_c = \Gamma_C[(1/M_c) + \sigma]$. Unlike the sum $\Gamma_C + \sigma M_c$ this satisfies the definition of entanglements in that the equivalent crosslinks σ and $1/M_c$ have a common interaction with Γ_C. For the case of complete wetting of filler particles by a rubber matrix we can take $\Gamma_C = 1 + 2.5C$ for equivalence with Smallwood's theory of modulus reinforcement,[12] or $1 + 2.5C + 14.1C^2$ if we adopt the refinement of Guth and Gold.[13] These theoretical factors do not apply if the effective wetting

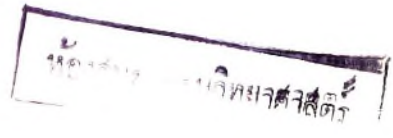

of the particles has been destroyed by prestressing or by vacuole formation with inert fillers during initial-curve modulus tests.

High-Order Effects of Fix Points in Gum and Reinforced Networks

Steric hindrance of chain segments by stretched short chains or hard inclusions may increase too rapidly with crosslinking to be expressed wholly as a first-order component of Γ. To allow for this possibility, we can introduce a purely mathematical definition of all such higher-order effects, i.e., without any limitation on their physical character. They are here referred to as Ω steric hindrance effects and defined as those whose fractional stress contribution is $\Omega[(1/M_c) + \sigma]$ in proportion to the $1/M_c + \sigma$ fix points in the network. On this definition the high-order departure from basic theory will make a deviant contribution $\Omega[(1/M_c) + \sigma](f/A)$ to an observed stress f/A.

On subtracting the Ω contribution and correcting for v_r as in eq. (2) the theoretical part of the network stress is $(1 - \Omega(1/M_c + \sigma))(fv_r^{1/3}/A)$; and with allowance, too, for σ and Γ_C, by equations (3)–(6) we have:

$$\{1 - \Omega[(1/M_c) + \sigma]\}(fv_r^{1/3}/A) = \Gamma_C \rho RT[(1/M_c) + \sigma][\alpha - (1/\alpha^2)]$$

$$\frac{fv_r^{1/3}}{A} = \frac{\Gamma_C \rho RT[\alpha - (1/\alpha^2)]}{[(1/M_c) + \sigma]^{-1} - \Omega} \tag{7}$$

It can be seen that the stress f/A tends to infinity in the limit $[(1/M_c) + \sigma]^{-1} \approx \Omega$. Therefore Ω may be regarded as the spacing of fix points which would transform the polymer into a rigid material. However, this concept of a critical segment size must be regarded with caution, because it involves extrapolating to an extreme where rubberlike properties disappear. The effect of Ω in increasing the modulus G is expressed by the equation:

$$G = \frac{\Gamma_C \rho RT}{[(1/M_c) + \sigma]^{-1} - \Omega}$$

$$= \Gamma_C \rho RT([(1/M_c) + \sigma] + \Omega[(1/M_c) + \sigma]^2 + \ldots) \tag{8}$$

where $\Gamma_C = 1$ for gum networks. Thus Ω can represent high-order effects due to short chains, reinforcing particles, and the limited flexibility and extensibility of real molecules.

This mathematical definition of Ω may be supplemented by a simple physical model for the modified theory. Taking L_A for the Loschmidt (Avogadro) number, there are high-order effects of $(L_A/2)[(1/M_c) + \sigma]$ crosslinks and entanglements if their subdivision of the molecules into $L_A[(1/M_c) + \sigma]$ chains causes steric hardening near filler particles and short chains at the limit of extensibility. Then for molecular weight $[(1/M_c) + \sigma]^{-1}$ between fix points the effective chain length may be reduced to average molecular weight $[(1/M_c) + \sigma]^{-1} - \Omega$. Thus high-order effects are represented physically by a crude model in which rubbery chains of molecular weight $[(1/M_c) + \sigma]^{-1} - \Omega$ are linked by short segments Ω

of equivalent tension but inability to extend further. Hence $\Omega[(1/M_c) + \sigma]$ measures a hard fraction of the network.

By an earlier incomplete definition of high-order effects their fractional contribution to G and $1/F(v_r)$ were expressed by Ω/M_c and ω/M_c, respectively, in which case:[7]

$$F(v_r) = \frac{\Omega - \omega}{\gamma} + \frac{\Gamma}{\gamma}\frac{\rho RT}{G} \tag{9}$$

On the present theory these deviant contributions are $\Omega[(1/M_c) + \sigma]$ and $\omega[(1/M_c) + \sigma]$ so that the factor $1 + \sigma M_c$ cancels γ in $(\Omega - \omega)/\gamma$ to yield linear graphs for swollen rubber, even when their intercept is substantial at high elongations. Experimentally the Ω concept has been justified by linear graphs of intercept $\Omega - \omega$ and slope $\Gamma/\gamma = 1$ for swollen NR at 50% elongation,[7] and later for relatively large $\Omega - \omega$ at up to 250% elongation.[10] Hence for swollen networks the non-Gaussian term $\Omega - \omega$ is constant for a fixed elongation, and the above equation simplifies to:

$$F(v_r) = \Omega - \omega + (\Gamma/\gamma)\rho RT/G \tag{10}$$

Here $\Gamma/\gamma = \Gamma_C/\gamma_C$ in accordance with eq. 6 and analogously $\gamma = \gamma_C(1 + \sigma M_c)$. For swollen gum rubber $\Gamma_C/\gamma_C = 1$ so that eq. (10) becomes simply:

$$F(v_r) = \Omega - \omega + \rho RT/G \tag{11}$$

The following analysis concerns the more complex case of dry rubber when highly stretched or reinforced, or strained by swelling alone.

Networks with Hard or Insoluble Components

Even for small strains a theory with the above mathematical form is likely to be especially helpful if there is a volume hard fraction C of carbon black or polymer crystallites. To some extent the proposed theory is physically reminiscent of the model proposed by Mullins and Tobin.[14]

The parameter Ω in Equations 7–8 of the new theory becomes Ω_C for C^* bonded particles in a total hard fraction $\Omega_C[(1/M_c) + \sigma] = C^* + \Omega[(1/M_c) + \sigma]$. On the other hand, a filler volume V per unit volume tends to reduce the elastic modulus G in the ratio $1:(1 + V)$ by diluting the rubber chains, the specific modulus of the network being $(1 + V)G$ or $(1 - C)^{-1}G$. This modulus is $\Gamma_C\rho RT/\{[(1/M_c) + \sigma]^{-1} - \Omega_C\}$ on the new theory so that:

$$G = \frac{1 - C}{1 - C^*}\frac{\Gamma_C\rho RT}{[(1/M_c) + \sigma]^{-1} - [\Omega/(1 - C^*)]} \tag{12}$$

Here $\sigma \approx 0.44 \times 10^{-4}$, and $\Gamma_C = 1 + 2.5C$ if we adopt the theoretical modulus factor $1 + 2.5C$ which Smallwood[12] derived for complete wetting of filler particles by a rubber matrix. However, neglecting $\Omega/(1 - C^*)$ for prestretched networks at low strains, we can put $\Gamma_C = 1$ and $C^* = 0$ because wetting is then elastically ineffective except for individual bonds that remain to contribute to the $1/M_c + \sigma$ fix points. But for high elongations

$\Omega/(1 - C^*)$ may be written with C for C^* because then the strain interaction of rubber and filler will make C effective as hard fraction even when $C^* \ll C$ at low strains. On these hypotheses, for prestressed networks:

$$G = (1 - C)\frac{\rho RT}{[(1/M_c) + \sigma]^{-1} - [\Omega/(1 - C)]} \tag{12a}$$

where $G = \rho RT(1 - C)[(1/M_c) + \sigma]$ at low strains. After a high prestress, inert fillers do not contribute to the $1/M_c + \sigma$ fix points; they have a simple diluent effect at low strains as expressed here by $1 - C = (1 + V)^{-1}$. For unswollen networks that have not been prestretched, the general equation, eq. (12), will have $C^* \approx C$ and $(1 - C)/(1 - C^*) \approx 1$ in the case of carbon fillers. Therefore taking the Smallwood factor $1 + 2.5C$ for Γ_C we have, for carbon particle reinforcement without prestretching or swelling:

$$G = \frac{\rho RT(1 + 2.5C)}{[(1/M_c) + \sigma]^{-1} - [\Omega/(1 - C)]} \tag{13}$$

The above equations imply that rubbery properties are lost and rigidity develops at a higher critical mesh spacing $(1/M_c + \sigma)^{-1} \to \Omega/(1 - C)$ as the volume fraction C of hard particles is increased. The rubber fraction $\Omega[(1/M_c) + \sigma]/(1 - C)$ that is effectively inextensible will reflect any reticulate or fibrous structure of hard inclusions.

For swollen rubber with carbon particle reinforcement the following theory introduces a concept of bonded interface rubber that is stretched hard by swelling. Equilibrium swelling data in Part II[9] show that carbon fractions C are roughly in proportion (ca. 1/1.15) to total hard fractions C_h for widely different carbon blacks. This indicates a hard skin on bonded particles in swollen rubber such that the bound filler fraction C^* may be taken to be 87% of the total hard fraction C_h. Therefore $(1 - C)/(1 - .87C_h)$ can replace $(1 - C)/(1 - C^*)$ in the general eq. (12). The alternative ratio of $1.15C$ to $1 - C_h$ is less convenient. On the other hand, the total hard fraction C_h will determine the modulus upturn so that for swollen rubber $\Omega/(1 - C_h)$ should replace $\Omega/(1 - C^*)$ in eq. 12. Moreover, since the hard interface is rubber network it can be regarded from a standpoint of modulus theory as fully wetted by the matrix. Complete wetting would require Γ_C to be the Smallwood or Guth-Gold type of theoretical factor.[12,13] With the foregoing modifications, eq. (12) is therefore proposed with the use of Smallwood's factor in a revised form $\Gamma_C = 1 + 2.5C_h$. Then for swollen networks that have not been prestretched:

$$G = \frac{1 - C}{1 - .87C_h}\frac{\rho RT(1 + 2.5C_h)}{[(1/M_c) + \sigma]^{-1} - [\Omega/(1 - C_h)]}$$

$$= \frac{(1 - C)\rho RT}{[(1/M_c) + \sigma]^{-1} - [\Omega/(1 - C_h)]}(1 + 3.4C_h) \tag{13a}$$

Here the term $1 + 3.4C_h$ is obtained by binomial expansion, C_h^2 terms and higher powers being neglected. Compared to the original Smallwood factor $(1 + 2.5C)$ the result $(1 - C)(1 + 3.4C_h)$, with $C_h \approx 1.15C$ for good solvents, is an increase to $(1 + 2.9C)$ for carbon particles in networks that have been swollen but not prestretched. With the coefficient of C adjusted to allow for C^2 interaction the writer shows elsewhere that carbon chain structure (shape factor) leads to an appreciable coefficient of C^2, and that this C^2 interaction coefficient is a linear measure of shape factor.[26]

Even swelling measurements on gum (unfilled) rubbers may require a small refinement ω corresponding to the Ω deviation of modulus, i.e., representing high-order effects of crosslinks. This ω deviation of equilibrium swelling may acquire a more significant value Λ_r if solvent-resistant rubber is induced by bonded particles of filler. Then for a volume fraction $\Lambda_r[(1/M_c) + \sigma]$ of effectively hard rubber we have by analogy with the Ω deviation of eq. (8):

$$F(v_r) = [(1/M_c) + \sigma]^{-1} - \Lambda_r \tag{14}$$

In the particular case of poor adhesion of polymer and filler, Kraus[15] has pointed out that swelling will form vacuoles which fill with solvent and cause the apparent swelling from weight measurements to be greater than the true value. This difficulty may be avoided by the new method here, in which mass-derived values are calculated on the total volume of polymer and filler. Then we obtain apparent compound swellings v_c where:

$$v_r = \frac{(1 + V)^2 v_c}{(1 + 2V)(1 + v_c V)} \tag{15}$$

This equation neglects a small term $v_c V^2/(1 + 2V)$ and comprises a factor $(1 + V)/(1 + 2V)$ to allow for the filler volume, the vacuole correction being $(1 + V)v_c/(1 + v_c V)$. In the case of unbonded particles these corrections almost cancel so that for practical purposes v_c is then equivalent to v_r (see Table I). For appreciable interface bonding but negligible linkage reinforcement it is shown in the Appendix that the resulting hard fraction is $C_h = [1 - (v_{ro}/v_c)]/(1 - v_{ro})$.

TABLE I
Equivalence of True v_r to the Mass-Derived v_c
When Solvent Vacuoles Form about Unbonded Particles

V	v_c	$\frac{(1 + V)^2 v_c}{(1 + 2V)(1 + v_c V)}$	Difference between v_c and v_r, %
0.2	0.1	0.101	−1
	0.2	0.198	+1
	0.3	0.291	+3
0.3	0.1	0.102	−1
	0.2	0.199	+0.5
	0.3	0.291	+3

Constraint of Swelling and Crosslink Reinforcement by Filler Particles

With reinforcing fillers such as carbon black, the substitution of v_c for v_r in eq. (14) means that firmly bonded particles are counted equivalent to solvent-resistant polymer and included in a compound hard fraction $\Lambda_C[(1/M_c) + \sigma]$.

By defining linkage reinforcement ϕ as the ratio of reinforced crosslinking $(1/M_c + \sigma)$ to the corresponding gum values $1/[\omega + F_0(v_r)]$; and considering only the rubber part of reinforced compounds, we have

$$[(1/M_c) + \sigma]^{-1} = \Lambda_r + F(v_r) \tag{14}$$

$$(1/M_c) + \sigma = \phi/[\omega + F_0(v_r)] \tag{16}$$

and

$$F(v_r) = [F_0(v_r)/\phi] - [\Lambda_r - (\omega/\phi)] \tag{16a}$$

In Figure 1 SBR data from Part II[9] show that for varying cure, eq. (16a) is linear with constant slope $1/\phi$. This is expected in view of Kraus's

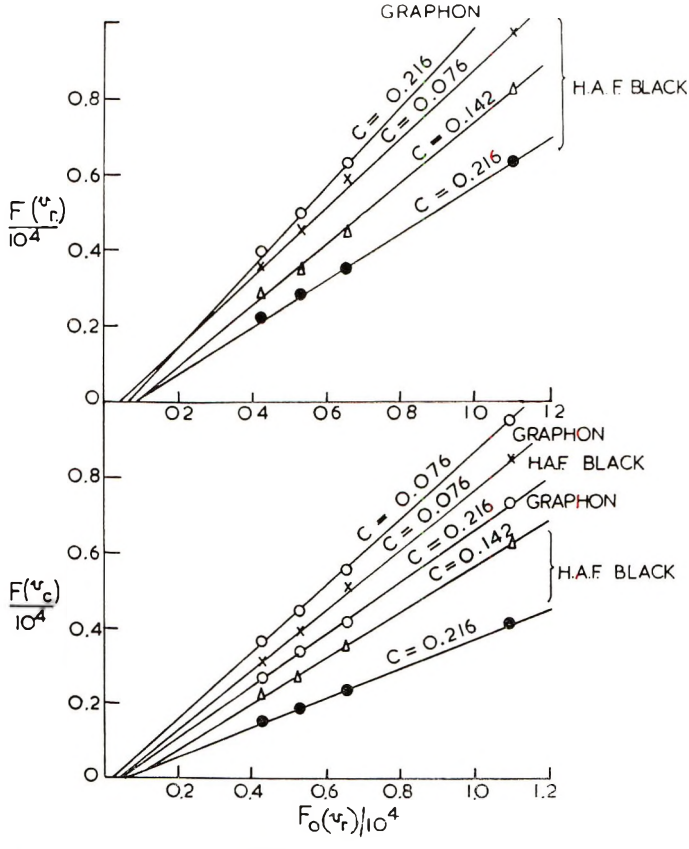

Fig. 1. Flory function $F_0(v_r)$ of SBR gum swelling related to carbon-reinforced values $F(v_r)$ or $F(v_c)$ for cure-varied fractions v_r of rubber or v_c of compound at equilibrium swelling.

discovery that cure has little effect on the ratios of swelling measurements for gum and corresponding reinforced vulcanizates.[16]

However, fluctuating intercepts in Figure 1 show that refinements are needed in the proposed new concepts of Λ hardening and linkage reinforcement. The present hypothesis is that effectively hard rubber on bonded particles is directly proportional to their volume concentration C^* and to the fix points $(1/M_{cg} + \sigma)$ of the gum matrix: but that the interfacial hard layer has considerable thickness only when the bonded chains are stretched hard, in this case through preventing swelling of filled holes in the matrix. Hence the ordinate intercepts of the lower graphs in Figure 1 are smaller because of less matrix swelling with the high black concentrations 50–65 phr. With increasing matrix crosslinking the reduced swelling must lead similarly to a diminishing specific measure Λ of the hardening per unit of matrix crosslinking and per unit volume of filler. On this basis the new theory can be developed quantitatively as follows.

We define C^* = volume fraction $C - C^1$ of bonded particles for C^1 unbound particles in a total fraction C per unit volume of rubber and filler; $1/M_c + \sigma$ = density of crosslinks and entanglements in the reinforced vulcanizate; $1/M_{cg} + \sigma$ = crosslinking and entanglement of a corresponding gum vulcanizate; Λ = specific hardening per unit of gum crosslinking and per unit volume of filler; $\Lambda(1/M_{cg} + \sigma)$ = volume fraction of hardened rubber per unit volume of filler (for carbon black this fraction is roughly constant and ca. 0.15[9]); ΛC^* = volume fraction of hardened rubber per unit of gum (matrix) crosslinking (this fraction decreases as crosslinking reduces Λ by reducing swelling); $\Lambda C^*(1/M_{cg} + \sigma)$ = volume fraction of hardened rubber on a volume fraction C^* of bonded particles in gum of crosslinking $(1/M_{cg} + \sigma)$; $\omega(1/M_{cg} + \sigma)$ = effective hard fraction in the absence of reinforcing particles; ϕ = linkage reinforcement defined by the ratio

$$[(1/M_c) + \sigma]/[(1/M_{cg}) + \sigma] = [(1/M_c) + \sigma][\omega + F_0(v_r)]$$

According to this analysis of eq. (14) there is an effectively hard polymer fraction $\Lambda_r(1/M_c + \sigma)$ comprising $\omega(1/M_{cg} + \sigma)$ for the gum alone, and a hardened fraction $\Lambda C^*(1/M_{cg} + \sigma)$ due to filler reinforcement; that is:

$$\Lambda_r\phi[(1/M_{cg}) + \sigma] = \omega[(1/M_{cg}) + \sigma] + \Lambda C^*[(1/M_{cg}) + \sigma] \quad (17)$$

where ϕ is the linkage reinforcement. On dividing through by $\phi[(1/M_{cg}) + \sigma]$ we obtain:

$$\begin{aligned} \Lambda_r &= (1/\phi)(\omega + \Lambda C^*) \\ &= (\omega/\phi)[1 + (\Lambda/\omega)C^*] \end{aligned} \quad (18)$$

In the limit $C^* = 0$ and $\phi = 1$, eq. (18) becomes $\Lambda_r = \omega/\phi = \omega$ for the case of gum rubber. On combining eqs. (18) and (16a), and multiplying through to remove ϕ from the right-hand side we have:

$$F_0(v_r) = \phi F(v_r) + \Lambda C^* \quad (19)$$

The tendency of filler cavities to dilate with swelling and the specific measure Λ of interfacial hardening due to this constrained tendency can be expected to vary with the total molecular extension $(\alpha_m - 1)$ in the same way as the corresponding modulus property Ω. It has been shown elsewhere[10] that Ω increases with $(\alpha_m - 1)^2$, this being proportional to $[(1/v_r^{1/3}) - 1]^2$ when gum modulus testpieces are additionally stretched by swelling. Therefore for pure swelling without mechanical stress we have by analogy:

$$\Lambda = b[(1/v_r)^{1/3} - 1]^2 \tag{20}$$

where b is an empirical constant to allow for a hard interface of highly-stretched rubber in swollen networks of filled rubber. This hypothesis is consistent with Boonstra's qualitative conclusion[17] that filler constraint depends on the overall swelling as varied by choice of solvents. It appears reasonable *a priori* as a trial substitution in eq. 19; and on dividing through by $F(v_r)$ we have:

$$\frac{F_0(v_r)}{F(v_r)} = \phi + \frac{bC^*[(1/v_r^{1/3}) - 1]^2}{F(v_r)} \tag{19a}.$$

By taking data from Part II[9] and for $C^* \approx C$ for carbon blacks, the refinement b is the average from the slope bC in Figure 2, where $F_0(v_r)/F(v_r)$ is plotted against $[(1/v_r^{1/3}) - 1]^2/F(v_r)$. Scatter of the points may be due to error of the approximation $C^* \approx C$ if C^* varies at all with cure crosslinking. Each line through the points is drawn to obtain a rough fit with a common slope factor $b = 3000$ where:

$$\frac{F_0(v_r)}{F(v_r)} = \phi + \frac{bC[(1/v_r^{1/3}) - 1]^2}{F(v_r)} \tag{21}$$

This choice $b = 3 \times 10^3$ comes with greater precision and discrimination from Part II[9] where b is selected by trial to obtain ϕ values by Equation 21 to satisfy the following requirements: (*1*) a reasonable assumption that Graphon gives negligible linkage reinforcement $\phi \approx 1$; (*2*) negligible ϕ variation with cure and filler concentration for negligible linkage reinforcement; (*3*) close agreement with the value for Graphon, $\phi \approx 0.98$, obtained by eq. (27) from $F(v_r)/F(v_c)$ data and C_h by eq. (47). Values of C_h for test (*3*) are obtainable by eq. (47) for the particular case of Graphon. There is no significant indication from Figure 2 that the coefficient b differs for HAF carbon and Graphon. A common coefficient of interfacial hardening is not unreasonable since vacuole formation by swelling is prevented even by the sparsely-bonded Graphon.

For a volume fraction C of filler the bonded fraction $C^* = C - C^1$ may be treated as if it were inextensible rubber. Then it is part of a compound hard fraction $\Lambda_C[(1/M_c) + \sigma]$; and, on introducing into eq. (14) a calibration factor γ_C, we have by adjustment of eqs. (17) and (14):

$$\Lambda_C[(1/M_c) + \sigma] = C^* + \omega[(1/M_{cg}) + \sigma] + \Lambda C^*[(1/M_{cg}) + \sigma] \tag{22}$$

$$[(1/M_c) + \sigma]^{-1} = \Lambda_C + \gamma_C F(v_c) \tag{23}$$

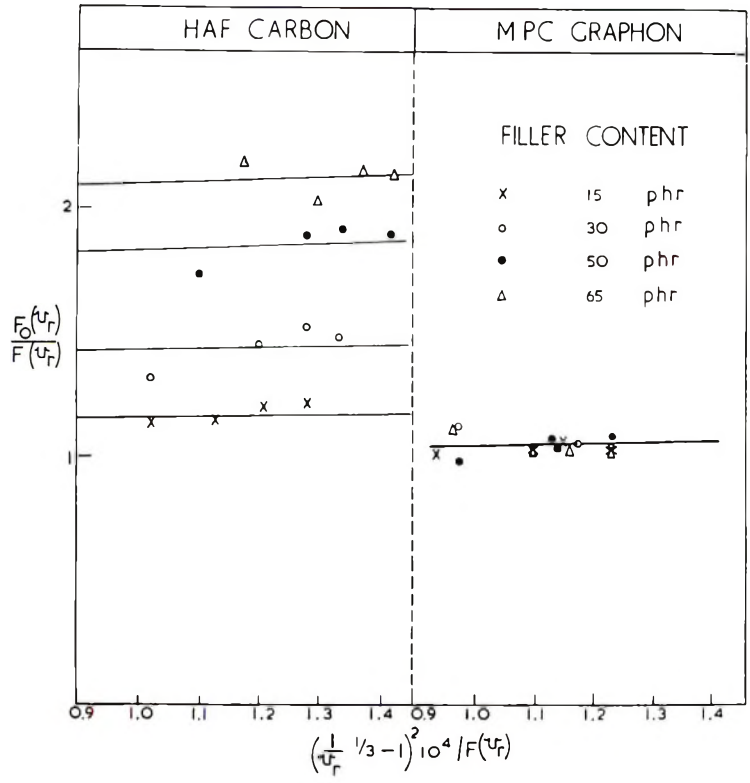

Fig. 2. Relation of $F_0(v_r)/F(v_r)$ to its hard interface component $bC[(1/v_r^{1/3}) - 1]^2/F(v_r)$ for carbon blacks in SBR. The gum crosslinking $1/F_0(v_r)$ is $0.91–2.3 \times 10^{-4}$ and the ordinate intercept is linkage reinforcement ϕ in eq. (21).

Thus for compound swellings v_c the calibration factors $\Lambda_C > 0$ and $\gamma_C > 1$ allow for overestimation of crosslinking due to the solvent resistant volume of reinforcing particles. Since carbon particles do not form vacuoles, the slope ϕ of eq. (19) can be used to determine γ_C experimentally from the slope of the combined eqs. 16 and (22)–(23), i.e.,

$$F_0(v_r) = [\phi\gamma_C/(1 - C^*)]F(v_c) + [(\Lambda + \omega)C^*/(1 - C^*)] \qquad (24)$$

From SBR data of Part II[9] the linear graphs in Figure 1 show the success of this eq. (24) and eqs. (16a)–(19) when applied over a range of crosslinking and carbon concentration. For this preliminary calibration we can take $C^* \approx C$ for carbon black. Table II shows the corresponding γ_C in eq. 24 as obtained from the inverse slopes $(1 - C^*)/\phi\gamma_C$ in Figure 1. As far as can be judged from the data in Table II a common relation $\gamma_C \approx 1 + C$ is true for the carbons HAF and Graphon having very different reinforcing ability. To include fillers with an unbound fraction C^1 this experimental result is here modified to a more general hypothesis:

$$\gamma_C = 1 + C - C^1 = 1 + C^* \qquad (25)$$

TABLE II
SBR Linkage Reinforcement ϕ by Carbon Particles; Swelling Calibration γ_C for Such Particles (Those Too Firmly Bonded to Form Vacuoles)

Carbon black loading in SBR			Linkage reinforcement ϕ [without allowing for Λ variation in eq. (19)]		Calibration factor γ_C from eq. (24) and Fig. 1 (taking $C^* \approx C$)	
Carbon black, wt-% (based on rubber)	Volume fraction C	$1 + C$	HAF Carbon	Graphon	HAF Carbon	Graphon
15	0.076	1.076	1.09	0.98	1.06	1.06
30	0.142	1.142	1.22	1.25	1.13	1.13
50	0.216	1.216	1.61	0.93	1.22	1.21
65	0.263	1.263	2.23	1.18	1.28	1.27

The justification for this theoretical step is that γ_C is not needed with mass-increment v_e data for inert fillers, eq. (19) being applicable with $C^* = 0$ and v_e replacing v_r to allow for vacuoles (see Table I).

By the above hypothesis [eq. (25)] with Λ from eq. (20) and neglecting $\omega C^*/(1 - C^*)F(v_e)$, on dividing eq. (24) by $F(v_e)$ we have:

$$\frac{F_0(v_r)}{F(v_e)} = \phi \frac{1 + C^*}{1 - C^*} + \frac{bC^*[(1/v_r^{1/3}) - 1]^2}{(1 - C^*)F(v_e)} \tag{26}$$

For bonded particles $C^* \approx C$ is sufficiently accurate for the bC^* refinement; then $\phi(1 + C^*)/(1 - C^*)$ may be calculated from $F_0(v_r)/F(v_e)$ by subtracting $bC[(1/v_r^{1/3}) - 1]^2/(1 - C)F(v_e)$. Alternatively, to express differing levels of reinforcement, the hardened (swollen) rubber at the filler surface may be represented in a total hard fraction C_h that is slightly greater than the volume fraction C^* of bonded filler. Then eq. 26 can be given a simpler but sufficiently accurate form:

$$\phi(1 + C_h)/(1 - C_h) = F_0(v_r)/F(v_e) \tag{27}$$

Properly interpreted, this is a general index of reinforcement, even when vacuoles are so prevalent that it is not much greater than 1 (for calcium silicate it is fractional at low concentrations). With strongly reinforcing particles $(1 + C_h) > 1$; and $\phi \gtrsim 1$ when there is little cure retardation due to surface acidity. By eq. (27) the reinforced number of fix points is:

$$1/M_e + \sigma = \phi/F_0(v_r) = [(1 - C_h)/(1 + C_h)]\, 1/F(v_e) \tag{28}$$

Here $C_h \approx 1.15C$ for carbon blacks.[9] For Graphon or inert fillers the Appendix shows that more precise C_h values leading to ϕ and $1/M_e + \sigma$ by eqs. (27) and (28) can be obtained experimentally from $C_h = [1 - (v_{ro}/v_e)]/(1 - v_{ro})$. With better bonded fillers such as normal carbon black, the linkage reinforcement ϕ and corresponding C_h by eq. (27) can be obtained by eq. (21) or from the slope of eq. (19). Then the results $\phi \gg 1$ give effective linkage reinforcement. But the actual $1/M + \sigma$ and in-

trinsic linkage reinforcement ϕ_0 can be obtained, when needed, by dividing by $(1 + 2{\cdot}5C_\phi)$ where $C_\phi = (C \ln \phi)/(1 + 2{\cdot}5C)$.

Stress Upturn and Strain Hardening

Prestressing of reinforced rubber will soften it at lower elongations, and the subsequent stress–strain curve can be very steep at quite low elongations, depending on the prestretch.[18,19] By multiplying the top and bottom of eq. (8) by $[(1/M_c) + \sigma]$ it can be seen that $-\ln\{1 - \Omega[(1/M_c) + \sigma]\}$ is the logarithm of this upturn component. For dry (unswollen) rubber at low elongations there is also an initial decrease in the modulus $F/[\alpha - (1/\alpha^2)]$ as the elongation $(\alpha - 1)$ is increased. The inconstant moduli which result from these complex and conflicting tendencies are analyzed by Figure 3 into logarithmic components $-\ln\{1 - \Omega[(1/M_c) + \sigma]\}$ and $C_2^*/\propto$. For low strains the inextensible fraction $\Omega[(1/M_c) + \sigma]\}$ is equal to the logarithmic modulus component $-\ln\{1 - \Omega[(1/M_c) + \sigma]\}$ and for low effective hard fractions it simplifies to:

$$\Delta \ln F = -\ln\{1 - \Omega[(1/M_c) + \sigma]\} \approx \Omega[(1/M_c) + \sigma] \qquad (29)$$

Even at zero elongation the basic theory may require a small correction for high-order effects so that Figure 3 acknowledges that there may be a residual modulus contribution $\omega[(1/M_c) + \sigma]$, though usually this is negligible for gum or prestressed rubbers.

Prestressed vulcanisates vary greatly in modulus and since the initial dip in their modulus-strain curve is greatest when the modulus is high, it is necessary for the dip to be expressed by a coefficient C_2^* of fractional change rather than the well-known C_2 of Mooney[20] and Rivlin and Saunders.[21] The present paper meets this need by a logarithmic form of analysis which for $\ln(1 + C_2^*/\alpha) \approx C_2^*/\alpha$ is roughly equivalent to replacing C_2 by $C_1C_2^*$ so that where $[C_2^*/\alpha] \ll 1$:

$$F/[\alpha - (1/\alpha^2)] = 2C_1 + (2C_1C_2^*/\alpha) \qquad (30)$$

The modulus $2C_1$ corresponds to the preferred notation G of this and earlier papers.[19,22] By eq. (30) and taking $\ln(1 + C_2^*/\alpha) \approx C_2^*/\alpha$ for elongations that are substantial but well below the modulus upturn we have as an approximation to the logarithmic form:

$$G = \frac{F/[\alpha - (1/\alpha^2)]}{1 + (C_2^*/\alpha)} \qquad (31)$$

For a complete analysis of Figure 3 that includes modulus upturn the success of a logarithmic equation is given in Part II.[9] The corresponding definition of modulus may be expressed for moderate strains by a logarithmic definition that is more accurate than eq. (31):

$$\ln\{F/[\alpha - (1/\alpha^2)]\} - (C_2^*/\alpha) = \ln G \qquad (32)$$

For swollen rubbers F must be replaced by $Fv_r^{1/3}$ and C_2^* becomes $C_2^*v_r^{4/3}$ in eq. (32). This empirical modification of eq. 2 is inaccurate for very low

elongations; but Blanchard has shown that particle contacts then cause anomalous stiffening in any case.[22,23] For unfilled rubbers the physical significance of low-strain deviation from elasticity theory was discussed recently by Gee.[24]

Prestretching leads to softer rubber vulcanizates at lower levels of subsequent strain, this softening action being well known as the Mullins effect. For prestretched rubber the present writer has evolved a new and contrasting concept of strain-hardening by subsequent lower strains. This strain-hardening of a pre-stretched network is distinct and opposite in character to the prestretch softening, though related mechanisms are probably involved. Equation (45) of the Appendix expresses the proposed concept of strain-hardening in terms of intrinsic molecular extensibility ϵ and a network coefficient h of strain hardening. Thus:

$$-\ln\left[1 - \Omega\left(\frac{1}{M_c} + \sigma\right)\right] = \omega\left(\frac{1}{M_c} + \sigma\right) + \frac{3}{5}\left(\frac{1}{\epsilon}\right)\left(\frac{1}{M_c} + \sigma\right)(\alpha - 1)^2 + \left[\frac{6}{5}\left(\frac{h}{\epsilon}\right) + \frac{11}{50}\left(\frac{1}{\epsilon^2}\right)\right]\left(\frac{1}{M_c} + \sigma\right)^2(\alpha - 1)^4 + \left[\frac{3}{5}\left(\frac{h^2}{\epsilon}\right) + \frac{9}{10}\left(\frac{h}{\epsilon^2}\right)\right]\left(\frac{1}{M_c} + \sigma\right)^3(\alpha - 1)^6 \quad (33)$$

Experience with this equation in Part II[9] shows that in unswollen rubber at moderate to high elongations there is so much strain hardening ($h > 0$) that both the terms in $(\alpha - 1)^2$ and $\omega(1/M_c + \sigma)$ are relatively insignificant. In that case:

$$-\ln\left[1 - \Omega\left(\frac{1}{M_c} + \sigma\right)\right] = \left[\frac{6}{5}\left(\frac{h}{\epsilon}\right) + \frac{11}{50}\left(\frac{1}{\epsilon^2}\right)\right]\left(\frac{1}{M_c} + \sigma\right)^2(\alpha - 1)^4 + \left[\frac{3}{5}\left(\frac{h^2}{\epsilon}\right) + \frac{9}{10}\left(\frac{h}{\epsilon^2}\right)\right]\left(\frac{1}{M_c} + \sigma\right)^3(\alpha - 1)^6 \quad (34)$$

For small deviations, $-\ln[1 - \Omega[(1/M_c) + \sigma]] \approx \Omega[(1/M_c) + \sigma]$, so that for the negligible strain hardening $h \approx 0$ of swollen rubbers, eq. (11) has $\Omega - \omega$ independent of crosslinking $1/M_c$ on putting $h = 0$ in the simplified eq. 33:

$$\Omega - \omega = \frac{3}{5}\left(\frac{1}{\epsilon}\right)(\alpha - 1)^2 + \left[\frac{6}{5}\left(\frac{h}{\epsilon}\right) + \frac{11}{50}\left(\frac{1}{\epsilon^2}\right)\right]\left[\frac{1}{M_c} + \sigma\right](\alpha - 1)^4 + \left[\frac{3}{5}\left(\frac{h^2}{\epsilon}\right) + \frac{9}{10}\left(\frac{h}{\epsilon^2}\right)\right]\left(\frac{1}{M_c} + \sigma\right)^2(\alpha - 1)^6 \quad (35)$$

When there is negligible strain hardening, $h \approx 0$ in eq. (33), the modulus upturn $(3/5\epsilon)[(1/M_c) + \sigma](\alpha - 1)^2$ will be roughly constant at break if non-Gaussian behaviour has a fixed limit due to chain breakage. In that case, the network extensibility will be proportional to the square root of the chain length, as in Treloar's theory for gum networks.[25]

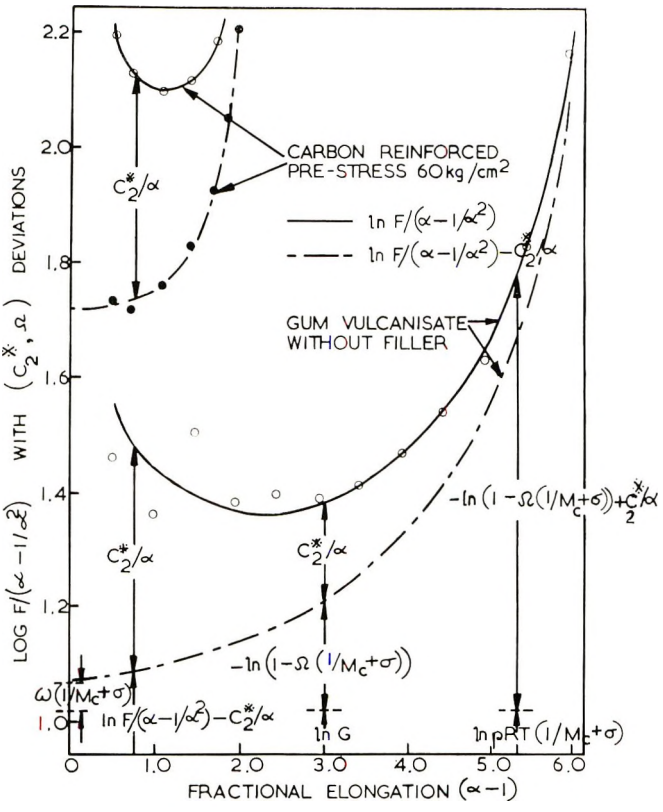

Fig. 3. Diagram showing filler effects and the proposed theoretical analysis of stress–strain curves of prestressed rubber into components $\Omega[(1/M_c) + \sigma]$ and C_2^*/α.

The hypothesis of strain hardening expressed by the above equations is easily applied if we replace $1/M_c + \sigma$ by the effective concentration of fix points from physical measurements at low strains. On substituting this effective constraint $1/[M_c]$ on the right-hand side of eq. (34), we have

$$-\ln\left[1 - \Omega\left(\frac{1}{M_c} + \sigma\right)\right] = \left[\frac{6}{5}\left(\frac{h}{\epsilon}\right) + \frac{11}{50}\left(\frac{1}{\epsilon^2}\right)\right](1/[M_c])^2(\alpha - 1)^4 + \left[\frac{3}{5}\left(\frac{h^2}{\epsilon}\right) + \frac{9}{10}\left(\frac{h}{\epsilon^2}\right)\right](1/[M_c])^3(\alpha - 1)^6 \quad (36)$$

For rubber molecules of finite primary weight, the use of $1/[M_c]$ will lead to some error, because crosslinks that are "ineffective" due to free-end chains will nevertheless contribute to the upturn of the stress–strain curve. Except in this usually unimportant respect the upturn is considered likely in practice to relate more closely to the physically effective constraint $1/[M_c]$ than it does to the actual number of fix points. For networks containing hard particles, this use of effective constraint in eq. (36) avoids the difficulty of attempting by theory to take the hard volume generally

into account [e.g., by eq. (12)]. The imperfection in tension-strain due to a hard filler in rubber is best studied empirically in the relation between low-strain modulus G and h in eq. (36), as will appear in Part 2.[9] Effective constraint $1/[M_c]$ is measured by the modulus parameter $(\rho RT)^{-1}G$ with G from eq. (2) at low strains, or more accurately from eqs. (32) and (36) by extrapolation of the resultant equation:

$$\ln\frac{F}{\alpha - (1/\alpha^2)} - \frac{C_2^*}{\alpha} = \ln G + \left[\frac{6}{5}\left(\frac{h}{\epsilon}\right) + \frac{11}{50}\left(\frac{1}{\epsilon^2}\right)\right]\frac{G^2}{(\rho RT)^2}(\alpha - 1)^4 + \left[\frac{3}{5}\left(\frac{h^2}{\epsilon}\right) + \frac{9}{10}\left(\frac{h}{\epsilon^2}\right)\right]\frac{G^3}{(\rho RT)^3}(\alpha - 1)^6 \quad (37)$$

On wholly empirical grounds Blanchard and Parkinson[19] used the fourth power of $\alpha - 1$ to express the stress upturn of reinforced networks. With $C_2^* = 0.7$ on present evidence the new eq. 37 is applicable by using a modified (empirical) coefficient for the sixth-power refinement, this being calculable from the prestretch to include even the steepest curve, i.e., up to the prestretch.[9]

DISCUSSION

Underlying the above analysis and equations is a general physical model and theory of polymer compounds as heterogeneous networks. They are pictured with a hard phase comprising rubber near the limit of extensibility together with any reinforcing particles and/or sterically hindered rubber segments. The hindered segments may be in a transition state, interacted with highly stretched chains and hard particles, or trapped inside particle aggregates and carbon gel fragments. On this theory polymeric materials have an effective hard phase which is augmented by filler reinforcement, decreases with prestretching, and grows with increasing strain up to the prestretch. In swollen rubber the hard phase includes rubber on particle surfaces that has been stretched hard by swelling, and rubber trapped inside coherent aggregates of filler or rubber and filler. The theory does not explicitly consider the configuration of the phases, this being taken generally but indirectly into account by extensibility and strain hardening. The latter properties have an experimental significance and semiempirical basis that will be made clearer in Part II of the paper.[9]

APPENDIX

Analysis of the Upturn Component of Tension–Strain Curves

For rubber networks that do not contain filler there is already a theory for non-Gaussian distribution of chain displacements at high elongations.[25] Then if r is the root-mean-square separation of chain ends, the

stress F on the stretched rubber is proportional to the inverse Langevin function $L^{-1}(r/nl)$ where nl is the fully extended length of the chains and:

$$L^{-1}(r/nl) = 3(r/nl) + (9/5)(r/nl)^3 + (297/175)(r/nl)^5 + \ldots .$$

For the proposed logarithmic analysis, powers greater than $(r/nl)^4$ are neglected, together with $(r/nl)^4$ terms except at high elongations; and expansion of $\ln\{1 + 99(r/nl)^4/[175 + 105(r/nl)^2]\}$ is approximated by taking $105(r/nl)^2 \approx 75$ to cover the highest elongations $r/nl \approx 0.85$ that are likely without breaking. Hence the stress logarithm $\ln F$ is taken proportional to:

$$\ln 3(r/nl) + (3/5)(r/nl)^2 - [(9/25)(r/nl)^4/2] + (99/250)(r/nl)^4$$

This approximation is accurate enough in most applications. The term $3(r/nl)$ represents Gaussian chain displacements, and by itself gives the well-known function $\alpha - (1/\alpha^2)$ in the basic theoretical eq. (2) for rubber modulus at low strain ratio α. Therefore taking $(99 - 45)/250$ to be not significantly different from $11/50$ for present purposes we obtain for the stress upturn deviation from basic theory:

$$\Delta \ln F = (3/5)(r/nl)^2 + (11/50)(r/nl)^4 \tag{38}$$

Approximation errors in the above derivation of $(11/50)(r/nl)^4$ are unimportant, especially as in the following calculation it becomes an $(\alpha - 1)^6$ term whose coefficient is in practice calculated from experimental data.[9]

To express the increase of r with elongation in eq. (38) the strain measure r/nl may be taken roughly proportional to $\alpha - 1$ for strains that are high enough to give appreciable $\Delta \ln F$. Then if K is the constant of proportionality, the principal non-Gaussian term will vary with elongation according to the relation:

$$(r/nl)^2 \approx \kappa^2(\alpha - 1)^2$$

where $1/\kappa$ measures the limiting elongation of the network. By introducing a new hypothesis that there is strain hardening in proportion to the square of the elongation we can now account for the fourth power dependence of log F on elongation which Blanchard and Parkinson[19] discovered with prestressed rubbers. Thus, taking $1/\kappa_0$ to represent the extensibility which the network would have if not subject to strain hardening:

$$\kappa/\kappa_0 = 1 + h[(1/M_c) + \sigma](\alpha - 1)^2 \tag{39}$$

Here $[(1/M_c) + \sigma]$ is the measure of crosslinking and entanglement, and h is a coefficient of strain hardening due to the chains being part of a stretched network that is not uniform. The factor $[(1/M_c) + \sigma]$ is introduced on empirical grounds (Part II) and because there can be no strain hardening due to short chains and network steric hindrances if there are no fix points to form the network.

On combining the above relationships we have:

$$(r/nl)^2 \approx \kappa_0^2(\alpha - 1)^2 + 2h\kappa_0^2[(1/M_c) + \sigma](\alpha - 1)^4 + h^2\kappa_0^2[(1/M_c) + \sigma]^2(\alpha - 1)^6 \quad (40)$$

In the kinetic statistical theory of polymer molecules their potential extensibility is proportional to the square root of the chain length. Hence with a new concept of mean square extensibility ϵ per unit molecular weight as a measure of intrinsic extensibility or polymer flexibility we have for the mean square extensibility $1/\kappa_0^2$ of the network chains:

$$1/\kappa_0^2 = \epsilon/[(1/M_c) + \sigma] \quad (41)$$

On combining eqs. (38) and (40) with the above expression for κ_0^2 we have for the principal non-Gaussian contribution to the logarithm of the stress

$$\frac{3}{5}\left(\frac{r}{nl}\right)^2 \approx \frac{3}{5}\left(\frac{1}{\epsilon}\right)\left(\frac{1}{M_c} + \sigma\right)(\alpha - 1)^2 + \frac{6}{5}\left(\frac{h}{\epsilon}\right)\left(\frac{1}{M_c} + \sigma\right)^2(\alpha - 1)^4 + \frac{3}{5}\left(\frac{h^2}{\epsilon}\right)\left(\frac{1}{M_c} + \sigma\right)^3(\alpha - 1)^6 \quad (42)$$

With allowance for strain hardening and on neglecting the eighth and higher powers of $\alpha - 1$, the next non-Gaussian term in eq. (38) can be resolved similarly into powers of $(\alpha - 1)^4$ and $(\alpha - 1)^6$ as follows:

$$\frac{11}{50}\left(\frac{r}{nl}\right)^4 \approx \frac{11}{50}\left(\frac{1}{\epsilon^2}\right)\left(\frac{1}{M_c} + \sigma\right)^2(\alpha - 1)^4 + \frac{9}{10}\left(\frac{h}{\epsilon^2}\right) \times \left(\frac{1}{M_c} + \sigma\right)^3(\alpha - 1)^6 \quad (43)$$

Here the coefficient 9/10 is a physically adequate approximation which does not differ significantly from the result 44/50 of a strictly mathematical analysis. By substituting in eq. (38) we have for the non-Gaussian contribution to $\ln F$:

$$\Delta \ln F \approx \frac{3}{5}\left(\frac{1}{\epsilon}\right)\left(\frac{1}{M_c} + \sigma\right)(\alpha - 1)^2 + \left[\frac{6}{5}\left(\frac{h}{\epsilon}\right) + \frac{11}{50}\left(\frac{1}{\epsilon^2}\right)\right]\left(\frac{1}{M_c} + \sigma\right)^2 \times (\alpha - 1)^4 + \left[\frac{3}{5}\left(\frac{h^2}{\epsilon}\right) + \frac{9}{10}\left(\frac{h}{\epsilon^2}\right)\right]\left(\frac{1}{M_c} + \sigma\right)^3(\alpha - 1)^6 \quad (44)$$

Comparing this with eq. (29) and adding $\omega[(1/M_c) + \sigma]$ to represent a residual non-Gaussian contribution and effective hard fraction in unstretched rubber yields:

$$-\ln\left[1 - \Omega\left(\frac{1}{M_c} + \sigma\right)\right] = \omega\left(\frac{1}{M_c} + \sigma\right) + \frac{3}{5}\left(\frac{1}{\epsilon}\right)\left(\frac{1}{M_c} + \sigma\right)(\alpha - 1)^2 + \left[\frac{6}{5}\left(\frac{h}{\epsilon}\right) + \frac{11}{50}\left(\frac{1}{\epsilon^2}\right)\right]\left(\frac{1}{M_c} + \sigma\right)^2(\alpha - 1)^4 + \left[\frac{3}{5}\left(\frac{h^2}{\epsilon}\right) + \frac{9}{10}\left(\frac{h}{\epsilon^2}\right)\right]\left(\frac{1}{M_c} + \sigma\right)^3(\alpha - 1)^6 \quad (45)$$

With unswollen rubbers, $h > 0$ so that $\omega(1/M_c + \sigma)$ and the term in $(\alpha - 1)^2$ are relatively negligible; the final term in $(\alpha - 1)^6$ is also essential only for appreciable values of $[3/5(h^2/\epsilon) + 9/10(h/\epsilon^2)][(1/M_c) + \sigma]^3$ together with high values of $(\alpha - 1)^6$ at the ultimate (steepest) part of the stress–strain curve. Hence there is approximate fourth-power dependence of log F on $(\alpha - 1)$ over a wide range of elongations, as discovered by Blanchard and Parkinson.[19,22]

Equations for Hard Fraction C_h from Equilibrium Swelling

We define x = volume of rubbery polymer, b = volume of filler and interface hard polymer, S = imbibed solvent volume at equilibrium, C_h = total hard fraction. Then

$$\begin{aligned} v_r &= x/(x + S) \\ &= x/(x + b + S - b) \\ v_c &= (x + b)/(x + b + S) \\ 1/v_c &= 1 + [S/(x + b)] \end{aligned}$$

Taking the result $1/v_c = 1 + [S/(x + b)]$ and the reciprocal of v_r:

$$\frac{1}{v_r} = \frac{1 + [S/(x + b)] - [b/(x + b)]}{[x/(x + b)]} = \frac{(1/v_c) - [b/(x + b)]}{[x/(x - b)]}$$

But $b/(x + b) = C_h$ and $x/(x + b) = 1 - C_h$

Therefore

$$\begin{aligned} 1/v_r &= [(1/v_c) - C_h]/(1 - C_h) \\ C_h &= [(1 - v_r)/v_c]/(1 - v_r) \end{aligned} \quad (46)$$

For negligible linkage reinforcement the measure v_r of swelling can be replaced by the gum matrix value v_{ro}. This avoids spurious v_r values due to vacuoles with noncarbon fillers, and it is equally suitable for Graphon carbon. In these cases:

$$C_h = [1 - (v_{ro}/v_c)]/(1 - v_{ro}) \quad (47)$$

This gives near perfect results for Graphon when substituted in eq. (27) (see Table V of Part II[9]). For HAF black it yields only apparent values C_h^1 since the above derivation makes no allowance for linkage reinforcement $\phi > 1$.

Relation between Equilibrium Swelling and Swollen Modulus

If it is assumed that trapped entanglements are the same at equilibrium for modulus and swelling, eq. (11) may be modified for swollen networks that contain filler particles. On the right of eq. (11) the modulus measure $\rho RT/G$ of mesh weight must be replaced for filled rubbers by $(1 - C)(1 + 3.4C_h)\rho RT/G$, with $\Omega/(1 - C_h)$ replacing Ω in accordance with eq. (13a). The small ω correction of $F(v_r)$ in eq. (11) may be retained because the increase from ω to Λ_r with carbon particle reinforcement may be neglected with sufficient accuracy for many purposes. Moreover swollen vacuoles do not invalidate the swelling function $F(v_r)$ for carbon reinforcement so that we can make the approximate equation:

$$F(v_r) \approx \frac{\Omega}{1 - C_h} - \omega + \frac{(1 - C)\rho RT}{G}(1 + 3.4C_h) \tag{48}$$

For the general case of swollen networks, including those with inert fillers that form vacuoles, $F(v_r)$ is replaced by $(1 + C_h)(1 - C_h)^{-1}F(v_c)$ in accordance with eq. (28). Then the term ω allowing for a solvent-resistant fraction is unnecessary because hardened rubber at the filler surface is taken into account in the total hard fraction C_h. Therefore on multiplying through by $(1 - C_h)/(1 + C_h)$ and binomial expansion of $(1 + C_h)^{-1}$ we have a more accurate equation than eq. (48):

$$F(v_c) = [\Omega/(1 + C_h)] + [(1 - C)\rho RT/G](1 + 1.4C_h) \tag{49}$$

Swollen modulus G may be calculated from eq. (2) or the logarithmic eq. (32), provided the strain is not too small or large. Equation (49) should be applicable generally to swollen networks that may contain hard inclusions, irrespective of their degree of bonding to the rubber.† Thus C_h should always be obtainable from swollen moduli G by linear slopes $(1 + 1.4C_h)$ relating $F(v_c)$ and $(1 - C)\rho RT/G$. Then for substantial linkage reinforcement $\phi > 1$ when eq. 47 is inapplicable, e.g., for normal carbon blacks, it is not necessary to rely on putting $C_h \approx 1.15C$. The latter approximation is established for swelling in a good solvent.

By further refinements (Polymer Letters[26]) the elastic reaction to swelling includes a hydrodynamic factor $1 + 2.5\theta_\phi$ to allow for effective wetting C_ϕ of filler particles if there is actual (intrinsic) linkage reinforcement $\phi_o > 1$ to enmesh the interface rubber. In this new approach, c.f. that of Porter[26] and others[27,28], $\phi_o = \phi_o(1 + 2.5\theta_\phi)$ and:

$$C_\phi = C \ln \phi_o = \frac{C \ln \phi}{1 + 2.5C} \tag{51}$$

† Note: Part II shows that eqs. (27)–(28) need a small empirical correction so that $0.97\,F(v_c)$ should replace $F(v_c)$. Accordingly, eq. (49) has the final corrected form:

$$0.97\,F(v_c) = [\Omega/(1 + C_h)] + [(1 - C)\rho RT/G](1 + 1.4C_h) \tag{50}$$

Therefore ϕ_o can be estimated from ϕ; and taking $\phi = F_o(v_r)/F(v_r)$ the functions $F(v_r)$ and $F(v_c)$ in equations 48–50 should strictly be corrected by $(1 + 2.5C_\phi)$.

References

1. P. J. Flory and J. Rehner, *J. Chem. Phys.*, **11**, 521 (1943).
2. P. J. Flory, *J. Chem. Phys.*, **18**, 108 (1950).
3. G. Gee, *Trans. Faraday Soc.*, **42**, 585 (1946).
4. S. M. Gumbrell, L. Mullins, and R. S. Rivlin, *Trans. Faraday Soc.*, **49**, 1945 (1953).
5. C. G. Moore and W. F. Watson, *J. Polym. Sci.*, **19**, 237 (1956).
6. L. Mullins, *J. Polym. Sci.*, **19**, 225 (1956).
7. A. F. Blanchard and P. M. Wootton, *J. Polym. Sci.*, **34**, 627 (1959).
8. L. Mullins, *J. Appl. Polym. Sci.*, **2**, 1 (1959).
9. A. F. Blanchard, *J. Polym. Sci. A-1*, this issue.
10. A. F. Blanchard, forthcoming paper, in preparation.
11. P. J. Flory, *Ind. Eng. Chem.*, **38**, 417 (1946).
12. H. M. Smallwood, *J. Appl. Phys.*, **15**, 758 (1944).
13. E. Guth and O. Gold, *Phys. Rev.*, **53**, 322 (1938).
14. L. Mullins and N. R. Tobin, *Proc. 3rd Rubber Tech. Conf.*, **1954**, 397.
15. G. Kraus, *J. Appl. Polym. Sci.*, **7**, 861 (1963).
16. G. Kraus, *Rubber World*, **136**, 67, 254 (1956).
17. B. B. Boonstra, *J. Appl. Polym. Sci.*, **11**, 389 (1967).
18. L. Mullins, *J. Rubber Res.*, **16**, 275 (1947); *J. Phys. Colloid Chem.*, **54**, 239 (1950).
19. A. F. Blanchard and D. Parkinson, *Ind. Eng. Chem.*, **44**, 799 (1952).
20. M. Mooney, *J. Appl. Phys.*, **11**, 582 (1940).
21. R. S. Rivlin and D. W. Saunders, *Phil. Trans. Roy. Soc.* (London), **A243**, 251 (1951).
22. A. F. Blanchard, *Trans. Inst. Rubber Ind.*, **32**, 124 (1956); *J. Polym. Sci.*, **14**, 355 (1954).
23. A. F. Blanchard, in *Applied Science of Rubber*, W. J. S. Naunton, Ed., Edward Arnold, London, 1961, p. 434.
24. G. Gee, *Polymer*, **7**, 373 (1966).
25. L. R. G. Treloar, *Physics of Rubber Elasticity*, Oxford Univ. (Clarendon) Press, 1949, p. 93.
26. A. F. Blanchard, Polymer Letters, in press.
27. M. Porter, *Rubber Chem. Technol.*, **40**, 866 (1867).
28. J. W. Sellers, M. P. Wagner, B. J. DeWitt, C. O. Stueber, and J. K. Bachmann, *J. Appl. Polym. Sci.*, **5**, 397 (1961).
29. O. Lorenz and C. R. Parks, *J. Polym. Sci.*, **50**, 299 (1961).

Received May 28, 1968

JOURNAL OF POLYMER SCIENCE: PART A-1 VOL. 8, 835–859 (1970)

Crosslinking, Filler, or Transition Constraint of Polymer Networks. II

A. F. BLANCHARD, *Dunlop Research Centre, Birmingham, England*

Synopsis

The theory of Part I is developed by application to filler reinforcement of NR and SBR. For unswollen but prestretched networks it quantifies entire stress–strain curves and applies new concepts of extensibility and strain hardening. Constraint of swelling is expressed by a constant ϕ, termed linkage reinforcement, and by an effective hard fraction C_h per cubic centimeter of compound. For rubber–filler swelling v_e the modified Flory functions $F(v_e)$ in part 1 need 3% correction. Then, relative to gum fix points $1/F_0(v_r)$:

$$\frac{1}{[M_e]} = \frac{\phi}{F_0(v_r)} = \frac{1 - C_h}{1 + C_h} \frac{1.03}{F(v_e)}$$

where $C_h \leqslant 1.15C$ for filler concentrations C per cubic centimeter of compound. The effective C_h comprises the volume fraction C^* of bonded particles and 5–10 Å of surface-bound rubber that has been stretched hard by swelling. When needed, the actual crosslink density and intrinsic linkage reinforcement ϕ_0 can be obtained by dividing by $(1 + 2.5C_\phi)$ where $C_\phi = (C \ln \phi)/(1 + 2.5C)$. The case $C_h \leqslant 1.15C$ with Graphon or inert fillers is identified and assessed by equations:

$$C_h = \frac{1 - (v_{r0}/v_c)}{1 - v_{r0}} \qquad 0.97\phi \frac{1 + C_h}{1 - C_h} = \frac{F_0(v_r)}{F(v_c)}$$

Results $C_h > 1.15C$ are invalid, but then $C_h \approx 1.15C^* \approx 1.15C$, e.g., for carbon blacks. Even Graphon is distinguished from inert fillers at low concentrations C by substantial constraint reinforcement $F_0(v_r)/F(v_c) > 1$. For prestressed dry rubber a modulus G, network extensibility $\alpha_b - 1$, and upturn coefficient μ_h express the whole curve; G and μ_h show identical constraint strength distributions. Network extensibility $\alpha_b - 1$ is the microbreaking strain (prestretch); for pure elastomer it is elongation at break. The relation of stress F to extension ratio α is:

$$\ln \frac{F}{\alpha - (1/\alpha)^2} - \frac{C_2^*}{\alpha} - j(\alpha_b - 1)^{1/2} \left(\frac{\alpha - 1}{\alpha_b - 1}\right)^6 = \ln G + \mu_h(\alpha - 1)^4$$

where $C_2^* = 0.7$ and $j = 0.4$ from NR/MPC data. Strain-hardening coefficients h are obtained from μ_h by the theory given in Part I. Hard modulus components $G_h = 0.7 \ln (h/h_0)$ vanish as $h \to h_0$ (gum) = 110. After high prestresses the residual $\ln(h^*/h_0)$ due to strong carbon–rubber linkages implies $G_h^* = 0.42$ kg/cm², i.e., ca. 10% of the normal cure crosslinks.

INTRODUCTION

For polymers swollen in solvent the Flory-Rehner equation was represented in Part I by $F(v_r)$ for network volume fraction v_r at equilibrium

swelling;[1] and with $[M_c]_s$ denoting the effective mesh weight from swelling measurements v_r. Therefore, with Flory's refinement for tetrafunctional crosslinks:[2]

$$[M_c]_s = \frac{-\rho v_1(v_r^{1/3} - v_r/2)}{\mu v_r^2 + \ln(1 - v_r) + v_r} = F(v_r) \tag{1}$$

Here $1/[M_c]_s$ measures the effective number of crosslinks (fix points), including entanglements σ, V_1 is the molar volume of the solvent, ρ is the polymer density, and μ is the interaction constant between polymer and solvent. According to the theory (Part I),[1] filler particles form an effective hard fraction C_h per cubic centimeter of compound; the volume fraction v_c of compound at equilibrium swelling is proposed as a general index of swelling, the rubber fraction v_r by mass-increment being unsuitable for fillers that form vacuoles.[1] On this new theory we have for $1/[M_c]_s$ fix points having ratio φ to gum values $1/F_0(v_r)$:

$$\frac{1}{[M_c]_s} = \frac{\phi}{F_0(v_r)} = \frac{1 - C_h}{1 + C_h}\frac{1}{F(v_c)} \tag{2}$$

Linkage reinforcement ϕ by a carbon volume fraction C does not vary with sulfur crosslinking of SBR. It has been suggested in Part I[1] that ϕ can be calculated from $F_0(v_r)/F(v_r)$ data by taking $b \approx 3 \times 10^3$ and $C^* \approx C$ in the following equation for networks with a bonded carbon fraction C^*:

$$\phi = \frac{F_0(v_r)}{F(v_r)} - \frac{bC^*[(1/v_r^{1/3}) - 1]^2}{F(v_r)} \tag{3}$$

In the present paper $b \approx 3 \times 10^3$ is tentatively established together with ϕ estimates for Graphon and HAF carbon black in SBR. Vacuoles invalidate ϕ from $F_0(v_r)/F(v_r)$ for inert fillers, but then, or for Graphon with negligible $\phi \approx 1$, we have from Part I:[1]

$$C_h = \frac{1 - (v_{r_0}/v_c)}{1 - v_{r_0}} \tag{4a}$$

$$\phi\left(\frac{1 + C_h}{1 - C_h}\right) = \frac{F_0(v_r)}{F(v_c)} \tag{4b}$$

The results of applying these equations are given in the present paper. The effective C_h includes rubber stretched hard on Graphon by swelling or trapped inside hard aggregates. Only eq. (4b) fits normal carbon blacks because these give appreciable linkage reinforcement $\phi > 1$.

For filler fractions $C \gg 0$ cm^{-3} and low strains $\alpha = 1.5$–2.0 below prestretch the modulus G was given a new basic definition:[1]

$$\ln \frac{Fv_r^{1/3}}{\alpha - (1/\alpha^2)} - \frac{C_2^*(v_r)^{4/3}}{\alpha} = \ln G \tag{5}$$

Here $C_2^* \approx 0.7$ corresponds to Mooney-Rivlin C_2;[3,4] the effective crosslinking $1/[M_c] = (\rho RT)^{-1}G$ by $1/M_c + \sigma$ fix points is equal to $(1 - C)[(1/M_c) + \sigma]$ for unswollen prestretched rubber ($v_r = 1$). For the stress upturn at higher strains, in Part I we introduced an hypothesis of strain-hardening, in contrast to prestretch softening (Mullins effect[5]). Nonlinear effects of crosslinks were expressed by a fractional stress-upturn $\Omega(1/M_c + \sigma)$, effective mesh weight $(1/M_c + \sigma)^{-1} - \Omega$, and hard fraction $\Omega[(1/M_c) + \sigma]$. They augment the logarithm of the above basic modulus G by $\Delta \ln F = -\ln[1 - \Omega\,[(1/M)_c + \sigma]]$; with μ_h characterizing strain-hardening up to the prestretch ($\alpha_b - 1$) we have from Part I:[1]

$$-\ln\left\{1 - \Omega\,[(1/M)_c + \sigma]\right\} = \mu_h(\alpha - 1)^4 + J\left(\frac{\alpha - 1}{\alpha_b - 1}\right)^6 \qquad (6)$$

On this theory the hard phase is augmented by filler and grows with increasing strain up to the pre-stretch. The present paper will determine μ_h and J from experimental data on MPC black in NR over a range of prestretches. For this purpose, on combining eqs. (5) and (6) we have a general equation for elongations up to the prestretch:

$$\ln \frac{F}{\alpha - (1/\alpha^2)} - \frac{C_2^*}{\alpha} - J\left(\frac{\alpha - 1}{\alpha_b - 1}\right)^6 = \ln G + \mu_h(\alpha - 1)^4 \qquad (7)$$

On wholly empirical grounds a much earlier paper of Blanchard and Parkinson[6] used the fourth power of $(\alpha - 1)$ to express the stress upturn of reinforced networks. From the new theory in Part I the empirical extension factor or upturn coefficient μ of earlier analyses[6,7] is given the theoretical value:

$$\mu_h = (1/\rho RT)^2\left[\frac{6}{5}\left(\frac{h}{\epsilon}\right) + \frac{11}{50}\left(\frac{1}{\epsilon^2}\right)\right]G^2 \qquad (8)$$

where h is a coefficient of strain hardening and ϵ is the mean square extensibility per unit molecular weight of chain, i.e., it measures the intrinsic flexibility and extensibility of the polymer molecules ($\epsilon = 5.6 \times 10^{-3}$ for NR). The sixth power term is added because stress upturn occurs at low elongations of reinforced networks, and then $\mu_h(\alpha - 1)^4$ is not adequate alone to represent the curves at their steepest as they approach the pre-stress.

EXPERIMENTAL

For gum and reinforced LTP vulcanizates the crosslinking and respective swelling functions $F_0(v_r)$ and $F(v_r)$ were varied widely by varying the sulfur and accelerator contents (Table I).

The compounds were all cured for 40 min at 148°C, with 15 min rise, and for each curative level the filler reinforcement was varied as shown in Table II.

TABLE I

	Parts			
Sulfur	1.0	1.75	2.0	2.5
Santocure	1.0	1.0	1.5	2.0

TABLE II

Filler, phr		
HAF carbon	Graphon (partially graphitized Spheron 6)	Calcium silicate
0	0	0
15	15	15
30	30	30
50	50	50
65	65	65

TABLE III

	Parts
LTP 1500	100.0
Zinc oxide	3.0
Stearic acid	1.0
Santoflex IP	0.75
Santoflex AW	0.75
Prime filler	0–65
Santocure	1–2.0
Sulfur	1–2.5

The compounds were first mill-mixed without the curatives, and then subdivided into four to add the four different curative combinations. The initial temperature of the mill rolls was 60 ± 5°C and the completed mixes had the general formula given in Table III.

Equilibrium swelling of the vulcanizates in solvent (toluene) was determined by measurements comprising the initial weight, the swollen weight, and the weight after drying out the solvent. Allowance was made for the filler volume and the small volume of sulfur and zinc oxide in the vulcanizate, it being assumed that the remaining ingredients were extracted by the solvent. This procedure is sufficiently accurate for all practical purposes.

For unswollen networks of reinforced rubber the stress–strain data of Blanchard and Parkinson are taken from Table I of an earlier publication,[6] and reanalyzed in accordance with the theory now proposed. Hence the MPC black composition and experimental procedure are as described by Blanchard and Parkinson, the key features being as follows.

Ring-shaped testpieces were used, and the experiments we carried out on a Goodbrand tensile testing machine. The rate of extension was 20 in./min, and the tests were carried out in a controlled atmosphere at 70 ± 2°F and 65% humidity; twelve different prestresses were used, namely, 30, 40,

50, 60, 70, 80, 100, 120, 140, 160, 180, and 200 kg/cm^2. There were two testpieces for each prestress, the prestress being worked out on the original cross section. Much of the set is incomplete elastic recovery and disappears on heating. Since only a small part of the observed set represents a true change in dimensions it was not taken into account. Four successive stress–strain curves were drawn on the machine, the ultimate stress in each case being equal to the ultimate stress during the first extension, i.e., the first prestress. The specimens were held at the prestress for 30 sec, and then the stress was released. In each case approximately 1 min elapsed between successive extensions although the time was not precisely controlled.

The 30-kg prestress is excluded from the present analysis because particle contacts contribute additional stiffening at less than 40 kg/cm^2. [7,8]

RESULTS AND DISCUSSION

Constraint of Swelling and Crosslink Reinforcement By Filler Particles

For individual cures of SBR vulcanizates the approximate linkage reinforcement $\phi \approx F_0(v_r)/F(v_r)$ by HAF carbon and Graphon are given in Table IV, together with more accurate results from eq. (3). Equation (3) was used for $b = 3 \times 10^3$ and with the approximation $C^* \approx C$ because even graphitized carbon forms enough strong bonds to prevent formation of swollen vacuoles. For HAF black the results $\phi \gg 1$ are interpreted as high linkage reinforcement rather than unlikely special effects of HAF carbon on solvent interaction μ, or abnormal interface hardening by swelling, though further experiments may be needed with varied solvents to eliminate fully the part of ϕ that is proportional to $[(1/v_r^{1/3}) - 1]$. The surface linkages probably include many of moderate strength which could be eliminated from the comparison by a high prestress or solvent temperature. The tentative choice $b = 3 \times 10^3$ to allow for interfacial hardening was made to satisfy the following requirements: (*1*) a reasonable assumption that Graphon gives negligible linkage reinforcement $\phi \approx 1$; (*2*) negligible ϕ variation with cure and filler concentration for negligible linkage reinforcement. (*3*) close agreement with the Graphon $\phi \approx 0.98$ obtained by eq. (4b) from $F_0(v_r)/F(v_c)$ data and C_h by eq. (4a).

Table IV shows that these requirements are satisfied. Slightly better agreement in Table VIII is obtained by eq. (10) which replaces $C^* \approx C$ by a more accurate approximation $C^* \approx 0.87C_h$ from later conclusions about carbon reinforcement. Therefore in calculations of ϕ from $F_0(v_r)/F(v_r)$ eq. (3) for vacuole-free carbon had the following alternative forms:

$$\phi = \frac{F_0(v_r)}{F(v_r)} - \frac{3C[(1/v_r^{1/3}) - 1]^2}{F(v_r) \times 10^{-3}} \tag{9}$$

$$\phi = \frac{F_0(v_r)}{F(v_r)} - \frac{2.6C_h[(1/v_r^{1/3}) - 1]^2}{F(v_r) \times 10^{-3}} \tag{10}$$

Development of the theory later allows replacement of these equations by a simpler and more accurate calculation of ϕ for carbon blacks.

As a generally valid measure of swelling by mass increment the calculated volume fraction v_c of compound at equilibrium is proposed to replace v_r. This mass increment v_c provides a common yardstick for inert and reinforcing fillers; for practical purposes it equals the true v_r where inert fillers form vacuoles (see Part I[1]). Assuming the filler does not inhibit vulcanization we then have $F_0(v_r)/F(v_c) \rightarrow 1$ in the limiting case of an inert filler. Hence the ratio $F_0(v_r)/F(v_c) > 1$ defines a new concept which is here

TABLE IV
Filler Linkage Reinforcement ϕ for Individual Cures and With Allowance for Interfacial Hardening by Swelling

Carbon black volume fraction C	Crosslinks without black $\times 10^4$	Approximate $\phi \approx F_0(v_r)/F(v_r)$ i.e., assuming no hardening		Accurate ϕ by eq. (9)		Accurate ϕ averaged for the range of cures[a]	
		HAF	Graphon	HAF	Graphon	HAF	Graphon
0.076	0.91	1.13	1.01	1.11	0.98		
	1.52	1.13	1.03	1.10	1.01	1.14	1.00
	1.88	1.19	1.05	1.16	1.02		
	2.34	1.21	1.03	1.18	0.99		
0.142	0.91	1.32	1.15	1.28	1.07		
	1.52	1.45	1.04	1.40	1.00	1.38	1.01
	1.88	1.52	1.05	1.46	1.00		
	2.34	1.47	1.04	1.42	0.99		
0.216	0.91	1.72	0.98	1.65	0.93		
	1.52	1.89	1.04	1.80	0.97	1.77	0.97
	1.88	1.90	1.07	1.82	1.00		
	2.34	1.89	1.07	1.80	0.99		
0.263	0.91	2.19	1.10	2.09	1.03		
	1.52	2.01	1.03	1.91	0.94	2.01	0.95
	1.88	2.15	1.02	2.04	0.93		
	2.34	2.13	1.02	2.02	0.92		

[a] Tables VIII and IX give final estimates of ϕ by more accurate methods which became possible for carbon blacks at a later stage in developing the theory.

termed constraint reinforcement. Experimental values of $F_0(v_r)/F(v_c)$ in Figure 1 show substantial constraint reinforcement, even by Graphon carbon, though Graphon is otherwise similar to inert fillers in giving negligible linkage reinforcement (Table IV). Therefore Graphon particles must form sufficient strong attachments to rubber to prevent it from pulling away to form swollen vacuoles, but not enough to increase the network crosslinking, as measured by equilibrium swelling.

In Figure 1 graphs of constraint reinforcement $F_0(v_r)/F(v_c)$ versus $[(1/v_r^{1/3}) - 1]^2/F(v_c)$ are drawn according to eq. (26) of Part I. The slope $bC^*/$

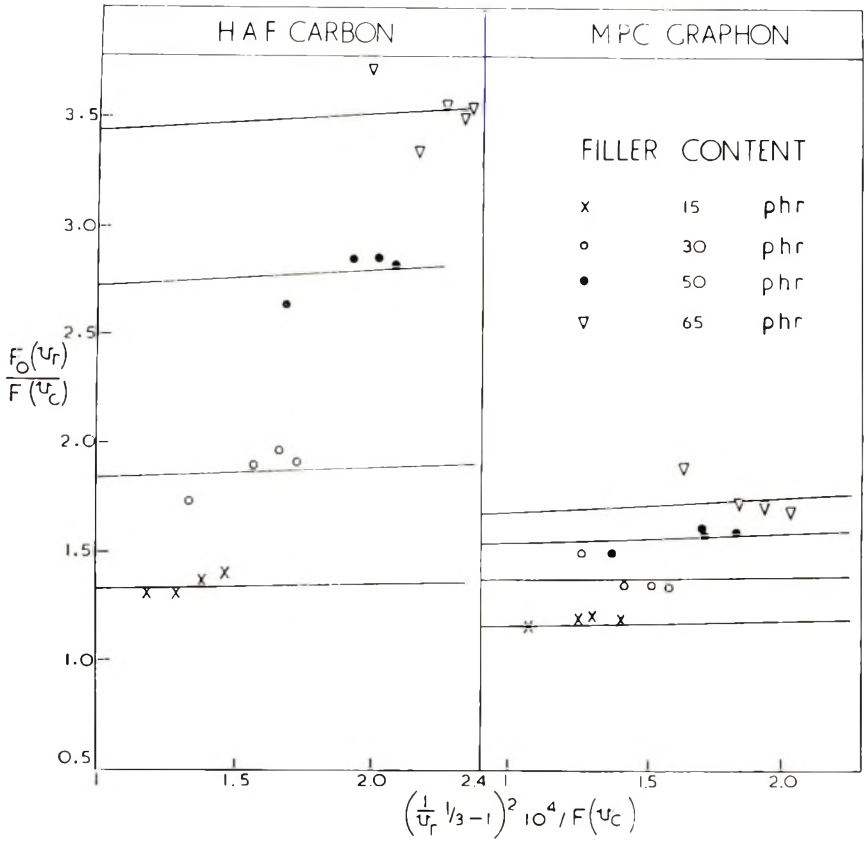

Fig. 1. Relation of $F_0(v_r)/F(v_c)$ to its hard interface component $bC[(1/v_r^{1/3}) - 1]^2/(1 - C)F(v_c)$ for carbon blacks in SBR. The ordinate intercept is the constraint constant defined by $0.97\ \phi\ (1 + C^*)/(1 - C^*)$ in eq. (13).

$(1 - C^*)$ allowing for interface hardening is a small correction in which the approximation $C^* \approx C$ is accurate enough for carbon blacks so that:

$$\frac{F_0(v_r)}{F(v_c)} = \phi \frac{1 + C^*}{1 - C^*} + \frac{b[(1/v_r^{1/3}) - 1]^2 C}{(1 - C)\,F(v_c)} \tag{11}$$

The lines drawn in Figure 1 are not accurately defined by the rather scattered points, but they have been drawn as in Figure 2 of Part I with a common slope parameter $b = 3000$ equal to that selected by the foregoing criteria (*1*)–(*3*). The corresponding intercepts $\varphi(1 + C^*)/(1 - C^*)$, here termed particle constraint constants, are obtained most conveniently for each individual cure by eq. (11) in the transposed form:

$$\phi \frac{1 + C^*}{1 - C^*} = \frac{F_0(v_r)}{F(v_c)} - \frac{3000[(1/v_r^{1/3}) - 1]^2 C}{(1 - C)\,F(v_c)} \tag{12}$$

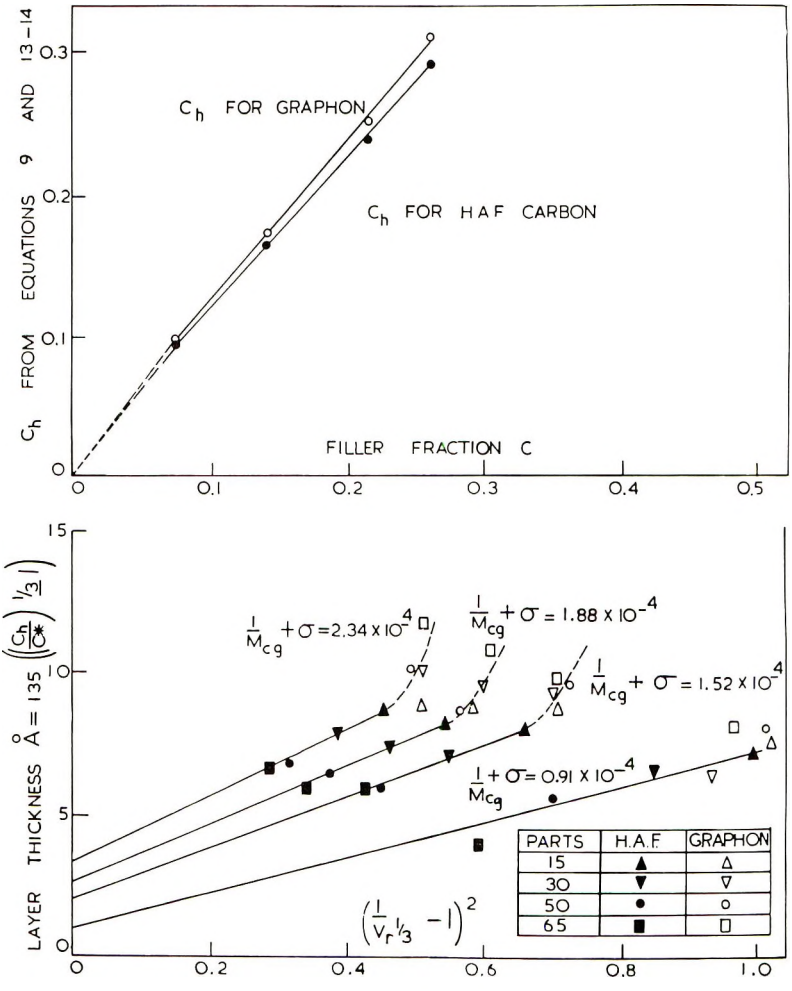

Fig. 2. Total hard fraction C_h and effective thickness of hard polymer interface when bonded SBR on a carbon volume fraction C is stretched hard by swelling.

The results for carbon blacks in Table V show that particle constraint constants vary little with cure, but increase as expected with carbon concentration C. The differing reinforcement levels may be expressed alternatively by a total hard fraction C_h that includes hardened (swollen) rubber at the filler surface. Then C_h absorbs the hard interface correction in a new binary index of reinforcement:

$$\phi \frac{1 + C_h}{1 - C_h} = \frac{F_0(v_r)}{F(v_r)} \tag{4b}$$

This constraint reinforcement provides a general measure of filler activity suitable for inert fillers as well as carbon blacks. Table V shows that it

discriminates most effectively between fillers at low concentrations where vacuoles cause fractional values for calcium silicate.

For bonded (carbon) particles Table IV, average estimates of the linkage reinforcement ϕ were used to calculate C_h and C^* from the data in Table V, i.e., from eqs. (4b) and (12). Though inaccuracies of these equations and ϕ will affect the absolute result, they cause little error in the relative magnitude C^*/C_h because both C^* and C_h are similarly affected. Therefore at the present stage of discussion only relative results C^*/C_h are considered

TABLE V
Constraint Reinforcement $F_0(v_r/F(v_c)$ and Particle Constraint Constant $\phi(1 + C^*)/(1 - C^*)$ for Fillers in SBR

Filler volume fraction C (silicate in parentheses)	Crosslinks without filler, $\times 10^4$	Constraint reinforcement $\approx \phi(1 + C_h)/(1 - C_h)$			Approximate [by eq. (12)] constraint constant[a] $\phi(1 + C^*)/(1 - C^*)$	
		HAF	Graphon	Calcium silicate	HAF	Graphon
0.076	0.91	1.30	1.15	0.65	1.27	1.13
(0.066)	1.52	1.29	1.18	0.76	1.26	1.15
	1.88	1.36	1.20	1.13	1.33	1.17
	2.34	1.38	1.18	0.95	1.34	1.15
0.142	0.91	1.72	1.50	0.99	1.66	1.44
(0.123)	1.52	1.88	1.35	1.06	1.80	1.28
	1.88	1.96	1.36	1.01	1.88	1.28
	2.34	1.90	1.34	1.11	1.81	1.26
0.216	0.91	2.64	1.50	1.63	2.50	1.39
(0.189)	1.52	2.84	1.57	1.44	2.68	1.43
	1.88	2.85	1.61	1.41	2.69	1.48
	2.34	2.82	1.60	1.48	2.65	1.45
0.263	0.91	3.72	1.87	1.74	3.50	1.70
(0.233)	1.52	3.37	1.73	1.72	3.14	1.53
	1.88	3.57	1.71	1.53	3.32	1.50
	2.34	3.50	1.69	1.46	3.24	1.47

[a] Constraint constants could be calculated by eq. (12) only for bonded (carbon) particles. Theoretical identification of the above quantities as $\phi(1 + C_h)/(1 - C_h)$ and $\phi(1 + C^*)/(1 - C^*)$ by eqs. (4b) and (12) is 3% too low, as will appear later.

suitable for inclusion in Table VI. They are well represented by a general estimate $C^*/C_h = 0.87$, the somewhat lower result 0.83 for Graphon being of doubtful significance because ϕ and C^* by eqs. (9) and (12) are less accurate at the lowest extreme of carbon activity (they are invalid for inert fillers). Since $C^* \approx C$, this general assessment is supported in Table VI by Graphon results $C/C_h = 0.88$ obtained later by a different method (Table VIII). It concerns swelling of reinforced number in a good solvent.

Theoretical identification of Table V data by eqs. (12) and (9) gives a general result $C^*/C \approx 0.90$ for carbon blacks. This is unacceptable because by definition $C^* \approx C$ for particles that do not form vacuoles. To correct

TABLE VI
Ratio of Bound Carbon Fraction $C^* \approx C$ to Total Hard Fraction C_h for Carbon Volume Fractions C in SBR

Carbon volume fraction C	Crosslinks without filler $\times 10^4$	C^*/C_h by eqs. (4b) and (12)		C/C_h by eq. (4a) for Graphon
		HAF	Graphon	
0.076	0.91	0.86	0.86	0.94
	1.52	0.85	0.84	0.82
	1.88	0.84	0.83	0.75
	2.34	0.82	0.83	0.81
0.142	0.91	0.87	0.87	0.67
	1.52	0.86	0.83	0.88
	1.88	0.86	0.82	0.86
	2.34	0.85	0.81	0.89
0.216	0.91	0.89	0.84	1.02
	1.52	0.88	0.81	0.92
	1.88	0.87	0.83	0.88
	2.34	0.86	0.80	0.89
0.263	0.91	0.92	0.85	0.85
	1.52	0.88	0.81	0.96
	1.88	0.88	0.79	0.97
	2.34	0.87	0.78	0.98
	Average	0.87[a]	0.83	0.88

[a] The average result 0.87 can be represented $C_h \approx 1.15C^* \approx 1.15C$ for good solvents.

this error, eq. (12) can be given a small adjustment of ca. 3% by an empirical factor 0.97 as follows:

$$0.97\phi \frac{1 + C^*}{1 - C^*} = \frac{F_0(v_r)}{F(v_c)} - \frac{3000[(1/v_r^{1/3}) - 1]^2 C}{(1 - C) F(v_c)} \tag{13}$$

Then eq. (4b) must be adjusted similarly because basically it is the same equation with the hard interface correction absorbed into a total hard fraction C_h. That eq. (4b) does need this adjustment is confirmed by trial combination with eq. (9) to match independent results $C_h \approx 1.15C$ from eq. (4a). Therefore:

$$0.97\ \phi \frac{1 + C_h}{1 - C_h} = \frac{F_0(v_r)}{F(v_c)} \tag{14}$$

Like the original eq. (4b), this experimental refinement applies to all fillers. With less active fillers than carbon black, C^* must replace C on the right of eq. (13) because interface hardening occurs only on bonded particles. In Table VII the C^* and C_h calculations from Tables IV and V show that eqs. (13) and (14) apply with satisfactory results consistent with $C^* = C$ and the independent discovery $C_h \approx 1.15C$ for swelling in good solvents.

Only carbon fillers allow use of eq. (9) to estimate ϕ in eqs. (13) and (14) and hence the above C^* and C_h. Therefore results of this method are

TABLE VII
Bonded Particle Fraction C^* and Total Hard Fraction C_h from Table V by Accurate Equations (13) and (14) and the Mean ϕ from Table IV

Crosslinks without filler $\times 10^4$	Carbon volume fraction C	Bonded particle fraction C^* from accurate eq. (13)		Total hard fraction C_h from accurate eq. (14)	
		HAF	Graphon	HAF	Graphon
0.91	0.076	0.069	0.076	0.080	0.085
1.52		0.065	0.085	0.077	0.097
1.88		0.092	0.093	0.103	0.106
2.34		0.095	0.085	0.110	0.097
0.91	0.142	0.107	0.190	0.124	0.209
1.52		0.147	0.132	0.168	0.159
1.88		0.168	0.132	0.188	0.162
2.34		0.149	0.125	0.173	0.155
0.91	0.216	0.185	0.192	0.211	0.229
1.52		0.219	0.206	0.246	0.250
1.88		0.220	0.222	0.248	0.262
2.34		0.213	0.213	0.243	0.259
0.91	0.263	0.284	0.297	0.312	0.339
1.52		0.233	0.248	0.267	0.305
1.88		0.260	0.238	0.293	0.299
2.38		0.248	0.229	0.284	0.294

limited to Graphon and HAF carbon in Table VI. However, vacuole-forming silicate is compared with Graphon in Table VIII by calculating ϕ and C_h in reverse order, the hard fraction C_h being obtained first from the equation:

$$C_h = \frac{1 - (v_{r_0}/v_c)}{1 - v_{r_0}} \tag{4a}$$

This simple relation was derived in Part I for negligible linkage reinforcement, $\phi \approx 1$. Taken together with eq. (14), the final revised form of eq. (4b), and the constraint reinforcement $F_0(v_r)/F(v_c)$, it gives near perfect results for Graphon in Table VIII. Notwithstanding vacuole formation at low silicate concentrations it also gives good results for the silicate filler.

Table VIII shows good agreement of average estimates of linkage reinforcement ϕ by the different methods for Graphon; and remarkably constant estimates $\phi = 1.01$ by combining eqs. (4a) and 14). Moreover, the data for calcium silicate are resolved into a consistently negligible linkage reinforcement $\phi \approx 1$ with a relatively small hard fraction C_h representing vacuoles at low filler concentrations. These results contrast with apparently fractional and varying linkage reinforcement obtained by methods in Table IX which take no account of vacuoles. One such method uses an equation valid for a firmly bonded hard phase:

$$\frac{1}{M_c} + \sigma = \frac{\phi}{F_0(v_r)} = 1.03\,\frac{(1 - 1.15C)}{(1 + 1.15C)}\,\frac{F_0(v_r)}{F(v_c)} \tag{15}$$

TABLE VIII

Hard Fraction C_h and Linkage Reinforcement ϕ from $C_h = [1 - (v_{r0}/v_c)]/(1 - v_{r0})$ and $\phi = 1.03[(1 - C_h)F_0(v_r)/(1 + C_h)F(v_c)]$ for Graphon and Calcium Silicate in SBR[a]

Crosslinks without filler $\times 10^4$	Filler volume fraction C		$C_h = [1 - (v_{r0}/v_c)]/(1 - v_{r0})$		$\phi = \frac{1.03\ (1 - C_h)F_0(v_r)}{(1 + C_h)F(v_c)}$		Graphon, ϕ by eq. (10)
	Carbon	Silicate	Graphon, $\phi \approx 1$ (true C_h)	Silicate, $\phi \approx 1$ (true C_h)	Graphon	Silicate	
0.91	0.076	0.066	0.081	−0.288	1.01	1.20	0.98
1.52			0.093	−0.071	1.01	1.11	1.01
1.88			0.102	+0.069	1.01	1.03	1.02
2.34			0.094	−0.034	1.01	1.04	0.99
0.91	0.142	0.123	0.212	−0.006	1.01	1.03	1.05
1.52			0.162	0.031	1.00	1.02	1.00
1.88			0.165	0.043	1.00	0.95	1.00
2.34			0.159	0.058	1.00	1.02	0.99
0.91	0.216	0.189	0.212	0.248	1.01	1.01	0.94
1.52			0.234	0.193	1.01	1.00	0.97
1.88			0.245	0.184	1.01	0.99	1.00
2.34			0.243	0.210	1.01	1.00	0.99
0.91	0.263	0.233	0.308	0.277	1.02	1.02	1.03
1.52			0.275	0.273	1.01	1.01	0.95
1.88			0.271	0.222	1.01	1.00	0.94
2.34			0.267	0.199	1.01	1.00	0.93

[a] The critical factor determining the final choice $b = 3000$ in eqs (9) and (10) was the need for consistent results with Graphon; and in Tables VII and VIII the different methods for obtaining ϕ do show good average agreement. That the accuracy of eq. (14) is very high is indicated by remarkably consistent ϕ values; they are less variable than those from eq. (9).

TABLE IX

Calculation of Linkage Reinforcement ϕ (Assuming No Vacuoles and Taking $C_h = 1.15C$) and Apparent Values ϕ^1 for Nonreinforcing Particles

Filler volume fraction C (silicate in parentheses)	Crosslinks without filler $\times 10^4$	$\phi = 1.03\left(\frac{1 - 1.15C}{1 + 1.15C}\right)\frac{F_0(v_r)}{F(v_c)}$		Calcium Silicate		
					Apparent results	
		HAF	Graphon	$\frac{F_0(v_r)}{F(v_c)}$	$\frac{F_0(v_r)}{F(v_r)}$	$\phi^1 = \frac{1.03(1 - 1.15C)F_0(v_r)}{(1 + 1.15C)F(v_c)}$
0.076	0.91	1.12	0.99	0.65	0.58	0.58
(0.066)	1.52	1.11	1.02	0.76	0.68	0.67
	1.88	1.18	1.04	1.13	1.00	1.00
	2.34	1.19	1.02	0.95	0.84	0.84
0.142	0.91	1.27	1.11	0.99	0.79	0.77
(0.123)	1.52	1.39	1.00	1.06	0.84	0.82
	1.88	1.45	1.01	1.01	0.86	0.78
	2.34	1.41	0.99	1.11	0.89	0.86
0.216	0.91	1.64	0.93	1.63	1.14	1.08
(0.189)	1.52	1.76	0.97	1.44	1.01	0.95
	1.88	1.77	1.00	1.41	0.99	0.93
	2.34	1.75	0.99	1.48	1.04	0.98
0.263	0.91	2.04	1.03	1.74	1.10	1.03
(0.233)	1.52	1.86	0.96	1.72	1.10	1.02
	1.88	1.97	0.95	1.53	0.98	0.91
	2.34	1.93	0.93	1.45	0.93	0.87

where C is the nominal volume fraction of hard material. This formula restates eq. 14 with the factor 1.03 inversely equivalent for all practical purposes to the empirical correction 0.97; and with $C_h \simeq 1.15C$ from the foregoing calculations on the vacuole-free carbons. The criterion for taking $C_h = 1.15C$ as invalid results, $C_h > 1.15C$, from eq. (4a), e.g., due to linkage reinforcement $\phi > 1$ by normal carbon blacks (see C_h^1 in Fig. 3). Table IX shows that the resulting eq. (15) is accurate enough for carbon blacks, but gives anomalous results with low concentrations of calcium silicate.

On bonded particles the rubber fraction $C_h - C^*$ made hard (inextensible) by swelling is $\Delta C^*[(1/M_{cg}) + \sigma]$ in eq. (18) of Part I so that:

$$\Lambda_r = \omega/\phi + (C_h - C^*)/\phi\,[(1/M_{cg}) + \sigma]$$

where

$$\phi\,[(1/M_{cg}) + \sigma] = \{[\omega + F_0(v_r)]/[\Lambda_r + F(v_r)]\}\,[\omega + F_0(v_r)]^{-1}$$

Here $\phi F(v_r) \approx F_0(v_r)$ is accurate enough in a small correction, and $\Lambda_r(C_h - C^*)$ is negligible compared to $(C_h - C^*)F(v_r)$. On substituting for Λ_r in eq. (16a) of Part I and with C approximating for C^* in eq. (3):

$$\frac{F_0(v_r)}{F(v_r)} = \phi + \phi\,(C_h - C^*) \tag{16}$$

and

$$C_h = C^* + \frac{b[(1/v_r^{1/3}) - 1]^2 C}{F_0(v_r)} \tag{17}$$

For HAF black and Graphon the values of C_h from eqs. (9) and (14) are plotted in Figure 2, and those for Graphon and calcium silicate by eq. (4a) are plotted in Figure 3.

The highly stretched fraction $C_h - C^*$ grows with the swelling index $[(1/v_r^{1/3}) - 1]^2$ and the crosslinking $[(1/M_{cg}) + \sigma) \approx 1/F_0(v_r)$ of the gum matrix. This inextensible coating effectively multiplies the particle radius by $(C_h/C^*)^{1/3}$. For a typical gum with $1/M_c + \sigma = 1.52 \times 10^{-4}$ and HAF or Graphon particles of diameter 270 Å, the layer thickness in Figure 2 is 5–10 Å for concentrations of 15–65 phr. Since linkage reinforcement reduces swelling the layer thickness decreases with black concentration. With the sparsely-bonded Graphon, which permits a high stretch by swelling, the dotted lines suggest that there may be some upturn deviation at low concentrations from linear dependence on $[(1/v_r^{1/3}) - 1]^2$. However, this feature is of doubtful significance, because Graphon is a borderline case for which the C_h/C^* based on eq. (13) is probably inaccurate, as indicated by the Graphon C/C_h in Table VI. With dynamic mechanical strain rather than swelling the hard layer may be thicker due to hindered bond rotation and transient chain interlocking in the region of hard particles. Smit[9] has

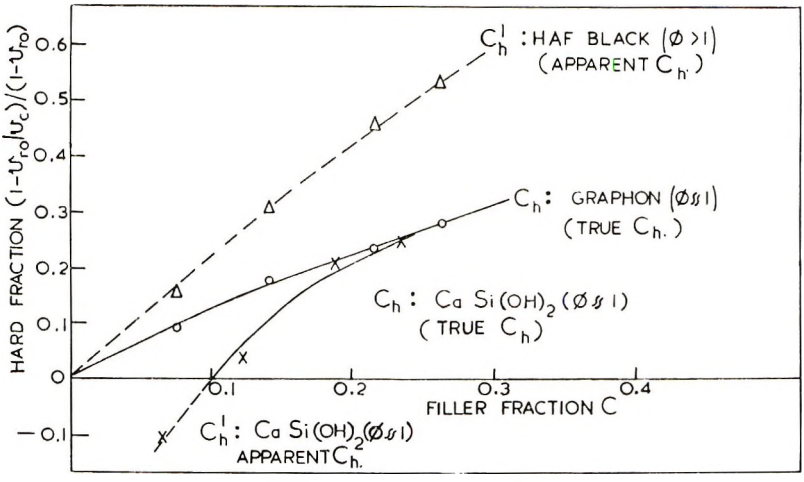

Fig. 3. Hard fraction $C_h = [1 - (v_{r0}/v_c)]/(1 - v_{r0})$ for negligible linkage reinforcement by Graphon and calcium silicate ($\phi \simeq 1$); and apparent values C_h^1 for HAF carbon ($\phi \gg 1$).

inferred at least 20 Å of glassy polymer to explain the variation of dynamic modulus with concentration and specific surface.

Stress Upturn and Strain Hardening of Unswollen Polymers

To illustrate stress–strain curves of prestressed rubber, Figure 4 shows some of the data obtained as described above. Equation (7) was set up partly on a hypothesis that the network extensibility is closely related to the prestretch $\alpha_b - 1$. This hypothesis is justified by the steepness of the stress–strain curve at just below the prestretch. The limit $\alpha_b - 1$ can be exceeded in practice only because the reinforced network changes through breakdown of some of the constraints. These considerations suggest that it is reasonable to investigate the proposed sixth power refinement by a trial function:

$$J = j(\alpha_b - 1)^i \tag{18}$$

where $\alpha_b - 1$ is the prestretch or network-breaking elongation and j and i have fixed numerical values. Then eq. (7) becomes:

$$\ln \frac{F}{[\alpha - (1/\alpha^2)]} - \frac{C_2^*}{\alpha} - j(\alpha_b - 1)^i \left(\frac{\alpha - 1}{\alpha_b - 1}\right)^6 = \ln G + \mu_h(\alpha - 1)^4 \tag{19}$$

Here C_2^* corresponds roughly to the Mooney-Rivlin C_2;[3,4] the modulus $(f/A)/[\alpha - (1/\alpha^2)]$ of basic theory has been replaced by a true constant G that is roughly equivalent numerically at low strains. Extrapolation of Eq. (19) can give this new modulus G after trials have fixed the C_2^*, j and i needed to express all the data by linear graphs. Hence the new theory characterizes stress–strain behavior by a modulus intercept ln G and slope

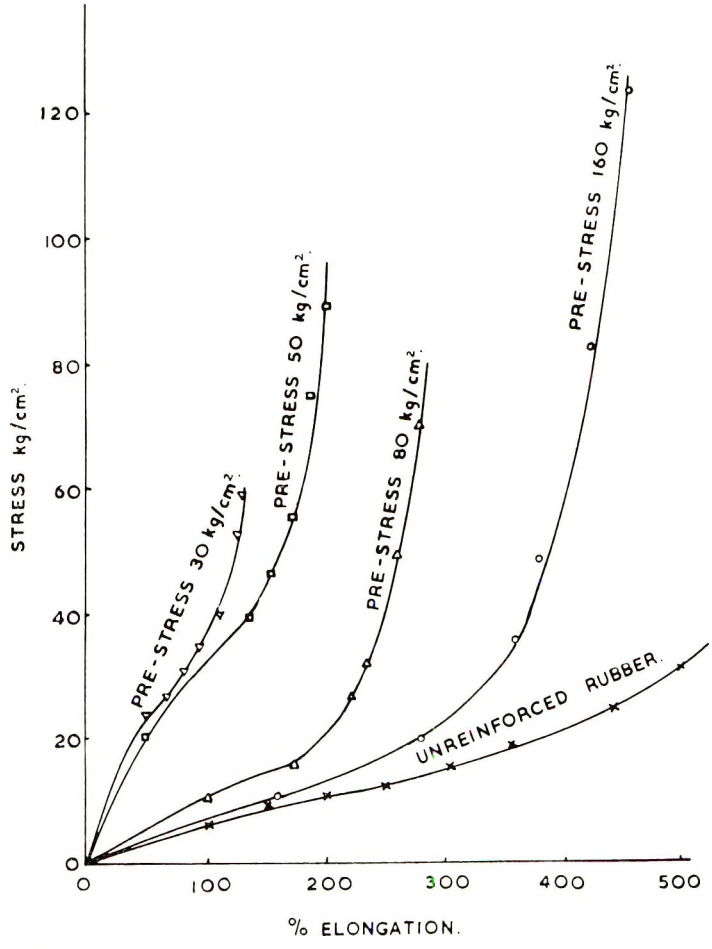

Fig. 4. Stress–strain curves for prestressed vulcanizates which have been reinforced by 50 phr of MPC carbon, i.e. $V = 0.26$ volumes of carbon per unit volume of natural rubber.

μ_h. Theoretical considerations in Part I have related the modulus G to crosslinking by the equation:

$$G = \rho RT/[M_c] = \rho RT(1 - C)[(1/M_c) + \sigma] \tag{20}$$

Thus for prestretched networks with a filler volume concentration C per cubic centimeter of rubber and filler the effective crosslinking $1/[M_c]$ is related to the $1/M_c + \sigma$ fix points by the equation:

$$1/[M_c] = (1 - C)[(1/M_c) + \sigma] \tag{21}$$

In these equations ρ is the polymer density, RT is the product of the gas constant and absolute temperature, and $(1 - C)$ takes account of the diluent effect of the filler in pre-stretched rubber.

On present evidence, one must have $j = 0.4$ and $i = 1/2$ to obtain the linear graphs shown in Figures 5 and 6, and these values represent even the prestress as an extreme point of the stress-strain curve. The smooth-out of the initial dip in the modulus strain curves shows that the empirical choice $C_2^* = 0.7$ to express this feature is the best available for unswollen rubber. For vulcanizates without reinforcement the sixth-power refinement is negligible as in Figure 6, except with highly cured gum for which we may take $\alpha_b - 1$ as the highest attainable prestretch. The coefficient 0.4 needs

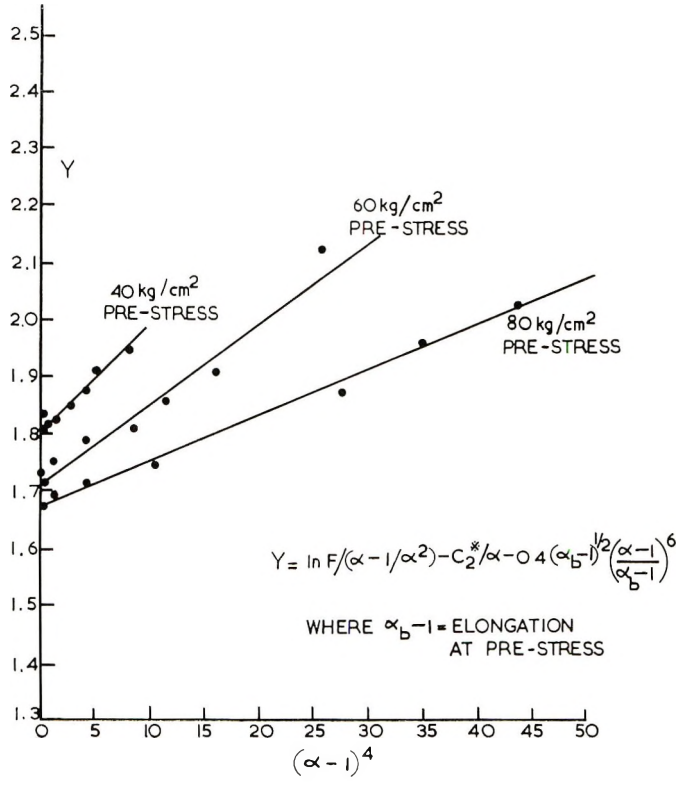

Fig. 5. Application of eq. (19) to stress–strain curves for 50 phr MPC carbon in NR, and elongations 50–250% after pre-stresses of 40–80 kg/cm². The equation has fixed constants $C_2^* = 0.7$, $j = 0.4$, and $i = 1/2$.

checking in the latter case. Equation (19) neglects the first two terms in eq. (33) of Part I, but for unswollen networks it is adequate at more than 100% elongation of gum rubber or for reinforced vulcanizates at elongations 50–500% after prestresses of 40–200 kg/cm² (Fig. 4). For networks other than reinforced NR the empirical parameter $C_2^* = 0.7$ may require adjustment; for swollen networks it becomes $C_2^* v_r^{4/3}$.

The empirical extension factor of earlier analyses[6,7] is now superseded by a property μ_h which can be expressed theoretically by the new equation derived in part I:

$$\mu_h = (1/\rho RT)^2 \left[\frac{6}{5}\left(\frac{h}{\epsilon}\right) + \frac{11}{50}\left(\frac{1}{\epsilon^2}\right)\right] G^2 \tag{8}$$

Here h is a coefficient of strain hardening and ϵ is the mean square extensibility per unit molecular weight of chain, i.e., it measures the intrinsic flexibility and extensibility of the polymer molecules. For reinforced

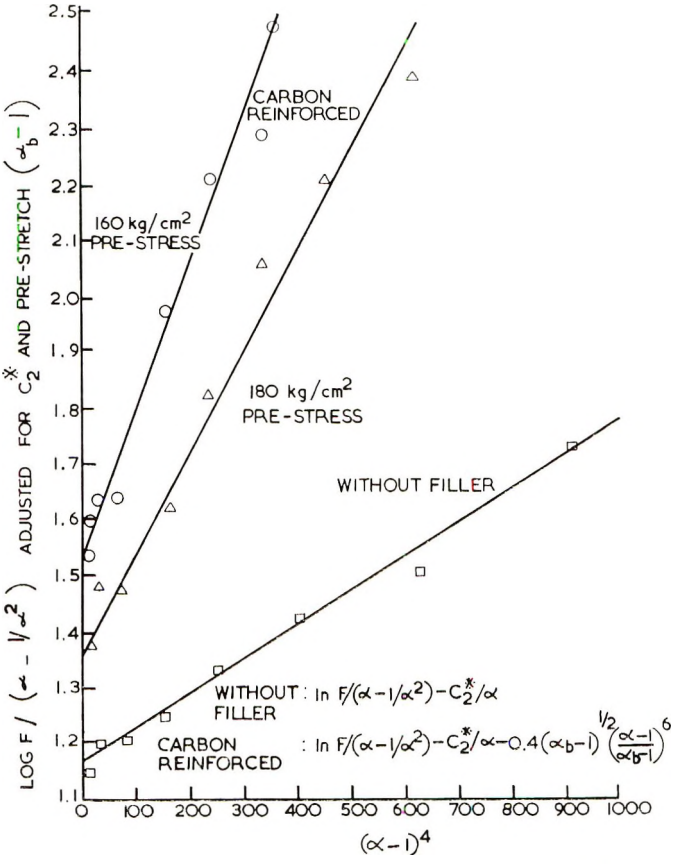

Fig. 6. Application of eq. (19) to stress–strain curves for 50 phr MPC carbon in NR, and elongations 150–500% after pre-stresses 160 and 180 kg/cm². The equation has fixed constants $C_2^* = 0.7$, $j = 0.4$, and $i = 1/2$.

rubber the term (11/50) $(1/\epsilon^2)$ is usually negligible in comparison with the expression (6/5) (h/ϵ) for strain hardening; and in that case the equation becomes:

$$\mu_h = (6/5)\ (1/\rho RT)^2\ (h/\epsilon) G^2 \tag{22}$$

From graphs such as Figures 5 and 6 the estimates of G from the intercept and the slope μ_h are given in Table X. In this case $\epsilon = 5.6 \times 10^{-3}$ for natural rubber gum corresponding to a potential extensibility of about 750% for chain length 10,000 and about 1050% for chain length 20,000. Hence

TABLE X
Values of G, μ_h, and h/ϵ for MPC-Reinforced Rubber after Prestressing and for Gum Rubber

Prestress, kg/cm²	Modulus G, kg/cm²	Upturn coefficient μ_h	Relative measure h/ϵ of the strain hardening on subsequent stretching $\times 10^{-4}$	
			Neglecting $11/50\epsilon^2$	Taking $\epsilon = 5.6 \times 10^{-3}$
MPC reinforced				
30	6.33	0.1111	121.62	121.04
40	6.08	0.0471	55.85	55.27
50	5.96	0.0312	38.51	37.93
60	5.61	0.0477	66.51	65.92
70	5.15	0.0161	26.61	26.03
80	5.13	0.0127	21.13	20.54
100	4.71	0.0096	19.00	18.41
120	4.45	0.0070	15.74	15.16
140	4.79	0.0046	8.80	8.22
160	4.53	0.0031	6.63	6.05
180	3.84	0.0022	6.55	5.96
200	4.36	0.0016	3.69	3.11
Gum rubber (600% prestretch)	3.22	0.0006	2.53	1.95

TABLE XI
Coefficients h of Strain Hardening and the Hard Fraction $\Omega[(1/M_c) + \sigma]$ from $-\ln^{-1}\{1 - \Omega[(1/M_c) + \sigma]\}$ at Prestretches $(\alpha_b - 1)$

Prestress, kg/cm²	Coefficient h of strain hardening on subsequent stretching	Fractional elongation $(\alpha_b - 1)$ at prestress	Hard fraction at prestretch (micro-breaking elongation) $\alpha_b - 1$, %
MPC-reinforced			
30	6780	1.27	40
40	3100	1.68	50
50	2120	1.93	57
60	3690	2.25	64
70	1460	2.54	69
80	1150	2.70	71
100	1030	3.25	77
120	849	3.72	80
140	460	3.97	81
160	339	4.34	83
180	334	4.97	86
200	174	5.33	85
Gum rubber (600% prestretch)	$h_0 = 109$	600% breaking elongation	59

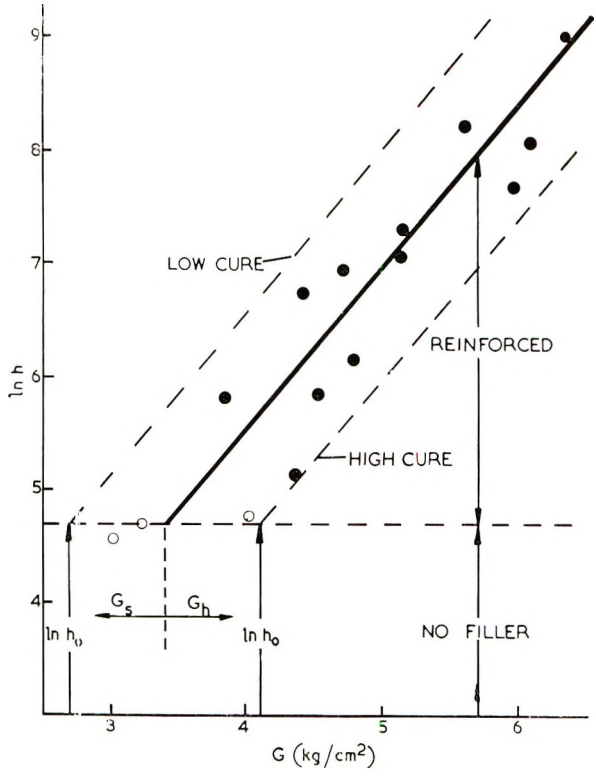

Fig. 7. Relation of modulus G after prestressing to subsequent strain hardening h for 50 phr MPC reinforcement of NR; hard and soft modulus components G_h and G_s corresponding to a reference level ln $h_0 = 4.7$ and $h_0 = 110$ for simple networks.

in Table XI the absolute coefficients h of strain hardening were obtained by using the relative measure h/ϵ from eq. (8) or (22), i.e.,

$$h/\epsilon = (5/6)\ (\rho RT)^2\ \mu_h/G^2 - (11/50)\ (1/\epsilon^2) \tag{23}$$

Even for the gum vulcanizate of modulus $G = 3.22$ kg/cm² the upturn coefficient $\mu_h = 0.0006$ is 4.3 times the theoretical value $(11/50\epsilon^2)\ (G/\rho RT)^2$ for no strain hardening.

The difference between ln G and $\ln\{F/[\alpha - (1/\alpha^2)]\} - C_2^*/\alpha$ at the prestress or network-breaking may be used to calculate the inextensible fraction $-\ln^{-1}\{1 - \Omega[(1/M_c) + \sigma]\}$ at the extreme point of the subsequent stress–strain curve. This will be understood by comparison of eqs. (6) and (7). The calculated hard fractions in Table XI are maximum values because more of the network breaks down at stresses higher than the prestress. Presumably the surviving linkages of carbon particles to network rubber lead to many chains of low extensibility and to molecular organization through steric hindrance to stretching of the adjacent chain segments.

For MPC-reinforced rubber after prestresses of 40–200 kg/cm² the logarithm of the coefficient h of strain hardening is plotted in Figure 7 against

the low-strain modulus G. The reference level ln h_0 represents gum rubber with a constant $h = h_0$ which in eq. (8) makes μ_h proportional to $[(1/M)_c + \sigma]^2$. Then, if chain breakage imposes a fixed limit to non-Gaussian behavior, we have from the non-Gaussian (upturn) components in eqs. (6) and (19) that the extensibility of simple gum networks is proportional to the square root of their chain length, as in Treloar's theory[10] of non-Gaussian chain displacements. The logarithmic relation implies that for a hard constituent contribution G_h the coefficient of strain-hardening is:

$$h = h_0 \exp \{1.43 G_h\} \tag{24}$$

where 1.43 is the slope of Figure 7. By extrapolating this linear graph in the direction of higher prestresses the reference level ln h_0 is intersected at a point representing no hard component G_h due to reinforcing particles. The soft component G_s is due mainly to normal cure linkages, but it may include other chemical contributions G_{sf} that have been induced by the filler surface without involving short chains and hard surface constraints.

By eqs. (24) and (22) or (23) the measurement of ln h should distinguish hard region constraints from normal intermolecular linkages and assess their respective contributions G_h and G_s. Previous failure[7,8] to observe this distinction was due to abbreviated measurements and calculations which did not allow for a substantial term in $(\alpha - 1)^6$ at high elongations. Even with gum rubber this sixth power is substantial for high sulfur and accelerated vulcanizates because their breaking elongation $\alpha_b - 1$ is less than 6.0 in eq. (19). Moreover, without a constant reference level h_0 for gum of varying cure, the distinctive stress upturn effect of filler linkages was difficult to detect by significant comparisons. Now, in accordance with eq. (24).

$$G_h = 0.7 \ln(h/h_0) \tag{25}$$

On present evidence ln $h_0 = 4.7$, so that $h = 110$ for gum networks, though more careful and precise measurements are needed to improve this estimate.

The new theory is very different in mathematical form from that of Sato and Furukawa,[11] and it does not attempt to provide a detailed local analysis of extensibility near bonded particles. However, the new theory is much easier to use and of wider application to both gum and reinforced rubbers over their entire range of strain. The main physical difference from the theory of Mullins and Tobin[12] is that hard regions are formed by highly-deformed rubber and strain-interaction with the filler, as well as broken down by the initial prestretch: whereas the Mullins-Tobin model pictures a 'hard' rubber phase with deformations occurring mainly in 'soft' regions. A qualitatively similar concept of heterogeneous structure due to denatured rubber in stretched vulcanizates has since come to my attention in a paper by Fujimoto.[13] The theory of Fujimoto is confined to reinforced rubber and does not provide a quantitative expression of the whole stress–strain curve.

Stress Breakdown and Strength of Reinforced Networks

Blanchard and Parkinson[6,7] showed that changes in modulus with prestressing may be related to a measure X of the force per linkage and to corresponding linkage strength factors $X = \alpha_b S/G^{2/3}$, which measure the strength of the strongest linkages broken by the prestress S. Empirically it was shown that the distribution of these strengths is described by two parameters G_r and K in the equations:

$$dG/G_r = -(K^3X^{1/2}/4) \exp\{-KX^{1/2}\}dX \tag{26}$$

$$G = G^* + G_rF(X) \tag{27}$$

where G^* is the residual modulus after high prestresses, G_r is a measure of the initial number of secondary linkages, and K is a measure of their strength. The appropriate function $F(X) \rightarrow 1$ for low prestresses and $F(X) \rightarrow 0$ after high prestresses is the gamma function:

$$F(X) = (K^3/4) \int_X^\infty X^{1/2}\exp[-KX^{1/2}]dX$$

$$= [1 + KX^{1/2} + K^2X/2]e^{-KX^{1/2}} \tag{28}$$

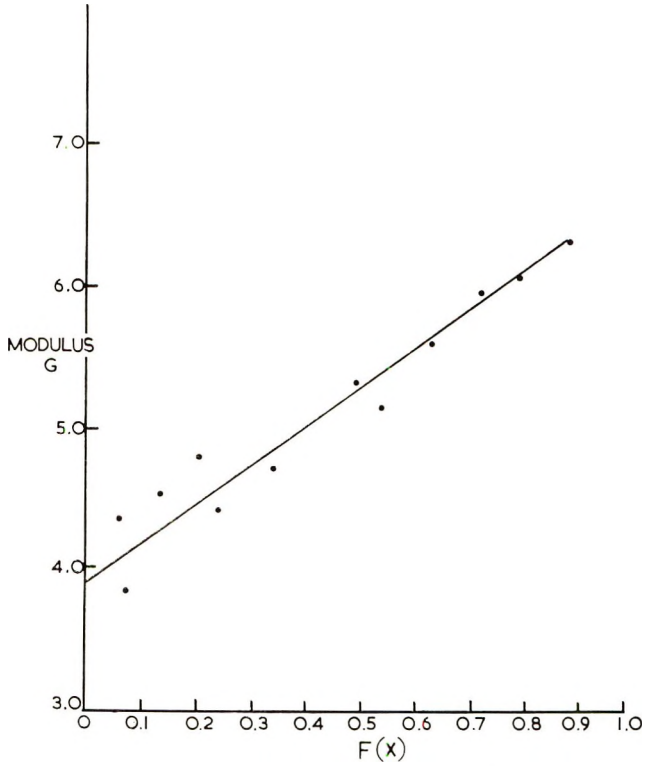

Fig. 8. Decrease in modulus G on prestressing for 50 phr MPC reinforcement of NR and with quantitative expression $F(X)$ by eq. (28) characterizing the stress breakdown and network strength.

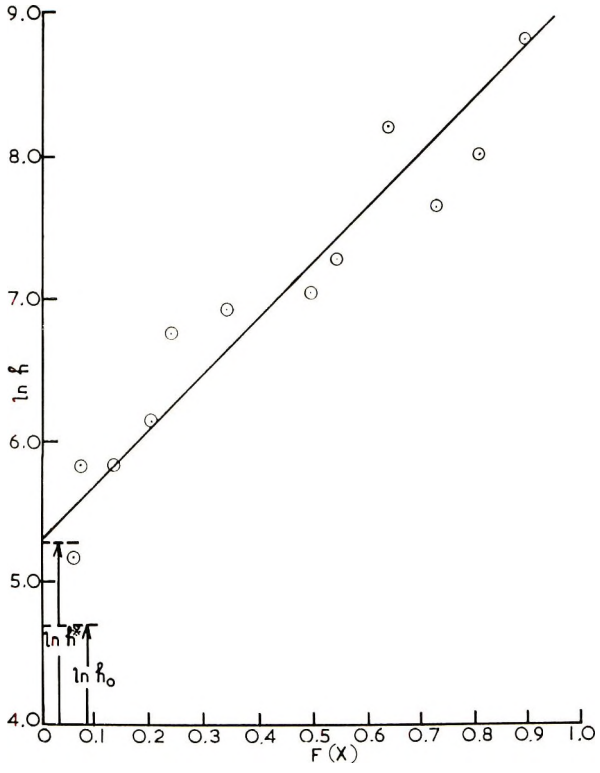

Fig. 9. Graph showing that $F(X)$ is a fundamental network parameter which also expresses the prestress-induced changes in the upturn of the stress–strain curve of reinforced rubber.

Thus the modulus can be resolved into one component $G_rF(X)$ which is a function of the prestress, and a further component G^* surviving high prestress which is attributed to strong (primary) linkages formed by sulfur and by carbon blacks.

The above law of softening has one strength distribution constant $K = 0.276$ common to linkages formed by various fillers and loadings in NR, and in SBR and butyl test cases.[6,7] Figure 8 shows that it is unaffected by the more satisfactory definition and calculation of G in the present paper. Moreover, it is now evident from Figure 9 that $F(X)$ can also express the prestress induced changes in the upturn of the curves, as reflected by the new coefficient h of strain hardening. Hence the strength distribution $F(X)$ with $K = 0.276$ is a fundamental parameter of filler–rubber networks. Other types of network may have different strength constants K which could be determined to fit a range of prestresses. With K initially unknown in $F(X)$, the network analysis will be exacting but not too laborious with the help of a computer.

F. T. Bueche[14,15] has proposed a theory of stress softening in which the broken linkages are primary chemical bonds of relatively highly stressed

rubber chains between filler particles. Blanchard[16] has suggested that sliding or desorption of network molecules at the particle surface may involve preferential absorption of short, unattached molecules and of other non-network material. Boonstra[17,18] and Dannenberg[19] have put forward the hypothesis that surface slippage of rubber attachments to carbon particles is the main mechanism of stress-softening and of carbon reinforcement. Mullins and Tobin[12] and Harwood *et al.*[20] have introduced the concept of a strain amplification factor due to filler particles. The latter authors regard prestress softening as a property of the polymer matrix, in which case Blanchard and Parkinson's $K = 0.276$ for various fillers would have to be interpreted as a common weakening action of spherical particles on parts of the matrix—though with carbon particles there are strong (persistent) bonds to prevent any impairment of the ultimate tensile strength. Whatever view is taken, the theory of Bueche shows that Blanchard and Parkinson's interpretation is open to criticism, in that K and $F(X)$ represent a distribution of stress as well as a distribution of strength. One answer to this objection is that K and $F(X)$ are in either case a measure of linkage strength, inasmuch as they reflect the ability of the linkages to survive when the rubber is stressed. Another is that the broken linkages are so closely associated with the hard filler particles that it is immaterial if some breaks occur at a distance from the filler–rubber interface.

The relation between $\ln h$ and $F(X)$ has slope 3.9 in Figure 9 and may be related to Figure 7 and 8 by writing it in the general form:

$$\ln h = \ln h^* + 1.43\, G_r F(X) \tag{29}$$

where $\ln h^* = 5.3$ for the natural rubber and MPC carbon of earlier experimental work.[6] The modulus component G_r in this equation is not the whole hard component G_h because that includes a tough residue G_h^* due to comparatively strong bonds between rubber and carbon black. By eq 25 this tough residue of primary linkages can be calculated from:

$$G_h^* = 0.7\, (\ln h^* - \ln h_0) \tag{30}$$

For the present case of MPC carbon in natural rubber it is $G_h^* = 0.42$ kg/cm^2; and it is still only $(1 + V)G_h^* = 0.53$ kg/cm^2 after allowing for network dilution by the carbon volume V per cubic centimeter of rubber. This is rather more than 10% contribution by the carbon–rubber linkages.

A much greater total of strong filler linkages is obtained if 3.22 kg/cm^2 from Figure 6 is taken for the gum modulus, and if the filler contribution is measured simply by the residual difference after high prestress i.e., by $(1 + V)\,G^* - 3.22 = 1.70$ kg/cm^2. This discrepancy indicates that hard-surface constraints due to rubber attachment are responsible for less than 1/3 of the primary linkages due to MPC black. Other filler-induced linkages, but not distinguishable from cure crosslinks, are reflected in Figure 7 by an increase $(1 + V)G_s - 3.22 = 1.07$ kg/cm^2 in the soft component of the modulus. These conclusions support the view of Kraus[21] that the linkages induced by carbon black are mainly between rubber molecules, the

number of linkages to the black being relatively small. The smaller moduli than in earlier comparisons[6,8] are due to the new definition of modulus G by eq. (19), in which a parameter C_2^* allows for the deviation of unswollen rubber from theoretical behaviour at low strains. This has little effect on relative assessments.

Effective ϕ values from equilibrium swelling will need correction by a hydrodynamic factor $1 + 2.5C_\phi$ if there is effective wetting C_ϕ of the filler due to intrinsic linkage reinforcement $\phi_0 > 1$. The filler loading term $C_\phi = (C \ln \phi)/(1 + 2.5C)$ vanishes when $\phi = 1.0$ for Graphon in Table 8: hence it seems preferable to the plain concentration factors which Porter[23] and others[24,25] have proposed without account of linkage reinforcement. A supplement in Polymer Letters[26] gives the results and derivation of the present refinement; and develops it for filler volume fractions 8 to 25% to allow for particle shape factor, e.g., chain structure of HAF carbon in SBR.

References

1. A. F. Blanchard, *J. Polym. Sci. A-1*, this issue.
2. P. J. Flory, *J. Chem. Phys.*, **18**, 108 (1950).
3. M. Mooney, *J. Appl. Phys.*, **11**, 582 (1940).
4. R. S. Rivlin and D. W. Saunders, *Phil. Trans. Roy. Soc.* (London), **A243**, 251 (1951).
5. L. Mullins, *J. Rubber Res.* **16**, 275 (1947); *J. Phys. Colloid Chem.*, **54**, 239 (1950).
6. A. F. Blanchard and D. Parkinson, *Ind. Eng. Chem.*, **44**, 799 (1952).
7. A. F. Blanchard, *Trans. Inst. Rubber Ind.*, **32**, 124 (1956); *J. Polym. Sci.*, **14**, 355 (1954).
8. A. F. Blanchard, *Applied Science of Rubber*, W. J. S. Naunton, Ed., Edward Arnold, London, 1961, p. 434.
9. P. P. A. Smit, *Rheol. Acta*, **5**, 277 (1966).
10. L. R. G. Treloar, *Physics of Rubber Elasticity*, Oxford Univ. (Clarendon) Press, 1949, p. 93.
11. Y. Sato and J. Furukawa, *Rubber Chem. Technol.* **35**, 857 (1962).
12. L. Mullins and N. R. Tobin, *Proc. 3rd Rubber Tech. Conf.*, **1954**, 397; *J. Appl. Polym. Sci.* **9**, 2993 (1965).
13. K. Fujimoto, *J. Soc. Rubber Ind. Japan*, **37**, 991 (1964).
14. F. Bueche, *J. Appl. Polym. Sci.*, **5**, 271 (1961).
15. F. Bueche, *J. Appl. Polym. Sci.*, **4**, 107 (1961).
16. A. F. Blanchard, *Proc. 4th Rubber Tech. Conf.*, **1962**, 361.
17. B. B. Boonstra, *Reinforcement of Elastomers* G. Kraus, Ed., Interscience, New York, 1965, Chap. 16.
18. B. B. Boonstra, *J. Appl. Polym. Sci.*, **11**, 389 (1967.)
19. E. M. Dannenberg, *Trans. Inst. Rubber Ind.*, **42**, 26 (1966).
20. J. A. C. Harwood, L. Mullins, and A. R. Payne, *J. Appl. Polym. Sci.*, **9**, 3011 (1965).
21. G. Kraus, *Rubber World*, **136**, 67, 254 (1956).
22. G. Kraus, *J. Appl. Polym. Sci.*, **7**, 861 (1963).
23. M. Porter, *Rubber Chem. Technol.* **40**, 866 (1967).
24. J. W. Sellers, M. P. Wagner, B. J. De Witt, C. C. Stueber and J. H. Bachmann, *J. Appl. Polym. Sci.* **5**, 397 (1961).
25. O. Lorenz and C. R. Parks, *J. Polym. Sci.* **50**, 299 (1961).
26. A. F. Blanchard, *Polymer Letters*, in press.

Received May 28, 1968

JOURNAL OF POLYMER SCIENCE: PART A-1 VOL. 8, 861–868 (1970)

Some Consideration of Excluded Volume Effects in Dilute Polymer Solutions

R. YEH and A. ISIHARA, *Statistical Physics Laboratory, Department of Physics and Astronomy, State University of New York, Buffalo, New York 14214*

Synopsis

A two-parameter model is proposed to analyze the viscosity of dilute polymer solutions, and critical comments are given on recent articles by Berry and by Norisuye et al. The data seem to follow our theoretical model better than other models. Light-scattering data are also analyzed. The data indicate that the distribution function of monomers decays as a simple exponential function for large r.

INTRODUCTION

Many years have passed since the excluded volume effects were first introduced into theoretical considerations of polymer solutions. Experimental efforts[1–10] have also been made to establish the excluded volume effects on the viscosity, light-scattering, and other data. To express the volume effects on these data a simple expansion parameter α originally introduced by Flory has been used widely. It has been found, however, that the expansion parameter determined from one data, say viscosity, differs from that from other data, say light scattering. Recently, Berry[5] found that $[\eta]/[\eta]_\theta$ is not a single-valued function of z except for $M \sim 10^6$. However, Norisuye et al. opposed this view on the ground[1] that Berry's values for the parameter z contained a reducing factor 1/1.55 which exaggerated his finding. Also, Norisuye et al. claimed the validity of a single parameter theory because the double logarithmic plots of α_η^3 and α_s^3 for polychloroprene (PCP) fell onto a single curve. Thus, there is still a controversial point. Actually, these discrepancies indicate the necessity of adopting a more refined theoretical treatment. Especially, if our interest is in establishing the excluded volume effects in comparison with the drainage effects, a viscosity formula which has both effects should be used for analyzing experimental data.

To meet this situation we have derived in a previous paper a formula for the intrinsic viscosity of chain polymers taking both effects into consideration. The result is characterized by a segment distribution function, through which the effects on the viscosity coefficient appear. Nevertheless, for detailed analyses of experimental data which are mostly analyzed in

terms of the expansion parameter, we found it necessary to express our formula in the same language. For this purpose, we shall adopt in this paper a simple model instead of the perturbation approach developed in the previous paper. We shall thus analyze some recent experimental data on the intrinsic viscosity.

We shall then try to find a possible form for the distribution function based on light-scattering data. The excluded volume effects appear in the scattered intensity, and since the intensity function is a Fourier transform of the distribution function we can infer a possible form for the distribution function. Although there is one disadvantage of not being able to determine the distribution function for all distances, light-scattering data, together with viscosity and other data, give some information on the excluded volume effects.

TWO-PARAMETER MODEL FOR VISCOSITY

Experimental data on viscosity and the second virial coefficient[1-6] of polymer solutions seem to suggest that α_s^2 depends only on a single parameter Z. α_s^2 is the ratio of the mean-square radius of gyration in good solvent with that in a θ-solvent, i.e., $\alpha_s^2 = \langle r^2\rangle/\langle r^2\rangle_\theta$. Z as usual, is defined by $(3/2\pi)^{3/2}(\beta/b^3)N^{1/2}$, where N is the number of monomer units in a single polymer molecule, b is the effective bond length, and β is the binary cluster integral for the interaction between nonbonded segments.

One of the important questions in the viscosity theory is whether or not $\alpha_\eta^3 = [\eta]/[\eta]_\theta$, the ratio of intrinsic viscosity in good solvent with that in θ-solvent, depends only on Z. To look into this question, we propose a simple model similar to the one first introduced by Bueche:[11]

$$W(\vec{r}) = A\,(9/\pi Nb^2)^{3/2}\exp\{(9r^2/Nb^2) - (CNb^2Z/4r^2)\} \qquad (1)$$

$W(\vec{r})$ is the probability of finding a monomer at $\vec{r}$ with the center of mass of the polymer fixed at the origin. The normalization condition $\int W(\vec{r})d\vec{r} = 1$ determines A. C is an adjustable parameter of order 1, to be determined so as to produce the best agreement with experimental data. In the absence of excluded volume effect ($C = 0$), the distribution function is reduced to a gaussian distribution of well known form, with $\langle r^2\rangle_\theta = 1/6\,Nb^2$.

Our model based on eq. (1) is similar in form to, yet mathematically more tractable than the self-consistent field models of Flory[12] and Reiss.[13] Equation (1) implies also a reasonable asymptotic dependence of $\langle r^2\rangle$ on N, namely $\langle r^2\rangle \sim N^{3/4}$ for large N.

A great advantage of adopting eq. (1) is in that it enables us to evaluate α_s^2 exactly in a closed form, and to compare with the usual Hermans-Overbeek approximation.[14] To see this, let us consider

$$I = \frac{\int_0^\infty x^4\,dx\exp\{-a^2x^2 - (b^2/x^2)\}}{\int_0^\infty x^2\,dx\exp\{-a^2x^2 - (b^2/x^2)\}} \qquad (2)$$

An exact integration yields

$$I_e = [1 + 2(1 + ab)(1 + 2ab)]/2a^2(1 + 2ab) \tag{3}$$

The Hermans-Overbeek[14] approximation gives

$$I_a = (3 + \sqrt{9 + 16a^2b^2})/4a^2 \tag{4}$$

The error of the Hermans-Overbeek approximation $\equiv 1 - I_a/I_e$ is small for $ab \gg 1$ or $ab \ll 1$, but is no less than 1% for $23 > ab > 0.2$. For our case, $\alpha_s^2 = 1$ if $a^2 = 3/2$, $b^2 = 3CZ/2$. So

$$\alpha_s^2 = 1 + [3CZ/(1 + 3\sqrt{CZ})] \tag{5}$$

The experimental values of Z vary from 0 to 4. In this domain, the Hermans-Overbeek approximation is not very accurate and has an average error of 7%. On the other hand, from eq. (5) we get

$$\alpha_s^3 = \{1 + [3CZ/(1 + 3\sqrt{CZ})]\}^{3/2} \tag{6}$$

As is shown in Figure 1, with a reasonable choice of $C = 0.83$, eq. (6) agrees with experimental data satisfactorily.

For the intrinsic viscosity $[\eta]$, we found previously[15,16] that

$$[\eta] = \alpha_s^2[\eta]_0/(1 + a\langle 1/r\rangle) \tag{7}$$

where $[\eta]_0 = \pi Nab^2/6m$, m is the mass of a monomer, $a = \zeta/6\pi\eta_0$ is the effective radius of a monomer determined from Stokes' law. By definition, $\langle 1/r\rangle = 4\pi N \int_0^\infty W(\vec{r})r dr$

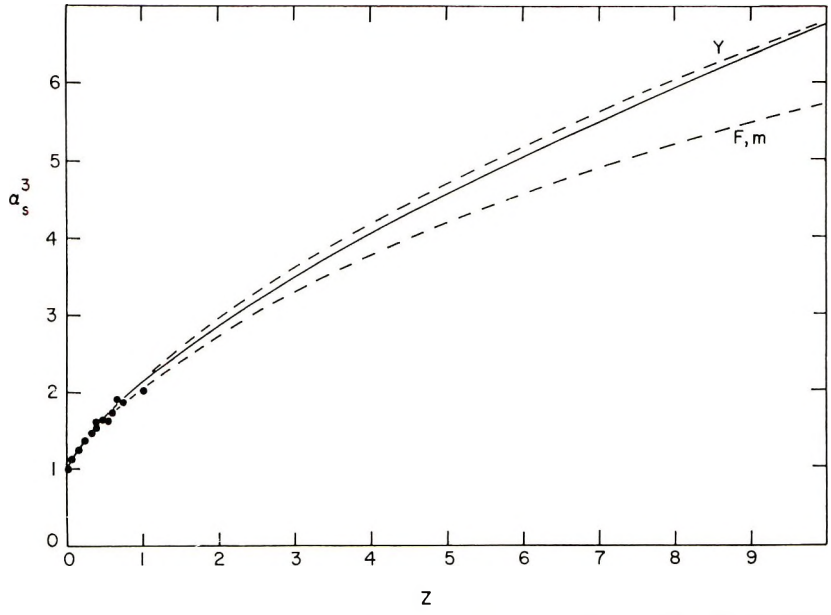

Fig. 1. Comparison of experimentally determined values for α_s^3 with the calculated values: (—) eq. (6), with $C = 0.83$; (--y) Yamakawa's formula; (- - F,m) modified Flory formula;[17] (●) data of polychloroprene in *trans*-decalin.

In θ-solvent, $\alpha_s = 1$, and hence

$$\alpha_\eta^3 \equiv \frac{[\eta]}{[\eta]_\theta} = \frac{\alpha_s^2}{1 + a\langle 1/r\rangle}(1 + a\langle 1/r\rangle_\theta) \tag{8}$$

From definition, we see that

$$\langle 1/r\rangle = f(Z)\langle 1/r\rangle_\theta$$
$$\langle 1/r\rangle_\theta = 6N^{1/2}/\sqrt{\pi}\, b$$

where

$$f(Z) = \frac{\exp\{3\sqrt{CZ}\}}{1 + 3\sqrt{CZ}} \int_0^\infty \exp\left\{-y - \frac{9CZ}{4y}\right\} dy \tag{9}$$

We have evaluated the integral numerically by Simpson's rule (with relative error less than 10^{-7}). For large Z, $f(Z)$ has the same asymptotic dependence as α_s^{-1}, namely, $f(Z) \sim \alpha_s^{-1} \sim Z^{-1/4}$. Also, $f(Z) \to 1$ as $Z \to 0$. With $C = 0.83$, the error of the usual approximation adopted by many authors, in which $\langle 1/r\rangle$ is replaced by $\alpha_s^{-1}\langle 1/r\rangle_\theta$, increases with Z. The approximation has an average relative error of 20% in the range of Z

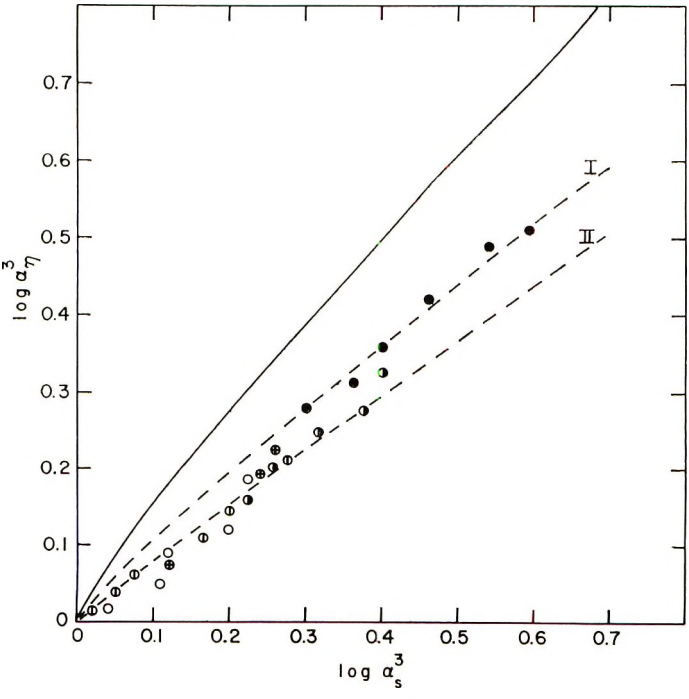

Fig. 2. Comparison of theory with the experimental data of polychloroprene (PCP) in log α^3_η *vs.* log α^3_s plot: (——) case of large N; [$\alpha_\eta^3 = \alpha_s^2 f(z)$]; (I) eq. (8) with $(6/\sqrt{\pi})N^{1/2}a/b = 0.9$; (II) eq. (8) with $(6/\pi)N^{1/2}a/b = 0.2$; (○, ◑, ⊕) experimental data for PCP in *trans*-decalin; (◑) PCP in *n*-butyl acetate at 25°C; (●) PCP in carbon tetrachloride at 25°C.

varying from 0 to 4. The error is defined by $1 - f(Z)\alpha_s$, with α_s given by eq. (5).

From eqs. (8) and (9), we get

$$\alpha_\eta^3 = \frac{(1 + 3\sqrt{CZ} + 3CZ)\,[1 + (6/\sqrt{\pi})\,N^{1/2}\,(a/b)]}{(1 + 3\sqrt{CZ})\,[1 + (6/\sqrt{\pi})\,N^{1/2}\,(a/b)\,f(Z)]} \tag{10}$$

Hence α_η^3 in general should depend on two parameters, Z and $N^{1/2}\,(a/b)$. This result is natural because a drainage effect is in general quite independent of an excluded volume effect. In other words, both parameters could be present in viscosity data. For large N ($a\,\langle 1/r\rangle_\theta > a\,\langle 1/r\rangle \gg 1$), or for small Z [$f(Z) \to 1$ as $Z \to 0$], the drainage effect in $[\eta]$ cancels with that in $[\eta]_\theta$, and eq. (8) reduces to $\alpha_\eta^3 = \alpha_s^2$. In this limit, $\alpha_\eta^3 \to \alpha_s^2/f(Z) \to N^{3/5}$, or $[\eta] \to M^{0.875}$ in agreement with many experiments.[15,16]

The relation between $\log \alpha_\eta^3$ and $\log \alpha_s^3$ is plotted in Figure 2 based on eqs. (6) and (8) (with $C = 0.83$). We find that the experimental data for polychloroprene (PCP) may be roughly divided into two categories: the carbon tetrachloride data which lie on the curve with $(6/\sqrt{\pi})\,N^{1/2}\,(a/b) = 0.9$, and the other data with $(6/\sqrt{\pi})\,N^{1/2}\,(a/b) = 0.20$. As one can see, the two sets of experimental points lie fairly distinctively on different curves, indicating the presence of a drainage effect. There is no significant overlap between these two groups of data contrary to the claim of Norisuey[1] that they lie on the same curve. Their claim is not convincing, although more data are needed before reaching final conclusion. It is rather surprising for us to find that even the last experimental point of Norisuye et al.[1] which is way off from the one-parameter curve falls naturally and nicely on our theoretical curve without any further adjustment. These authors had to "lift up" the point in order to establish the single-parameter theory. Thus, the present viscosity data do not seem to exclude the existence of a drainage effect. Equation (8) depends on two arbitrary parameters, of which the parameter $(6/\sqrt{\pi})\,N^{1/2}\,(a/b)$ is found to be rather small (0.2–0.9).[15,16] However, more refined considerations may possibly change the parameters.

Analysis of Light-Scattering Data

Viscosity data provides little information about the monomer distribution function $W(\vec{r})$, since it gives only moments of $W(\vec{r})$. On the other hand, light-scattering experiments are supposed to yield much more, since the square root of the angular scattering function, $P^{1/2}(\theta)$, is essentially the Fourier sine transform of $W(\vec{r})$.[18]

Light-scattering data[6–10] seem to obey a very simple empirical rule (Fig. 3):

$$P^{-1}(\theta) = 1 + hx \tag{11}$$

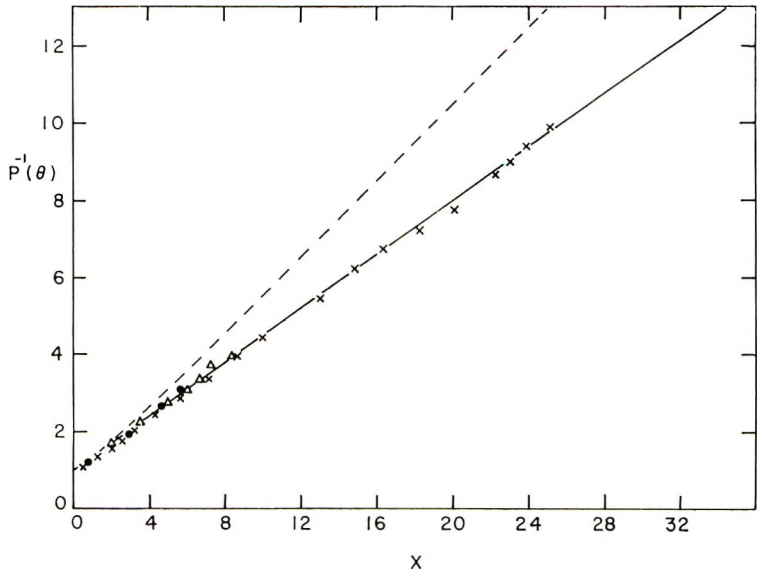

Fig. 3. Comparison of experimentally determined values for $P^{-1}(\theta)$ with the calculated values: (——) eq. (11) with $h = 9/26$; (--) Debye's formula; (X) experimental values for polystyrene–benzene, 40°C, (●) polystyrene–cyclohexane, 35°C; (Δ) polystyrene–cyclohexane, 45°C.

We note in this empirical formula that $P^{-1}(\theta)$ is determined by one single parameter x:

$$x^{1/2} = \frac{4\pi}{\lambda} \langle r^2 \rangle^{1/2} \sin \frac{\theta}{2}$$

λ is the wavelength of the incident light, and θ is the scattering angle. It is found that $h = 9/26$ gives the best fit. However, $h = 1/3$ will be used for the following discussion. This is the value which we expect from Debye's formula for small x.

If the one-parameter theory is correct, we must rule out all the distribution functions obtained from the self-consistent field approaches, including eq. (1). The reason is that a distribution function of the form $\exp\{-Ar^m - Br^n\}$ will introduce in $P(\theta)$ at least two independent parameters.

If we accept eq. (11) as a rigorous relation, we can obtain the monomer distribution function $W(\vec{r})$ and the pair distribution function $\rho(\vec{r})$ by inverse Fourier transform.[18] We find

$$W(\vec{r}) = \frac{3}{2\pi^2 \langle r^2 \rangle r} K_1\left(\sqrt{3}\, \frac{r}{\langle r^2 \rangle^{1/2}}\right)$$

$$\rho(\vec{r}) = \frac{3}{4\pi \langle r^2 \rangle r} \exp\left\{-\frac{\sqrt{3}r}{\langle r^2 \rangle^{1/2}}\right\} \tag{12}$$

K_1 is the modified Bessel function of the second kind. The singularity at the origin may be considered artificial, as $W(\vec{r})$ at small r requires measure-

ments at very short wavelength. Data at small value of x may be used only to determine $W(\vec{r})$ and $\rho(\vec{r})$ for large r. At large values of x, some deviation from eq. (11) might be found.

According to eq. (12), the decay of the two distribution functions are essentially $\exp\{-\sqrt{3}r/\langle r^2\rangle^{1/2}\}$ for larger r. In fact, any linear relationship between $[P^{-1}(\theta) - 1]$ and x implies a simple exponential decay of $W(\vec{r})$. Such a decay is not the case in the standard gaussian type distribution or in the distribution based on a lattice model.[19] It suggests, contrary to earlier conjectures,[20] that the excluded volume effect changes not only the value of $\langle r^2\rangle$, but also the shape of the distribution function. For further details an independent confirmation of eq. (12) is desirable by x-ray or neutron-scattering measurements.[21] [The static response function $\chi_0(\vec{r})$ is directly proportional to $\rho(\vec{r})$ of eq. (12).]

Finally, the dependence of $P(\theta)$ on a single parameter x suggests that $W(\vec{r})$ may depend on Z only through $\langle r^2\rangle$. If $\langle r^2\rangle$ appears in $W(\vec{r})$, the equation

$$\int_0^\infty r^4\, W(\vec{r})\, dr = \int_0^\infty r^2\, W(\vec{r})\, dr\, \langle r^2\rangle \tag{13}$$

may be considered as a constraint on $\langle r^2\rangle$. A question arises whether a solution of eq. (13) exists. Although the gaussian distribution satisfies eq. (13), its consequence, i.e. the Debye formula,[22]

$$P(\theta) = (2/x^2)\,(e^{-x} - 1 + x) \tag{14}$$

does not agree with experiment (Fig. 3). Therefore, taking into consideration eq. (6), one might be inclined to use $W(\vec{r}) = y^n \exp\{-\sqrt{3}\, y\}$, with $y = r/\langle r^2\rangle^{1/2}$. However, there is no solution for real positive n which satisfies eq. (13).

SUMMARY

We are led to the conclusion that to determine the drainage and excluded volume effects, we need more thorough experiments on samples of small N or large Z. Such experiments will give more information concerning drainage effects. For very large N or very small Z, however, the ratio α_η^3 as determined currently will not show drainage effects. The recent claims of Kawahara et al.[2] needs further investigation.

For large r the distribution function might decay exponentially. For small r, light-scattering experiments at short wavelength are needed to determine the distribution function.

The Hermans-Overbeek approximation used in excluded volume calculation is not very accurate, (approximately 7% error).

We wish to thank the Computing Center of the State University of New York at Buffalo for kind support in carrying out the numerical calculation of this work.

This work was supported by the National Science Foundation.

We wish to thank Dr. G. C. Berry for sending us preprints prior to publication (ref. 5).

References

1. T. Norisuye, K. Kawahara, A. Teramoto, and H. Fujita, *J. Chem. Phys.*, **49**, 4330 (1968).
2. K. Kawahara, T. Norisuye, and H. Fujita, *J. Chem. Phys.*, **49**, 4339 (1968).
3. W. R. Krigbaum and D. K. Carpenter, *J. Phys. Chem.*, **59**, 1166 (1955).
4. G. V. Schultz and R. Kirste, *Z. Physik. Chem.* (Frankfurt), **30**, 171 (1961).
5. G. C. Berry, *J. Chem. Phys.*, **44**, 4550 (1966); *ibid.*, **46**, 1338 (1967).
6. D. McIntyre, J. Mazur, and A. M. Wims, *J. Chem. Phys.*, **49**, 2887 (1968).
7. J. Mazur, D. McIntyre, and A. M. Wims, *J. Chem. Phys.*, **49**, 2896 (1968).
8. J. Mazur and F. McCrackin, *J. Chem. Phys.*, **49**, 648 (1968).
9. D. McIntyre, A. Wims, L. C. Williams, and L. Mandelkern, *J. Phys. Chem.*, **66**, 1932 (1962)
10. P. Debye, D. Chu, and H. Kaufmann, *J. Polym. Sci. A*, **1**, 2387 (1963).
11. F. Bueche, *J. Chem. Phys.*, **21**, 208 (1953).
12. P. J. Flory, *J. Chem. Phys.*, **17**, 186 (1949).
13. H. Reiss, *J. Chem. Phys.*, **47**, 186 (1967).
14. J. J. Hermans and J. Th. G. Overbeek, *Rec. Trav. Chim.*, **67**, 761 (1948).
15. R. Yeh and A. Isihara, *J. Chem. Phys.*, **51**, 1215 (1969).
16. A. Isihara, *Adv. Polym. Sci.*, **5**, 531 (1968).
17. H. Yamakawa and G. Tanaka, *J. Chem. Phys.*, **47**, 3991 (1967).
18. A. Isihara, *J. Chem. Phys.*, **40**, 1137 (1964).
19. M. E. Fisher, *J. Chem. Phys.*, **44**, 616 (1966).
20. H. B. Gray, Jr., V. A. Bloomfield, and J. E. Hearst, *J. Chem. Phys.*, **46**, 1493 (1967).
21. P. G. de Gennes, *Physics*, **3**, 37 (1967).
22. P. Debye, B. Chu, and D. Woermann, *J. Chem. Phys.*, **36**, 1803 (1962).

Received July 22, 1969

JOURNAL OF POLYMER SCIENCE: PART A-1 VOL. 8, 869–884 (1970)

Thermally Stable Silarylene-1,3,4-Oxadiazole Polymers

HANNA NAGY KOVACS, ALVIN D. DELMAN, and BERNARD B. SIMMS, *Naval Applied Science Laboratory, Brooklyn, New York 11251*

Synopsis

The effects of incorporating a *p*-phenylene- (or *m*-phenylene)-1,3,4-oxadiazole fragment into the backbone of poly[1,4-phenylene(diphenylsilyl)-1,4-phenylene-2,5-(1,3,4-oxadiazole)], which was developed by the authors, was investigated. Bis[*p*-carbohydrazidophenyl)diphenylsilane was copolymerized with dipentachlorophenyl terephthalate or isophthalate to produce the prepolymers poly[*N*-(*p*-diphenylsilylbenzoyl)-*N'N''*-(terephthaloyl)-*N'''*-(*p*-benzoyl)dihydrazide] and poly[*N*-(*p*-diphenylsilylbenzoyl)-*N'*,-*N''*-(isophthaloyl)-*N'''*-*p*-benzoyl) dihydrazide], respectively. The polyhydrazides were converted by thermal dehydration into poly[1,4-phenylene(diphenylsilyl)-1,4-phenylene-(1,3,4-oxadiazole-2,5-diyl)-1,4-phenylene-2,5-(1,3,4-oxadiazole)] and poly[1,4-phenylene(diphenylsilyl)-1,4-phenylene-(1,3,4-oxadiazole-2,5-diyl)-1,3-phenylene-2,5-(1,3,4-oxadiazole)]. The new polymers were soluble in organic solvents. Films cast from these solutions exhibited good adhesion to glass and metal surfaces. Thermal analysis showed that the heat stability of all these polymers was about the same and that they were resistant to decomposition when heated in air to about 400°C. The results also indicated that these polymers were somewhat less heat-resistant than samples of poly-[1,4-phenylene(diphenylsilyl)-1,4-phenylene-2,5-[1,3,4-oxadiazole)] synthesized from bis(*p*-carbohydrazidophenyl)diphenylsilane and bis-(*p*-carbopentachlorophenoxyphenyl)diphenylsilane.

INTRODUCTION

In a previous paper[1] the synthesis and good thermal stability of silicon-containing Schiff base and benzimidazole derivatives were reported. This work was followed by the synthesis of silicon-containing acide amide, benzimidazole and oxadiazole polymers.[2] Results of thermal analysis[3] indicated that these polymers were unusually stable when heated in air up to 400°C. Poly[1,4-phenylene(diphenylsilyl)-1,4-phenylene-2,5-(1,3,4-oxadiazole)][2] (I) exhibited specially good resistance to thermal oxidation and was soluble in several organic solvents. Solution-cast films from the polymer were flexible and exhibited good adhesion to glass and metal surfaces even after being heated for prolonged time at 300°C.

This is in contrast to other heat-resistant fully aromatic poly-1,3,4-oxadiazoles[4,5] which were insoluble in organic solvents.

Realizing that polymers with high inherent viscosities generally exhibit superior properties over those with lower molecular weights, studies were

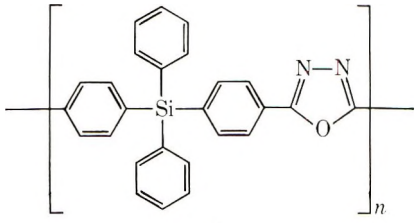

I

undertaken to modify the synthesis route for the preparation of polymer I with longer chain size. In addition new silicon-containing 1,3,4-oxadiazole polymers were synthesized. Results of investigations concerning the synthesis and thermal stability of these polymers are presented in this paper.

RESULTS AND DISCUSSION

Synthesis of Intermediate Compounds

A more economical procedure was developed for our previously described method[2] for the oxidation of diphenyldi(*p*-tolyl)silane (II) with chromic anhydride to produce bis(*p*-carboxyphenyl)diphenylsilane (III) in larger quantities. Speck's[6] potassium permanganate oxidation method was also modified to convert II to dicarboxylic acid III. Bis(*p*-chlorocarbonylphenyl)diphenylsilane (IV), bis(*p*-carbomethoxyphenyl)diphenylsilane (V) and bis[*p*-carbo-(*p*-nitrophenoxy)phenyl]diphenylsilane (VI) were prepared from III as described before.[2]

Diacid chloride IV was interacted with pentachlorophenol in the presence of triethylamine to produce bis(*p*-carbopentachlorophenoxyphenyl)-diphenylsilane (VII) which was made before by another method.[2]

The reaction of excess of hydrazine with V, VI, and VII yielded bis(*p*-carbohydrazidophenyl)diphenylsilane (VIII) which melted when freshly prepared at 170–172°C. However, in 24 hr the melting point changed considerably.

It should be mentioned that the melting point determination of dihydrazide VIII was carried out with constant agitation using a thin glass rod. Several melting points and resolidifications were observed indicating different crystalline forms until at 204–205°C dihydrazide VIII finally melted completely. Infrared spectra of samples taken during and at the end of the melting point determinations showed that dihydrazide VIII did not change chemically during the heating process.

It is interesting to note that efforts to recrystallize VIII from acetone gave mono(*N*-isopropylidene)bis(*p*-carbohydrazidophenyl)diphenylsilane (IX) instead.

Dipentachlorophenyl terephthalate (X) and dipentachlorophenyl isophthalate (XI) were prepared in high yield from the reaction of pentachlorophenol with terephthaloyl chloride or isophthaloyl chloride in the presence of triethylamine.

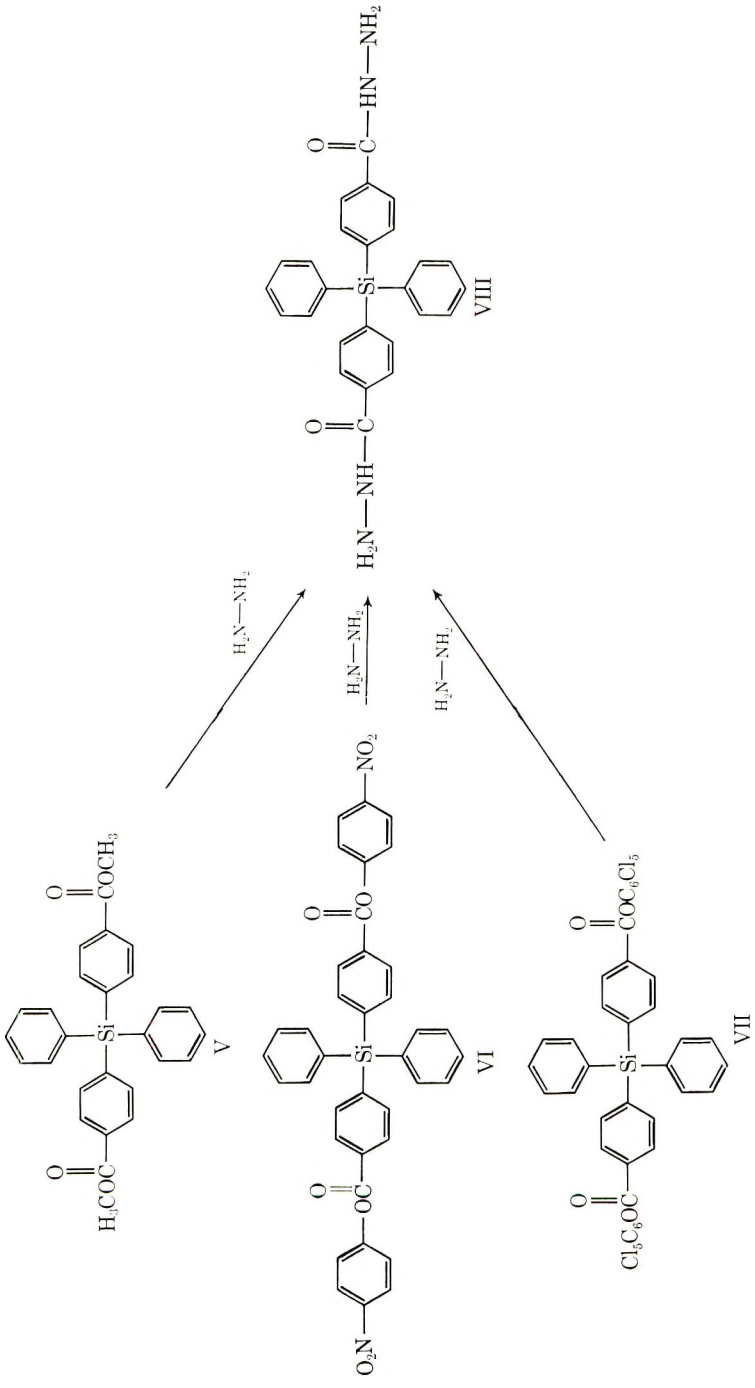

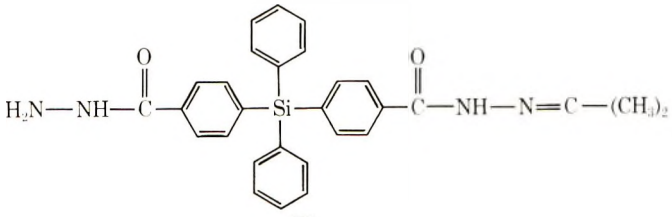

IX

The preparation of X and XI by esterification of terephthalic acid and isophthalic acid with pentachlorophenol, with the use of dicyclohexylcarbodiimide to dehydrate, was found to be too slow because of the low solubility of the acids in the solvent. The separation of diesters X and XI from the dicyclohexylurea by-product was laborious.

Polymer Synthesis

Poly[1,4-phenylene(diphenylsilyl)-1,4-phenylene-2,5-(1,3,4-oxadiazole)] (I). Dihydrazide VIII was interacted with diacid chloride IV, or diester VII to form poly[*N*-(*p*-diphenylsilylbenzoyl)-*N'*-(*p*-benzoyl) hydrazide] (XII) with inherent viscosities of 0.37 and 0.59, respectively. The polymer

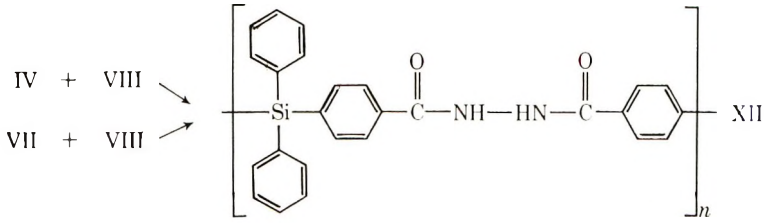

XII $\xrightarrow{\Delta}$ I

samples were converted by thermal cyclodehydration into the poly(1,3,4-oxadiazole (I). The sample of I prepared from IV had inherent viscosities in chloroform and pyridine of 0.32 and 0.19, respectively. The specimen synthesized from VII was completely soluble in pyridine and dissolved only partially in chloroform. The inherent viscosity of the pyridine solution was 0.37. It appears from several measurements that the solubility of polymer I in chloroform is limited to molecular weights corresponding to an inherent viscosity of 0.38 (0.29 in pyridine). When a film of the material of inherent viscosity 0.38 was cast from chloroform solution and heated at atmospheric pressure for about 1 hr at 290–300°C. its inherent viscosity was increased to 0.43 in pyridine. A comparison of the results with previous data indicates that both specimens prepared by the new methods had higher molecular weights than the sample made according to the earlier procedure.[2] It is interesting to note that other samples prepared from diester VII also had higher inherent viscosities than those made from the acid chloride IV. This might be due to the fact that the acid chloride end groups hydrolyzed to form terminal carboxylic acid units

which because of lower reactivity were less able than the ester chain ends to interact further.

During the preparation of several batches of polymer I from the diester it was observed that the reaction temperature was an important factor in obtaining prepolymer XII with high molecular weight. When the reactants in dimethylaniline were quickly heated to reflux rather than gradually raising the temperature, a sample with substantially lower viscosity (0.33) was obtained. Tar formation was observed in a relatively short time when the polymerization reaction was conducted in *N*-methylpyrrolidone, quinoline and diethylaniline.

Poly[1,4-phenylene(diphenylsilyl)-1,4-phenylene-(1,3,4-oxadiazole-2,5-diyl)-1,4-phenylene-2,5-(1,3,4-oxadiazole)] (XIII). A reaction mixture of dihydrazide (VIII) and dipentachlorophenyl terephthalate (X) in dimethylaniline was heated for 65 hr to produce poly[*N*-(*p*-diphenylsilylbenzoyl)-*N'*,*N''*-(terephthaloyl)-*N'''*-(*p*-benzoyl) dihydrazide] (XIV) with inherent viscosity of 0.59 in dimethylacetamide.

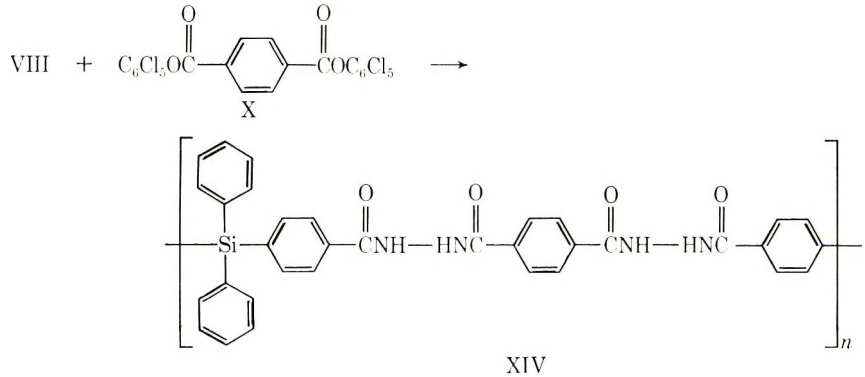

XIV

Polydihydrazide XIV was heated at 280–300°C under reduced pressure to form the poly-1,3,4-oxadiazole (XIII) with inherent viscosity of 0.42 in pyridine. This polymer was completely soluble in pyridine and partially dissolved in chloroform and methylene chloride.

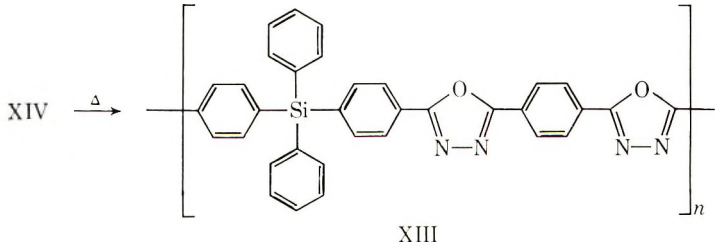

XIII

Poly[1,4-phenylene(diphenylsilyl)-1,4-phenylene-(1,3,4-oxadiazole-2,5-diyl)-1,3-phenylene-2,5-(1,3,4-oxadiazole) (XV). A similar copolymerization of dihydrazide VIII with dipentachlorophenyl isophthalate (XI) in the same solvent for 120 hr yielded poly[*N*-(*p*-diphenylsilylbenzoyl)-

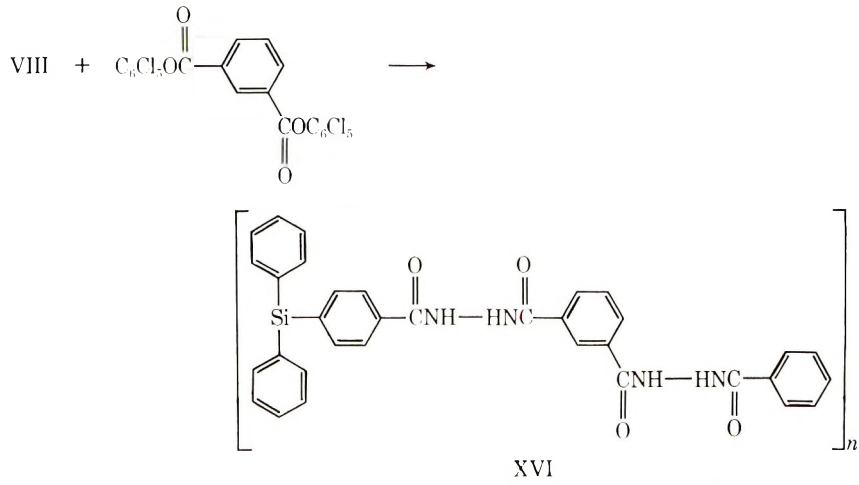

XVI

N,N''-(isophthaloyl)-*N'''*-(*p*-benzoyl)dihydrazide] (XVI) with inherent viscosity of 0.53 in dimethylacetamide.

It is interesting to note, that much longer heating time was required to produce prepolymer XVI with about the same viscosity as polyhydrazide XIV.

The thermocyclodehydration of polyhydrazide XVI at 280–310°C produced the poly(-1,3,4-oxadiazole) (XV) with inherent viscosity of 0.33 in pyridine. When the dehydration was conducted at temperatures below 300°C lower molecular weight samples of XV were obtained which dissolved completely in chloroform and had inherent viscosities of 0.38 and 0.22 in this solvent and pyridine, respectively. This polymer was somewhat less soluble in organic solvents than polyoxadiazoles I and XIII.

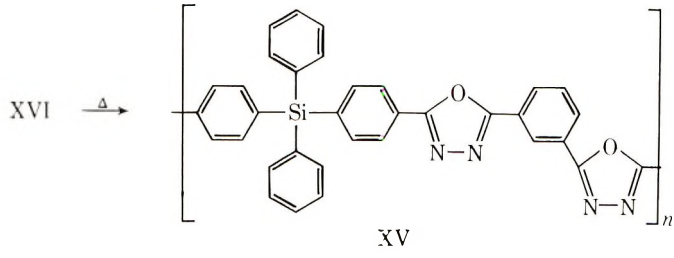

XV

Films of all of the silicon-containing oxadiazoles which were cast from chloroform and methylene chloride solutions exhibited good adhesion to glass and metal surfaces. When these films were heated in air at about 300°C and redissolved, they showed increased inherent viscosity in pyridine and were less soluble in the chlorinated solvents.

Thermal Properties

Thermal Cyclodehydration. TGA thermograms show that polyhydrazides XII, XIV, and XVI lost 0.2–1% of weight, when heated to 100°C. This decrease is attributed to volatilization of adsorbed water.[7] The DTA

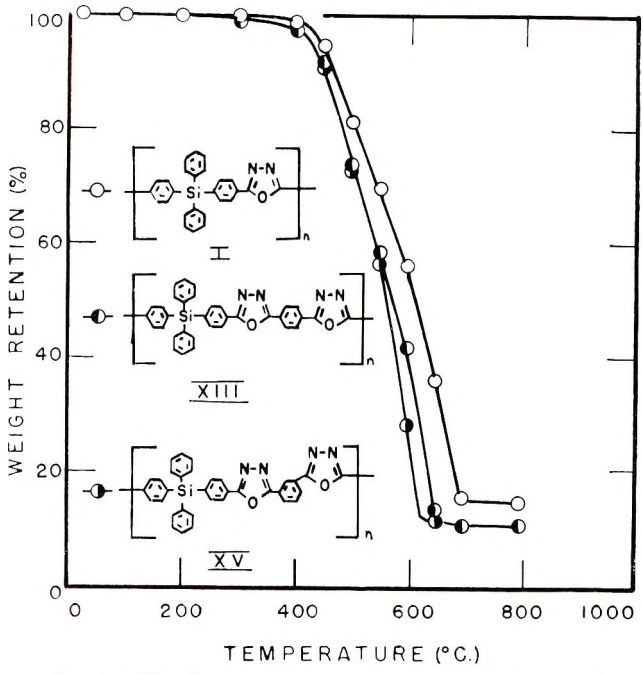

Fig. 1. TGA thermograms: (○) I; (◐) XIII; (◑) XV.

curves show that these polyhydrazides underwent an endothermic transformation at about 280–340°C that is associated with the thermocyclodehydration of the polymers. This is substantiated by TGA data which show that the polymers underwent weight losses that correspond to the amount of water produced from the cyclodehydration process.

Heat Stability. Figure 1 presents the TGA thermograms made from polyoxadiazoles I, XIII, and XV. The results indicate that all of the polymers underwent no weight loss due to decomposition when heated to 350°C. Above this temperature the products lost weight very slowly to about 425°C, and then the rate of decrease became more rapid. This suggests that the polymers might be useful for extended time periods at 350°C and for shorter time intervals at higher temperatures. The DTA thermograms of the polymers are presented in Figure 2. Results show that the polymers underwent no changes below the temperature at which decomposition began. Polymer I started to undergo an exothermic change at about 410°C, while XIII and XV began such transformations at approximately 380°C. These data agree with TGA results which indicated that polymer I was slightly more heat-stable than polymers XIII and XV. All of the thermograms exhibit exothermic peaks at about 500°C and 580°C. From studies made by other investigators,[8,9] these exothermic peaks are attributed to the decomposition of oxadiazole rings, and diphenylsilarylene units, respectively. The exothermic peaks and shoulders occurring at temperatures above 600°C are probably associated with further thermal oxidation of residual decomposition products.

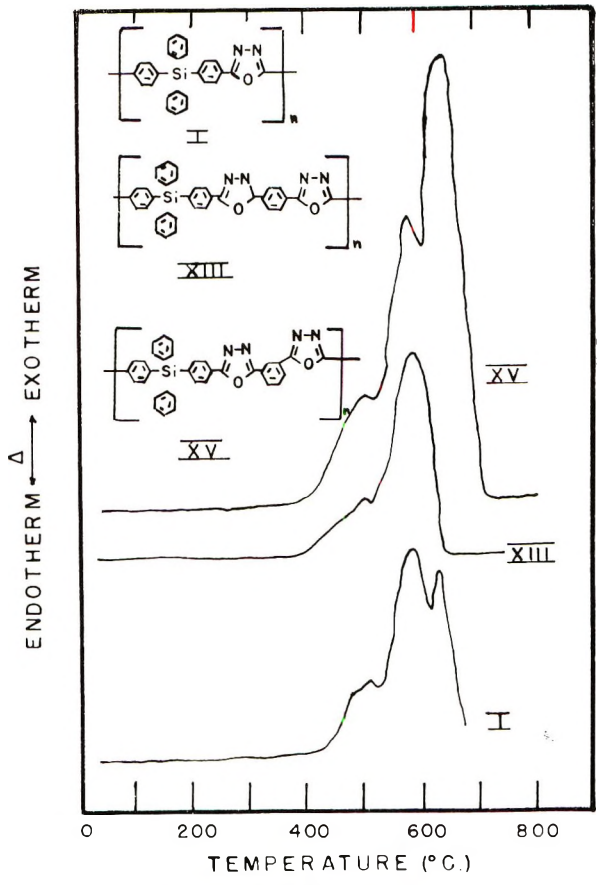

Fig. 2. DTA thermograms.

Polyoxadiazoles I, XIII, and XV underwent no weight loss when heated in air for 6 hr at 300°C. After 6 hr at 350°C, polyoxadiazoles I, XIII, and XV showed weight decreases of 0.5, 1.8, and 1.7%, respectively. Over the same time period at 400°C, these products exhibited weight losses of 14.0, 14.3, and 16.5%, respectively. Once again, as in the case of the TGA and DTA experiments, the results suggest that polymer I is slightly more heat-stable than polyoxadiazoles XIII and XV.

Films of the polymers cast from solutions onto aluminum foil and heated for 25 hr in air at 350°C and then for 6 hr at 400°C showed only slight discoloration, excellent adhesion to the substrate, and did not crack when flexed manually. Films on sodium chloride crystals when heated similarly showed no change when their infrared spectra were compared with those of the original polymers, except for the development of a very weak peak at 4.48 μ. The appearance of this new band is ascribed[3,9] to the formation of small quantities of isocyanate or nitrile groups due to the decomposition of some of the oxadiazole rings in the backbone or chain ends of the molecules.

EXPERIMENTAL

Infrared Spectroscopy

Perkin-Elmer model 337, grating infrared spectrophotometer equipped with sodium chloride optics was employed to make spectra from solution cast films and Nujol mulls of the products over the region of 2.5–15.0 μ.

Melting Point

Thomas-Hoover and Vandercamp equipment was used to obtain uncorrected melting point measurements of the intermediate compounds.

Elemental Analysis

The products were analyzed by the Schwarzkopf Microanalytical Laboratories, Woodside, New York.

Viscosity

Inherent viscosity of the hydrazide prepolymers was determined at 30°C from dimethylacetamide solutions containing 0.2% of polymer and 5% lithium chloride. Similar measurements of the polyoxadiazoles were made from chloroform and pyridine solutions containing 0.2% of polymer.

Solvents

N,*N*-Dimethylaniline and *N*-methylpyrrolidone were distilled before they were used for the synthesis of polyhydrazides.

Thermal Analysis

Resistance of the polymers to thermal decomposition in air was determined by thermogravimetric (TGA), differential thermal (DTA), and isothermogravimetric (IGA) analysis techniques as described before.[3] Before making TGA and IGA determinations of solution cast films, they were preheated in air for about 30 min at 290–300°C to remove any adsorbed moisture and solvent.

Synthesis of Intermediate Compounds

Diphenyldi(*p*-tolyl)silane (II). This was prepared by the method of Maienthal et al.[10]

Bis(*p*-carboxyphenyl)diphenylsilane (III). A modification of the procedure described earlier[2] was used to prepare III. To a vigorously stirred mixture of 90 ml of glacial acetic acid, 30 ml of acetic anhydride, and 7.2 ml of concentrated sulfuric acid cooled to +10°C was added about 1.5 g of chromic anhydride. After a short while, about 0.3 g of II was added. This sequence was repeated until a total of 12 g (0.12 mole) of chromic anhydride and 4.4 g (0.012 mole) of II was alternately added over 50 min while maintaining the temperature at 13–15°C. Stirring was continued for another 75 min while not allowing the temperature to rise above 17°C.

The reaction mixture was poured over crushed ice and stirred vigorously for 1 hr. The solidified product was filtered and washed several times with water to a pale color, and then dissolved in ether. The ether solution was separated from a gummy residue, dried over anhydrous magnesium sulfate, and filtered. The drying agent was washed thoroughly with ether. The filtrate and washings were combined and concentrated under vacuum until crystals started to form. Then petroleum ether (bp 37–48°C) was added in excess, and 3.63 g (71% yield) of crude dicarboxylic acid III was isolated, mp 258–262°C. The crude product was dissolved in ether and petroleum ether was added until the solution became faintly cloudy. The solution was treated with charcoal, filtered, concentrated until crystals appeared, diluted with an equal volume of petroleum ether, and filtered to give pure III, mp 266–268°C.

A modification of Speck's procedure[6] was also used to obtain III. To a boiling solution of 3.64 g (0.01 mole) of II in 40 ml of aqueous pyridine (70%) was added 7.95 g (0.05 mole) of potassium permanganate over 70 min with vigorous stirring. Reflux was continued for another hour. Then excess oxidant, if any, was destroyed by adding 2 ml of methyl alcohol. The solution was filtered, and the residue was washed with 10 ml of water. The combined filtrate and washing was poured over ice and acidified to pH 2. The precipitate was separated by filtration and washed thoroughly with water. Additional dicarboxylic acid III was recovered by converting the manganese dioxide residue to the water-soluble sulfate with aqueous sodium hydrosulfite and hydrochloric acid, and separating the insoluble dicarboxylic acid III by filtration. The fractions of III were combined, worked up as above to isolate 3.09 g (73% yield) of crude product, mp 254–258°C, and recrystallized, mp 266–268°C. The infrared spectrum of the products prepared by both procedures were identical with that of a sample made previously.[2]

Bis(*p*-carbopentachlorophenoxyphenyl)diphenylsilane (VII). To a solution of 1.198 g (4.5 mmole) of pentachlorophenol and 0.56 ml (4 mmole) of triethylamine in 15 ml of methylene chloride was added 0.901 g (1.95 mmole) of bis(*p*-chlorocarbonylphenyl)diphenylsilane (IV)[2] dissolved in 10 ml of the same solvent. After standing at room temperature for 3 hr, the clear solution was concentrated under vacuum to about 10 ml, heated to boiling temperature, diluted with 50 ml of ethyl acetate, and cooled in an ice bath. The crystalline mixture was filtered, washed with ethyl acetate, and triturated with 75 ml of benzene to dissolve pentachlorophenyl ester VII. The insoluble triethylamine salt was discarded. The benzene solution was concentrated to 5 ml, diluted with 90 ml of acetone, and cooled in an ice bath to recover 1.02 g of VII, mp 268–270°C. The methylene chloride–ethyl acetate mother liquor was evaporated to dryness, and the crystalline residue was washed with hot acetone to obtain an additional 0.335 g of the insoluble diester VII, mp 262–264°C., for a total yield of 75%. The melting point of the crude product was raised to 269–271°C[2] by recrystallization from a 1:10 mixture of benzene and ethyl acetate.

The infrared spectrum was identical with that of a sample of VII synthesized previously[2] by another method.

Bis(*p*-carbohydrazidophenyl)diphenylsilane (VIII). To a vigorously stirred boiling solution of 9 ml of 97% hydrazine in 270 ml of dry methyl alcohol was added over 20 min 3.6 g (3.9 mmole) of pentachlorophenyl ester VII. The mixture was refluxed for 2 hr, and the clear solution was allowed to stand overnight at room temperature and for 1 hr in ice. The crystals that separated were filtered and washed with benzene and ice-cold methyl alcohol to give 1.7 g (96% yield) of crude VIII, mp 170–172°C. In 24 hr the melting point changed to 202–203°C. Several melting points and resolidifications were observed before dihydrazide VIII finally melted. The dihydrazide was recrystallized from dimethylacetamide and ethyl alcohol (1:10) or tetrahydrofuran and benzene (1:10) and dried at 100°C, mp 204–205°C. As in the case of the crude material, the purified crystals went through a series of transformations during the melting point determination: softening at 114–116°C, solidifying at 140°C, softening again at 172–174°C, resolidifying at 175°C, and finally melting at 204–205°C. When dihydrazide VIII was heated to 180°C and allowed to cool to room temperature, it melted at 204–205°C without any intermediate changes. Infrared spectral data indicated that the product was not chemically changed when heated during the melting point determination. The transformations, including the final melting point, were observed only when a thin glass rod was inserted into the melting point tube containing a sample of VIII. During the heating process the rod was constantly moved while in contact with the sample. When the melting point of VIII was determined by the conventional method it softened at 110–118°C and liquified slowly, becoming clear at about 200°C.

ANAL. Calcd for $C_{26}H_{24}N_4O_2Si$: C, 69.00%; H, 5.34%; N, 12.38%; Si, 6.20%. Found: C, 68.91%; H, 6.03%; N, 12.01%; Si, 6.13%.

VIII was also prepared by adding in small portions 2.18 g (3.27 mmole) of *p*-nitrophenyl ester VI[2] to a mixture of 5 ml of 97% hydrazine, 200 ml of dry methyl alcohol, and 15 ml of benzene. A clear solution was obtained after refluxing the reaction mixture for 15 min. Refluxing was continued for 2 hr. After standing at room temperature for 20 hr and in ice for 1 hr, 1.33 g (90% yield) of VIII was recovered, mp 200–202°C.

VIII was similarly prepared by refluxing 1 g (2.2 mmole) of dimethyl ester V with 1.5 ml of 97% hydrazine in 8 ml of dry methyl alcohol for 3 hr. Heavy crystal separation was observed after the reaction mixture was at room temperature for 20 min. On cooling the mixture in an ice bath, 900 mg (90% yield) of VIII, was separated, mp 200–202°C.

When dihydrazide VIII was triturated at room temperature with acetone, it dissolved and, after a few seconds, crystalline mono(*N*-isopropylidene)-bis(*p*-carbohydrazidophenyl)diphenylsilane (IX), mp 298–300°C, separated. IX was recrystallized from dimethylacetamide, mp 305–306°C. The same product in analytically pure form crystallized when acetone was

added to dihydrazide VIII in tetrahydrofuran and the solution was refluxed for a few minutes.

ANAL. Calcd for $C_{29}H_{28}N_4O_2Si$: C, 70.72%; H, 5.73%; N, 11.38%; Si, 5.70%. Found: C, 71.11%; H, 6.41%; N, 11.43%; Si, 5.70%.

Dipentachlorophenyl Terephthalate (X). A solution of 2.03 g (0.01 mole) of terephthaloyl chloride in 40 ml of methylene chloride was added to 6.66 g (0.025 mole) of pentachlorophenol and 2.93 ml (0.021 mole) of triethylamine in 80 ml of methylene chloride, and a heavy precipitate formed immediately. The crystalline product was separated by filtration and washed with methylene chloride to produce 6.1 g (92% yield) of X, mp 328–330°C. X was recrystallized from boiling xylene, mp 334–336°C (decomp.) (measured in a Vandercamp apparatus preheated to 230°C.). The infrared spectrum of X showed a peak at 5.67 μ that is characteristic of the pentachlorophenyl ester group.

ANAL. Calcd for $C_{20}H_4Cl_{10}O_4$: C, 36.24%; H, 0.61%; Cl, 53.50%. Found: C, 36.58%; H, 0.75%; Cl, 53.65%.

X was also synthesized by adding 2.06 g (0.01 mole) of dicyclohexylcarbodiimide in 15 ml of dry ethyl acetate to a solution of 2.66 g (0.01 mole) of pentachlorophenol in 15 ml of dry ethyl acetate. After standing at room temperature for 10 min, a suspension of 0.42 g (0.0025 mole) of terephthalic acid in 90 ml of ethyl acetate was added to the reaction mixture. The mixture was refluxed for 26 hr and filtered. The insoluble fraction was washed with ethyl acetate, large quantities of hot chloroform, and tetrahydrofuran to remove the dicyclohexylurea by-product and leave 0.90 g (54% yield) of the ester X, mp 320–326°C. X was recrystallized from a mixture of benzene and tetrahydrofuran (2.5:1), mp 334–336°C, softens at 304–306°C.

Dipentachlorophenyl Isophthalate (XI). Diester XI was prepared in 94% yield from isophthaloyl chloride and pentachlorophenol according to the procedure described for the preparation of X. The crude product, mp 258–268°C was recrystallized from boiling xylene, mp 296–298°C (determined in a Vandercamp apparatus, preheated to 230°C). The infrared spectrum of XI showed the characteristic ester peak at 5.65 μ.

ANAL. Calcd for $C_{20}H_4Cl_{10}O_4$: C, 36.24%; H, 0.61%; Cl, 53.50%. Found: C, 36.47%; H, 0.67%; Cl, 53.48%.

X1 was also prepared by adding 24.75 g (0.12 mole) of dicyclohexylcarbodiimide in 200 ml of ethyl acetate to a stirred solution of 31.92 g (0.12 mole) of pentachlorophenol in 150 ml of the same solvent. After standing at room temperature for 10 min, 4.98 g (0.03 mole) of isophthalic acid was added to the reaction mixture in small portions. The mixture was diluted with 150 ml of solvent and refluxed for 20 hr. The solid reaction products were separated and washed several times with tetrahydrofuran to dissolve most of the dicyclohexylurea by-product. The insoluble residue was dissolved in 600 ml of boiling xylene and the solution was cooled to

70°C. The remainder of the dicyclohexylurea, that separated out was filtered off and discarded. After several hours, a crystalline precipitate formed and was isolated by filtration to give 10 g (50% yield) of XI, mp 280-286°C. XI was recrystallized from xylene, mp 296–297°C.

Synthesis of Polymers

Poly[*N*-(*p*-diphenylsilylbenzoyl)*N'*-(*p*-benzoyl)hydrazide] (XII). A mixture of 2.763 g (3 mmole) of pentachlorophenyl ester VII and 1.358 g (3 mmole) of dihydrazide VIII in 65 ml of dimethylaniline was heated with constant stirring under nitrogen in a Wood's metal bath at 135–140°C for 2 hr, during which time the solution cleared. Gel formation occurred while the solution was then heated at 155–160°C for 19 hr. The reaction mixture was diluted with 16 ml of dimethylaniline and then heated for 74 hr at 178–183°C, and finally refluxed for 48 hr. After cooling to room temperature, the precipitate was separated by filtration and washed with ethyl acetate, methyl alcohol, and methylene chloride to obtain 2 g (79% yield) of polyhydrazide XII with inherent viscosity of 0.59. XII is soluble in dimethylacetamide, dimethylformamide, pyridine, and dimethyl sulfoxide. The infrared spectrum of polyhydrazide XII was identical with that of a sample prepared previously by another method.[2]

ANAL. Calcd for $(C_{26}H_{20}N_2O_2Si)_n$: C, 74.26%; H, 4.79%; N, 6.66%; Si, 6.68%. Found: C, 74.01%; H, 5.15%; N, 6.67%; Si, 6.50%.

Tar formation was observed with dihydrazide VIII and dipentachlorophenyl ester VII in diethylaniline were refluxed for 12 hr and worked up to obtain a 61% yield of polyhydrazide XII with inherent viscosity of 0.36.

XII was also synthesized by adding 461.4 mg (1 mmole) of acid chloride IV in 15 ml of *N*-methylpyrrolidone to a stirred, ice-cooled solution of 452.6 mg (1 mmole) of dihydrazide VIII and 0.28 ml (2 mmole) of triethylamine in 20 ml of the same solvent. Triethylamine hydrochloride began to separate immediately. The reaction mixture was stirred for 1 hr in an ice bath and at room temperature for 20 hr. To esterify the acid chloride endgroups, 12 ml of dry methyl alcohol was added, and the resulting clear solution was allowed to stand at room temperature for 1 hr. It was then poured into 600 ml of water and the mixture was stirred for 1 hr. The precipitate was separated by filtration and washed with water, methyl alcohol, tetrahydrofuran, and petroleum ether to obtain 832 mg (99% yield) of polyhydrazide XII with inherent viscosity of 0.37. The material was dried at 100°C for elemental analysis.

ANAL. Calcd for $(C_{26}H_{20}N_2O_2Si \cdot 0.5H_2O)_n$: C, 72.70%; H, 4.92%; N, 6.52%; Si, 6.53%. Found: C, 72.67%; H, 5.28%; N, 6.34%; Si, 6.38%.

Poly[*N*-(*p*-diphenylsilylbenzoyl)-*N'*,*N''*-(terephthaloyl)-*N'''*-(*p*-benzoyl)dihydrazide] (XIV). A well stirred suspension of 0.905 g (2 mmole) of dihydrazide VIII and 1.325 g (2 mmole) of terephthalate X in 44 ml of dimethylaniline was heated under nitrogen for 1 hr at 135–140°C in a

Wood's metal bath. The reaction mixture was then heated at 158–160°C for 16 hr, during which time a precipitate was formed. Then 10 ml of dimethylaniline was added, the mixture was heated at 178–180°C for 24 hr and then refluxed for 24 hr, during which time the precipitate dissolved. On cooling to room temperature, a light beige precipitate formed, which was isolated by filtration, and washed with methyl alcohol and ethyl acetate to produce 1.1 g (94% yield) of polyhydrazide XIV with inherent viscosity of 0.59. XIV was soluble in the same solvents as XII. The infrared spectrum of XIV exhibited amide I and amide II peaks at 6.08 and 6.40 μ, respectively, and silicon-phenyl vibrations at 7.0 and 9.0 μ. Polymer XIV was dried at 100°C under reduced pressure for analysis.

ANAL. Calcd for $(C_{34}H_{26}N_4O_4Si \cdot H_2O)_n$: C, 67.98%; H, 4.69%; N, 9.32%; Si, 4.67%. Found: C, 67.70%; H, 4.89%; N, 8.78%; Si, 4.85%.

Poly[*N*-*p*(-diphenylsilylbenzoyl)-*N'*,*N''*-(isophthaloyl)-*N'''*-(*p*-benzoyl)-dihydrazide] (XVI). A stirred mixture of 1.358 g (3 mmole) of dihydrazide VIII and 1.988 g (3 mmole) of isophthalate XI in 66 ml of dimethylaniline was gradually heated under nitrogen in a Wood's metal bath to 130–135°C. Within 30 min a clear solution was obtained. Then the bath temperature was raised to 150–155°C and after 0.5 hr it was increased to 180–185°C. and maintained for 112 hr. Finally, the mixture was refluxed for 7 hr and allowed to stand overnight at room temperature. The liquid portion was decanted and a very hard film remaining on the walls of the reaction flask was removed, pulverized, and washed with methyl alcohol, ethyl acetate, and ether to give 1.54 g (88% yield) of polyhydrazide XVI with inherent viscosity of 0.53. The polymer was soluble in the same solvents as polyhydrazides XII and XIV. The infrared spectrum of XVI showed peaks at 6.06 and 6.45 μ for amide I and amide II linkages, respectively, and at 7.0 and 9.0 μ for silicon-phenyl bonds. Polymer XVI was dried under reduced pressure at 100°C before analysis.

ANAL. Calcd for $(C_{34}H_{26}N_4O_4Si)_n$: C, 70.08%; H, 4.49%; N, 9.61%; Si, 4.82%. Found: C, 70.09%; H, 4.87%; N, 9.38%; Si, 4.90%.

Poly[1,4-phenylene(diphenylsilyl)-1,4-phenylene-2,5-(1,3,4-oxadiazole)] (I). At 1 mm pressure, a 500-mg sample of polyhydrazide XII with an inherent viscosity of 0.55, and containing pentachlorophenyl chain ends, was heated in a Wood's metal bath at 160–170°C for 40 min, at 280–290°C for 2 hr, and finally at 300–310°C for 3 hr to produce polyoxadiazole I with inherent viscosity in pyridine of 0.37. The polymer was only partially soluble in chloroform. The infrared spectrum of I and that of a sample prepared previously by another method[2] were identical.

ANAL. Calcd for $(C_{26}H_{18}N_2OSi)_n$: C, 77.58%; H, 4.50%; N, 6.96%; Si, 6.98%. Found: C, 77.08%; H, 4.62%; N, 6.87%; Si, 7.22%.

When a sample of the polymer with inherent viscosity of 0.37 was heated, in an open test tube with constant stirring for 1 hr at 290–300°C, the viscosity increased to 0.43.

ANAL. Calcd for $(C_{26}H_{18}N_2OSi)_n$: Si, 6.98%; Found: Si, 7.26%.

The trituration with chloroform of a sample of polyoxadiazole I with inherent viscosity in pyridine of 0.32 dissolved 81% of the polymer. The soluble fraction had inherent viscosities of 0.38 and 0.29 in chloroform and pyridine, respectively. The chloroform-insoluble portion had an inherent viscosity of 0.45 in pyridine. When the chloroform-soluble fraction was heated at 290–300°C for 50 min at atmospheric pressure, its inherent viscosity in pyridine increased from 0.29 to 0.43.

Polyoxadiazole I with inherent viscosities of 0.32 and 0.19 in chloroform and pyridine, respectively, was prepared from a sample of polyhydrazide XII, which was obtained from the acid chloride IV, and had an inherent viscosity of 0.37. XII was heated under reduced pressure (1 mm) at 165–175°C for 40 min, at 280–290°C for 2 hr, at 290–300°C for 5 hr, and finally at 300–310°C for 6 hr.

ANAL. Calcd for $(C_{26}H_{18}N_2OSi)_n$: C, 77.58%; H, 4.50%; N, 6.96%; Si, 6.98%. Found: C, 78.01%; H, 4.14%; N, 6.72%; Si, 6.92%.

When a sample of the same polyoxadiazole I was heated to 315–322°C in air, it softened and could be formed into a thread with a glass rod. Within 3 hr at this temperature range the sample hardened and its silicon content increased from 6.92 to 7.45%.

Poly[1,4-phenylene(diphenylsilyl)-1,4-phenylene-(1,3,4-oxadiazole-2,5-diyl)-1,4-phenylene-2,5-(1,3,4-oxadiazole)] (XIII). This polymer was made by heating a 200-mg sample of polyhydrazide XIV, with an inherent viscosity of 0.59, at 1 mm pressure in a Wood's metal bath at 150–160°C for 75 min, at 280–290°C for 5 hr, and at 290–300°C for 6 hr. The light beige polymer was completely soluble in pyridine and dissolved partially in chloroform and in methylene chloride. It had an inherent viscosity of 0.42 in pyridine. The infrared spectrum of the product showed a broad doublet at 6.37 and 6.5 μ and a peak at 10.4 μ that is associated with the oxadiazole structure, and vibration frequencies at 7.0 and 8.9 μ that is attributed to silicon-phenyl binding.

ANAL. Calcd for $(C_{34}H_{22}N_4O_2Si)_n$: C, 74.71%; H, 4.06%; N, 10.25%; Si, 5.13%. Found: C, 75.51%; H, 4.14%; N, 9.85%; Si, 5.17%.

When a chloroform-soluble fraction of polyoxadiazole XIII was cast, a flexible film formed from which adsorbed moisture could not be removed completely by heating it under reduced pressure at a 100°C. The water was removed by heating the film for several minutes at 300°C. After 1 hr at 290–310°C the polymer became insoluble in chloroform without cross-linking, and its inherent viscosity in pyridine increased from 0.28 to 0.32.

ANAL. Calcd for $(C_{34}H_{22}N_4O_2Si)_n$: Si, 5.13%. Found: Si, 5.14%.

Poly[1,4-phenylene(diphenylsilyl)-1,4-phenylene-(1,3,4-oxadiazole-2,5-diyl)-1,3-phenylene-2,5-(1,3,4-oxadiazole)] (XV). A 200-mg sample of polyhydrazide XVI with inherent viscosity of 0.53 was heated at 1 mm pressure for 20 min at 150–160°C, 3.5 hr at 280–290°C, 4 hr at 290–300°C and finally 4 hr at 300–310°C, to form the poly(1,3,4-oxadiazole) (XV)

with inherent viscosity in pyridine of 0.33. This sample of the polymer was partially soluble in chloroform and dissolved slowly in hot pyridine. A chloroform-soluble specimen with inherent viscosities in chloroform and pyridine of 0.38 and 0.22, respectively, was obtained when polyhydrazide XVI was heated for 2 hr at 150–160°C, 7 hr at 280–290°C, and 6 hr at 290–300°C.

ANAL. Calcd for $(C_{34}H_{22}N_4O_2Si)_n$: C, 74.71%; H, 4.06%; N, 10.25%; Si, 5.13%. Found: C, 74.39%; H, 4.27%; N, 10.06%; Si, 5.15%.

The inherent viscosity of a sample of polyoxadiazole XV was increased from 0.22 to 0.29 in pyridine when it was heated in air at 290–300°C for 45 min.

ANAL. Calcd for $(C_{34}H_{22}N_4O_2Si)_n$: Si, 5.13%. Found: Si, 5.11%.

When a specimen of polyoxadiazole XV was heated under reduced pressure for 10 min at 340°C, it was found to be 80% soluble in chloroform and had an inherent viscosity 0.22 in pyridine. An additional 9% of the polymer was dissolved by triturating with pyridine. The inherent viscosity of the latter fraction was 0.37 in pyridine.

The authors are grateful to Jack Mironov for preparing the DTA thermograms.

The opinions or assertions contained in this paper are the private ones of the authors and are not to be construed as official or reflecting the views of the Naval Service at large.

References

1. H. Nagy Kovacs, A. D. Delman, and B. B. Simms, *J. Polym. Sci. A-1*, **4**, 1081 (1966).
2. H. Nagy Kovacs, A. D. Delman, and B. B. Simms, *J. Polym. Sci. A-1*, **6**, 2103 (1968).
3. A. D. Delman, H. Nagy Kovacs, and B. B. Simms, *J. Polym. Sci. A-1*, **6**, 2117 (1968).
4. A. H. Frazer and F. T. Wallenberger, *J. Polym. Sci. A*, **2**, 1147 (1964).
5. A. H. Frazer and D. R. Wilson, paper presented at American Chemical Society Meeting, September 1968, Atlantic City; *Polymer Preprints*, **9**, No. 2, 1150 (1968).
6. S. B. Speck, U. S. Pat. 2,722,524 (Nov. 1, 1955).
7. A. H. Frazer and I. M. Sarasohn, *J. Polym. Sci. A-1*, **4**, 1649 (1966).
8. G. P. Brown, J. A. Hill, and C. B. Murphy, *J. Polym. Sci.*, **55**, 419 (1961).
9. J. L. Cotter and G. J. Knight, *Chem. Commun.*, **1966**, 336.
10. M. Maienthal, M. Hellmann, C. P. Haber, L. A. Hymo, S. Carpenter, and A. J. Carr, *J. Amer. Chem. Soc.*, **76**, 6392 (1954).

Received August 20, 1969
Revised August 20, 1969

JOURNAL OF POLYMER SCIENCE: PART A-1 VOL. 8, 885–899 (1970)

Studies on Monomer Reactivity Ratios. I. An Electronegativity Model

JAMES R. HOYLAND, *Battelle Memorial Institute, Columbus Laboratories, Columbus, Ohio 43201*

Synopsis

A model based on an electronegativity scheme is proposed for treatment of monomer reactivity ratios in free-radical bulk copolymerization. Values for each monomer are assigned to three parameters: a relative localization (or resonance stabilization) energy, a radical electronegativity, and a monomer electronegativity. Parameters for 17 monomers are given and calculated reactivity ratios are tabulated for a large number of copolymerizations. Agreement with experiment is usually obtained to within experimental error except for systems involving acrylonitrile. Computed parameters are rationalized on the basis of molecular orbital theory.

INTRODUCTION

The calculation of monomer reactivity ratios in free-radical polymerization represents an extreme challenge to the theoretician in that any approach taken is beset with both obvious and hidden pitfalls. Ideally, one wishes to compute the free energies of activation ΔF_{11}^* and ΔF_{12}^* for the reactions

$$\begin{aligned} \text{—}M_1\cdot + M_1 &\rightarrow \text{—}M_1\cdot \\ \text{—}M_1\cdot + M_2 &\rightarrow \text{—}M_2\cdot \end{aligned} \qquad (1)$$

and set $r_1 = \exp\{-(\Delta F_{11}^* - \Delta F_{12}^*)/RT\}$. This formulation does not lend itself to practical calculations, since one cannot, in general, compute the entropy of activation. Therefore, the usual assumption is made that the activation entropies are about the same for the two reactions and that the free-energy terms can be replaced by enthalpies of activation. One must therefore exclude from any attempted calculation reactions in which steric effects are known to be of considerable importance. Furthermore, penultimate effects of necessity are neglected. These are obvious difficulties but there are other more subtle points which may be raised. The most important of these is whether there is only one mode of attack of the monomers M_1 and M_2 leading to a single low-lying transition state, or whether there are several possible modes leadng to transition states of rather comparable energy. This latter question could be answered if it were possible to carry out a complete study of the reaction energy surface as a function of all possible geometric variables. Unfortunately, this is not possible at least

from an *ab initio* standpoint. Therefore, previous investigators have resorted to empirical studies based for the most part on the familiar π-electron Hückel theory. At best such an approach can allow a correlation to be drawn between observed reactivity ratios and some computed reactivity index. For example, Hayashi et al.[1] found that there appeared to be a definite correlation between the increased π-electron conjugation energy in a radical–monomer pair and reactivity. Levinson[2] improved these calculations and studied a greater number of monomer pairs. Large errors were found in many calculated values, however, and such a method is far from predictive. A more pragmatic approach is needed if quantitative prediction is desired. The familiar Q–e scheme[3] can be thought of as such an approach in that theoretical intuition guided the selection of a model which was then tested as to its ability to account for experimental data.

The original interpretation of the Q–e parameters was that Q is related to resonance stabilization of the radical and the product, e_1e_2 can be thought of as the attraction or repulsion of static charges. As such, Q should be related to the localization energy of the vinyl group double bond. Such an interpretation has been made by Fueno et al.[4] and by Levinson.[2] An equally plausible correlation has been made by Lüssi[5] between Q and the π-electron bond order of the vinyl group. The significance of the e values is more difficult to ascertain and the original interpretation has not persisted. No really satisfactory correlation has been developed for this parameter. Levinson[2] has suggested that the e value may be related to the average electron affinity of the monomer and the corresponding radical but this seems doubtful. This point will be discussed later in further detail.

The Q–e scheme has served as the main instrument for interpretation and calculation of reactivity ratios since its inception. This is due to its inherent simplicity and the fact that it is capable of giving a fairly good qualitative picture of the trends of reactivity ratios. It is not accurate enough to provide a quantitative treatment, however, even if the relatively large experimental errors are taken into account. This and the following paper serve to offer two alternatives to the Q–e scheme which are somewhat more sophisticated, are more accurate for prediction of reactivity ratios, but simple enough to be generally applicable.

ELECTRONEGATIVITY MODEL

The concept of electronegativity originated in the work of Pauling,[6] who pointed out that, in general, there is an enhancement of the bond strength of a diatomic molecule A—B over the additive mean of the bond energies of A—A and B—B. This led to the postulate that this enhancement is related to the absolute value of the difference of the electronegativities of the two atoms in question. A precise definition cannot be given to this quantity, but intuitively it is a measure of the electron-attracting power of an atom or molecule. Large differences in electronegativities between the two atoms of a diatomic molecule imply a stabilization brought about by

charge transfer or the mixing of ionic configurations into the wave function thereby lowering the energy of the molecule.

We wish to apply this same concept to the prediction of monomer reactivity ratios. In this case it is postulated that the energy of a transition state for the reaction $—M_a\cdot + M_b$ will be lowered if there is a significant difference in the electronegativities of the radical $—M_a\cdot$ and the monomer M_b. We further assume that the other important effect in lowering this transition state energy is the resonance stabilization of the radical $—M_b\cdot$ which is formed or, alternatively, the localization energy of the monomer M_b. For a given monomer pair M_1 and M_2 we therefore postulate that the r_1r_2 following equations can be written for the reactivity ratios r_1 and r_2:

$$\log r_1 = L(2) - L(1) + |X_R(1) - X_M(1)| - |X_R(1) - X_M(2)| \quad (2)$$

$$\log r_2 = L(1) - L(2) + |X_R(2) - X_M(2)| - |X_R(2) - X_M(1)| \quad (3)$$

where L is a relative localization energy of the monomers, X_R is the radical electronegativity, and X_M is the monomer electronegativity. It is arbitrarily assumed that L and X_R are equal to zero for styrene in order to define a starting point.

The parameters for the 17 monomers listed in Table I were computed in the following way. Initially parameters for styrene, methyl acrylate, methyl methacrylate, 2-vinylpyridine, and 4-vinylpyridine were found by a numerical least-squares fit using the reported reactivity ratios at 60°C. Probable experimental error was taken into account by assuming any computed reactivity ratio that fell within the error bounds was exact. If this

TABLE I
Parameter Values

Monomer	Monomer abbreviation	L	X_R	X_M
Styrene	ST	0	0	0.126
Methyl acrylate	MA	0.574	0.570	0.818
Methyl methacrylate	MM	−0.014	0.522	0.478
2-Vinylpyridine	2VP	−0.130	0.268	0.236
4-Vinylpyridine	4VP	−0.094	0.324	0.322
Acrylonitrile	AN	0.372	0.834	0.834
p-Methoxystyrene	PMXS	−0.038	<0.016[a]	0.016
p-Chlorostyrene	PCLS	−0.094	0.260	0.182
p-Methylstyrene	PMES	0.016	<0.108[a]	0.108
Methyl vinyl ketone	MVK	0.234	0.620	0.894
2-Methyl-5-vinylpyridine	2M5VP	−0.036	0.184	0.176
Vinyl acetate	VAC	1.326	0.500	0.500
Methacrylonitrile	MAN	0.006	0.700	0.700
Methacrylic acid	MACD	−0.202	0.616	0.720
Methacryloxymethylpentamethyldisiloxane	MMPD	0.076	0.480	0.306
5-Ethyl-2-vinylpyridine	5E2VP	−0.074	0.190	0.142
Vinylidene chloride	VCL2	0.800	0.670	0.350

[a] Insufficient experimental data to determine this value.

failed to occur, the deviation of the computed value from the observed one was set equal to

$$\Delta = \min \left\{ \begin{matrix} |r_{\text{calc}} - r_{\text{exp}} - \epsilon| \\ |r_{\text{calc}} - r_{\text{exp}} + \epsilon| \end{matrix} \right\} \tag{4}$$

where ϵ is the probable experimental error, i.e., the experimental value is $r_{\text{exp}} \pm \epsilon$. The quantity numerically minimized was $\Sigma\Delta^2$. Approximate values for the other 12 monomers were then derived by hand calculation and a final computer refinement was then carried out on all 17 monomers. It is these final refined values which are given in Table I. It should be noted in passing that in the case of vinylidene chloride as monomer 2, one must use an intrinsic value for r_1 which is twice that observed because of symmetry considerations.

DISCUSSION OF RESULTS

Computed reactivity ratios for various monomer pairs are given in Table II, along with the experimental values and those calculated from the Q–e scheme. The Q–e parameters and the experimental data are taken from the literature.[7] The agreement between computed and experimental results is generally to within the observed error bounds, except for systems in which acrylonitrile is one of the monomers. Errors are especially large for the vinylpyridine–acrylonitrile systems. Experimental data scatter in 2-vinylpyridine or 2-methyl-5-vinylpyridine with acrylonitrile is quite large and causes one to be skeptical of data on any of these systems. Penultimate effects are known to exist in the styrene–acrylonitrile system[8] and probably are also operative in the vinylpyridines. It is improbable that they are large enough to cause more than a small fraction of the discrepancies observed since the styrene-acrylonitrile system is well accounted for by the present method. Numerically, the computed values of r_1 for the vinylpyridine–acrylonitrile systems (M_1 is the vinylpyridine) are consistently about twice the lowest observed value which indicates that the rate constant for the reaction of acrylonitrile with a vinyl pyridine radical is anomalously large. No explanation for this effect is obvious.

A comparison of results computed by the Q–e scheme, the present method, and experimental values shows the definite superiority of the electronegativity technique in accounting for most of the detailed variations in the reactivity ratios for the systems considered. The Q–e scheme fails badly for the systems ST–2VP, ST–4VP, MM–2VP, MM–4VP, MA–AN, MAN–MM, MACD–MAN, 5E2VP–ST, MA–VCL2, MM–VCL2, MVK–VCL2, and MACD–VCL2 which are well accounted for by the present method. There are, of course, a few instances in which the Q–e predictions are better than those of the electronegativity scheme, such as ST–MM and AN–VCL2.

Ideal Systems

An ideal system is defined as one for which the product r_1r_2 is equal to unity. Such systems are predicted to occur in the electronegativity scheme under certain circumstances which are less stringent than for the Q–e method. For the latter case, an ideal system can only occur if $e_1 = e_2$. In the electronegativity model, a given system will be ideal in either of two cases, these being those shown in eqs. (5).

Case A:

$$X_R(i) \geq X_M(j) \qquad i,j = 1,2$$

Case B:

$$X_R(i) \leq X_M(j) \qquad i,j = 1,2 \qquad (5)$$

An example of case A is the system MMPD–MM, while an example of case B is PMXS–ST. The system MM–VCL2 is predicted to be intrinsically ideal but, because of the symmetry considerations mentioned above, the product of the observed reactivity ratios is 0.5.

Relation to the Q–e Method

It is of interest to examine the relationship of the parameters of the electronegativity and Q–e schemes in the hope that a better understanding of each may be forthcoming. Both methods contain terms which are related to resonance stabilization so that it would be assumed that there should be a definite relationship between these. In particular, one would expect a linear relationship between $-\log Q$ and L. Unfortunately, this does not occur, as shown by Table III and Figure 1. The scatter is particularly bad near the origin and there seems to be little correlation between the two quantities in this region. The equation for a linear least-squares fit, however, reveals that, overall, $-\log Q \approx L$. This equation is

$$-\log Q = -0.02 + 1.04L \qquad (6)$$

It was pointed out previously that the original interpretation of the parameter e as representing a static charge is no longer taken seriously. A charge-transfer interpretation can be given to this parameter, in that stabilization of the transition state will be more pronounced through charge transfer for systems in which the difference in e values is large. Levinson's postulate[2] of the relationship between e and the average electron affinity of the monomer and radical then represents only the electron-accepting tendency but does not take into account the ease of electron donation. From the Mulliken definition[9] of electronegativity,

$$X = {}^1/_2(I + A) \qquad (7)$$

where I and A are the ionization potential and electron affinity, respectively, it is obvious that this parameter takes into account both the electron donating and accepting character of a molecule. We therefore feel that the parameter e should be related to the average of the monomer and radical

TABLE II
Computed Reactivity Ratios[a]

M_1	M_2	r_1	r_2	r_1, Q–e	r_2, Q–e	r_1, exp	r_2, exp	Comment
ST	MA	0.76	0.17	0.78	0.18	0.75 ± 0.03	0.18 ± 0.02	
ST	MM	0.43	0.46	0.52	0.47	0.50 ± 0.02	0.50 ± 0.02	
ST	2VP	0.57	1.05	0.61	1.51	0.55 ± 0.03	1.14 ± 0.1	
MA	2VP	0.16	1.54	0.17	1.79	0.17 ± 0.01	1.58 ± 0.05	
MM	2VP	0.44	0.87	0.40	1.12	0.41 ± 0.03	0.83 ± 0.05	
ST	4VP	0.51	0.79	0.75	0.92	0.54 ± 0.03	0.70 ± 0.10	b
MM	4VP	0.58	0.85	0.71	0.98	0.57 ± 0.01	0.79 ± 0.05	b
MA	4VP	0.21	1.50	0.32	1.67	0.22 ± 0.01	1.7 ± 0.2	b
ST	AN	0.46	0.08	0.34	0.05	0.40 ± 0.05	0.04 ± 0.04	
MA	AN	0.61	1.53	1.00	0.69	0.77 ± 0.20	1.33 ± 0.17	c
MM	AN	1.31	0.18	0.90	0.31	1.20 ± 0.14	0.15 ± 0.07	b
2VP	AN	0.93	0.08	0.93	0.06	0.47 − 22.0	0.08 ± 0.04	c
4VP	AN	0.91	0.10	1.03	0.14	0.41 ± 0.09	0.11 ± 0.01	b
PMXS	ST	0.85	1.18	0.96	0.94	0.82 ± 0.07	1.16 ± 0.09	d
PMXS	MM	0.36	0.33	0.34	0.30	0.32 ± 0.05	0.29 ± 0.03	
PCLS	ST	1.09	0.71	1.20	0.67	1.03 ± 0.03	0.74 ± 0.03	
PCLS	MM	0.87	0.42	1.10	0.54	0.89 ± 0.05	0.41 ± 0.02	b
PCLS	PMXS	0.78	0.60	0.98	0.56	0.86 ± 0.08	0.58 ± 0.03	b
PMES	MM	0.40	0.46	0.44	0.34	0.44 ± 0.02	0.40 ± 0.02	b
PMES	PCLS	0.65	1.09	0.65	1.00	0.61 ± 0.03	1.15 ± 0.05	b
ST	MVK	0.29	0.35	0.44	0.25	0.29 ± 0.04	0.35 ± 0.02	b
AN	MVK	0.63	1.58	0.47	1.63	0.61 ± 0.04	1.78 ± 0.22	b, d
2M5VP	ST	0.97	0.82	1.12	0.85	1.05 ± 0.14	0.85 ± 0.04	
2M5VP	MA	0.96	0.17	1.19	0.21	0.88 ± 0.10	0.17 ± 0.01	b
2M5VP	MM	0.55	0.47	0.76	0.51	0.61 ± 0.08	0.46 ± 0.02	b
2M5VP	AN	0.58	0.09	0.59	0.07	0.27 ± 0.04	0.12 ± 0.01	b
MM	VAC	23.0	0.04	22.2	0.03	22.2 ± 0.9	0.07 ± 0.03	

MA	VAC	8.51	0.08	9.90	0.05	9.00 ± 2.5	0.10 ± 0.10	
AN	VAC	4.17	0.05	4.20	0.03	4.00 ± 0.3	0.06 ± 0.01	
2VP	VAC	18.0	0.02	43.5	0.02	30 ± 15	0 ± ?	e
MAN	ST	0.26	0.27	0.31	0.25	0.16 ± 0.06	0.30 ± 0.10	b
MAN	MM	0.57	0.77	1.09	0.78	0.65 ± 0.06	0.67 ± 0.10	b
MAN	VAC	13.2	0.03	18.7	0.02	12.0 ± 2.0	0.01 ± 0.01	e
MACD	ST	0.66	0.16	0.91	0.13	0.70 ± 0.05	0.15 ± 0.01	b
MACD	MAN	1.69	0.59	2.32	0.42	1.64 ± 0.05	0.62 ± 0.05	b, d
MACD	VAC	32.8	0.02	51.0	0.01	20 ± ?	0.01 ± ?	e
MMPD	ST	0.56	0.79	0.63	0.66	0.58 ± 0.02	0.77 ± 0.02	f
MMPD	MM	1.21	0.83	1.04	0.92	1.13 ± 0.10	0.93 ± 0.10	d, f
MMPD	AN	1.31	0.15	1.49	0.26	1.44 ± 0.15	0.19 ± 0.04	f
MMPD	VAC	25.4	0.04	26.3	0.03	24.0 ± 5.0	0.16 ± 0.16	f
5E2VP	ST	1.14	0.81	1.44	0.69	1.20 ± 0.20	0.79 ± 0.03	b
5E2VP	MM	0.66	0.40	0.80	0.34	0.69 ± 0.03	0.39 ± 0.01	b
5E2VP	MA	1.17	0.15	1.21	0.14	1.16 ± 0.08	0.18 ± 0.01	b
5E2VP	AN	0.71	0.07	0.54	0.04	0.43 ± 0.05	0.02 ± 0.02	b
ST	VCL2	1.87	0.09	1.80	0.17	1.85 ± 0.05	0.09 ± 0.01	
MA	VCL2	0.90	0.88	1.65	0.57	0.84 ± 0.06	0.99 ± 0.10	
MM	VCL2	2.44	0.21	3.31	0.30	2.53 ± 0.10	0.24 ± 0.03	b
AN	VCL2	0.44	0.53	1.00	0.49	0.91 ± 0.10	0.37 ± 0.10	b
MVK	VCL2	1.87	0.34	2.52	0.36	1.8 ± ?	0.55 ± ?	e
MACD	VCL2	3.47	0.18	8.81	0.08	3.00 ± 0.45	0.15 ± 0.03	e
VAC	VCL2	0.11	4.72	0.10	6.87	0.05 ± 0.05	4.80 ± 1.20	

[a] All experimental data are for bulk polymerization at 60°C unless otherwise noted.
[b] Single measurement at 60°C.
[c] Wide scatter in experimental data.
[d] Predicted to be an ideal system.
[e] Single measurement at 70°C.
[f] Single measurement at 50°C.

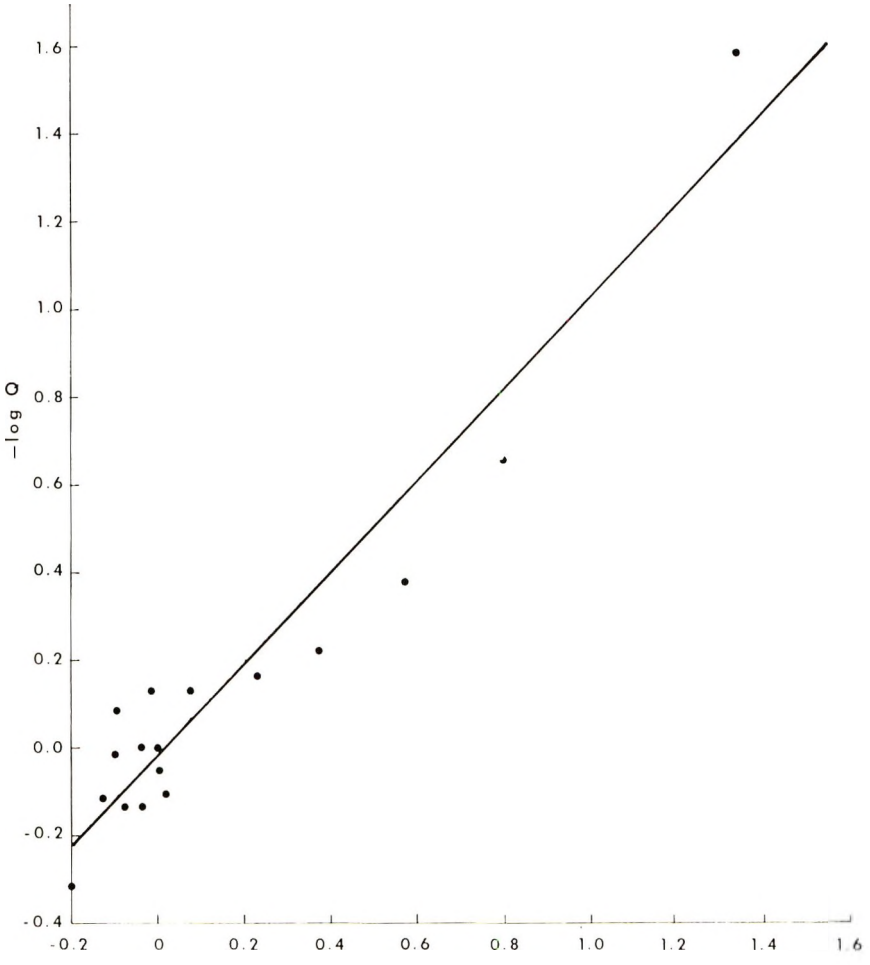

Fig. 1. Plot of $-\log Q$ vs. L.

electronegativities, $\bar{X}$. A plot of e versus $^1/_2(X_M + X_R)$ is shown in Figure 2 and seems to give credence to this supposition. A least-squares fit of the data indicates the following relationship between e and $\bar{X}$:

$$e = -1.01 + 2.47\bar{X} \tag{8}$$

Molecular Orbital Considerations

A purely *ab initio* quantum-mechanical consideration of reactivity ratios, as pointed out earlier, is clearly impossible. Likewise, any attempt to use semiempirical or purely empirical procedures can do little more than indicate a correlation between some computed value and reality. Because of these facts, the following discussion will be completely qualitative and will attempt only to show that the observed trends in the parameters are realistic. Furthermore, since at least a qualitative correspondence

holds between the values of L and $-\log Q$, and since Q can be related to the monomer localization energy, the discussion will be confined to the electronegativities.

We began with the Mulliken definition of electronegativity, given by eq. (7) and, for simplicity, we will confine our discussion to conclusions which can be drawn from Hückel theory.[10] Within this context, which admittedly is far from reality, the ionization potential of a monomer is given

TABLE III
Comparison with Q–e Values[a]

Monomer	L	$-\log Q$	$\frac{1}{2}(X_R + X_M)$	e
ST	0	0	0.063	−0.80
MA	0.574	0.377	0.694	0.60
MM	−0.014	0.130	0.500	0.40
2VP	−0.130	−0.114	0.252	−0.50
4VP	−0.094	0.086	0.323	−0.20
AN	0.372	0.222	0.834	1.20
PMXS	−0.038	−0.134	—	−1.11
PCLS	−0.094	−0.014	0.221	−0.33
PMES	0.016	−0.104	—	0.98
MVK	0.234	0.161	0.757	0.68
2M5VP	−0.036	0.004	0.180	−0.58
VAC	1.326	1.580	0.500	−0.22
MAN	0.006	−0.050	0.700	0.81
MACD	−0.202	−0.369	0.668	0.65
MMPD	0.076	0.130	0.393	0.19
5E2VP	−0.074	−0.135	0.166	−0.74
VCL2	0.800	0.658	0.510	0.36

[a] Q–e values taken from ref. 7.

by the negative of the energy ϵ_n of the highest-lying occupied molecular orbital (MO). Likewise, the electron affinity is the negative of the energy of the lowest-lying unoccupied MO, ϵ_{n+1}, so that the electronegativity of the monomer in the Hückel approximation should be given by

$$X_M = -(\epsilon_n + \epsilon_{n+1})/2. \tag{9}$$

In the same way, one predicts that for a radical the electron affinity and the ionization potential should be the same, namely, the negative of the energy of the singly occupied MO, $\bar{\epsilon}_n$, so that

$$X_R = -\bar{\epsilon}_n. \tag{10}$$

This latter approximation appears ridiculous but can be rationalized by the observation that, in general, the ionization potential of a radical is a good deal larger than predicted, ($I = -\bar{\epsilon}_n + \delta$) and the electron affinity is much less ($A = -\epsilon_n - \delta'$), so that if δ and δ' are about the same order of magnitude then the value of X_R is that given by eq. (10).

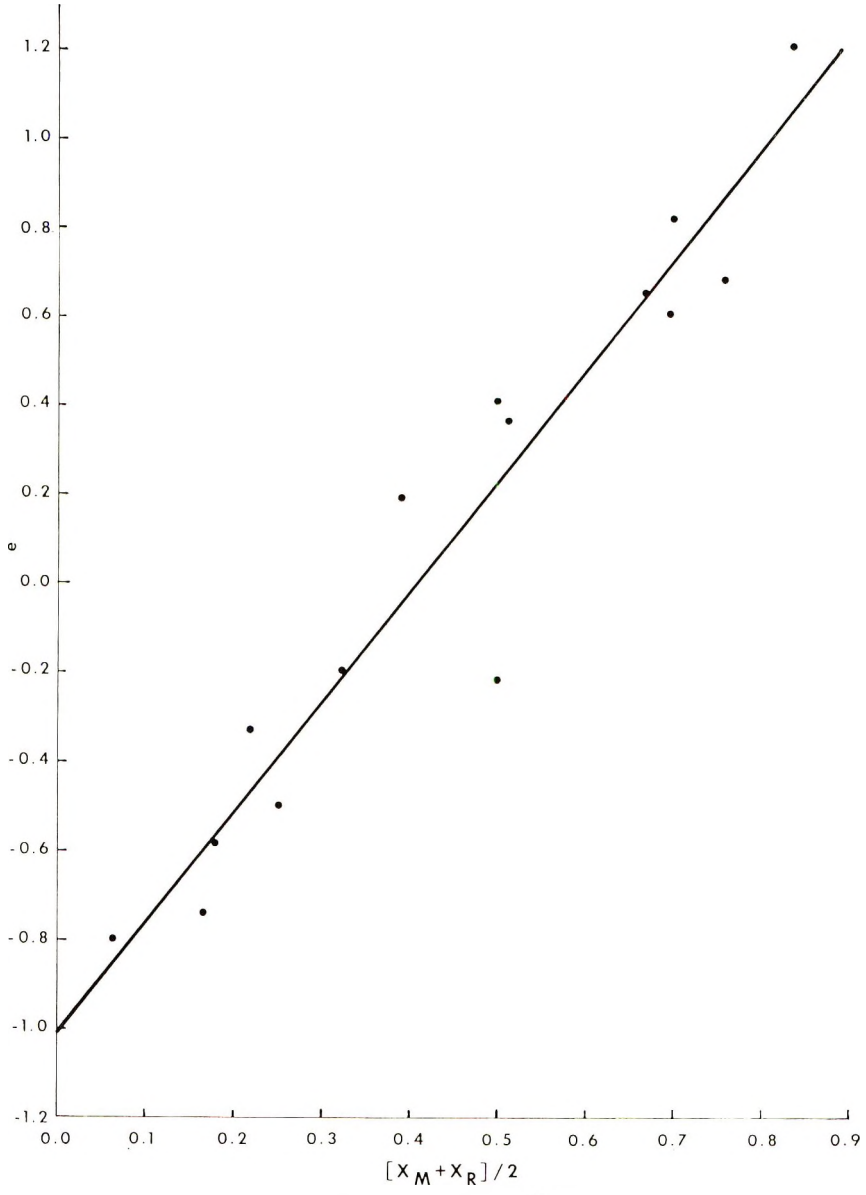

Fig. 2. Plot of e vs. $\bar{X}$.

We begin with a discussion of styrene, vinylpyridines, and their substituted derivatives. In the Hückel approximation, one has the following:

$$\epsilon_n(\mathrm{ST}) = \alpha + k\beta$$
$$\epsilon_{n+1}(\mathrm{ST}) = \alpha - k\beta$$
$$\bar{\epsilon}_n(\mathrm{ST}) = \alpha - \delta\beta \qquad \delta \ll k \qquad (11)$$

where α and β are the usual Hückel coulomb and resonance integrals. The value of $\bar{\epsilon}_n$ is different from α due to hyperconjugation with the remainder of the polymer chain. Ignoring the value of α for the moment, we simplify these equations to read:

$$\begin{aligned} \epsilon_n(\mathrm{ST}) &= k\beta \\ \epsilon_{n+1}(\mathrm{ST}) &= -k\beta \\ \bar{\epsilon}_n(\mathrm{ST}) &= -\delta\beta \end{aligned} \tag{12}$$

We now define the zero of energy to be $-\delta\beta$ so that

$$\begin{aligned} \epsilon_n(\mathrm{ST}) &= (k + \delta)\beta \\ \epsilon_{n+1}(\mathrm{ST}) &= (-k + \delta)\beta \\ \bar{\epsilon}_n(\mathrm{ST}) &= 0 \end{aligned} \tag{13}$$

so that $X_\mathrm{R}(\mathrm{ST}) = 0$, $X_\mathrm{M}(\mathrm{ST}) = -\delta\beta$. Since $\beta < 0$, we have that $X_\mathrm{M}(\mathrm{ST}) > X_\mathrm{R}(\mathrm{ST})$.

The vinylpyridines differ from styrene in that one of the ring carbons has been changed to a nitrogen so that the coulomb integral at this site is now $\alpha + \gamma\beta$. The first-order change in the energy levels due to the presence of the nitrogen atom is to lower ϵ_n, ϵ_{n+1}, $\bar{\epsilon}_n$ from the styrene values. The magnitude of the shift will depend on the coefficient in the appropriate MO at the point of substitution of N for C. This effect will be more pronounced in 4VP than in 2VP. For either system, however, we can write, approximately:

$$\begin{aligned} \epsilon_n(\mathrm{VP}) &= (k + \delta + \xi)\beta \\ \epsilon_{n+1}(\mathrm{VP}) &= (-k + \delta + \xi)\beta \\ \epsilon_n(\mathrm{VP}) &= \xi'\beta \end{aligned} \tag{14}$$

More detailed calculations reveal that ϵ_{n+1} is lowered by a greater amount than ϵ_n but this is not too important. Therefore,

$$\begin{aligned} X_\mathrm{M}(\mathrm{VP}) &= X_\mathrm{M}(\mathrm{ST}) - \xi\beta \\ X_\mathrm{R}(\mathrm{VP}) &= X_\mathrm{R}(\mathrm{ST}) - \xi'\beta \end{aligned} \tag{15}$$

so that $X_\mathrm{M}(\mathrm{VP}) > X_\mathrm{M}(\mathrm{ST})$, $X_\mathrm{R}(\mathrm{VP}) > X_\mathrm{R}(\mathrm{ST})$, the observed shifts in electronegativity being correct. The prediction that larger effects occur in 4VP is also correct.

Substitution of an ethyl group for the hydrogen at the five-position of 2VP can be treated by second-order perturbation theory. If a heteroatom model is adopted,[11] the effect will be primarily in raising the energy levels ϵ_n, ϵ_{n+1}, and $\bar{\epsilon}_n$. The shifts should be in the order $\epsilon_n > \bar{\epsilon}_n > \epsilon_{n+1}$ on the basis of the form of the MO's and will be much smaller than the shifts engendered

by the substitution of a nitrogen in the styrene ring. Therefore, for 5E2VP, we would predict the following pattern of energy levels:

$$\begin{aligned} \epsilon_n\ (5\text{E}2\text{VP}) &= (k + \delta + \xi - \eta_1)\beta \\ \epsilon_{n+1}(5\text{E}2\text{VP}) &= (-k + \delta + \xi - \eta_2)\beta \\ \bar{\epsilon}_n(5\text{E}2\text{VP}) &= (\xi' - \eta_3)\beta \end{aligned} \tag{16}$$

where $\eta_1 > \eta_3 > \eta_2$. We conclude $X_{\text{M}}(5\text{E}2\text{VP}) < X_{\text{M}}(2\text{VP})$, $X_{\text{R}}(5\text{E}2\text{VP}) < X_{\text{R}}(2\text{VP})$, and $[X_{\text{R}}(5\text{E}2\text{VP}) - X_{\text{M}}(5\text{E}2\text{VP})] > [X_{\text{R}}(2\text{VP}) - X_{\text{M}}(2\text{VP})]$. These predictions are substantiated by the results shown in Table I.

The parameters for *p*-methylstyrene can be rationalized in the same manner by using second-order perturbation theory. The methyl group perturbs ϵ_n and ϵ_{n+1}, raising them somewhat, the larger effect occurring on ϵ_n. The radical level $\bar{\epsilon}_n$ is also raised, so that X_{R} should become negative for PMES. In summary, it is concluded that:

$$\begin{aligned} &\epsilon_n(\text{PMES}) = (k + \delta - \mu_1)\beta \\ &\epsilon_{n+1}(\text{PMES}) = (-k + \delta - \mu_2)\beta \\ &\mu_2 < \mu_1 \\ &X_{\text{M}}(\text{PMES}) = -(2\delta - \mu_1 - \mu_2)\beta/2 < X_{\text{M}}(\text{ST}) \end{aligned} \tag{17}$$

A discussion of 2-methyl-5-vinylpyridine follows most easily by substituting a nitrogen into the appropriate position in the ring of *p*-methylstyrene. Since the MO's ϕ_{n+1} and ϕ_n are nodal at this position, actual calculations were carried out. The main effect in the molecule is to lower the value of ϵ_{n+1}, while ϵ_n is lowered by a much smaller amount. Therefore, the value of X_{M} for 2M5VP is somewhat larger than that of PMES. The nitrogen substitution has a somewhat larger effect in the radical, lowering the value of $\bar{\epsilon}_n$ significantly from that of PMES, so that $X_{\text{R}}(2\text{M}5\text{VP}) > X_{\text{R}}$-(PMES).

Although the methoxyl group, $-\text{OCH}_3$, is much more strongly conjugating than a methyl group, it appears to be adequate to treat its effect on ϵ_n, ϵ_{n+1}, and $\bar{\epsilon}_n$ in styrene by perturbation theory, at least as a first approximation. The effect in PMXS, then, is to raise all of these levels, ϵ_n being the most strongly perturbed, followed by $\bar{\epsilon}_n$ and ϵ_{n+1}. This causes a sharp reduction in the electronegativities so that $X_{\text{M}}(\text{PMXS}) < X_{\text{M}}(\text{ST})$, X_{R}-(PMXS) $< X_{\text{R}}(\text{ST})$. Since the perturbation is much stronger than in PMES, the shifts from the styrene values should be a good deal larger. These predictions are in agreement with the computed results.

The substitution of a chlorine atom at the para position of styrene is much more difficult to treat adequately. The intuitive feeling that such a substitution should affect the energy levels in much the same way as the

corresponding methyl and methoxyl substitutions is not confirmed. The Hammett σ_p-constants[12] for CH_3, OCH_3, and Cl bear this out, these being -0.17, -0.27, and $+0.23$, respectively. The Cl atom primarily withdraws electrons from the styrene system, probably through participation, at least in part, of *d*-orbital conjugation.[12] This will result in a lowering of the levels ϵ_n, ϵ_{n+1}, and $\bar{\epsilon}_n$, with a corresponding increase in X_M and X_R. The effect appears to be more strongly pronounced in the radical.

For a discussion of acrylonitrile, we begin from the parent unperturbed molecule butadiene. The energy levels, ϵ_n, ϵ_{n+1}, and $\bar{\epsilon}_n$, of the latter system are not very different from styrene and as a first approximation we take them to be the same. The formation of acrylonitrile from butadiene involves the substitution of one of the terminal carbons by a nitrogen and a marked shortening of the C—N bond length. The coulomb integral for the nitrogen is more electronegative than that of carbon, and we expect that the resonance integral for the C≡N bond will be larger in absolute magnitude than for a C=C bond. The presence of the more electronegative nitrogen lowers the energy levels sharply. Since the form of the MO's indicates that this effect is greater in butadiene than in styrene, and the nitrogen is probably more electronegative than in the vinyl pyridines, the magnitude of the shifts is much larger. The orbital ϕ_n is C≡N bonding, so that the larger resonance integral for the C≡N bond further lowers ϵ_n. The opposite effect occurs for ϵ_{n+1}, since ϕ_{n+1} is C≡N antibonding so that this level is raised somewhat by the change in β. The radical level $\bar{\epsilon}_n$ is most strongly perturbed by the change in the coulomb integral, and is lowered. The form of the MO $\bar{\phi}_n$ indicates it is slightly C≡N antibonding but the magnitude of the coefficients makes this consideration unimportant. Overall, a large increase in ionization potential and electron affinity occurs for both radical and monomer so that X_M and X_R are drastically increased. Calculations predict that the balancing of these changes is such that X_R is lowered somewhat more than X_M. In summary, we can write:

$$\begin{aligned}
\epsilon_n(\mathrm{AN}) &= (k + \delta + \nu_1)\beta \\
\epsilon_{n+1}(\mathrm{AN}) &= (-k + \delta + \nu_2)\beta \qquad \nu_2 < \nu_1 \\
\bar{\epsilon}_n(\mathrm{AN}) &= \nu_3\beta \qquad \nu_3 > (\nu_1 + \nu_2)/2 \qquad (17) \\
X_M(\mathrm{AN}) &= -(\nu_1 + \nu_2 + 2\delta)\beta/2 \\
X_R(\mathrm{AN}) &= -\nu_3\beta \\
&\qquad \nu_3 \approx (\nu_1 + \nu_2 + 2\delta)/2
\end{aligned}$$

Methacrylonitrile can be treated adequately by considering the perturbation of the methyl group on the acrylonitrile levels. The magnitude of ϵ_n is most strongly shifted, followed by $\bar{\epsilon}_n$ and ϵ_{n+1}. The net effect of raising these levels is to increase both X_M and X_R by about the same amount.

$$\epsilon_n(\mathrm{MAN}) = \epsilon_n(\mathrm{AN}) - \gamma_1\beta$$
$$\epsilon_{n+1}(\mathrm{MAN}) = \epsilon_{n+1}(\mathrm{AN}) - \gamma_2\beta$$
$$\bar{\epsilon}_n(\mathrm{MAN}) = \bar{\epsilon}_n(\mathrm{AN}) - \gamma_3\beta$$
$$\gamma_1 > \gamma_3 > \gamma_2$$
$$\gamma_3 \approx (\gamma_1 + \gamma_2)/2 \qquad (18)$$
$$X_\mathrm{M}(\mathrm{MAN}) = X_\mathrm{M}(\mathrm{AN}) + (\gamma_1 + \gamma_2)\beta/2$$
$$X_\mathrm{R}(\mathrm{MAN}) = X_\mathrm{R}(\mathrm{AN}) + \gamma_3\beta$$

At this point, the discussion must become more qualitative since the naive ideas of Hückel theory cannot account for the detailed behavior of MVK, MA, MM, and MACD, especially in comparison with the nitriles. We first consider acrolein (ACR), for which sufficient experimental data was not available to include it in the monomers considered. Again butadiene serves as a starting point. The oxygen atom is substituted for a terminal carbon and, being more electronegative than the nitrile nitrogen, we expect the levels ϵ_n and ϵ_{n+1} to shift by a greater amount. The resonance integral for the C=O bond should be about the same as for the C=C bond so that, in this case, we expect ϵ_{n+1} to be lowered by a slightly greater amount than ϵ_n. In any case, we expect $X_\mathrm{M}(\mathrm{ACR}) > X_\mathrm{M}(\mathrm{AN})$. Similarly, we would expect $X_\mathrm{R}(\mathrm{ACR}) > X_\mathrm{R}(\mathrm{AN})$, and $X_\mathrm{M}(\mathrm{ACR}) > X_\mathrm{R}(\mathrm{ACR})$. Perturbation by a methyl group now shifts the levels in much the same way as in methacrylonitrile. An examination of the coefficients in the various MO's leads one to expect that the shifts should be somewhat smaller since methyl substitution is at a different position. The value of X_R for MVK cannot be accounted for, however, by such a shift. We would expect that $X_\mathrm{R}(\mathrm{MVK}) > X_\mathrm{R}(\mathrm{MAN})$, while the opposite is true. This is an obvious breakdown of the assumption of eq. (10). The value of $X_\mathrm{M}(\mathrm{MKV})$ is reasonable, however.

The situation encountered in MVK also applies to methyl acrylate. The acrolein molecule is now perturbed by the introduction of the methoxyl group, causing a larger perturbation of the levels than the methyl group. The X values for MA are reasonable, then, in comparison with MVK, but not in comparison with the nitriles in the case of X_R.

The levels of methyl methacrylate can be considered either from the standpoint of perturbing MVK with a methoxyl group, or perturbing MA with a methyl group. In either case, the low value of X_M for MM cannot be rationalized by the simple model adopted. The shift in $X_\mathrm{R}(\mathrm{MM})$ from either MVK or MA is reasonable. A similar difficulty is noted in the value of X_R for methacrylic acid in relation to that of MVK. One would expect $X_\mathrm{R}(\mathrm{MACD})$ to be much the same as for MM. Many of these effects are undoubtedly detailed functions of molecular geometry. Likewise, the parameters derived from experimental data may be quite different from those expected due to compensation for somewhat different contributions from various factors in determining the activation energy.

The remaining molecules (VAC, MMPD, VCL2) can only be treated by sophisticated calculations which are impossible to carry out at this time. The parameters for VCL2 seem reasonable but those of the other systems seem anomalous, especially the vinyl acetate values.

SUMMARY

The model presented in this paper for the treatment of reactivity ratios for free-radical bulk polymerization offers a definite advantage in accuracy over the Q–e scheme for most of the systems studied. Anomalous results for many systems involving acrylonitrile indicate that this monomer does not behave in a predictable manner and simple reactivity schemes will all undoubtedly fail to predict good values for the reactivity ratios of such systems.

References

1. K. Hayashi, T. Yonezawa, C. Nagata, S. Okamura, and K. Fukui, *J. Polym. Sci.*, **20,** 537 (1956).
2. G. S. Levinson, *J. Polym. Sci.*, **60,** 43 (1962).
3. T. Alfrey, Jr. and C. C. Price, *J. Polym. Sci.*, **2,** 101 (1947).
4. T. Fueno, T. Tsuruta, and J. Furukawa, *J. Polym. Sci.*, **40,** 487 (1959).
5. H. Lüssi, *Makromol. Chem.*, **103,** 47 (1967).
6. L. Pauling, *J. Amer. Chem. Soc.*, **54,** 3570 (1932).
7. G. E. Ham, Ed., *Copolymerization*, High Polymer Series, Vol. 18, Interscience, New York, 1964.
8. G. E. Ham, *J. Polym. Sci.*, **14,** 87 (1954).
9. R. S. Mulliken, *J. Chem. Phys.*, **2,** 782 (1934).
10. A. Streitwieser, *Molecular Orbital Theory for Organic Chemists*, Wiley, New York, 1961.
11. H. H. Jaffe, *Chem. Revs.*, **53,** 191 (1953).
12. J. R. Hoyland and L. Goodman, *J. Phys. Chem.*, **64,** 1816 (1960).

Received August 21, 1969

JOURNAL OF POLYMER SCIENCE: PART A-1 VOL. 8, 901–907 (1970)

Studies on Monomer Reactivity Ratios. II. A Charge-Transfer Model

JAMES R. HOYLAND, *Battelle Memorial Institute, Columbus Laboratories, Columbus, Ohio 43201*

Synopsis

A charge-transfer model is proposed for the treatment of monomer reactivity ratios in free-radical bulk polymerization. The procedure involves the assignment of three parameters to each monomer, which can be interpreted as being related to the energies of the highest occupied monomer orbital, the singly occupied radical orbital, and the lowest lying virtual orbital of the monomer. Parameters are found for 17 monomers and computed reactivity ratios for a large number of copolymer systems are tabulated and compared with experiment. Similarities of the present model and the electronegativity scheme are discussed.

INTRODUCTION

The problems involved in predicting monomer reactivity ratios have been discussed at length in the previous paper (Part I).[1] It was concluded that quantum mechanical calculations of these reactivity ratios are clearly impossible without the introduction of many simplifying assumptions. For molecules of even moderate size, however, these assumptions must be so drastic that the question of whether a meaningful procedure is being followed becomes very important. It was suggested in Part I that a more meaningful procedure for the theoretician to follow might be to propose a model involving quantities which are felt to be important in determining reactivity ratios, and to test this model by assessing its ability to account for experimental data. Parameters found from a fit of the experimental data can then be examined from empirical or semiempirical quantum mechanical reasoning. It is strongly felt that such an approach will, in the long run, prove more fruitful than attempts to compute reactivity ratios solely on the basis of some form of empirical quantum mechanics.

Examples of successful models put forward on this basis are the Q–e scheme[2] and the electronegativity model described in Part I. In this paper, an alternate approach is proposed based on the idea of charge transfer.

CHARGE-TRANSFER MODEL

The basic quantum mechanical ideas of charge-transfer phenomena were first put forward by Mulliken,[3] although the reasoning behind these ideas

is much older. We consider two neutral species, D and A, reacting to form a molecule or a complex. If one of the species, D, can function as an electron donor and the other, A, as an electron acceptor, then the wavefunction for the system can be written as a linear combination of functions which represent covalent and ionic structures, D—A and D^+—A^-. The degree of charge transfer, and hence the strength of the bond, should be dependent upon the ionization potential of D and the electron affinity of A, at least as a first approximation.

We propose to make use of this concept in the prediction of monomer reactivity ratios. It is proposed that the energy of a transition state will be stabilized if a favorable charge-transfer situation is operative. Since we do not claim to be setting forth a rigorous theory or one which necessarily conforms to all facets of reality, a further dubious assumption is made, namely that only the most energetically favorable charge-transfer mode between monomer and radical (R^+—M^- or R^-—M^+) need be considered.

In addition to charge-transfer effects, it is expected that the monomer localization energy should also be an important parameter just as in the Q–e and electronegativity schemes. It is therefore proposed that the following equation can be written for the monomer reactivity ratios:

$$\log r_1 = -L(1) + L(2) + \Delta E_{CT}(1\cdot 2) - \Delta E_{CT}(1\cdot 1) \tag{1}$$

The terms L represent the relative monomer localization energies and $\Delta E_{CT}(i\cdot j)$ is a charge-transfer energy between monomer j and radical i. We now define the quantities $\hat{E}_U(i)$, $E_R(i)$, and $\hat{E}_O(i)$ as the energies of the lowest unoccupied orbital in the monomer i, the energy of the singly occupied orbital in the radical i, and the energy of the highest occupied orbital in monomer i, respectively. Therefore, the charge-transfer energies can be written as

$$\Delta E_{CT}(i\cdot j) = \min \begin{Bmatrix} \hat{E}_U(j) - E_R(i) \\ E_R(i) - \hat{E}_O(j) \end{Bmatrix} \tag{2}$$

It would appear at first that four parameters are needed for each monomer, but it is readily shown that this number can be reduced to three. Two new quantities, E_U and E_O, are defined by the following equations:

$$E_U(i) = \hat{E}_U(i) + L(i) \tag{3}$$

$$E_O(i) = \hat{E}_O(i) - L(i) \tag{4}$$

Inspection of eqs. (1) and (2) indicates there are four possible expressions for $\log r_1$ depending on the relative magnitudes of $\hat{E}_U(j)$, $E_R(i)$, and $\hat{E}_O(j)$. These are each examined below and it is shown that only three independent parameters for each monomer are needed.

Case I. The first case considered is defined by a pattern of energy levels $\hat{E}_U(2) - E_R(1) < E_R(1) - E_O(2)$ and $E_U(1) - E_R(1) < E_R(1) - \hat{E}_O(1)$.

The expression for $\log r_1$ then becomes

$$\log r_1 = L(2) - L(1) + \hat{E}_U(2) - \hat{E}_U(1)$$
$$= E_U(2) - E_U(1) \quad (5)$$

Case II. The pattern of energy levels is characterized by the relations $\hat{E}_U(2) - E_R(1) < E_R(1) - \hat{E}_O(2)$ and $E_R(1) - \hat{E}_O(1) < \hat{E}_U(1) - E_R(1)$. In this case,

$$\log r_1 = L(2) - L(1) + \hat{E}_U(2) + \hat{E}_O(1) - 2E_R(1)$$
$$= E_U(2) + E_O(1) - 2E_R(1) \quad (6)$$

Case III. This is the converse of case II, in that $E_R(1) - \hat{E}_O(2) < \hat{E}_U(2) - E_R(1)$ and $\hat{E}_U(1) - E_R(1) < E_R(1) - \hat{E}_O(1)$. We therefore have

$$\log r_1 = L(2) - L(1) + 2E_R - \hat{E}_O(2) - \hat{E}_U(1)$$
$$= 2E_R - E_U(1) - E_O(2) \quad (7)$$

Case IV. The relationships governing case I are reversed, leading to $E_R(1) - \hat{E}_O(2) < \hat{E}_U(2) - E_R(1)$ and $E_R(1) - \hat{E}_O(1) < \hat{E}_U(1) - E_R(1)$, so that

$$\log r_1 = L(2) - L(1) - \hat{E}_O(2) + \hat{E}_O(1)$$
$$= E_O(1) - E_O(2) \quad (8)$$

Therefore, we need consider only the parameters E_U, E_O, and E_R for each monomer.

The values of the parameters for the monomers considered are given in Table I. These were derived in exactly the same manner as those for the

TABLE I
Parameter Values

Monomer	Abbreviation	E_U	E_R	E_O
Styrene	ST	3.006	0	−3.292
Methyl acrylate	MA	2.902	−0.584	−4.458
Methyl methacrylate	MM	2.662	−0.518	−3.638
2-Vinylpyridine	2VP	2.744	−0.278	−3.274
4-Vinylpyridine	4VP	2.740	−0.338	−3.404
Acrylonitrile	AN	2.678	−0.864	−4.474
p-Methoxystyrene	PMXS	3.096	0.004	−3.150
p-Chlorostyrene	PCLS	2.860	−0.280	−3.258
p-Methylstyrene	PMES	3.050	>−0.122[a]	−3.294
Methyl vinyl ketone	MVK	2.456	−0.658	−4.174
2-Methyl-5-vinylpyridine	2M5VP	2.940	−0.180	−3.284
Vinyl acetate	VAC	3.946	−0.540	−5.026
Methacrylonitrile	MAN	2.362	−0.760	−3.880
Methacrylic acid	MACD	2.160	−0.660	−3.880
Methacryloxymethylpentamethyldisiloxane	MMPD	2.886	−0.522	−3.554
5-Ethyl-2-vinylpyridine	5E2VP	2.900	−0.214	−3.244
Vinylidene chloride	VCL2	3.566	−0.684	−4.324

[a] Insufficient data to determine this parameter.

electronegativity scheme described in Part I, and this paper should be referred to for computational details. The value of E_R for styrene was set equal to zero to serve as the reference point.

RESULTS

Calculated values of reactivity ratios for the systems considered are given in Table II along with the experimental results. Comments concerning individual cases have not been included in the Table II since they are the same as those in Table II of the preceding paper, except for predicted ideal cases. Likewise, the reactivity ratios computed from the Q–e scheme are not included.

The calculated results are generally in excellent agreement with experiment. Acrylonitrile copolymers are an exception as in the electronegativity scheme. Vinylpyridine–acrylonitrile systems and vinylidene chloride–

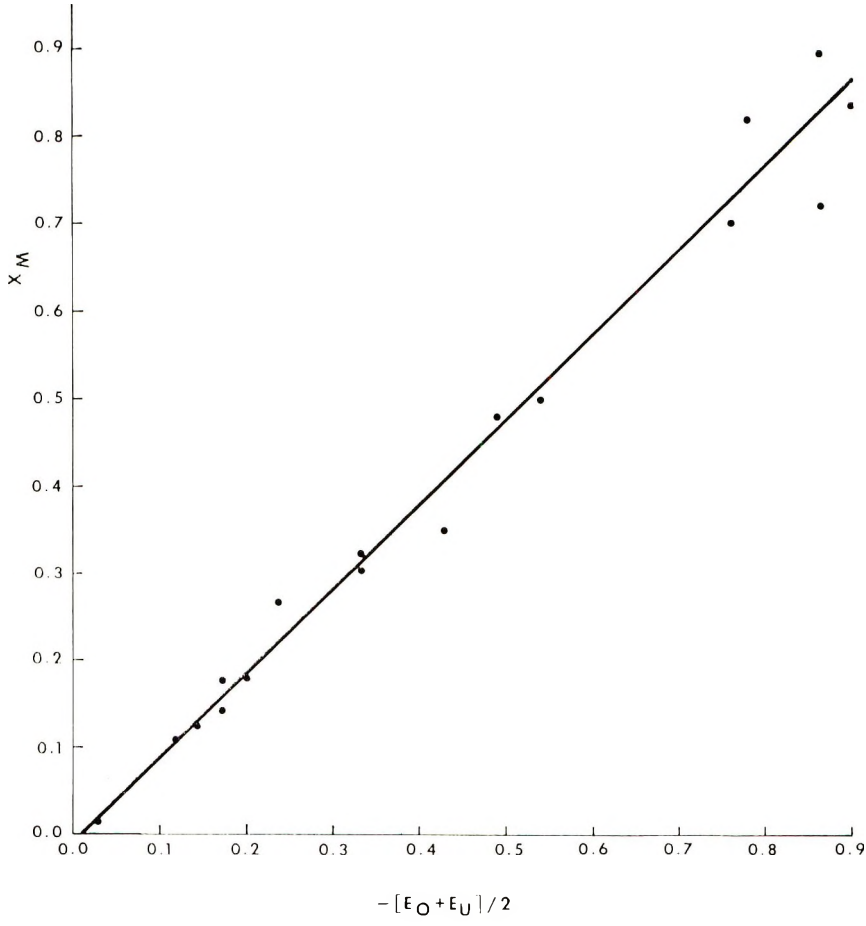

Fig. 1. Plot of X_M vs. $-(E_0 + E_U)/2$.

TABLE II
Computed Reactivity Ratios

M_1	M_2	r_1	r_2	r_1, exp	r_2, exp
ST	MA	0.79	0.17	0.75 ± 0.03	0.18 ± 0.02
ST	MM	0.45	0.45	0.50 ± 0.02	0.50 ± 0.02
ST	2VP	0.55	1.04	0.55 ± 0.03	1.14 ± 0.10
MA	2VP	0.16	1.53	0.17 ± 0.01	1.58 ± 0.05
MM	2VP	0.43	0.88	0.41 ± 0.03	0.83 ± 0.05
ST	4VP	0.54	0.77	0.54 ± 0.03	0.70 ± 0.10
MA	4VP	0.22	1.49	0.22 ± 0.01	1.70 ± 0.20
MM	4VP	0.58	0.86	0.57 ± 0.01	0.79 ± 0.05
ST	AN	0.47	0.08	0.40 ± 0.05	0.04 ± 0.04
MA	AN	0.60	1.13	0.77 ± 0.20	1.33 ± 0.17
MM	AN	1.19	0.17	1.20 ± 0.14	0.15 ± 0.07
2VP	AN	0.91	0.07	0.47 − 22.0	0.08 ± 0.04
4VP	AN	0.89	0.10	0.41 ± 0.09	0.11 ± 0.01
PMXS	ST	0.81	1.23	0.82 ± 0.07	1.16 ± 0.09
PMXS	MM	0.37	0.32	0.32 ± 0.05	0.29 ± 0.03
PCLS	ST	1.08	0.71	1.03 ± 0.03	0.74 ± 0.03
PCLS	MM	0.92	0.42	0.89 ± 0.05	0.41 ± 0.02
PCLS	PMXS	0.78	0.58	0.86 ± 0.08	0.58 ± 0.03
PMES	PCLS	0.65	1.09	0.61 ± 0.03	1.15 ± 0.05
PMES	MM	0.41	0.45	0.44 ± 0.02	0.40 ± 0.02
ST	MVK	0.28	0.33	0.29 ± 0.04	0.35 ± 0.02
AN	MVK	0.59	1.67	0.61 ± 0.04	1.78 ± 0.22
2M5VP	ST	1.02	0.86	1.05 ± 0.14	0.85 ± 0.04
2M5VP	MA	0.95	0.16	0.88 ± 0.10	0.17 ± 0.01
2M5VP	MM	0.55	0.44	0.61 ± 0.08	0.46 ± 0.02
2M5VP	AN	0.57	0.08	0.27 ± 0.04	0.12 ± 0.01
MM	VAC	22.1	0.04	22.2 ± 0.90	0.07 ± 0.03
MA	VAC	9.04	0.09	9.00 ± 2.50	0.10 ± 0.10
AN	VAC	4.17	0.05	4.00 ± 0.30	0.06 ± 0.01
2VP	VAC	16.9	0.02	30.0 ± 15.0	0 ± ?
MAN	ST	0.26	0.23	0.16 ± 0.06	0.30 ± 0.10
MAN	MM	0.57	0.57	0.65 ± 0.06	0.67 ± 0.10
MAN	VAC	14.0	0.03	12.0 ± 2.0	0.01 ± 0.01
MACD	ST	0.65	0.14	0.70 ± 0.05	0.15 ± 0.01
MACD	MAN	1.59	0.63	1.64 ± 0.05	0.62 ± 0.05
MACD	VAC	35.2	0.02	20 ± ?	0.01 ± ?
MMPD	ST	0.55	0.76	0.58 ± 0.02	0.77 ± 0.02
MMPD	MM	1.21	0.82	1.13 ± 0.10	0.93 ± 0.10
MMPD	AN	1.47	0.14	1.44 ± 0.15	0.19 ± 0.04
MMPD	VAC	27.3	0.03	24.0 ± 5.0	0.16 ± 0.16
5E2VP	ST	1.12	0.78	1.20 ± 0.20	0.79 ± 0.03
5E2VP	MM	0.70	0.40	0.69 ± 0.03	0.39 ± 0.01
5E2VP	MA	1.22	0.15	1.16 ± 0.08	0.18 ± 0.01
5E2VP	AN	0.73	0.07	0.43 ± 0.05	0.02 ± 0.02
ST	VCL2	1.82	0.09	1.85 ± 0.05	0.09 ± 0.01
MA	VCL2	0.89	0.89	0.84 ± 0.06	0.99 ± 0.10
MM	VCL2	2.42	0.21	2.53 ± 0.10	0.24 ± 0.03
AN	VCL2	0.41	0.53	0.91 ± 0.10	0.37 ± 0.10
MVK	VCL2	1.77	0.32	1.8 ± ?	0.55 ± ?
MACD	VCL2	3.47	0.16	3.00 ± 0.45	0.15 ± 0.03
VAC	VCL2	0.10	5.06	0.05 ± 0.05	4.80 ± 1.20

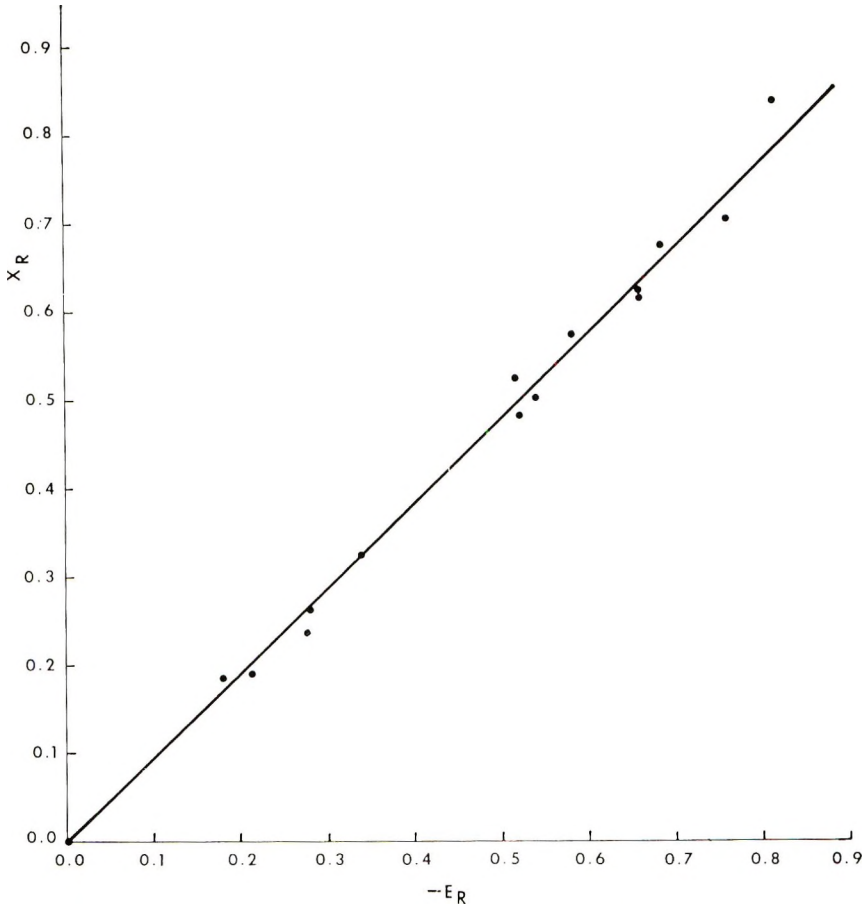

Fig. 2. Plot of X_R vs. $-E_R$.

acrylonitrile are especially poor. All other monomers appear to be amenable to this treatment, however.

Ideal Systems

Ideal systems are naturally predicted within the charge-transfer scheme. These systems occur if cases I or IV discussed in the previous section hold for both log r_1 and log r_2 simultaneously. Only two ideal systems are predicted by the charge-transfer scheme, these being PMXS–ST and MM–MMPD. The system MM–VCL2 is predicted to be intrinsically ideal as in the electronegativity model.

Relationship to the Electronegativity Scheme

In Part I it was assumed that the electronegativity could be written as $^1/_2(I + A)$, where I and A are the ionization potential and the electron

affinity, respectively. These latter quantities were then approximately related molecular orbital energy levels such that

$$X_M = -{}^1/_2(\epsilon_n + \epsilon_{n+1}) \tag{9}$$

$$X_R = -\bar{\epsilon}_n \tag{10}$$

Comparison with the present method indicates that ϵ_n, ϵ_{n+1}, and $\bar{\epsilon}_n$ should be related to $\hat{E}_O$, $\hat{E}_U$, and E_R, respectively. We note also that $E_O + E_U = \hat{E}_O + \hat{E}_U$, so that we expect that there should be a linear relationship between X_M and $-{}^1/_2(E_U + E_O)$ and between X_R and $-E_R$. Figures 1 and 2 show that this is the case, a least-squares treatment indicating the following results:

$$X_M = -0.009 + 0.964[-E_O - E_U]/2 \tag{11}$$

$$X_R = 0.952(-E_R) \tag{12}$$

The results for reactivity ratios computed by either the charge-transfer or the electronegativity model do not indicate that either method is superior to the other. The level of agreement with experiment is about the same for both methods as is the amount of labor required for their use. Further application to other systems may allow a future decision to be made concerning which method is capable of better explaining detailed behavior.

SUMMARY AND CONCLUSIONS

The results of this paper and those described in Part I have demonstrated that it is possible to construct reactivity schemes for polymer reactivity ratios which can give a more quantitative account of experimental trends than the traditional Q–e method. Most systems studied are well accounted for by either scheme and the exceptions may indicate that other processes are occurring or that some other factors not considered make an important contribution to the transition state energy. Work is continuing on attempts to include other factors which may have considerable influence.

References

1. J. R. Hoyland, *J. Polym. Sci. A-1*, this issue.
2. T. Alfrey, Jr. and C. C. Price, *J. Polym. Sci.*, **2**, 101 (1947).
3. R. S. Mulliken, *J. Amer. Chem. Soc.*, **72**, 600 (1950).

Received August 21, 1969

JOURNAL OF POLYMER SCIENCE: PART A-1 VOL. 8, 909–916 (1970)

Stereoregular Poly(styrenesulfonic Acid)

N. N. AYLWARD,* *Chemistry Department, Aberdeen University, Old Aberdeen, Scotland*

Synopsis

A convenient method is described for the preparation of poly(*n*-propyl *p*-vinylbenzene sulfonate) by using the monomer, *n*-propyl *p*-vinylbenzene sulfonate and butyllithium initiation in tetrahydrofuran at −75°C. The structure of this polymer enables complete hydrolysis to the corresponding poly(styrenesulfonic acid), which was characterized with respect to molecular weight and sulfonic acid content. The polyacid was shown by potentiometric titration to be strongly ionophoric.

INTRODUCTION

Poly(styrenesulfonic acids) are usually synthesized by polymerization of a salt of the monomer,[1,2] or sulfonating[3] atactic polystyrenes,[4–6] which may be monodisperse.[7] These methods may lead to one sulfonic acid group to each benzene ring with the molecular weight distribution being unchanged. Stereoregular PSSA has not been studied in detail.

In this paper the monomer, *n*-propyl *p*-vinylbenzene sulfonate, has been examined with respect to polymerization by butyllithium in tetrahydrofuran at −75°C. The polarity and resonance stabilization,[8,9] of the monomer are expected to be such that it may be reactive in anionic polymerization. In solution in tetrahydrofuran, contact ion pairs,[10] an appreciable concentration of solvent separated ion pairs, and a small proportion of very highly reactive free ions may be anticipated to be the main means of propagation.[10,11] With these latter two species the monomer does not co-ordinate before reaction, but approaches the anion in the syndiotactic sense, which is sterically preferred because of the usual nonbonded interactions.[12–14] Polymerization should then proceed as from a single propagating species to produce, at low temperatures, predominantly syndiotactic polymer.

EXPERIMENTAL

Materials

Solvent. Reagent-grade tetrahydrofuran was freed of inhibitor, refluxed over sodium, and distilled. It was then stirred and refluxed over

* Present address: Olin Building, Case Western Reserve University, Cleveland, Ohio 44106.

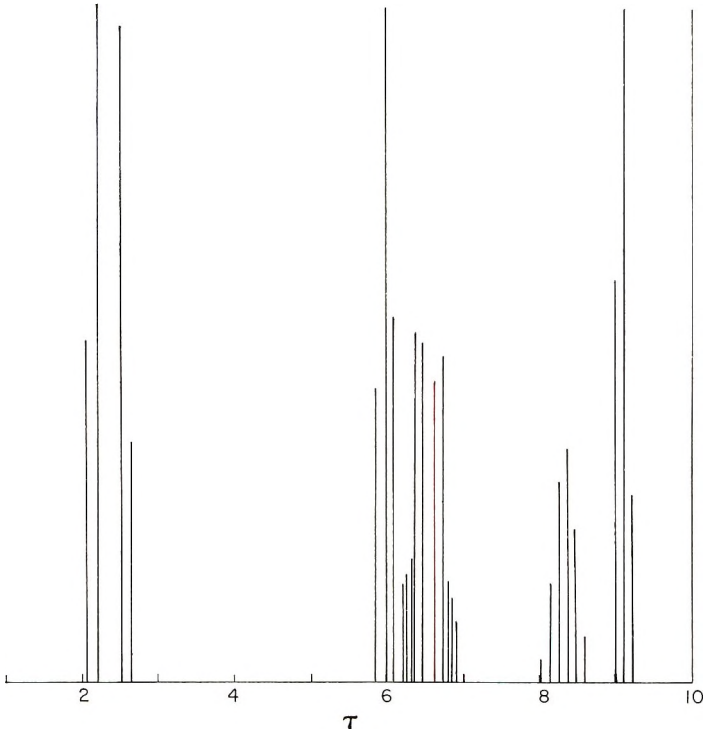

Fig. 1. NMR line spectrum of *n*-propyl *p*-(β-bromoethyl)benzene sulfonate taken in deuterochloroform with 1% tetramethylsilane reference.[10]

calcium hydride and distilled in an argon atmosphere. The tetrahydrofuran fraction boiling at 66.3°C was collected and used in polymerization work. Final purification and drying of solvent was achieved using a high vacuum grid to enable distillation of solvent into a vessel containing a small quantity of outgassed butyllithium.

Prepurified grade argon was used as the inert atmosphere in all reactions.

***n*-Butyllithium.** *n*-Butyllithium was prepared from *n*-butyl chloride and a slight excess of lithium wire in low-boiling petroleum ether as the solvent.[15] The reaction mixture was centrifuged under argon and the supernatant withdrawn with a syringe and stored in serum capped bottles at −20°C under argon. Several preparations, ranging in molarity from 3 to 4*M*, were employed.

***n*-Propyl *p*-Vinylbenzene Sulfonate.** This monomer was prepared in three stages as described by Spinner et al.[16] β-Bromoethyl benzene is chlorosulfonated to a mixture of (β-bromoethyl)benzenesulfonyl chlorides which are separated by fractional crystallization. The *para* isomer is converted to the propyl ester by using the modification of Chen and Hammett.[17] The purity of the *n*-propyl *p*-(β-bromoethyl)benzene sulfonate is conveniently determined at this stage by NMR (Fig. 1) and infrared spectra.[18] Of particular diagnostic value are the doublets of the

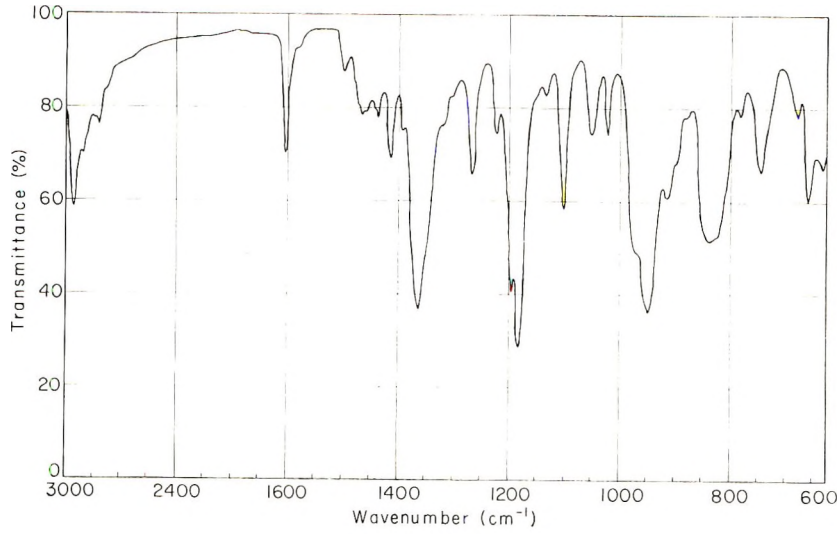

Fig. 2. Infrared spectrum of *n*-propyl *p*-(β-bromoethyl)benzene sulfonate.

phenyl protons at 2.11 and 2.55 τ and the proton resonance of group, $-CH_2CH_2-Br$, centered at 6.53 τ, also group $-SO_2-CH_2-$ at 5.97 τ.

The infrared spectrum shown in Figure 2, was taken as a smear between potassium bromide disks. The spectrum is similar to that published,[18] with ν_{asym} SO_2 = 1363 cm^{1-}, ν_{sym} SO_2 = 1150–1200 cm^{-1}, and νSO–C = 947 cm^{-1}.[19] n_D^{25} was 1.5388.

The final step of the preparation involves dehydrobromination. The vinyl compound is distilled with great difficulty;[16] n_D^{25} = 1.5374. It was normally kept over calcium hydride at 0°C with a trace of 4-*tert*-butyl pyrocatechol as stabilizer.

Anal. Calcd for $C_{11}H_{14}O_3S$: C, 58.37%; H, 6.23%; S, 14.17%. Found: C, 58.3%; H, 6.6%; S, 14.1%.

Polymerizations

The Pyrex glass reaction vessel used for the polymerizations constituted part of a high-vacuum grid maintained at $<10^{-5}$ mm Hg and registered with a Vacustat pressure gauge. The vessel could therefore be flamed out under high vacuum and the monomer and solvent added from vessels containing sodium films. Condensation of the solvent vapor was effected by the use of liquid nitrogen. The polymerization vessel, which contained a serum cap, was then isolated from the grid and connected by way of a tap and the serum cap to an argon line which entered the vessel by means of a hypodermic needle through the serum cap. By the use of these techniques the advantages of high vacuum operations and the ease of using rubber seals were combined. Initiator could then be added through the same serum cap by using a syringe. In addition, the vessel was kept at −75°C by a bath of methanol and solid carbon dioxide. Stirring was

effected by an internal PTFE-coated stirrer operated magnetically from below.

The polymerization was carried out by distilling tetrahydrofuran (CaH_2-, Na-, and BuLi-dried) into the reaction vessel. This was brought to room temperature and argon passed over the solution. The monomer, *n*-propyl *p*-vinylbenzene sulfonate (CaH_2- and Na-dried), which is impossible to distill in a normal still, was passed to the reaction vessel through a tube (0.25 mm bore) which had been previously heated with argon passing through it. Involatile monomers were always transferred by this procedure through very flexible tubes by a difference in argon pressure between the two vessels maintained at room temperature. The reaction mixture, 10% (v/v), was stirred to obtain a homogeneous solution and then taken to −75°C. Butyllithium solution was added by syringe in a similar manner to that of Wenger et al.,[20] in that impurities can be titrated out, but when excess butyllithium is present the whole solution immediately turns pink. The solution was left for 9 hr but no diminution of color occurred. Termination was effected by the addition of just sufficient methanol to remove the color.

The polymer solution was precipitated in a small volume of dry methanol and purified by solution in methyl ethyl ketone and precipitation in methanol. It was dried at 60°C in a vacuum oven. The yield was almost quantitative.

ANAL. Calcd for $C_{11}H_{14}O_3S$: C, 58.37%; H, 6.23%; S, 14.17%. Found: C, 58.7%; H, 6.4%; S, 14.1%.

To hydrolyze this polymer to PSSA, 1 g of polymer was suspended in 100 ml of 8*N* hydrochloric acid and the solution refluxed for 3 hr. This was continued for a period of 24 hr to ensure complete hydrolysis. The solution was cooled, filtered, and dialyzed to remove acid and alcohol. Evaporation of the solution of the polyacid gave white PSSA.

Hydrolysis was shown to be definitely complete by the absence of the ester triplets at 9.04 and 5.97 τ in the NMR spectrum and the similarity of the infrared spectrum to a published example.[21]

Characterization of the Polymers

The most detailed quantitative knowledge of the microtacticity of a polymer is often obtained from its high-resolution nuclear magnetic resonance spectrum,[22] while useful information can be obtained from x-ray diagrams and empirical absorption measurements.

NMR Measurements. Polymer solutions were normally 10% (w/v) with 1% of internal standard. Standards were either tetramethylsilane or 3-trimethylsilylpropane 1-sulfonate, depending on their solubility in the solvent being used. The Varian 60 Mcps instrument was operated at 30°C.

Figure 3 gives the NMR spectrum of poly(*n*-propyl *p*-vinylbenzene sulfonate) taken in deuterochloroform. Comparison with that of *n*-propyl

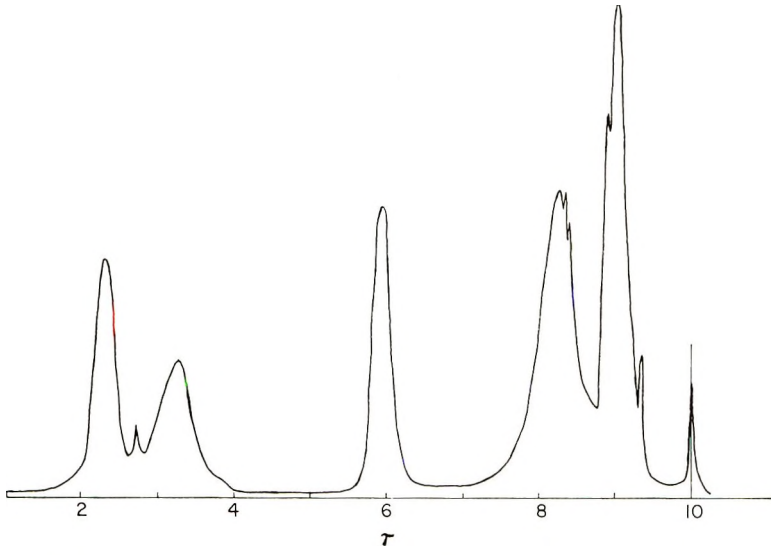

Fig. 3. NMR spectrum of poly(*n*-propyl *p*-vinylbenzene sulfonate) taken in deuterochloroform with 1% tetramethylsilane reference.[10]

p-(β-bromoethyl)benzene sulfonate (Fig. 1) adequately proves the structure of the polymer. That of the polymer is remarkable in that the methine peak of the backbone seems to have been moved extensively and is no longer visible. The main phenyl resonances at 3.28 and 2.32 τ can be assigned to the *ortho* and *meta* protons,[23] respectively. The shielding of all these protons compared with the low molecular weight analog (5.97, 2.55, and 2.11 τ) results from the protons being in the diamagnetic shielding of neighboring phenyl groups.[23] In particular, the large shift of the methine protons is considered to be particularly likely for the trans-trans conformation of syndiotactic polymer as the methine protons are then sandwiched between neighboring phenyl groups. A TGTG′TGTG′ conformation would seem difficult and offer less diamagnetic shielding. The NMR results are taken to furnish independent evidence for the syndiotacticity of the polymer. If there had been a high isotactic content, the methine resonance would be expected to be distinguishable from the backbone methylene protons, as found for isotactic polystyrene.[24]

The spectrum of the PSSA was taken in concentrated hydrochloric acid. The phenyl protons occur in two main peaks at 2.26 and 3.16 τ with a small peak at 3.56 τ. These appear at higher field than those of *n*-propyl *p*-(β-bromoethyl)benzene sulfonate, but are lower than those of the poly(*n*-propyl *p*-vinylbenzene sulfonate). Presumably the diamagnetic shielding is less able to operate for the polyacid. The backbone methylene peak occurs at 8.20 τ.

Infrared Characterization. Polymers were ground with dry potassium bromide and made into disks. Comparison of the spectrum of poly(*n*-propyl *p*-vinylbenzene sulphonate), shown in Figure 4, with that shown

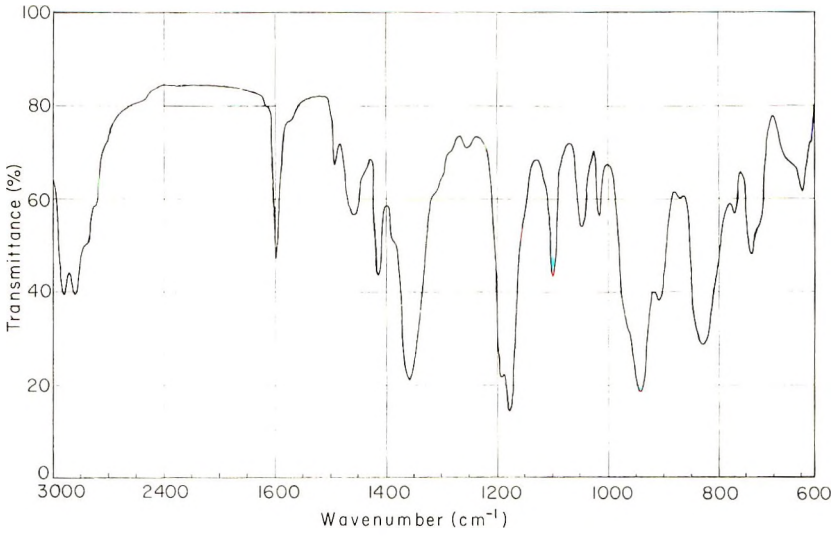

Fig. 4. Infrared spectrum of poly(*n*-propyl *p*-vinylbenzene sulfonate).

in Figure 2 indicates the formula of the polymer is as expected. As for the low molecular weight analog, the ν_{asym} SO_2 vibration occurs at 1357 cm^{-1}, ν_{sym} SO_2 at 1150–1200 cm^{-1}, and νSO–C between 900 and 1000 cm^{-1}. Assignment of most of the other bands may be tentatively carried out by comparison with spectra obtained for *p*-disubstituted benzenes of various types.[25,26] Comparison with the polycarbonate, $-[C_6H_4-C(CH_3)_2-C_6H_4-O-CO-O-]_n-$, suggests the bands might be assigned as follows: ν_{14}, 1597; ν_{19A}, 1492; ν_{18A}, 1015; ν_{11}, 828 cm^{-1}.

The infrared spectrum of the PSSA was almost identical to that of a published atactic sample,[21] but the resolution was less.

Molecular Weight Determinations. The presence of unknown quantities of trace impurities in the monomer often required that sufficient initiator should be added to produce a low degree of polymerization. Most of the polymers were therefore thought to be of very low molecular weight, and it was desirable to determine if the polymerization was capable of giving material that could be classed as polymeric. The Mechrolab vapor pressure osmometer, Model 301A, was used, although only an approximate molecular weight was expected.

For an 0.005*M* solution of the polymer in acetone, molecular weights of $4.0–5.0 \times 10^3$ were obtained. The instrument is claimed to be accurate to 4–5%, even for polymers in this range, provided measurements are extrapolated to zero concentration of solute.

Potentiometric Titrations. pH measurements were carried out by using a Radiometer glass electrode, type B, in conjunction with an internal bridge calomel electrode. These electrodes were used with a Radiometer null-point pH meter, type PHM 4c. The pH values of 0.05*M* potassium hydrogen phthalate and 0.05*M* sodium borate, used for standardization,

were as listed by Gold.[27] At a concentration of $4 \times 10^{-3}M$ the polyacid was fully dissociated, as calculated from the pH of the solution. This was verified by potentiometric titration, which enabled the polymer to be characterized as having one sulfonic acid group to each benzene ring. The complete dissociation of the sulfonic acid group is typical of strongly ionophoric polyelectrolytes.

DISCUSSION

The anionic polymerization of the monomer, *n*-propyl *p*-vinylbenzene sulfonate, by butyllithium provides another example of this method of producing high molecular polymers. Normally in this system, initiation consists of the addition of *n*-butyllithium across the monomer double bond,[29] and one polymer chain is produced by each initiator molecule.[30] Chain termination is negligible, but initiation and propagation proceed at comparable rates.[31] Electron-attracting substituents on the aromatic ring generally increase the relative rate of reaction of substituted styrenes with the styryl anion.[32] This supports the concept that anionic charge is on the carbon alpha to the aromatic ring. Provided that attack on the ester grouping is not important, this polymerization should offer the possibility of preparing monodisperse polymer, as for styrene.[33]

The hydrolysis of this polymer to PSSA proceeds to completion and should be particularly facile, especially in aqueous sodium hydroxide, as several mechanisms may operate together such as S_{N1} and S_{N2}[34] attack at the α-carbon of the ester group. Alternatively, unimolecular or bimolecular reaction may occur to yield propylene, or perhaps neighboring group participation is important as found in the hydrolysis of other polymers.

Little supplementary evidence for the tacticity appears to be provided by the properties of the PSSA. As for poly(vinylsulfonic acid)[35] and atactic PSSA,[5] this polyacid may be considered a typical strong polyacid. While no quantitative assessment of its tacticity can be given, it is proposed that the polyacid is highly syndiotactic.

I thank Professor G. M. Burnett, Dr. P. Meares, Dr. J. J. Hermans, and the Technical Staff of Aberdeen University.

References

1. R. H. Wiley and S. F. Reed, *J. Amer. Chem. Soc.*, **78**, 2171 (1956).
2. R. A. Mock, C. A. Marshall, and T. E. Slykhouse, *J. Phys. Chem.*, **58**, 498 (1954).
3. E. E. Gilbert, *Sulfonation and Related Reactions*, Interscience, New York, 1965, p. 76.
4. A. S. Tevlina and Y. B. Trostyanskaya, *Vysokomol. Soedin.*, **5**, 1178 (1963).
5. J. P. Dux and J. Steigman, *J. Phys. Chem.*, **62**, 288 (1958).
6. M. Kato, T. Nakagawa, and H. Akamatu, *Bull. Chem. Soc. Japan*, **33**, 323 (1960).
7. W. R. Carroll and H. Eisenberg, *J. Polym. Sci. A*, **2**, 599 (1666).
8. J. Furukawa and T. Tsuruta, *J. Polym. Sci.*, **36**, 275 (1959).
9. T. Yonezawa, T. Higashimura, K. Katagiri, K. Hayashi, S. Okamura, and K. Fukui, *J. Polym. Sci.*, **26**, 311 (1957).

10. D. N. Bhattacharyya, C. L. Lee, J. Smid, and M. Szwarc, *J. Phys. Chem.*, **69**, 612 (1965); *ibid.*, **69**, 624 (1965).

11. T. E. Hogen-Esch and J. Smid, *J. Amer. Chem. Soc.*, **88**, 307 (1966); ibid., **87**, 669 (1965).

12. L. L. Ferstandig and F. C. Goodrich, *J. Polym. Sci.*, **43**, 373 (1960).

13. J. W. L. Fordham, *J. Polym. Sci.*, **39**, 321 (1959).

14. C. E. H. Bawn, W. H. Janes, and A. M. North, in *Macromolecular Chemistry, Paris 1963* (*J. Polym. Sci. C*, **4**), M. Magat, Ed., Interscience, New York, 1963, p. 427.

15. H. Gilman, W. Langham, and F. W. Moore, *J. Amer. Chem. Soc.*, **62**, 2327 (1940).

16. I. H. Spinner, J. Ciric, and W. F. Graydon, *Can. J. Chem.*, **32**, 143 (1954).

17. C. H. Chen and L. P. Hammett, *J. Amer. Chem. Soc.*, **80**, 1329 (1958).

18. T. G. Brydges, D. G. Dawson, and J. W. Lorimer, *J. Polym. Sci. A-1*, **6**, 1009 (1968).

19. N. S. Ham, A. N. Hambly, and R. H. Laby, *Austral. J. Chem.*, **13**, 443 (1960).

20. F. Wenger and S. S. Yen, *Makromol. Chem.*, **43**, 1 (1961).

21. R. Hart and R. Janssen, *Makromol. Chem.*, **43**, 242 (1966).

22. F. A. Bovey, *Pure Appl. Chem.*, **12**, 525 (1966).

23. F. A. Bovey and G. V. D. Tiers, *Fortsch. Hochpolym.-Forsch.*, **3**, 139 (1963).

24. R. J. Kern and J. V. Pustinger, *Nature*, **185**, 236 (1960).

25. C. Y. Liang, *Newer Methods of Polymer Characterization*, B. Ke, Ed., Interscience, New York, 1964, p. 33.

26. C. Y. Liang and S. Krimm, *J. Mol. Spectry.*, **3**, 554 (1959).

27. V. Gold, *pH Measurements*, Methuen, London, 1956, p. 118.

28. A. Katchalsky, N. Shavit, and H. Eisenberg, *J. Polym. Sci.*, **13**, 69 (1954).

29. R. C. P. Cubbon and D. Margerison, *Proc. Chem. Soc.*, **1960**, 146.

30. D. J. Worsfold and S. Bywater, *Can. J. Chem.*, **38**, 1891 (1960).

31. E. N. Kropacheva, B. A. Dolgoplosk, and E. M. Kuznetsova, *Dokl. Akad. Nauk SSSR*, **130**, 1253 (1960).

32. J. Smid and M. Szwarc, *J. Polym. Sci.*, **61**, 31 (1962).

33. T. Altares, D. P. Wyman, and V. R. Allen, *J. Polym. Sci. A*, **2**, 4533 (1964).

34. C. K. Ingold, *Structure and Mechanism in Organic Chemistry*, Cornell Univ. Press, Ithaca, N. Y., 1953, p. 341.

35. H. Eisenberg and G. R. Mohan, *J. Phys. Chem.*, **63**, 671 (1959).

Received December 10, 1968
Revised September 11, 1969

JOURNAL OF POLYMER SCIENCE: PART A-1 VOL. 8, 917-927 (1970)

Endgroup Analysis of Isolated Poly(methyl Methacrylate) from Graft Copolymers of Wool

KOZO ARAI, SHIGEO KOMINE, and MICHIHARU NEGISHI,
Faculty of Technology, Gunma University, Kiryu, Japan

Synopsis

In order to elucidate the termination mechanism in the graft copolymerization of methyl methacrylate to unreduced and reduced wool fibers, graft copolymers were prepared by means of the LiBr–$K_2S_2O_8$ redox sytem without homopolymer or with $K_2S_2O_8$ only with homopolymer at 30°C. The graft polymers (PMMA) were isolated almost completely from the wool trunk by an HCl-digestion method, leaving a few amino acid residues on the end of the graft polymers. Dinitrophenylation of the isolated polymer was carried out by various methods. The spectral features were almost the same as for dinitrophenylated amino acids of the usual type such as valine, leucine, and methionine, with a maximum in ultraviolet light at 340–345 mμ. From colorimetric analysis of the number of dinitrophenylated amino acid endgroups and the measurement of the average molecular weight of the isolated polymers, the number of amino acid endgroups linked to the graft polymers was calculated to be about one and two per polymer chain in reduced and unreduced wool, respectively, independent of the reaction system, graft-on, and molecular weight of graft polymers. From these facts, it was suggested that the most of isolated polymers are the truly grafted polymers. Also, the termination reactions have been explained as follows. In the unreduced wool, the restriction of mobility of the radical end might be expected, for the confinement of growing chains in wool fibers. This would be favorable to termination by recombination rather than by the disproportionation, since the former has a lower activation energy than the latter. Thus, the formation of intra- or intermolecular crosslinks might be considered between polypeptide chains. On the other hand, in the reduced wool, the mobility of graft polymers might be considered to be greater than that of unreduced wool because of its open structure. Therefore, termination would be principally by disproportionation between graft polymer radicals.

INTRODUCTION

Graft copolymerization of vinyl monomers on various fibers, films, and many other solid materials has been reported during the past two decades. Even though the internal deposition of polymers occurs preferentially inside the solid materials, homopolymer is formed in the reaction medium and on the surface. It is not certain whether solvent extraction processes for removing homopolymers are effective as with systems in which high molecular weight homopolymers are occluded. The results of electron microscopic observation for radiation grafting of styrene to wool[1] and rayon

fibers,[2] indicate that both extractable and unextractable homopolymers are likely to exist in these grafted fibers.

Grafting mechanisms have been studied by Speakman et al.[3,4] from the point of view of the initiation reaction in aqueous persulfate or hydrogen peroxide systems. However, it is not evident whether the deposited polymers are truly grafted polymer or internal homopolymer.

In our previous reports, it was shown that extractable homopolymers not formed to any appreciable extent in wool fibers grafted with the aqueous LiBr–$K_2S_2O_8$ redox system.[5]

The purpose of the present investigation is to determine quantitatively the number of truly grafted poly(methyl methacrylate) chains and to elucidate the mechanism of the termination reaction in the viscous matrix of wool fiber as recognized in the previous report.[6] Quantitative determination of amino acid endgroups incorporated in separated graft polymer chains has been made by the 2,4-dinitrofluorobenzene method.

EXPERIMENTAL

Merino wool tops were purified by Soxhlet extraction with acetone for about 24 hr, followed by washing with cold water and air drying.

Commercially available methyl methacrylate (MMA) was washed with 5% NaOH solution and water, dried with anhydrous sodium sulfate, and distilled under reduced pressure in a stream of nitrogen before use.

Lithium bromide, potassium persulfate, sodium bicarbonate, thioglycollic acid (TGA), diethylene glycol monobutyl ether (BC), 2,4-dinitrofluorobenzene (FDNB), and triethylamine were of first or special reagent grade and used without further purification. Various dinitrophenylated amino acids (DNP-amino acids) were of special reagent grade (Wako Pure Chemical Industries, Ltd.).

Reduction of Wool Fibers

The wool (1 g) was treated for 24 hr at 30°C with 0.2*N* solution of TGA adjusted to pH 4.7 (100 ml), washed with water, ethanol, again with water (200 ml each), pressed out with filter paper, and then subjected to grafting.

Graft Copolymerization

The preparation of the LiBr–$K_2S_2O_8$ system for grafting was carried out by the procedure reported in previous paper.[7] A 1-g portion of reduced or unreduced wool was treated with a solution containing 27.5 g LiBr, 0.2 g $K_2S_2O_8$, 22.5 g BC, 44.8 g H_2O, and 1.0, 2.0, 5.0, or 10 g MMA (LiBr–$K_2S_2O_8$ system).

Graft copolymerization by the system accompanied by the formation of a large amount of homopolymer was also carried out. The wool fibers were treated with solution containing 0.2 g $K_2S_2O_8$, 22.5 g BC, 72.3 g H_2O, and 5.0 g MMA ($K_2S_2O_8$ system).

TABLE I
Grafted Wool Samples Prepared under Various Grafting Conditions

Sample	Expt. no.	Reaction system	Monomer added, g	Graft-on, %
Unreduced wool	G1	$LiBr–K_2S_2O_8$	5.0	93.9
	G2	$LiBr–K_2S_2O_8$	5.0	86.7
	G3	$LiBr–K_2S_2O_8$	1.0	31.5
	G4	$LiBr–K_2S_2O_8$	2.0	84.5
	G5	$LiBr–K_2S_2O_8$	5.0	92.5
	G6[a]	$K_2S_2O_8$	5.0	92.0
Reduced wool	RG1	$LiBr–K_2S_2O_8$	5.0	146.9
	RG2	$LiBr–K_2S_2O_8$	2.0	127.8
	RG3	$LiBr–K_2S_2O_8$	5.0	205.8
	RG4	$LiBr–K_2S_2O_8$	10.0	219.0
	RG8	$K_2S_2O_8$	5.0	108.1

[a] Time of reaction; 30°C., 24 hr.

The grafting was carried out for 3 hr at 30°C, unless otherwise specified, until the reaction was almost completed. After the reaction, the wool fibers were washed with water alone in the case of $LiBr–K_2S_2O_8$ system. In the case of $K_2S_2O_8$ system, the wool fibers were extracted with acetone in a Soxhlet apparatus for about 24 hr, washed with water, and air-dried.

The extent of grafting was shown by the percentage weight increase on the original wool fibers. The grafted wool samples prepared by various grafting conditions are listed in Table I.

Separation of Graft Polymers

The grafted wool fibers (0.5 g) were digested in 35 ml of 6*N* HCl for about 30 min at 110°C until an intense reddish-blue coloration appeared. The partially digested materials were then filtered off from the colored solution by a glass filter and washed with 6*N* HCl. Again, the digestion was allowed to proceed for 24 hr at 110°C in a flask with reflux condenser attached, and the material was then thoroughly washed with boiling water until neutral and dried. Very white, fibrous, insoluble residues could be obtained by the two step digestion technique.

Determination of Nitrogen Content in Isolated Polymers

The isolated PMMA samples were dissolved in benzene, filtered off, and then precipitated in methanol. Purification was repeated three times with the use of acetone–methanol as a solvent–precipitant pair. Nitrogen analysis of the polymers was followed by the semimicro Kjeldahl method.[8]

A pellet of purified polymer (0.5–1.0 g) and 1 g of catalyst composed of 5 g selenium metal, 150 g anhydrous potassium sulfate, 10 g mercuric oxide, and 50 g copper sulfate crystal, were placed in Kjeldahl digestion flask. They were heated very gently until the substance was thoroughly wetted with the acid and frothing ceases. The temperature then was raised

gradually; the acid was boiled for 20 min, allowed to cool, and then diluted to about 20 ml by the addition of 15 ml of water. About 30 ml of 48% NaOH solution was poured in the flask, the ammonia evolved was distilled into 50 ml of 0.01N H_2SO_4. Distillation was carried out until the distillate becomes neutral; the 500-ml receiver was nearly filled and then the distillate was diluted accurately to 500 ml by the addition of water. A 50-ml portion of distillate was pipetted out and the excess of acid was titrated with 0.005N NaOH, the titration curves being obtained with use of a glass electrode (Horiba PH meter Type M-5). From the difference of neutralized volumes at pH 7.0 with a blank titration, the evolved molar ammonia (N mole) was computed:

$$N = (a - b)\,(f/200) \times 10^{-2}$$

where a and b denote the volume (milliliters) of 0.005N NaOH required for blank and real titration, respectively; f is a factor for 0.005N NaOH.

Nitrogen analysis was carried out three runs for each sample, average values are shown in Table II.

TABLE II
Number of Nitrogen Atoms per Polymer Chain Determined by Nitrogen Analysis

Sample	Average molecular weight of isolated polymers	Number of nitrogen atom per polymer chain
G5	4.2×10^5	Not detected
RG3	6.2×10^4	1.4

Dinitrophenylation

It is known that 2,4-dinitrofluorobenzene (FDNB) characteristically reacts with free amino, phenolic hydroxyl, and sulfydryl groups. Dinitrophenylation of the amino acid residues linked on the end of the separated graft polymer (PMMA) chain, was performed by the two different methods.

Sodium Bicarbonate System. The isolated polymes (0.5 g) remaining in the fiber state were suspended with occasional shaking in 50 ml of a mixture of 1% sodium bicarbonate and the same volume of 1% FDNB ethanol solution for 24 hr at 30°C. according to the modified procedure of Fraenkel-Conrat.[9]

Triethylamine System. By the method advocated by Whalley,[10] the coupling reaction was performed for 24 hr at 30°C in a mixed solution containing 10 ml of 9–10% benzene solution of the isolated polymers, 0.5 ml. FDNB, and few drops of triethylamine.

Purification of Dinitrophenylated Polymers

After the reaction was completed, three different procedures of purification for dinitrophenylated polymer (DNP-polymer) were tested to determine the best method for removing excess FDNB and the by-products of the reaction.

Extraction Method. Yellow fibrous materials (0.5 g) obtained by the sodium bicarbonate system were washed several times with 5% sodium bicarbonate solution on the filter paper and with water and then extracted four times, each for 24 hr, with 30 ml of cold methanol (good solvent for FDNB and a poor solvent for PMMA). Extraction was then carried out five times with a solvent mixture comprising 9 parts of methanol and 1 part of diethyl ether (a good solvent for FDNB and dinitrophenol). After the extraction, the material was washed with methanol and then water. Bright yellow DNP-polymer was obtained.

Precipitation Method. Acetone–diethyl ether (9:1)–methanol–petroleum ether (5:5) was used as a solvent–precipitant pair. Reprecipitation was repeated 3 to 4 times until the precipitant was no more discolored.

Alternatively, acetone–cold methanol was used as a solvent–precipitant pair. Reprecipitation was repeated 3 to 4 times. This procedure was applied for all DNP-polymers obtained by the above described methods.

Determination of DNP-Amino Acid Endgroups

The purified DNP-polymer dissolved in ethyl acetate. Yellow DNP-polymer solutions of concentration range 0.5–4.0 g/l. were prepared. The absorption spectra with a maximum in ultraviolet light at 340–345 mμ were

TABLE III
Average Molecular Weight of DNP-Polymer and Number of DNP-Amino Acid Endgroups per Polymer Chain Determined by the DNP Method for the Sodium Bicarbonate System

Sample	Purification method	Average molecular weight of DNP-Polymer determined by viscosity or osmotic pressure measurement	Number of DNP-amino acid end-groups per polymer chain
G1	A[a]	3.8×10^5	2.4
G1	B[b]	5.2×10^5	2.4
G1	C[c]	4.7×10^5 4.9×10^5 [d]	2.4
G2	C	4.6×10^5	2.1
G3	C	1.7×10^5	2.1
G4	C	2.5×10^5	2.3
G5	C	4.2×10^5 4.1×10^5 [e]	2.4
G6	C	3.3×10^5	2.5
RG1	A	4.4×10^4	0.9
RG2	B	4.7×10^4 5.0×10^4 [e]	1.0
RG3	C	6.2×10^4	0.9
RG4	C	1.7×10^5	0.9
RG8	C	7.8×10^4	0.9

[a] DNP-polymer purified by the extraction method.

[b] DNP-polymer purified by the precipitation method with acetone–ethyl ether (solvent)–methanol–petroleum ether (precipitant).

[c] DNP-polymer purified by the precipitation method with acetone(solvent)–methanol (precipitant).

[d] Isolated polymer.

[e] Determined by osmotic pressure measurement.

obtained by Hitachi spectrophotometer (Type EPS-2U) using 1-cm quartz cells. The spectral absorption curves were almost the same with these of the DNP-amino acids of the usual type. For the estimation of DNP-amino acids endgroups, calibration curve has been obtained with DNP–DL-methionine or DNP–L-leucine, both of which show an absorption maximum at 343 mμ in ethyl acetate. The intensity of absorption was corrected by subtracting the absorption of the same concentration of the isolated polymer solution.

Molecular Weight Determination of DNP-Polymer

The average molecular weight ($\bar{M}$) of the isolated poly(methyl methacrylate) and its DNP-polymer were measured viscometrically in benzene solution at 30°C from the following equation:[11]

$$[\eta] = 8.69 \times 10^{-5} M^{0.76}$$

The number-average molecular weight was also obtained for some DNP-polymers from osmotic pressure measurements in toluene at 37°C with the use of a high-speed membrane osmometer (Hewlett Packard, Model 502). These results are shown in Tables II and III.

RESULTS AND DISCUSSION

Nitrogen Content

As shown in Table II, evolved ammonia was not detected in the graft polymers prepared from unreduced wool fibers (G5), which had a high molecular weight, while the graft polymers of low molecular weight (RG-3), which were prepared from reduced wool, had 1.4 nitrogen atoms per polymer chain. This clearly suggests that the wool polypeptide molecules could be almost digested to individual amino acids leaving a few amino acid residues on the end of the isolated poly(methyl methacrylate).

DNP-Amino Acid Endgroup

The spectral absorption curves from 280 to 440 mμ for DNP-polymers are shown in Figure 1. No difference was observed between the spectral absorption curves of DNP-polymers obtained by the sodium bicarbonate and triethylamine method. The absorption curves for DNP-polymers obtained from unreduced and reduced fibers are almost the same, showing an absorption maximum at 343 mμ and shoulder near 410 mμ. The spectral absorption curve for DNP–DL methionine is also shown in Figure 1. These characteristic absorption of DNP-polymer is similar to those of the common DNP-amino acids, e.g., methionine, valine, leucine, etc. The spectral features for DNP-proline, which has heterocyclic groups, and di-DNP-amino acids (except di-DNP-lysine), were clearly shown to be different from those of our DNP-polymers. Therefore, it may be reasonable to consider that the DNP-amino acids incorporated in the isolated polymer would be of the common type of DNP-amino acid.

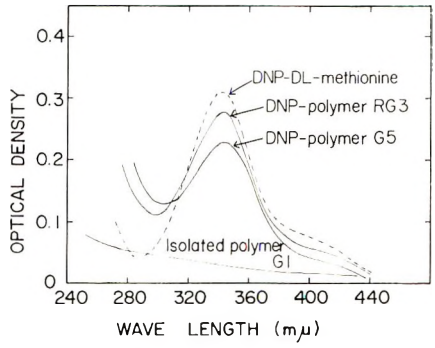

Fig. 1. Absorption spectra of DNP-DL-methionine(2.97×10^{-5} mole/l.), isolated polymer G1(1.5g/l.), and DNP-polymer G5(4.0g/l.) or DNP-polymer RG3 (1.5 g/l.) in ethyl acetate.

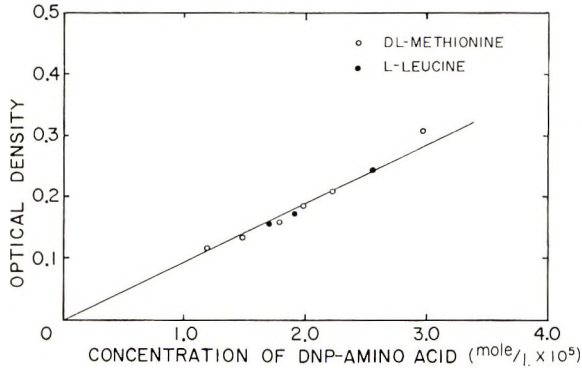

Fig. 2. Optical density vs. molar concentration of (○) DNP-DL-methionine and (●) DNP-L-leucine.

Furthermore, it has been suggested on the basis of kinetic considerations of graft copolymerization[12] or infrared spectroscopical investigation for the polymer fractions obtained by the solvent-extractive fractionation technique[13] that the cysteine residues on wool keratin are the main sites of grafting. Thus, the absorption spectra of DNP-methionine might be expected to be taken as the reference standard curve for estimation of amino acid endgroups incorporated in the isolated poly(methyl methacrylate). The calibration curves for DNP-DL-methionine and DNP-L-leucine are the same as shown in Figure 2. There is a linear relation between optical density and molar concentration of these DNP-amino acids. The molar extinction coefficient is 1.0×10^4. A linear relation is also obtained between optical density and the concentration of DNP-polymer as shown in Figures 3 and 4 for G5 and RG3.

From the number of DNP-amino acid endgroups and average molecular weight of the isolated polymers, the endgroups per polymer chain were calculated as shown in Tables III and IV. Though three different procedures were performed for purification of DNP-polymers, no difference in

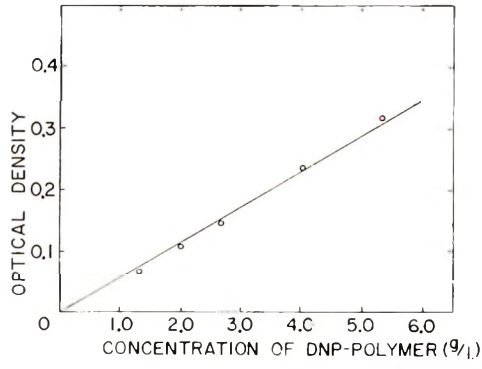

Fig. 3. Optical density vs. concentration of DNP-polymer G5 prepared by the extraction method.

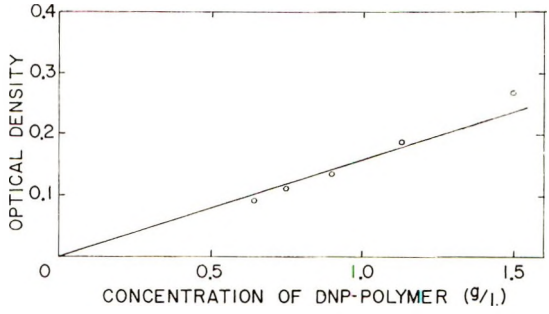

Fig. 4. Optical density vs. concentration of DNP-polymer RG3 prepared by the precipitation method with acetone(solvent)–methanol(precipitant).

the ultraviolet and visible absorption spectral features and no appreciable change in the number of endgroups per polymer chain are observed.

However, use of the precipitation methods gives somewhat greater values for average molecular weight than the extraction method for DNP-polymers prepared under the same reaction conditions. The swelling action and solubility of the DNP-polymers tend to increase in poor solvents for poly(methyl methacrylate), e.g., diethyl ether and methanol. Thus, for the precipitation method, particularly, much larger amounts of the lower molecular weight fractions of DNP-polymers would be likely to solubilize in the precipitant used. Accordingly, care should be taken in determination of endgroups in systems consisting of a mixture of homopolymers and grafted polymers bonding DNP-amino acid endgroups. It seems preferable to use acetone–cold methanol as a solvent–precipitant pair for the purification of DNP-polymer.

The results of Tables III and IV indicate that the number of amino acid endgroups incorporated in the isolated polymers is about one and two per polymer chain in reduced and unreduced wool fibers, respectively. It is noteworthy that the number of endgroups does not depend on the molecular weight of the graft polymer, but on the reduction treatment.

TABLE IV
Average Molecular Weight of DNP-polymer and Number of DNP-Amino Acid Endgroups per Polymer Chain Determined by the DNP Method for the Triethylamine System

Sample	Average molecular weight of DNP-polymer determined by viscosity measurement	Number of DNP-amino acid endgroups per polymer chain
G5	3.6×10^5	2.3
G6	3.1×10^5	2.8
RG3	4.2×10^4	0.8
RG8	5.5×10^4	1.0

Saha's Patent Blue V method[14] for the determination of amino groups was also tried, and nearly the same results were obtained. This experiment was less accurate than our DNP-method, however.

Interpretation of Number of Endgroups

The fact that the polymers deposited in the unreduced wool fibers have about two DNP-amino acid endgroups, does not limit this to one endgroup linked to each end of a long polymer chain. There is a possibility that one end of polymer chain might have two dinitrophenylated groups. Such amino acid residues might include cystine, lysine histidine, tryosine and cysteine, but not di-DNP-histidine and di-DNP-tryosine residues.

Also, the possibility of existence of di-DNP-lysine was ruled out by the following experiment.

Grafted wool fibers (designated as G1) were FDNB-treated in the sodium bicarbonate system, successively digested with HCl, and then purified by the precipitation method resulting in colorless polymers. The ultraviolet absorption spectral features were seen to agree wholly with those of the isolated graft polymer shown in Figure 1. Thus, it is reasonable to consider that the graft polymer chain does not contain di-DNP-lysine. The absence of S-DNP-cysteine is not eliminated by this method, since it readily decomposes with acid digestion.[15]

In order to confirm the absence of di-DNP-cystine or S-DNP-cysteine on the end of the isolated PMMA, the grafted wool fibers (G5) were thoroughly reduced with TGA, or methylated by diazomethane[16] after reduction, to block —SH and phenolic —OH groups, successively digested with HCl, and then FDNB-treated. In any treated sample, about two endgroups per polymer chain were obtained. This figure is the same value as that for grafted polymer without these treatment, indicating the absence of di-DNP-cystine and S-DNP-cysteine on the end of the isolated PMMA. Therefore, it is clear that one DNP-amino acid endgroup is situated on each end of the graft polymer chain. This fact would also give support to consideration of the —SH group as the main site of grafting.

It is clear that one DNP-amino acid residue is linked only to one end of a polymer chain for polymers deposited in reduced wool fibers. Further-

more, the number of endgroups for polymer obtained from the $K_2S_2O_8$ system is the same value as that for polymers from the LiBr–$K_2S_2O_8$ system. When the homopolymers on the fiber surface were removed as much as possible with running water, the extracted polymers were only 7 and 15% from grafted fibers for unreduced (G6) and reduced wool fibers (RG8), respectively. Here, it is noteworthy that most of the polymers deposited in unreduced wool fibers seem to be truly grafted on polypeptide chains, even though large amounts of homopolymers were formed in the reaction medium.

Therefore, it is suggested that intra- or intermolecular crosslinks between polypeptide chains are formed in unreduced wool fibers. Naturally, it could be considered that the growing graft polymer radicals were terminated by the mechanism of recombination in the unreduced wool fibers.

On the other hand, it is possible to consider the following various mechanisms which might occur in the reduced wool fibers: (a) termination by recombination between graft polymer radicals; (b) termination by disproportionation between graft polymer radicals; (c) chain transfer of graft polymer radical to thiol groups existing in high concentration on polypeptide chains; (d) termination between graft polymer radical and primary radical; (e) termination between graft polymer radical and homopolymer radical.

The number of DNP-amino acid endgroups for reduced wool fibers is nearly unity, and is independent of whether homopolymers are formed in the reaction system and also of the yield or molecular weight of DNP-polymer with the various purification methods. These facts seem to indicate that the isolated polymers do not consist of a mixture of grafted polymers and homopolymers, but rather mainly of grafted polymers.

As the consequence, there is every possibility that reactions (b), (c) and (d) might occur in reduced wool fibers.

Restriction of mobility of radical ends might be expected, because of the confinement of the growing chains in unreduced wool fibers.[6] This would be favorable to termination by the recombination rather than by disproportionation, since the former reaction has a lower activation energy than the latter.[17] On the other hand, in the case of the reduced wool fibers, the mobility of graft polymers might be considered to be greater than that of unreduced wool, because of its open structure. Thus, it might be considered that the principally termination by disproportionation between the growing polymer chains would be apt to take place. This point is presently under investigation.

References

1. P. Ingram, J. L. Williams, and V. Stannett, *J. Polym. Sci. A-1*, **6**, 1895 (1968).
2. W. M. Kaeppner and R. Y.-M. Huang, *Textile Res. J.*, **35**, 504 (1965).
3. G. W. Madras and J. B. Speakman, *J. Soc. Dyers Colourists*, **70**, 112 (1954).
4. L. T. Wolfram and J. B. Speakman, *J. Soc. Dyers Colourist*, **77**, 477 (1961).
5. M. Negishi, K. Arai, S. Okada, and I. Nagakura, *J. Appl. Polym. Sci.*, **9**, 3465 (1965).

6. M. Negishi, K. Arai, and K. Tabei, *Sen-i Gakkaishi*, **25**, 311 (1969).
7. M. Negishi, K. Arai, and S. Okada, *J. Appl. Polym. Sci.*, **11**, 115 (1967).
8. J. O. Cole and C. R. Parks, *Ind. Eng. Chem. Anal. Ed.*, **18**, 61 (1946).
9. H. Fraenkel-Conrat, *Biochem. Biophys. Acta*, **9**, 551 (1952).
10. W. B. Whally, *J. Chem. Soc.*, **1950**, 2241.
11. T. G. Fox, J. K. Kinsinger, H. F. Mason, and E. M. Schuele, *Polymer*, **3**, 71 (1962).
12. M. Negishi, K. Arai, and S. Okada, *J. Appl. Polym. Sci.*, **11**, 2427 (1967).
13. K. Arai, M. Negishi, and T. Okabe, *J. Appl. Polym. Sci.*, **12**, 2585 (1968).
14. S. Maiti and M. K. Saha, *J. Polym. Sci. A1*, **5**, 151 (1967).
15. H. Zahn and K. Trautmann, *Z. Naturforsch.*, **96**, 518 (1954).
16. T. Kuwamura, Y. Nakamura, and M. Negishi, *Sen-i Gakkaishi*, **13**, 547 (1957).
17. A. Blumstein, *J. Polym. Sci. A*, **3**, 2665 (1965).

Received August 20, 1969
Revised September 16, 1969

JOURNAL OF POLYMER SCIENCE: PART A-1 VOL. 8, 929–941 (1970)

Preparation of Optically Active *N*-Bornyl Maleimide and Poly(*N*-Bornyl Maleimide)

HIDEMASA YAMAGUCHI and YUJI MINOURA, *Faculty of Engineering, Osaka City University, Sumiyoshi-ku, Osaka, Japan*

Synopsis

Optically active *N*-bornyl maleimide (NBMI) was prepared with maleic anhydride and *d*-camphor amine and the polymerizations of *N*-bornyl maleimide were carried out with benzoyl peroxide (BPO), α,α'-azobisisobutyronitrile (AIBN) and *n*-butyllithium. The specific rotations of the polymers obtained by BPO, AIBN, and *n*-BuLi were +5.1 to +8.4, +10.0 to +10.1 and −7.0 to −9.0, respectively. The results of the x-ray analysis for the above polymers showed that these polymers had the same structure. The specific rotation of the polymer initiated by BPO increased with increasing intrinsic viscosity. The effect of the polymer endgroup on the specific rotation was discussed.

INTRODUCTION

The polymerization and the copolymerization of *N*-substituted maleimides have been studied by several authors.[1–4] Optically active *N*-substituted maleimide and optically active poly-*N*-substituted maleimide have not been prepared, in spite of a number of studies on optically active polymers.

The present paper, reported the preparation of optically active bornyl maleimide (NBMI) and its optically active polymer. NBMI was synthesized by the cyclization reaction of *N*-bornyl maleic acid, which was obtained from maleic anhydride and camphor amine as following.

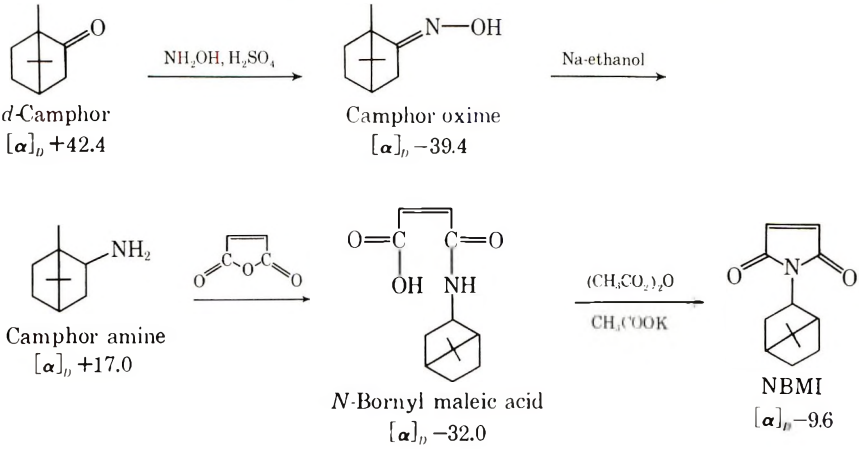

Optically active NBMI was polymerized with benzoyl peroxide (BPO) or α,α'-azobisisobutyronitrile (AIBN) as free radical initiators and *n*-butyllithium (*n*-BuLi) as an anionic initiator, and optically active poly(*N*-bornyl maleimide) (PNBMI) was obtained.

The intrinsic viscosity of the polymers was 0.030–0.064 (MW 2400–5100). It was found from the results of the x-ray analysis that the polymers initiated by BPO, AIBN, and *n*-BuLi had the same structure. The specific rotation of PNBMI obtained by BPO, AIBN, and *n*-BuLi was +5.1 to +8.4, +10.0 to +10.1, and −7.0 to −9.0, respectively. The optical rotatory dispersions of these asymmetric polymers had the same positive Cotton effects which were found to fit the simple Drude equations. The λ_c values of the polymers initiated by BPO, AIBN, and *n*-BuLi were 258–260, 253, and 256 mμ, respectively.

It was thought that the differences in the specific rotation for the polymers initiated by BPO, AIBN, and *n*-BuLi (i.e., +8.1, +10.1, and −9.1) and having the same degree of polymerization were attributable to differences in the endgroups of the polymers. The specific rotation of the polymer initiated by BPO increased with increasing intrinsic viscosity.

Furthermore, the effects of temperature and solvents on the specific rotation of NBMI and PNBMI were investigated.

EXPERIMENTAL

Materials

d-Camphor, $[\alpha]_D$ +42.4 (in ethanol), was a commercial product used without further purification. Commercially supplied hydroxylamine sulfate, maleic anhydride, acetic anhydride, and potasium acetate were used without further purification.

The solvents, THF, EtOH, Et_2O, $(CH_3CO)_2O$, etc., were purified by usual methods.

BPO was purified by recrystallization twice from chloroform. AIBN was purified by recrystallization from methanol. A hexane solution of *n*-BuLi was supplied commercially, and its concentration was determined by the usual double titration method of Gilman.[5,6]

Optically Active Camphor Oxime. Camphor oxime was obtained from *d*-camphor and hydroxylamine; 70% yield; mp 119.5–120°C; $[\alpha]_D$ −39.4 in ethanol. (Lit.[7,8] mp 118°C, $[\alpha]_D$ −42.4 in alcohol).

ANAL. Calcd for $C_{10}H_{17}ON$: C, 71.9%; H, 10.0%; N, 8.4%. Found: C, 72.1%; H, 10.3%; N, 8.5%.

Optically Active *d*-Camphor Amine. Camphor amine was obtained by the reduction of *d*-camphor oxime; 95.5% yield; mp 159–162°C; $[\alpha]_D$ +17.0 in ethanol. (Lit.[9] mp 163°C, $[\alpha]_D$ +45.5).

ANAL. Calcd for $C_{10}H_{19}N$: C, 78.4%; H, 12.4%; N, 9.1%; MW, 153. Found: C, 77.3%; H, 11.8%; N, 8.8%; MW, 161.

Optically Active *N*-Bornyl Maleic Acid. A solution of camphor amine in dry diethyl ether was added dropwise to a dry diethyl ether solution of maleic anhydride with vigorous stirring over a period of 30 min in a three-necked flask. After stirring for 1.5 hr, the crude product precipitated from the reaction system was filtered and was purified by the recrystallization from methanol. *N*-Bornyl maleic acid was obtained in 83.7% yield; mp 183–184.5°C; $[\alpha]$ −32.0 in ethanol.

ANAL. Calcd for $C_{14}H_{21}O_3N$: C, 66.4%; H, 8.4%; N, 5.5%; MW, 251. Found: C, 66.9%; H, 8.4%; N, 5.6%; MW, 245.

Optically Active *N*-Bornyl Maleimide. A solution of *N*-bornyl maleic acid, potassium acetate, and benzoquinone in acetic anhydride was reacted at 80 ~ 85°C in a three-necked flask with vigorous stirring over a period of 30 min. After 3 hr, the reaction mixture was poured into water. The viscous slurry obtained was washed with water to remove acetic acid and dried under vacuum. The crude product was purified by sublimation at 120°C under 12 mm Hg. NBMI recrystallized from methanol was obtained as crystalline needles in 32% yield; mp 58.5–60.5°C; $[\alpha]_D$ −9.6 in ethanol.

ANAL. Calcd for $C_{14}H_{19}O_2N$: C, 72.1%; H, 8.2%; N, 6.0%; MW, 233. Found: C, 71.2%; H, 8.1%; N, 5.5%; MW, 237.

Its infrared spectrum is shown in Figure 1a.

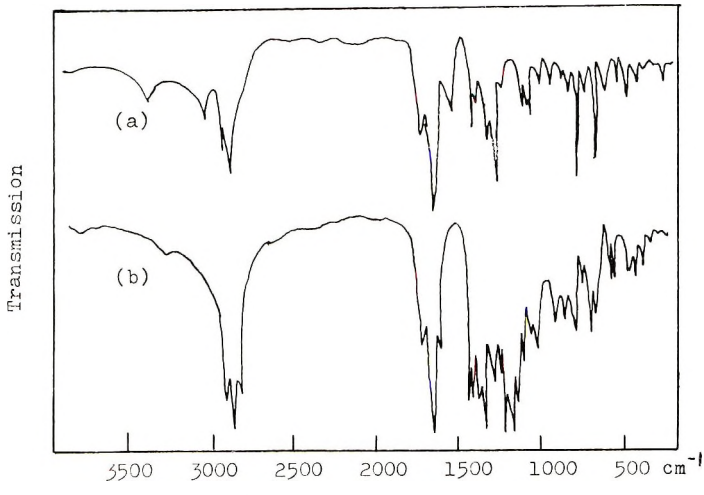

Fig. 1. Infrared spectrum of (*a*) *N*-bornyl maleimide and (*b*) poly(*N*-bornyl maleimide).

Polymerization Procedure

The polymerizations were carried out by BPO, AIBN, and *n*-BuLi as initiators in THF by the sealed tube method at 50°C. The required amounts of NBMI, initiator, and THF were placed in a tube; the tube was degassed completely, sealed off, and placed in a thermostat controlled at

50°C ± 0.1°C. After the polymerization, the tube was opened and the polymer solution was precipitated into methanol and dried to constant weight under vacuum.

Measurements

The infrared spectra were measured with KBr pellet on a Perkin-Elmer 337 photospectrometer.

The intrinsic viscosity of polymer was measured in THF at 30°C with an Ubbelohde viscometer.

Molecular weights of monomer and polymers were determined with a Knauer vapor pressure osmometer, methyl ethyl ketone and benzene being used as solvents.

The proton magnetic resonance spectra were obtained with a Hitachi 60 Mcps nuclear magnetic resonance spectrometer.

The x-ray powder diffractograms were obtained with the use of Cu Kα as a source on a Toshiba x-ray diffractometer.

Optical rotations were measured with a Shimazu Liebig-type polarimeter with filtered sodium light. Optical rotatory dispersion data were obtained by a Shimazu model QV-50 polarimeter equipped with a xenon source. The D-line optical rotations at various temperatures were measured by a Yanagimoto Model ORD-3 polarimeter.

RESULTS AND DISCUSSION

Optically Active *N*-Bornyl Maleimide

Reaction of *d*-camphor with hydroxylamine sulfate yielded camphor oxime. Camphor oxime was reduced by Na ethanol to camphor amine, which was reacted with maleic anhydride to form *N*-bornyl maleic acid. NBMI was prepared by the cyclization of *N*-bornyl maleic acid according to a modification of the procedure of Searle.[10] In order to identify the product as NBMI, infrared spectra, NMR spectra and elementary analysis were measured. As shown in Figure 1*a*, the infrared spectrum of NBMI had an absorption band at 1700 cm^{-1} due to the carbonyl group, but no absorption band at 3260 cm^{-1} due to the amide group.

The 60 Mc NMR spectra of *N*-bornyl maleic acid, NBMI, and PNBMI measured in chloroform-d_1 and carbon tetrachloride are shown in Figure 2. NMR spectra for PNBMI initiated by BPO, AIBN, and *n*-BuLi were identical. As shown in Figure 2*a* for *N*-bornyl maleic acid, the signals due to methyl, methylene and methine protons of bornyl group were observed in the range 5.5–9.5 τ. The signal due to the HC=CH protons were observed at 3.0–3.7 τ. The signal due to the proton of the amine group was at 1.4–1.6 τ. After the cyclization reaction (as shown in Fig. 2*b* of NBMI), the quartet signal (3.0–3.7 τ) due to the HC=CH protons of *N*-bornyl maleic acid is converted to a singlet (3.4τ). Furthermore, the signals due to the

TABLE I
Polymerization of *N*-Bornyl Maleimide[a]

Run	NBMI, mole/l.	Initiator	Initiator concn, mole/l.	Polymerization time, hr	Conversion, %	$[\eta]^b$	$[\alpha]_D^c$	λ^c
1	1.50	BPO	0.01	106	3.7	0.030	+6.3	258
2	2.14	BPO	0.01	106	3.8	0.035	+6.6	259
3	2.62	BPO	0.01	23	8.7	0.042	+8.1	259
4	2.81	BPO	0.01	53	15.7	0.050	+8.4	260
5	2.14	BPO	0.001	163	8.1	0.064	+8.4	258
6	2.14	AIBN	0.01	72	14.3	0.030	+10.1	253
7	2.14	AIBN	0.001	120	5.2	0.040	+10.0	253
8[d]	1.29	*n*-BuLi	0.047	24	28.4	0.062	−7.0	—
9[e]	1.29	*n*-BuLi	0.047	24	2.3	0.037	−9.1	—

[a] Polymerized at 50°C in THF.
[b] Measured at 30°C in THF.
[c] Measured in THF at 25°C.
[d] Polymerized in THF.
[e] Polymerized in benzene.

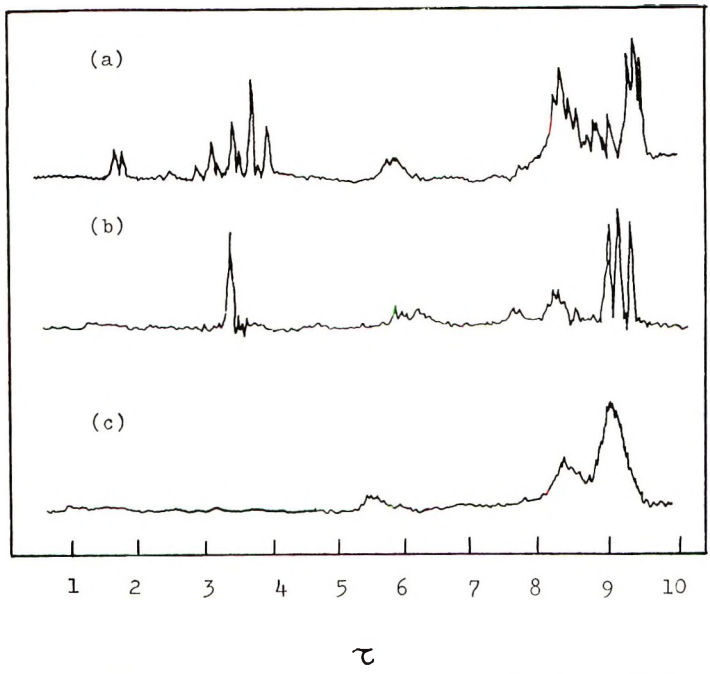

Fig. 2. Proton magnetic resonance spectra of (*a*) *N*-bornyl maleic acid; (*b*) *N*-bornyl maleimide, and (*c*) poly (*N*-bornyl maleimide).

proton of the amide group and the proton of the carboxyl group were extinguished. It was found that *N*-bornyl maleic acid cyclized to NBMI and the protons of HC=CH of the cyclized product became equivalent.

From the results of NMR, infrared spectra, and elemental analysis (C, H, and N), the product was identified as NBMI. NBMI obtained had $[\alpha]_D - 9.6$ in ethanol. The optical rotatory dispersion curve of NBMI is shown in Figure 3. The rotatory dispersion curve was found to fit a simple Drude equation, as shown in Figure 4.

The λ_c was 351 mμ. The specific rotations of NBMI in THF were measured at various temperatures from 15°C to 40°C. As shown in Figure 5, the temperature dependence coefficient $\Delta[\alpha]_D/\Delta T$ was found to be +0.042. The specific rotation of NBMI in THF was unchanged upon the addition of ethanol into a solution (Fig. 6).

Optically Active Poly(*N*-bornyl Maleimide) (PNBMI) by Anionic Polymerization

Anionic polymerization of optically active NBMI was carried out with *n*-BuLi at 50°C in THF and benzene.

The polymerization conditions, the intrinsic viscosity, and specific rotation of the PNBMI are shown in Table I.

Anal. Calcd for PNBMI: C, 72.1%; H, 8.2%; N, 6.0%. Found: C, 70.8%; H, 8.4%; N, 6.0%.

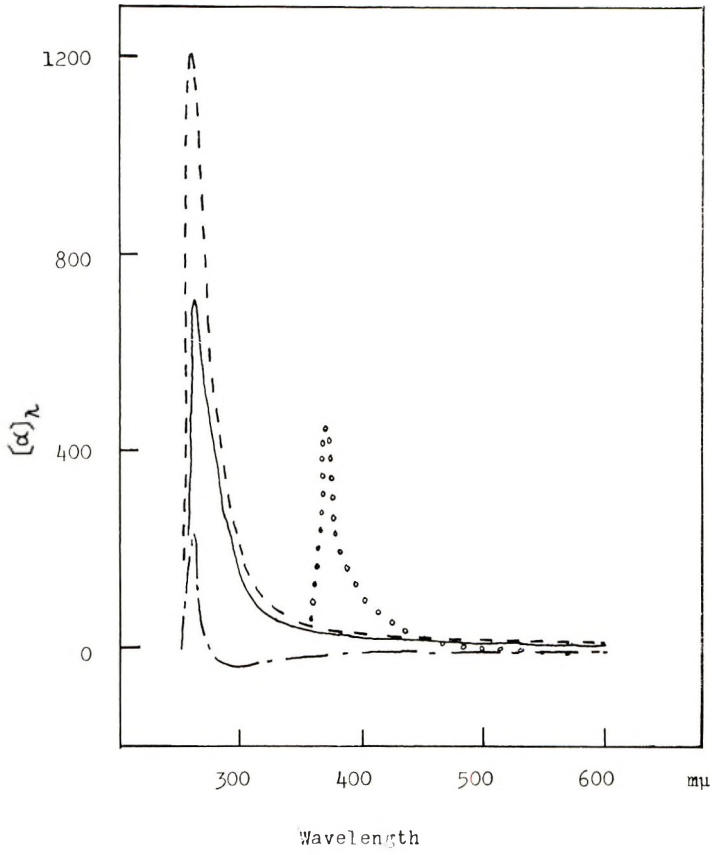

Fig. 3. Optical rotatory dispersions of (----) poly(*N*-bornyl maleimide) initiated by AIBN, (——) poly(*N*-bornyl maleimide) initiated by BPO, (-·-) poly(*N*-bornyl maleimide initiated by *n*-BuLi, and (◦◦◦◦) *N*-bornyl maleimide; in THF at 25°C.

The obtained polymers had the $[\eta]$ of 0.037–0.062 dl/g (MW 2900–4900), and the number-average degree of polymerization of PNBMI was 12–21.

The infrared spectrum of the polymer is shown in Figure 1*b*. The polymers had absorption bands at 1750 and 1700 cm^{-1} due to the carbonyl group and had no absorption band at 690 cm^{-1} due to *cis* carbon-carbon double bond.

The NMR spectrum for PNBMI is shown in Figure 2*c*. The signal (3.4 τ) due to HC=CH protons of NBMI disappeared after polymerization.

The x-ray powder diffractogram of PNBMI initiated by *n*-BuLi is shown in Figure 7. It is apparent from the diffractogram that the polymer had interference in the region 7.5–14.5, i.e., the polymer had two interplanes at 6.10 and 13.6 Å. It would be thought from the result that the polymer had a fiber period of 6.10 Å and had a slightly helical conformation as reported by Cubbon.[11] Cubbon polymerized *N*-substituted maleimides (*N*-ethyl, isopropyl, *n*-butyl, isobutyl, *tert*-butyl, *n*-octyl, benzyl, and phenyl malei-

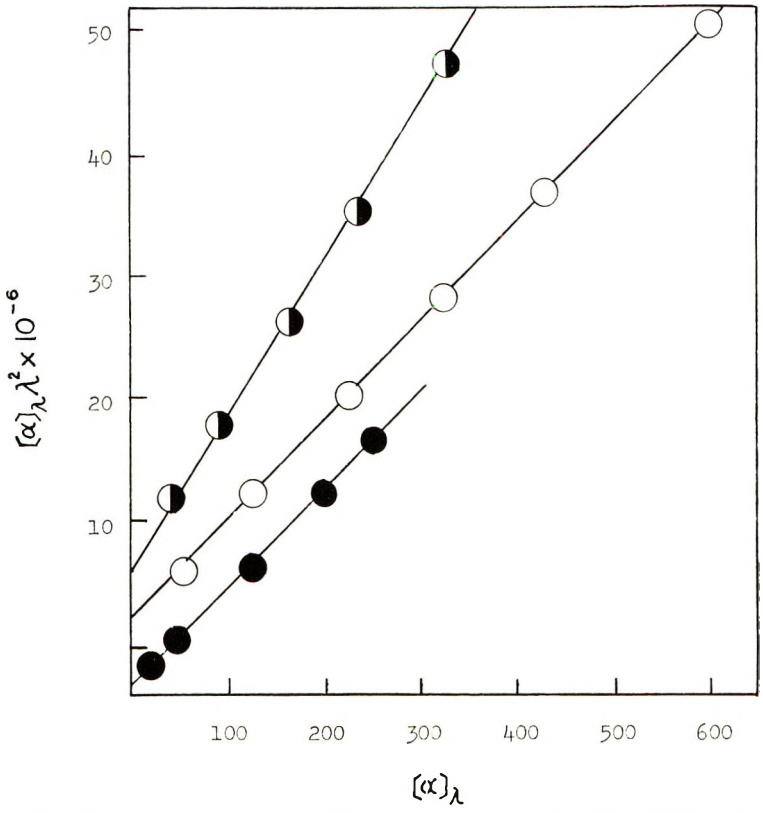

Fig. 4. Simple Drude dispersion of (●) poly (*N*-bornyl maleimide) initiated by BPO; (○) PNBMI initiated by AIBN; (◑) *N*-bornyl maleimide monomer.

mide) and carried out x-ray analysis to study the structure of poly-*N*-substituted maleimide. It was suggested that the x-ray data could be accounted for if these polymers were predominantly *threo*-diisotactic conformation, and the *threo*-diisotactic polymers could form a 3_1 helix.

The specific rotation for polymers obtained in THF and benzene as solvents were −9.1 and −7.0,respectively. These optical rotatory dispersion were measured as shown in Figure 3. Positive Cotton effects were found; the results did not fit the simple Drude equation. The chromophore which caused optical activity was presumed to be the carbonyl group of the NBMI unit.

Optically Active Poly(*N*-bornyl Maleimide) (PNBMI) by Free-Radical Polymerization

Radical polymerization of optically active NBMI was carried out with BPO and AIBN at 50°C in THF. The polymerization conditions, intrinsic viscosity, and specific rotation of the polymers are shown in Table I.

The polymers initiated by BPO had an intrinsic viscosity of 0.030–0.064 dl/g (MW 2400–5200), and a number-average degree of polymerization 10–22.

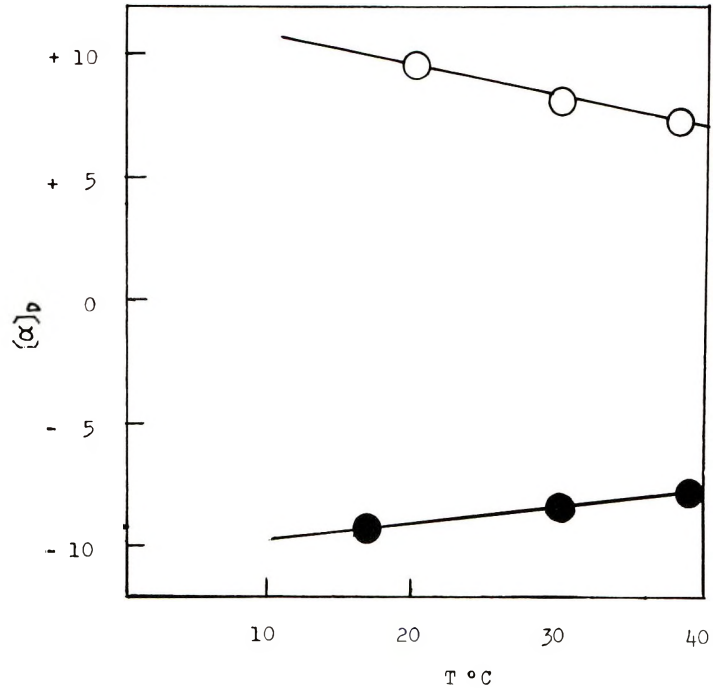

Fig. 5. Temperature dependence on the specific rotation of (●) *N*-bornyl maleimide and (○) poly (*N*-bornyl maleimide) initiated by BPO.

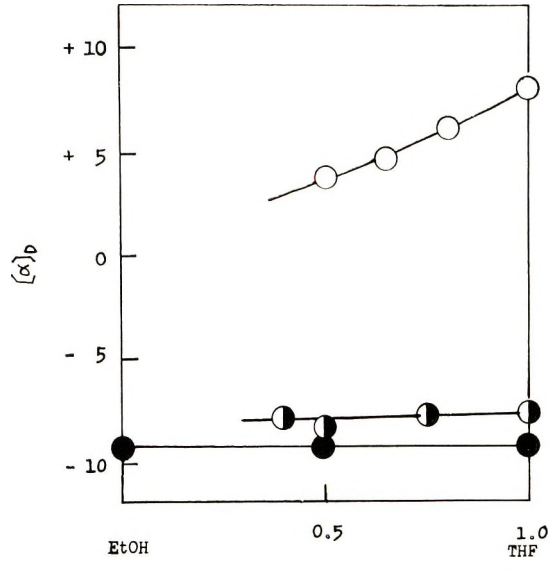

Fig. 6. Effect of solvents on the degree of the specific rotation of (●) *N*-bornyl maleimide; (○) poly (*N*-bornyl maleimide) initiated by BPO; (◑) poly (*N*-bornyl maleimide) initiated by *n*-BuLi.

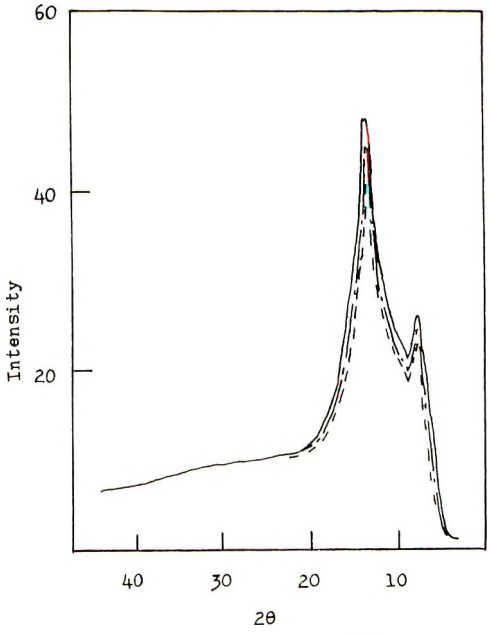

Fig. 7. X-Ray diffractometer scans: (——) poly (*N*-bornyl maleimide) initiated by *n*-BuLi; (--) poly (*N*-bornyl maleimide) initiated by BPO; (–·–) poly (*N*-bornyl maleimide) initiated by AIBN.

ANAL. Calcd for PNBMI: C, 72.1%; H, 8.2%; N, 6.0%. Found: C, 70.6%; H, 8.2%; N, 5.7%.

The polymers initiated by AIBN had as intrinsic viscosity of 0.030–0.040 dl/g (MW 2400–3200), and the number-average degree of polymerization was 10–14.

ANAL. Calcd for PNBMI: C, 72.1%; H, 8.2%; N, 6.0%. Found: C, 71.2%; H, 8.3%; N, 5.9%.

The intrinsic viscosity of the polymers initiated by BPO and AIBN decreased with increasing concentration of initiator.

The infrared spectra of these polymers initiated by BPO and AIBN were the same as that of the polymer initiated by *n*-BuLi (Fig. 1*b*).

The NMR spectra of PNBMI initiated by BPO and AIBN were same as that of the polymer initiated by *n*-BuLi (Fig. 2*c*).

The x-ray powder diffractograms of PNBMI initiated by BPO and AIBN are shown in Figure 7. These polymers had a fiber period of 6.0 Å, as, did the polymer initiated by *n*-BuLi. It was apparent from x-ray analysis and the infrared spectra that the polymers obtained by free-radical and anionic initiation had same structure.

The polymers initiated by BPO and AIBN had positive specific rotation as shown Table I. These optical rotatory dispersions were found to show a positive Cotton effect and to fit the simple Drude equation (Figs. 3 and 4). The value of λ_c for the polymer initiated by BPO was 258–260 mμ and that

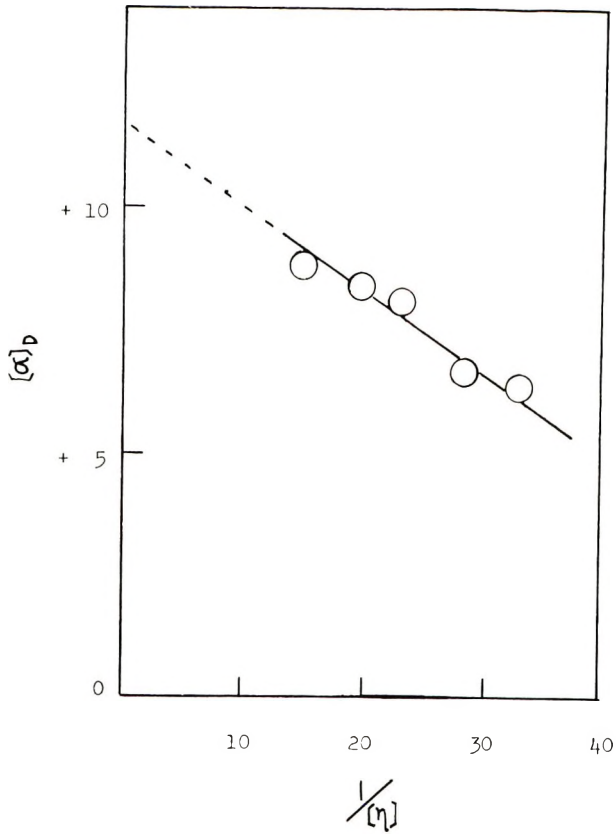

Fig. 8. Correlation between specific rotation and $1/[\eta]$ for poly (*N*-bornyl maleimide) initiated by BPO.

for the polymer initiated by AIBN was 253 mμ. These values of λ_e seems to be independent of the degree of polymerization of these polymers. The chromophore which caused optical activity appeared to be the carbonyl group of the NBMI unit.

The correlation between the specific rotation and the value of $[\eta]$ for the polymer initiated by BPO is shown in Figure 8. The specific rotation increased with increasing $[\eta]$, and the effect of the endgroup on the specific rotation was confirmed. The specific rotation for polymer of infinite degree of polymerization was estimated to be +11.7 by extrapolation.

There are some differences between the specific rotation for the PNBMI of the same degree of polymerization initiated by BPO, AIBN, and *n*-BuLi. That is, the specific rotation for the polymers obtained by different initators were +8.1, 10.0, and −9.1 for BPO, AIBN, and *n*-BuLi, respectively. This is attributable to differences in the polymer endgroups or to differences in the polymer configuration.

The optical rotatory dispersions for these polymers were measured to confirm the above suggestion. The optical rotatory dispersions for all the

polymers were found to have the same shape and to show positive Cotton effects (Fig. 3). The optical rotatory dispersion of the polymer initiated by *n*-BuLi showed a negative value in the range of long wavelength and the positive Cotton effect was less pronounced than that of the polymer initiated by free radical initiators had. The intensity of maximum rotation values for these polymers decreased in the following order: PNBMI initiated by AIBN > BPO > *n*-BuLi. It may be thought from above results that these polymers have two chromophores: the carbonyl group of NBMI unit (λ_c = about 260 mμ) and the endgroup of each polymer (λ_c < about 260 mμ). The former gave a positive optical rotation dispersion curve, and the latter gave a negative curve. The optical rotatory dispersion curve of the polymer initiated by *n*-BuLi seems to be affected by the latter chromophore. Thus the polymer had a negative specific rotation and a weak of maximum rotation. In addition, it is quite possible that anoinic initiators might produce *threo*-diisotactic structures which would be optically active centers which induce negative rotation near carbonyl absorption. It is possible that the free-radical initiators induce *threo*-disyndiotactic centers of atactic sequences which are inactive optically. Thus, these polymer show positive rotation.

Temperature and Solvent Dependence of Optical Rotation of Polymer

The specific rotation of PNBMI in THF at various temperatures was measured; the results are shown in Figure 5. The specific rotation for the polymer initiated by BPO decreased with increasing temperature, and a temperature dependence coefficient $\Delta[\alpha]/\Delta T$ of -0.097 was obtained. In contrast, the specific rotation for NBMI monomer increased with increasing temperature (Fig. 5). The results indicate that the optical activity of polymer is not attributable to the helical conformation but caused by the optically active bornyl group.

The specific rotation of PNBMI was measured in a THF–ethanol (precipitant) mixed solvent; the results are shown in Figure 6. The specific rotation for NBMI was independent upon the addition of ethanol. The specific rotation for the polymer initiated by *n*-BuLi was almost independent of the addition of ethanol, whereas that for the polymer initiated by BPO decreased with increasing amounts of ethanol. The end-group of PNBMI initiated by *n*-BuLi was the butyl group and did not show a solvent effect, but that of PNBMI initiated by BPO was the ester group which did show a solvent effect. The effect of ethanol on the optical rotation appeared only for PNBMI initiated by BPO.

These results indicate that the optical activity of oligomers obtained by the polymerization of optically active monomer was influenced markedly by the optically inactive end group.

The authors would like to express their grateful acknowledgment to Dr. A. Shimada and Mr. M. Fukuyo for x-ray analysis.

References

1. G. V. Paesschen and D. Timerman, *Makromol. Chem.*, **78**, 112 (1964).
2. Y. Minoura and Y. Suzuki, paper presented at the 15th Meeting, Polymer Science, Japan, 1966.
3. L. E. Coleman and J. A. Conrady, *J. Polym. Sci.*, **38**, 241 (1959).
4. M. Yamada and I. Takase, *Kobunshi Kagaku*, **23**, 348 (1966).
5. H. Gilman, F. K. Cartledge, and S.-Y. Sim, *J. Organometal. Chem.*, **1**, 8 (1963).
6. H. Gilman and F. K. Cartledge, *J. Organometal. Chem.*, **2**, 447 (1964).
7. E. Nägeli, *Ber.*, **16**, 497 (1883).
8. E. Beckmann, *Ann.*, **250**, 354 (1889).
9. M. O. Forster, *J. Chem. Soc.*, **73**, 391 (1898).
10. N. E. Searle, U. S. Pat. 2,444,536 (1948).
11. R. C. P. Cubbon, *Polymer*, **6**, 419 (1965).

Received June 4, 1969
Revised September 16, 1969

JOURNAL OF POLYMER SCIENCE: PART A-1 VOL. 8, 943–959 (1970)

Thermal Behavior of Poly-*p*-xylylene-*m*-carborane

ALVIN D. DELMAN, *Naval Applied Science Laboratory, Brooklyn, New York 11251**

Synopsis

Thermal analysis, infrared spectroscopy, and gel-permeation chromatography studies were undertaken to determine the behavior of poly(*p*-xylylene-*m*-carborane) at elevated temperature. Results show that the polymer softened at about 200°C, probably because of polymorphism. Chlorine atoms from chain ends also ruptured at this temperature. This initiated subsequent hydrogen abstraction and thermal oxidation reactions that resulted in the decomposition of the polymer. The process of degradation closely parallels the thermal oxidation of polybenzyl and other polymers with readily activated methylene groups. The volatile products that formed at 300 and 400°C were produced because of the cleavage of methylene groups and their oxidation products. Larger polymer segments containing phenylene and *m*-carborane groups were evolved at higher temperatures. Some crosslinking occurred when the polymer was heated in air at temperatures above 200°C. The degree of polydispersity of the polymer fraction that remained soluble in organic solvents increased with corresponding increase of temperature.

INTRODUCTION

A series of papers[1–4] reported on the heat stability of novel experimental polymers containing a carborane polyhedron in the backbone or side chains. As a phase of a continuing program, this paper describes the results of investigation of the thermal properties of a polymer composed of *p*-xylylene and *m*-carborane groups.

EXPERIMENTAL

Materials

The *p*-xylylene-*m*-carborane polymer discussed herein was developed and synthesized by Quantum, Inc., Wallingford, Conn. by the reaction of dilithio *m*-carborane and α, α'-dichloro-*p*-xylylene.[5] The recurring structure of the polymer is as follows shown in I, $—CB_{10}H_{10}C—$ represents the *m*-carborane nucleus.

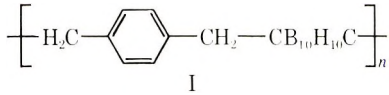

I

* The Wool Bureau, Inc., 225 Crossways Park Dr., Woodbury, New York, 11797.

Procedures

The procedures employed for thermogravimetric analysis (TGA) and isothermogravimetric analysis (IGA) were described before.[1]

Differential thermal analysis (DTA) was conducted by heating simultaneously a 1–2 mg sample of polymer sandwiched between alumina (Fisher Certified Reagent Grade, Catalog No. A-591), in a 1-cc platinum crucible and an identical vessel containing an equal volume of alumina as the reference material at 5°C/min. in air in a Du Pont model 900 differential thermal analyzer equipped with a 1200°C DTA cell. The furnace temperature and the temperature difference between the sample and the alumina were measured with a Pt/Pt + 13% Rh differential thermocouple.

Infrared absorption spectra were made from solution-cast films, Nujol mulls, and KBr pellets with a Perkin-Elmer model 337 grating instrument having KBr optics. In addition, 50-mg samples of polymer in aluminum foil boats were heated in air for 20 min at 100°C intervals over the temperature range of 300–800°C in a Wilks Scientific Corp., model 40, Pyro-Chem pyrolysis infrared accessory fitted with NaCl windows and a KRS-5 multiple internal reflection (MIR) plate. The uncondensed and condensed pyrolysis products were recorded with the spectrophotometer described above over the 2.5–15.0 and 2.5–25.0 μ range, respectively.

Mass spectra were obtained over the 0–150 mass range of an Ultek model Quad 250 residual gas analyzer.

Molecular size and polydispersity measurements were obtained by injecting a solution containing about 0.06% of polymer dissolved in dry toluene into a Waters Associates, Inc. gel-permeation chromatography (GPC) instrument for 30 sec. The solution was pumped at 1 ml/mg through a system of three columns packed with crosslinked polystyrene of 1000, 250, and 45 Å, respectively. The columns were calibrated as described before.[6]

RESULTS AND DISCUSSION

Molecular Size and Polydispersity

To obtain an approximation of the number of recurring units in the molecules, GPC measurements were made of several model compounds that were structurally related to poly-*p*-xylylene-*m*-carborane. The results are presented in Table I.

TABLE I
GPC Measurement of Model Compounds

Model compound	Size, Å	
	Calculated	Found
Toluene	6.5	6.4
p-Xylene	8.0	7.6
m-Carborane	—	8.8
Dibenzyl-*m*-carborane	16.4	15.8

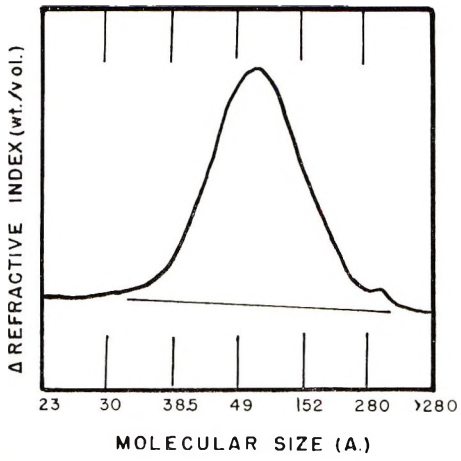

Fig. 1. GPC curve of polymer sample with low polydispersity.

A comparison of these data with bond lengths recorded in the literature[7,8] suggests that the recurring units is more closely related to the distance between the carbon atoms of the *m*-carborane nucleus than to the size of the entire polyhedron. Hence, from the x-ray diffraction study of bis(bromomethyl)-*o*-carborane made by Koster and Grassberger[9] and the geometry of the related icosahedral arrangement for the *ortho* and *meta* isomers,[10] it is estimated that the C–C′ bond length of the *meta* polyhedron is about 2.6 Å. This value and that of 6.58 Å for the size of the repeating unit of poly-*p*-xylylene[11] suggest that 9.2 Å is a close approximation for the dimension of the recurring structure of poly-*p*-xylylene-*m*-carborane.

Figure 1 shows the GPC fractionation curve of the polymer specimen. The chromatogram has a peak at about 66 Å and a shoulder beginning at approximately 280 Å. If it is assumed that the chain ends of the polymer are comprised of C-H and C-Cl linkages having bond lengths[7] of about 1.1 and 1.8 Å respectively, then the major component of the polymer which is depicted by the peak at 66 Å is a heptamer species. The shoulder near 288 Å indicates the presence of a small quantity of higher molecular weight chains. The number-average size (A_n) and weight-average size (A_w) of the polymer was calculated by the Waters Associates, Inc. method to be 66 and 127.7 Å, respectively. The degree of polydispersity (A_w/A_n) of the polymer molecules was 1.93.

Heat Stability

Thermogravimetric Analysis (TGA). The results of TGA measurements of the polymer are presented in Figure 2. These data indicate that the product rapidly underwent a small weight decrease at about 100–200°C which was probably due to the rupture of chain ends and the vaporization of a small amount of absorbed moisture. It seems reasonable to assume that the loss of weight, which occurred slowly at about 200°C and became

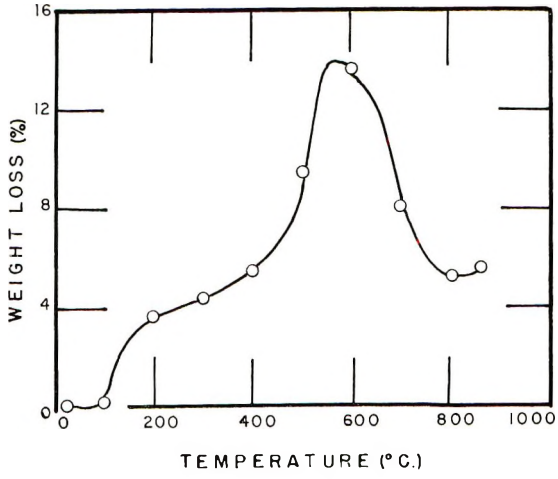

Fig. 2. TGA thermogram of polymer sample with low polydispersity.

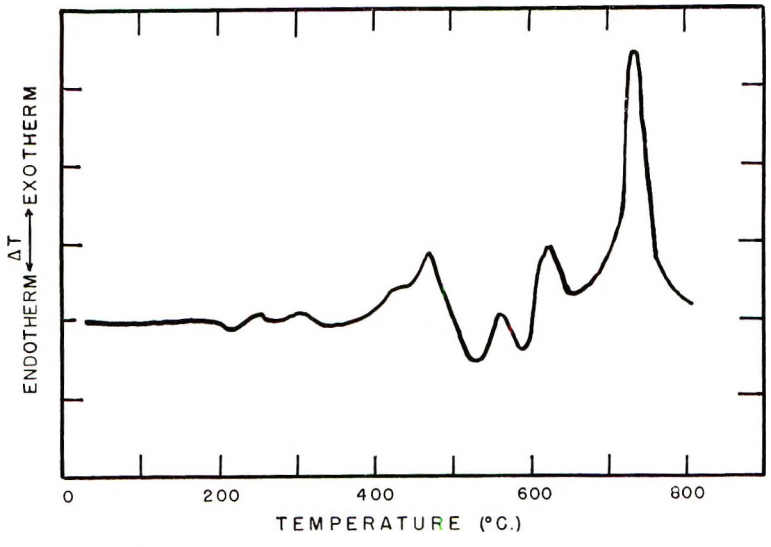

Fig. 3. DTA thermogram of polymer sample with low polydispersity.

rapid at 450–580°C, was associated with the thermal decomposition of the polymer backbone. The weight increases observed at 580–800°C are attributed to the reaction of oxygen with carborane nuclei. Since earlier studies[1,2,12] suggested that the carborane polyhedron had a stabilizing influence over the thermal cleavage of alkyl groups to which they were attached, it is also considered possible that part of the weight gain was the result of some of the methylene groups having undergone oxidation without rupture. The small weight loss noted above 800°C was probably caused by the pyrolysis of some residual organic material.

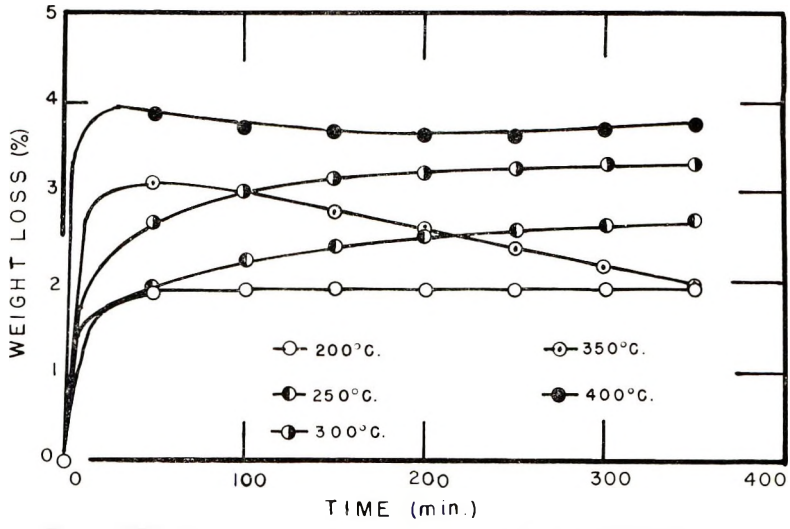

Fig. 4. IGA thermograms of polymer sample with low polydispersity.

Differential Thermal Analysis (DTA). Figure 3 shows the DTA thermogram obtained from a polymer sample. The weak endothermic trend in the region of 200–300°C corresponds very well with the temperature range at which the product was observed to soften when it was heated in a glass capillary tube. It is interesting to note that low molecular weight α-poly-*p*-xylylene also melts at this temperature range due to recrystallization.[13,14] Consequently, it is possible that the relatively low molecular weight sample of poly-*p*-xylylene-*m*-carborane behaved in a similar manner at this temperature. It is believed that the low intensity of the transformation was due to the superposition on the endotherm of an exothermic reaction that produced the weight loss observed at this temperature range during the TGA experiment.

The weak exotherm starting at about 230°C was apparently caused by a decomposition reaction. The degradation of poly-*p*-xylylene[15] and several products having structures with methylene groups connected to a carborane polyhedron[3] have also been reported to occur just after they melted.

From DTA data reported in the literature,[14] it seems reasonable to assume that the exothermic peaks at approximately 315 and 470°C, were caused by the thermal decomposition of *p*-xylylene groups. The exotherms occurring above 470°C. were probably the result of oxidation reactions involving the carborane polyhedron and residual organic products. This conclusion is supported by TGA data which showed that the polymer underwent a weight gain at 580-800°C. and a small weight decrease at temperatures above 800°C. while it was being heated in air.

Isothermogravimetric Analysis (IGA). Figure 4 shows the weight changes of the polymer when it was heated in air under isothermal conditions. These data indicate that all of the samples underwent a relatively small weight loss during the initial 30-min heating period; the rate of

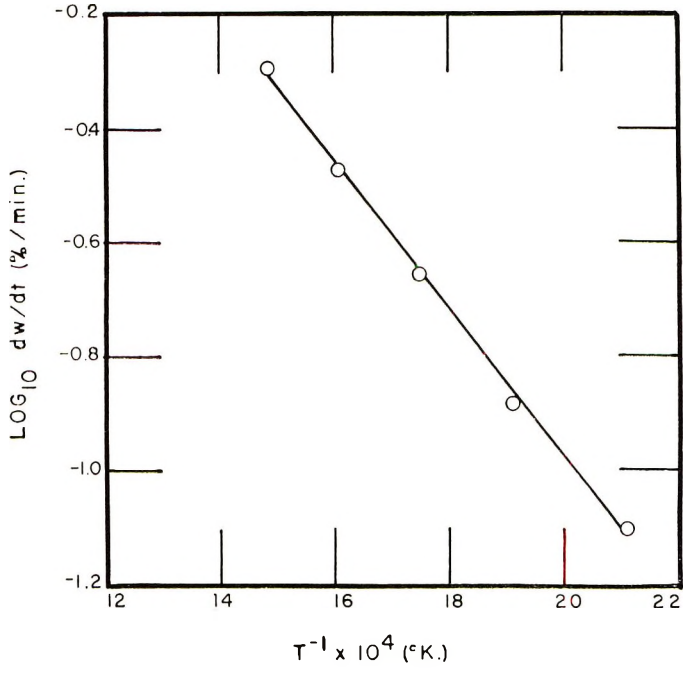

Fig. 5. Kinetic plot of IGA data.

decrease becoming more rapid as the temperature was increased. Thereafter, the specimens continued to lose weight while being heated at 200, 250, and 300°C and underwent weight increases at 350 and 400°C. At the latter temperature the specimen exhibited additional small weight decreases during the final 3-hr heating period.

The results agree with observations made from TGA and DTA data which suggested that the polymer underwent thermal rupture and oxidation reactions while being heated in air. Since poly-*p*-xylylene is known to undergo surface oxidation even at 200°C,[16] it is suspected that the above reactions occurred simultaneously. Evidently, thermal cleavage predominated up to 300°C, whereas oxidation prevailed at 350 and 400°C. The greater extent of oxidation at 350°C over that observed at 400°C might have been because less chain rupture and volatilization took place at the lower temperature and, therefore, more of the residual product remained to react with oxygen.

Visual examination of the IGA residues showed that the color of the polymer had darkened at 300–400°C. It is interesting to note that poly-*p*-xylylene was also observed to leave a dark brown residue after it was heated at 420–440°C.[17] It is inferred from this that the discoloration of poly-*p*-xylylene-*m*-carborane was due to the thermal oxidation of *p*-xylylene groups rather than to the decomposition of *m*-carborane nuclei.

Figure 5 shows an Arrhenius plot which was constructed from the maximum rates of weight decrease of the polymer at 200–400°C. The activa-

tion energy is 6 kcal/mole. Since the maximum rates of weight change were observed near the beginning of each heating period, the value obtained probably relates to the activation energy required to initiate the first thermal reaction of the polymer.

In this connection, it is interesting to note that during the first 50 min at 200°C the polymer underwent a weight decrease of 1.9% and then no further changes were observed. This loss corresponds to the rupture of chlorine atoms from chain ends and subsequent abstraction of hydrogen atoms from terminal linkages and/or the polymer backbone according to reactions such as (1) and/or (2a) and (2b).

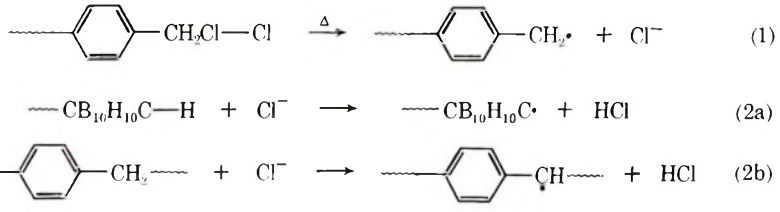

Little activation energy is required for reactions (2a) and (2b), which is exothermic for all C-H bonds.[18] Although the literature[19,20] suggests that activation energies of 18–20 kcal/mole are generally needed to produce reactions (2a) and (2b), the presence in the polymer molecules of strong electron-withdrawing *m*-carborane groups which increased the reactivity of the dechlorination process may explain why the determined value was lower than usual.[21]

The results of micro-Soxhlet extractions of the IGA residues and the original polymer for about 16 hr are presented in Table II. These data

TABLE II
Micro-Soxhlet Extraction

Specimen	Toluene-soluble fraction, %
Original polymer	100.0
200°C IGA residue	80.0
250°C IGA residue	64.3
300°C IGA residue	58.3
350°C IGA residue	21.3
400°C IGA residue	78.6

show that all of the residues were only partially soluble in chloroform, while the unheated polymer dissolved completely. In addition, the results indicate that the soluble material decreased in quantity with corresponding increases in temperature up to 350°C and increased substantially again at 400°C.

It seems reasonable to assume that the decline in the amount of soluble material was due to the formation of a three dimensional network when the polymer was heated in air. The larger amount of soluble product recovered

after 400°C over the quantities obtained from the 250,300, and 350°C experiments was most likely the result of more extensive rupture of the crosslinkages at the higher temperature. The decrease of solubility when the polymer was heated at 200°C suggests that at least some of the chlorine atoms that ruptured at that temperatur abstracted hydrogen atoms from the main chain according to reaction (2b), and that molecules with active groups combined subsequently to form crosslinks as in reaction (3). Since oxygen was present during the isothermal heating experiments, it is also possible that network formation was due to oxidation processes such as in reaction (4a)–(4c). From the weight changes shown in Figure 4, oxidation did not occur to any great extent, if at all, at 200°C.

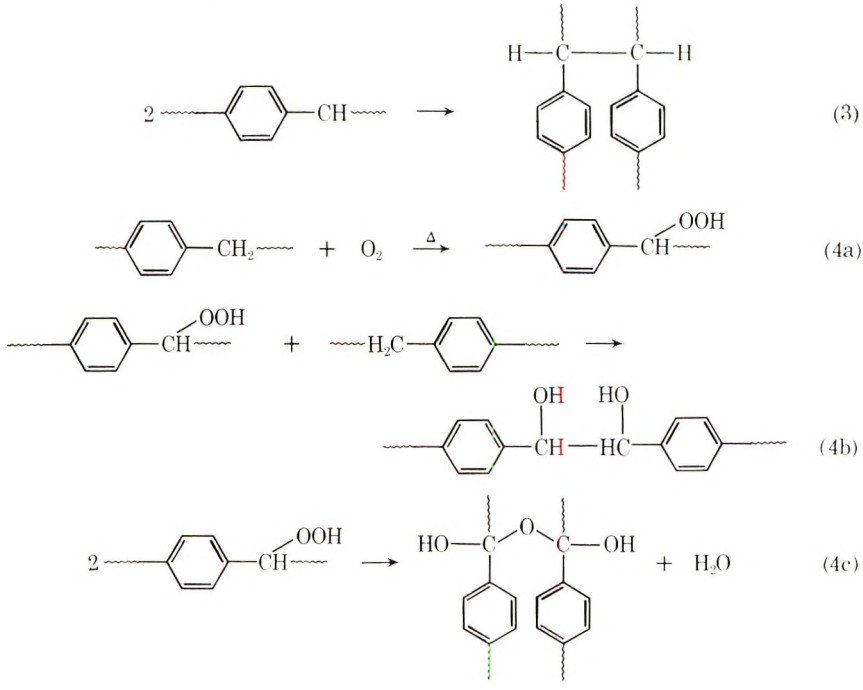

Reactions (4b) and (4c) would at least partially explain the weight increases observed at 350 and 400°C. At the latter temperature, thermal degradation probably took place by C–C bond rupture of the backbone and network structures as shown in eqs. (5).

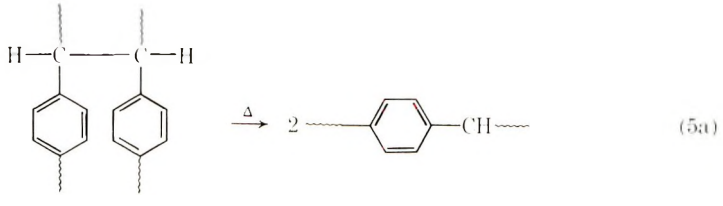

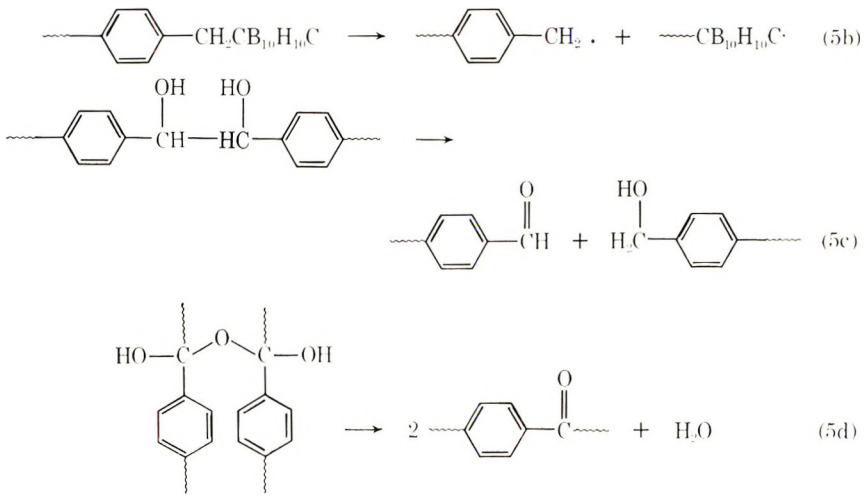

Figure 6 presents the GPC curve of the toluene soluble fraction from the IGA residue obtained after heating the polymer at 400°C. The curves made from soluble portions of the other residues appeared visually to have the same shape as the one given by the original polymer. By comparing Figures 1 and 6, it is evident that the product that was recovered after the 400°C treatment had a broader range of molecular weight species than the unheated polymer. The increase of polydispersity was probably due to the rupture of crosslinkages such as those produced by reactions (5a) and (5d), and the subsequent recombination of at least some of the active molecular segments.

The average size and polydispersity of the toluene soluble fractions from the IGA residues are compared to that of the original polymer in Table III.

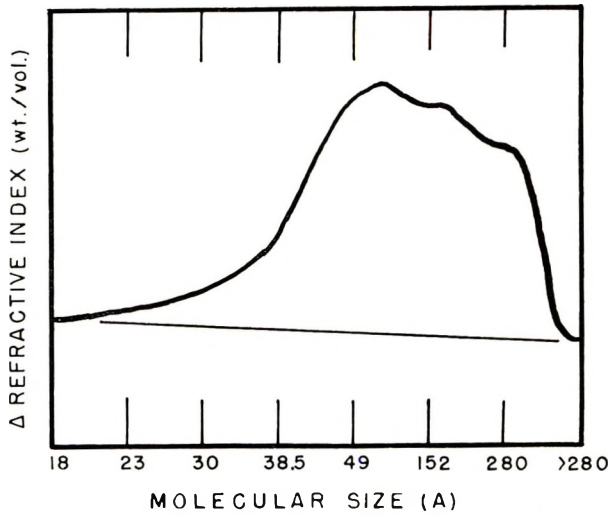

Fig. 6. GPC curve of toluene-soluble phase from 400°C IGA residue.

TABLE III
Average Molecular Size And Polydispersity

Specimen	Size, Å		Polydispersity
	A_w	A_n	A_w/A_n
Original polymer	127.7	66.0	1.93
200°C soluble fraction	126.6	65.0	1.95
250°C soluble fraction	212.7	66.9	3.18
300°C soluble fraction	217.6	63.8	3.41
350°C soluble fraction	236.9	65.8	3.60
400°C soluble fraction	475.6	76.1	6.25

It is apparent from the change of values obtained for the A_w/A_n ratios that the degree of polydispersity remained the same after the polymer was heated at 200°C. At the higher temperatures, however, the values for the A_w/A_n ratio increased with corresponding increases of temperature.

Infrared and Mass Spectrometry

The infrared spectrum of poly-*p*-xylylene-*m*-carborane shown in Figure 7 is consistent with its molecular structure. The spectrum of the residue from the sample that was heated at 200°C was the same as that from the original polymer. However, the intensity of CH_2 and *p*-C_6H_4 absorption modes in the spectra prepared form the residues obtained at 250-400°C progressively decreased as the temperature of the polymer was increased. The results provide additional evidence that, except for some network formation induced by the rupture of chlorine atoms from chain ends, the polymer backbone was structurally unchanged after being heated in air at 200°C. These data also confirm that radical decomposition occurred at higher temperatures.

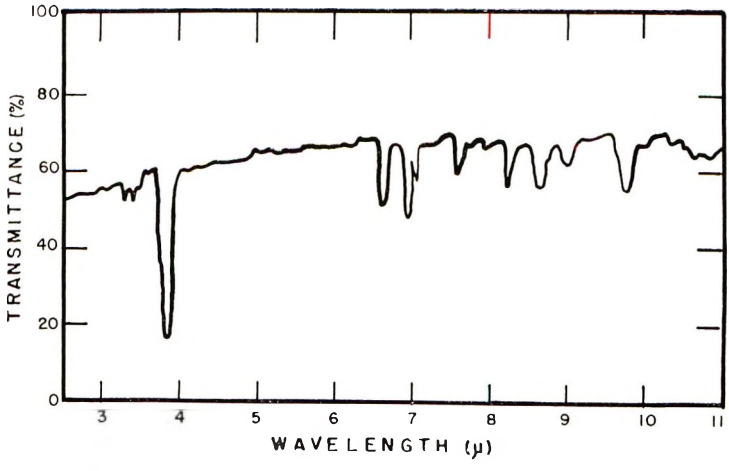

Fig. 7. Infrared spectrum of poly-*p*-xylylene-*m*-carborane.

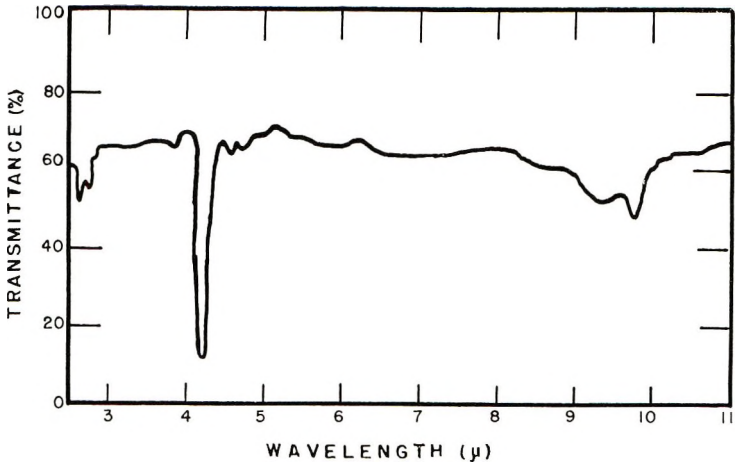

Fig. 8. Infrared spectrum of uncondensed pyrolysis products.

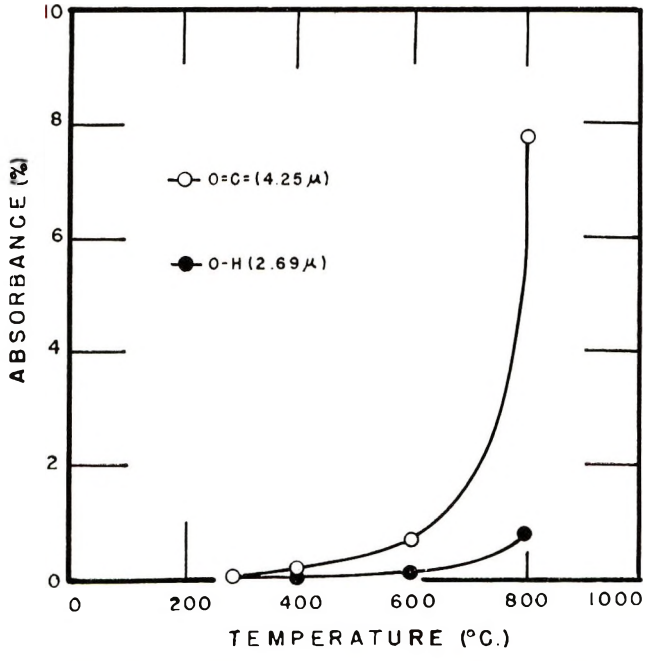

Fig. 9. Infrared absorbance of uncondensed pyrolysis products as a function of temperature.

Further insight into the structural changes that the polymer underwent during the heating process was obtained from experiments with the Pyro-Chem unit. The infrared spectrum of uncondensed gases that evolved when the polymer was heated for 20 min at 800°C is presented in Figure 8.

The spectrum exhibits O-H bands at 2.69 and 2.77 μ that are attributed to water, a weak B-H mode at 3.87 μ that is associated with the *m*-car-

borane polyhedron or its decomposition products, and an intense C=O vibration at 4.25 μ due to the presence of carbon dioxide. The absorption frequencies connected with water and carbon dioxide were also present in the spectra that were made after the polymer was heated at 400–700°C, while the B-H vibration was only evident in the spectrum from the sample treated at 800°C.

Figure 9 shows the change of intensity of the absorption bands at 2.69 and 4.25 μ as a function of temperature. It is evident from the results that the amount of water and carbon dioxide that was formed as a result of thermal oxidation of the polymer increased exponentially as the temperature was increased.

It seems reasonable to suppose that carbon dioxide was produced because of secondary thermal decomposition reactions such as (6a) and (6b). The formation of water is attributed to the dehydration of hydroperoxides or their reaction products as in (4c), (5d), (7a), and (7b), where (4c) and (5d) were probably intermediate steps of (7a).

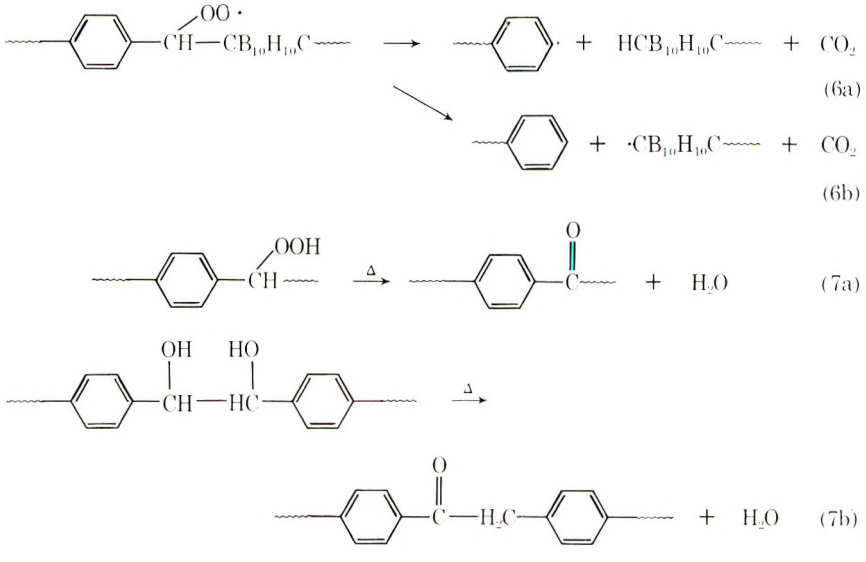

In addition to carbon dioxide and water, mass spectra of the uncondensed volatiles showed that hyrogen chloride was evolved during the pyrolysis of the polymer in the Pyro-Chem units. This supports the supposition made before that chlorine atoms were located at chain ends of the polymer molecules and that they ruptured during the heating process.

The formation of hydrogen chloride at the initial stage of thermal degradation probably had an activating influence upon the decomposition of peroxides that were produced during the heating process.[22]

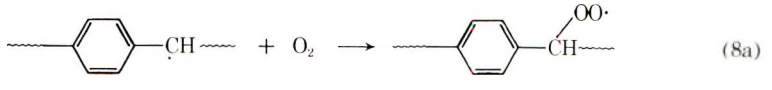

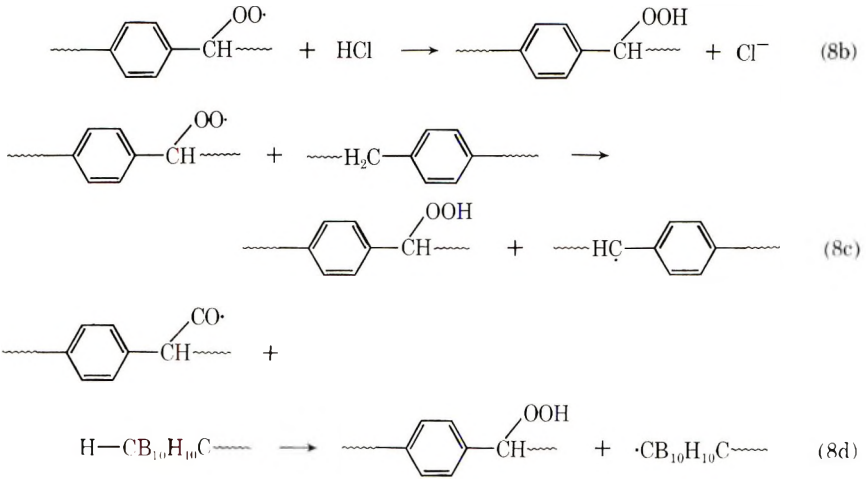

Reactions such as (8b) are generally much faster than (8c) and (8d). Therefore, the presence of HCl would tend to maintain a higher concentration of radicals than would otherwise be available to interact and, as a result, could subsequently initiate more crosslinking and chain rupturing reactions than would probably occur in its absence.

This phenomenon was further investigated by examining another specimen of poly-*p*-xylylene-*m*-carborane that was synthesized in the same manner.[5] In addition to heptamer species, the GPC curve on Figure 10 shows peaks at 13.5, 19, and 27 Å that indicate the presence of monomer, dimer, and trimer fractions in the sample.

Figure 11 compares the TGA thermogram made from this specimen with that obtained from the previous sample. It is evident from these data that the product which contained the lower molecular weight species was less heat stable than the material with only heptamer and some larger size mole-

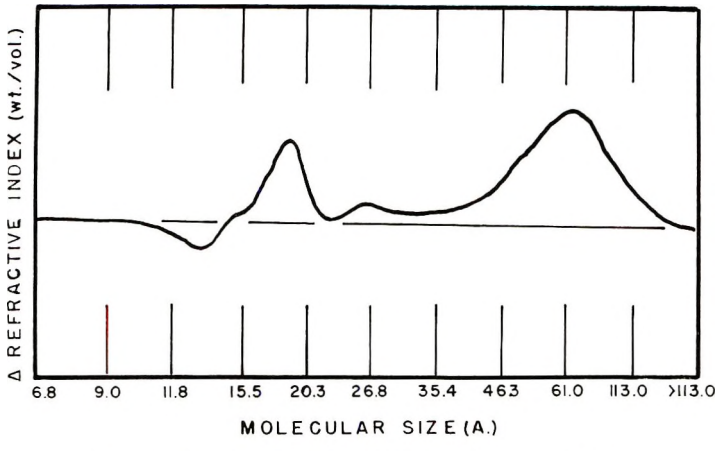

Fig. 10. GPC curve of polydisperse polymer sample.

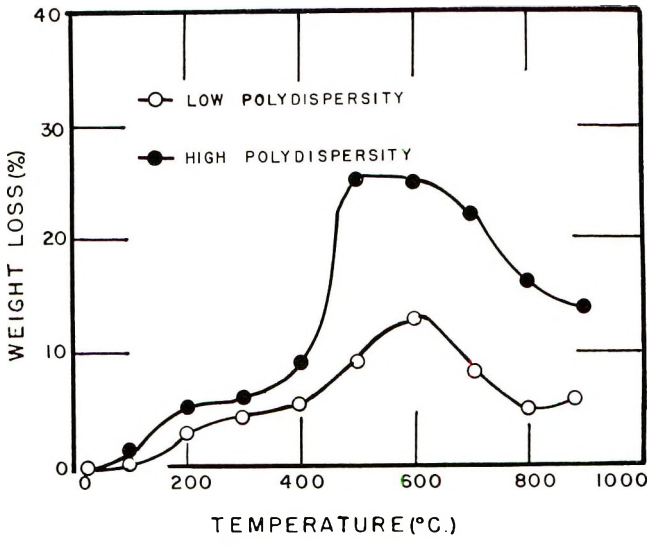

Fig. 11. Effect of molecular weight on heat stability.

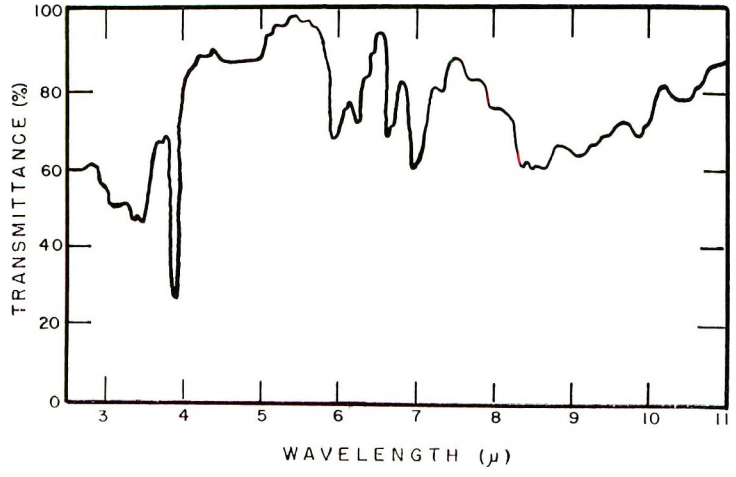

Fig. 12. Infrared spectrum of condensed pyrolysis products.

cules. Since the monomer, dimer, and trimer fractions are presumed to have contained a higher chlorine content than the larger molecules, these data seem to substantiate that the production of hydrogen chloride because of the cleavage of chain ends had a detrimental influence on the thermal resistance of the polymer.

Figure 12 shows the infrared spectrum of condensed gases that were produced when the polymer was heated in the Pyro-Chem unit at 800°C for 20 min. The condensed pyrolyzates that formed when the polymer was heated at 500–700°C. gave similar spectra, while those that were produced at 300 and 400°C showed absorption bands only for methylene groups and

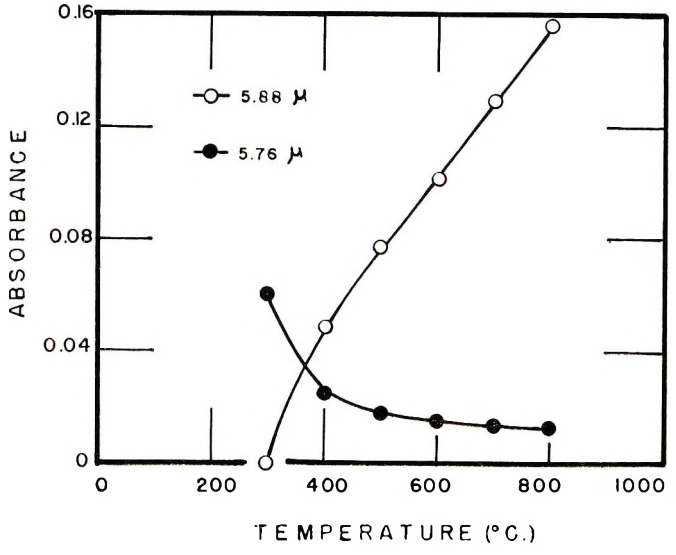

Fig. 13. Infrared absorbance of condensed pyrolysis products as a function of temperature.

their oxidation products. The absence in the latter spectra of vibration frequencies associated with carborane and phenylene groups confirms that these structures are more resistant to thermal oxidation than the methylene units of the chains.

All of the spectra made from the condensed gases contained absorption bands at 5.76 and 5.88 μ that were not present in the spectrum of the original polymer. Figure 13 shows that the 5.76 μ band became progressively less intense while the 5.88 μ mode grew as the pyrolysis temperature was increased.

The 5.76 μ band has been attributed to anhydride and/or ester linkages, and the 5.88 μ mode is generally associated with acid, aldehyde, and/or ketone configurations.[23] The appearance of such structures in the spectra from the condensed gases indicates the occurrence of thermal cleavage reactions such as (5c) and (5d) during the heating process. The rupture of volatile segments from chains that were thermally oxidized according to (7a) and (7b), or as follows, would also explain the presence of carbonyl bonding in the condensed gaseous products.

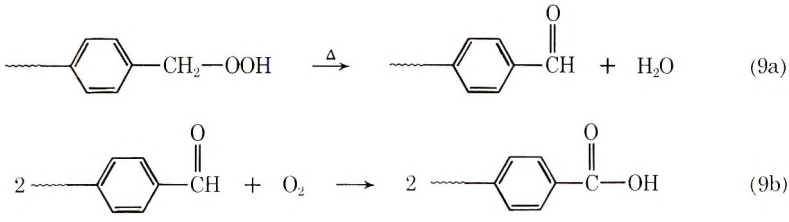

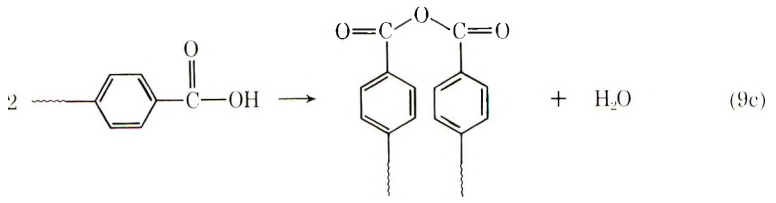

It is interesting to note that the different oxidative degradation reactions that have been presented to explain the structure of the pyrolyzates that formed when poly-*p*-xylylene-*m*-carborane was heated in air closely parallels the oxidation routes that have been proposed for polybenzyl.[24] In the case of the latter polymer it has been suggested that the primary steps of degradation involved an attack of methylene linkages by oxygen to produce benzhydrol and benzophenone linkages. However, it might be inferred from the fact that the infrared spectrum of the condensed gases produced at 300°C showed a 5.76 μ band, but did not contain an absorption mode at 5.88 μ, that a primary step of the decomposition of poly-*p*-xylylene-*m*-carborane involved the oxidation of methylene groups to give anhydride linkages instead of ketonic bonding.

Since it seems more reasonable to expect that anhydrides would form as a result of secondary rather than primary reactions, the explanation of this posed an interesting problem. In this connection, it is known that the frequency of a carbonyl group is related directly to the electron attracting or repelling power of any structure in the immediate vicinity of the group. For example, when a carbon atom of a carbonyl group is directly attached to a single aryl unit it absorbs at a lower wavelength of the infrared spectrum than when it is connected to two electron withdrawing structures; the influence of the α-aryl group being additive with that of any other structure which can affect the C=O frequency.[25] Thus, it seems more reasonable to assume that the 5.76 μ band of the infrared spectrum from the condensed pyrolysis products is associated with aldehyde and/or ketone instead of anhydride configurations. Such structures could have been produced as a result of reactions such as (5c), (5d), (7a), (7b), and (9a). The fact that B-H bond absorption at 3.87 μ from carborane nuclei and frequencies from phenylene groups were not observed in the spectra from pyrolyzates obtained at 300 and 400°C suggests that volatile products containing C=O structures were formed at these temperatures because of the rupture of thermally oxidized methylene groups. Larger molecular segments possessing carborane and phenylene groups were cleaved and volatilized at 500°C. and higher temperatures.

The author wishes to express his appreciation to J. Mironov and J. J. Kelly for conducting the thermal analysis studies, to B. B. Simms, Head of the Organic Chemistry Branch of the Naval Applied Science Laboratory for his continued interest and encouragement, to J. C. Montermoso of Quantum, Inc., Wallingford, Conn. for his cooperation, and to E. A. Bukzin of the Naval Ship Systems Command, Washington, D. C. and W. B. Shetterly of the Naval Ship Engineering Center, Hyattsville, Md. for sponsoring this work.

The opinions or assertions contained in this paper are the private ones of the author and are not to be construed as official or reflecting the views of the Naval Service at large.

References

1. A. D. Delman, J. J. Kelly, A. A. Stein, and B. B. Simms, *J. Polym. Sci. A-1*, **5**, 2119 (1967).

2. A. D. Delman, A. A. Stein, J. J. Kelly, and B. B. Simms, *J. Appl. Polym. Sci.*, **11**, 1979 (1967).

3. A. D. Delman, J. J. Kelly, A. A. Stein, and B. B. Simms, paper presented at the 2nd International Conference on Thermal Analysis, Worcester, Mass., August 1968, Vol. 1, 539, Academic Press, New York, 1969.

4. A. D. Delman, J. J. Kelly, and B. B. Simms, *J. Polym. Sci. A-1*, in press.

5. R. L. Taylor, Quantum, Inc., Project Serial No. SR 007 04 01, Task 1050, Bureau of Ships Contract NObs 94080, Final Report, December 14, 1966.

6. A. D. Delman, J. J. Kelly, J. Mironov, and B. B. Simms, *J. Polym. Sci. A-1*, **4**, 1277 (1966).

7. *Handbook of Chemistry and Physics*, 46th ed., Chemical Rubber Co., Cleveland, Ohio, 1965–66.

8. J. D. Roberts and M. C. Caserio, *Basic Principles of Organic Chemistry*, Benjamin, New York, 1964.

9. R. Koster and M. A. Grassberger, *Angew. Chem. Intern. Ed.*, **6**, 218(1967).

10. F. G. A. Stone and R. West, *Advances in Organometallic Chemistry*, Vol. 3, Academic Press, New York, 1965.

11. W. D. Niegisch, *J. Appl. Phys.*, **37**, 4041 (1966).

12. S. Papetti, B. B. Schaeffer, P. P. Gray, and T. L. Heying, *J. Polym. Sci. A-1*, **4**, 1623 (1966).

13. L. A. Errede and J. M. Hoyt, *J. Amer. Chem. Soc.*, **82**, 436 (1960).

14. L. A. Errede and R. S. Gregorian, *J. Polym. Sci.*, **60**, 21 (1962).

15. R. S. Corley, H. C. Haas, M. W. Kane, and D. I. Livingston, *J. Polym. Sci.*, **13**, 137 (1954).

16. L. A. Errede and N. Knoll, *J. Polym. Sci.*, **60**, 33 (1962).

17. A. T. Kalashnik, I. Ye. Kardash, T. S. Shpitonova, and A. N. Pravednikov, *Vysokomol. Soedin.*, **8**, 526 (1966).

18. W. A. Waters, *Mechanisms of Oxidation of Organic Compounds* Wiley, New York, 1964.

19. V. Ioan, L. Teodocorescu, S. Titeica, and C. D. Nenitsecu, *Acad. Rep. Populars Romine, Studii cercetari chim.*, **7**, 345 (1959).

20. R. Cockelbergs, A. Crucq, A. Frennet, and G. Lienard, *J. Chim. Phys.*, **56**, 967 (1959).

21. F. W. Evans, R. J. Fox, and M. Szwarc. *J. Amer. Chem. Soc.*, **82**, 6414 (1960).

22. J. H. Raley, F. F. Rust, and W. E. Vaughan, *J. Amer. Chem. Soc.*, **70**, 2767 (1948).

23. K. Nakanishi, *Infrared Absorption Spectroscopy-Practical*, Holden-Day, San Francisco, Calif., 1962.

24. R. T. Conley, *J. Appl. Polym. Sci.*, **9**, 1107 (1965).

25. L. J. Bellamy, *The Infra-Red Spectra of Complex Molecules*, Wiley, New York, 1958.

Received September 10, 1969
Revised October 8, 1969

JOURNAL OF POLYMER SCIENCE: PART A-1 VOL. 8, 961–972 (1970)

Thermal Degradation of Thin Films of Isotactic Polypropylene and Polypropylene with Ketonic Additives

ISMAT ABU-ISA, *General Motors Research Laboratories, Warren, Michigan 48090*

Synopsis

The rate of oxidation of 0.3–0.7 mil films of pure polypropylene is much more rapid than with thicker films. The rate of oxidation increases with the increase in the partial pressure of oxygen and with temperature. The apparent activation energy in oxygen is 22.5 kcal/mole. 1,3-Diphenyl-2-propanone added to the polymer acts as an oxidation initiator while *p*-phenylacetophenone and 4-phenylbenzophenone slightly retard the oxidation. The effects of the additives are more pronounced when the oxidation was carried out in air or at the lower temperatures (90°C) when the oxidation was conducted in pure oxygen. The degree of crystallinity based on the infrared data was found to increase with the degree of oxidation of the polymer.

INTRODUCTION

Similarity exists between the mechanism of thermal degradation of hydrocarbon polymers and that of the low molecular weight hydrocarbons.[1] However, the thermal oxidation of hydrocarbons usually requires added free-radical initiators except at very high temperatures, whereas the oxidation of the polymers is autocatalytic and proceeds surprisingly fast at temperatures as low as 60°C.[2] The fact that the oxidation of polypropylene is autocatalytic is sometimes attributed to trace impurities in the polymer or to the peroxide homolysis. The peroxides are found in trace amounts during the processing of the polymer.

A number of reports have been published dealing with the autoxidation of isotactic polypropylene. Chien and co-workers[4–8] used oxygen absorption, ESR, and other techniques to study the mechanism and evaluate the rate constants of individual steps of the thermal degradation of the polymer. Other studies on the mechanisms of degradation of isotactic polypropylene and the effect of stabilizers and impurities on the thermal degradation of the polymer include the work of Stivala and Reich,[1,9–11] Hawkins,[2,3,12] Hansen,[13] and others.[14,15] However, all of the degradation studies on polypropylene dealt with rather thick films of the polymer (2–100 mils), polymer powders, or polymer solutions. In such cases, limitations exist due to the influence of diffusion factors, the bulk of the polymer,

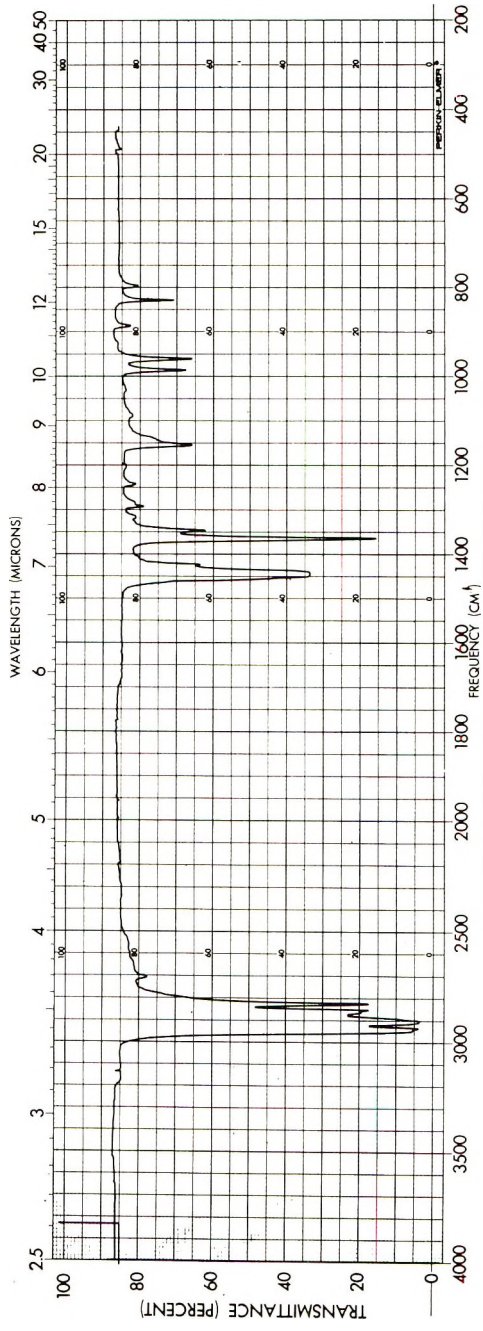

Fig. 1. Infrared spectrum of polypropylene.

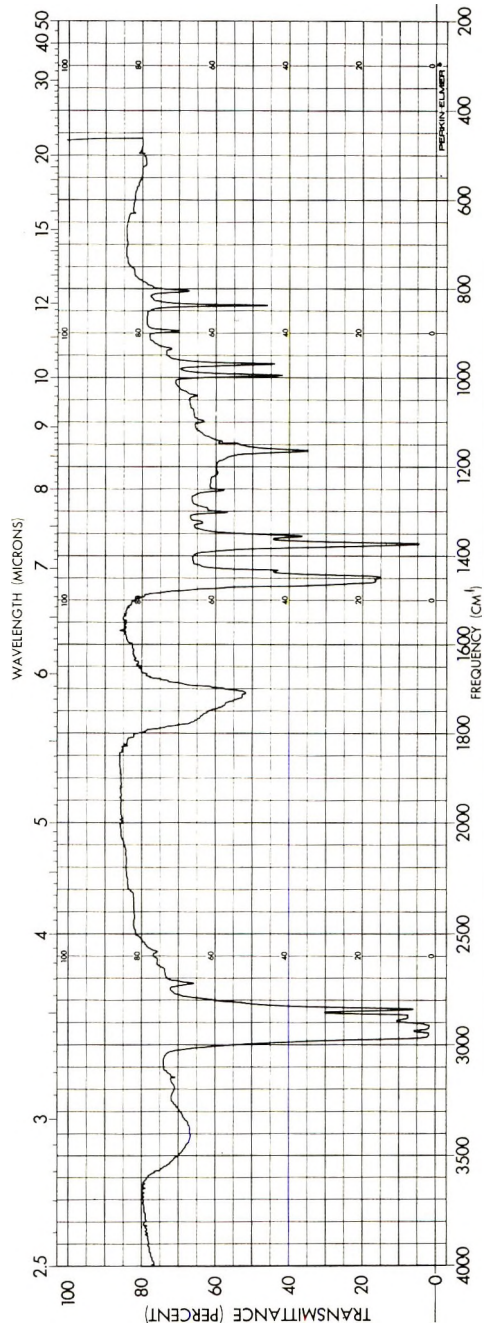

Fig. 2. Infrared spectrum of an oxidized sample of polypropylene.

and the solvent. It would be of interest, therefore, to obtain data on the oxidation of thin films of the polymer where the above limitations are not in effect.

The present investigation involves a study of the thermal degradation of thin films of isotactic polypropylene using oxygen absorption and infrared techniques. The effects of three ketonic additives on the thermal degradation of the polymer were also studied. Ketonic groups play an important role in the ultraviolet degradation of polypropylene. An attempt was also made to correlate the change in density and, hence, crystallinity of the polymer with the degree of oxidation from infrared data.

EXPERIMENTAL

Materials

The polypropylene used in this work was obtained from Hercules Incorporated. It is Profax 6501, unstabilized iostactic polypropylene. The weight-average molecular weight is 38000–47000. Crystallinity is between 40% and 70%. The sample was used without any further purification. The infrared spectrum of a thin film made from this sample is shown in Figure 1. Figure 2 shows the infrared spectrum of the same sample after oxidation.

The additives used in this study included 1,3-diphenyl-2-propanone (practical, Eastman Kodak), recrystallized twice from *n*-heptane; *p*-phenylacetophenone (white label, Eastman Kodak), recrystallized twice from a 50/50 mixture (by volume) of methyl alcohol and toluene; 4-phenylbenzophenone (white label, Eastman Kodak), recrystallized twice from methyl alcohol.

Apparatus

The apparatus used for making thin films of the polymer was made from an 18-in. section of glass tubing having a stopcock with a wide opening at the bottom. It was connected at the top through a ground glass joint to a glass bushing through which a stirrer was fitted. Also at the top, a stopcock was attached to allow purging of the system with the required gas. A 50-ml quantity of toluene was placed in the apparatus and allowed to heat to 120°C. A 3-g portion of the polymer and a specified amount of the additive, when used, were then added to the hot toluene. The polymer and the additive were allowed to dissolve in the toluene with constant stirring. A portion of the solution was then poured on a hot glass plate placed under the apparatus and drawn into a film using a hot draw-down blade. The film was allowed to dry on the hot plate for a period of three minutes, after which it was peeled off and stored in a vacuum desiccator for a period of not less than 18 hr before it was used. Film thicknesses between 0.3 mil and 0.7 mil were obtainable by using this procedure.

The oxygen absorption apparatus consisted of a glass tube 1.2 in. in diameter, closed at one end, and connected at the other end through an

O-ring joint to a 0.75-in. (OD) tubing which has a two-way stopcock at the top and an O-ring connection on the sides. The stopcock allowed the evacuation and refilling of the apparatus with the proper gas. The O-ring connection was joined to a buret which is used to measure, by means of a mercury leveling bulb, the amount of oxygen absorbed during a degradation experiment.

Molecular Sieve 5A and glass wool were placed at the bottom of the tube. The polymer film, about 0.1 g in weight, was rolled and placed on the top of the glass wool. The apparatus was evacuated and placed in a thermostated oil bath heated to the required temperature. After a period of 15 min in the oil bath, the apparatus was flushed several times with oxygen or air and filled with the gas at one atmosphere of pressure. Oxygen absorption readings were then taken. In all cases, a reference cell was used to follow volume changes not caused by the absorption of oxygen by the polymer.

The infrared spectra of the polymer films before and after degradation were taken on a Perkin-Elmer 621 grating spectrophotometer.

RESULTS

The results of the thermal degradation of thin films of polypropylene with no additives are shown in Table I. The rates of oxidation reported in the table are taken from the slope of oxygen absorption versus time curves after the elapse of the induction period. A_{995}, A_{970}, and A_{CO} are the intensities of the bands occurring at 995, 970, and 1710 cm.$^{-1}$, respectively, in the infrared spectrum of the polymer. As seen from Table I, the induction period and the rate of polymer oxidation are reasonably similar and do not show dependency on the thickness of the films.

Results of oxidation of polypropylene containing the ketones 1,3-diphenyl-2-propanone, *p*-phenylacetophenone, and 4-phenylbenzophenone are shown in Table II. The A_{CO} (unoxidized) is the intensity of the peak in the infrared spectrum corresponding to the carbonyl group and shows the relative concentration of the ketone in the polymer film just before it was degraded. The amount of ketone added to the polymer solution before casting ranged between 1.55×10^{-5} to 1.61×10^{-3} mole/g of polymer. However, due to the volatility of the ketones, the true measure of their concentration in the polymer are the values A_{CO}/A_{970} listed in the tables. The 1,3-diphenyl-2-propanone acts as an oxidation initiator, thus, increasing the rate of oxidation and shortening the induction period. The *p*-phenylacetophenone and the 4-phenylbenzophenone act as mild oxidation inhibitors.

Pure polypropylene films, as well as films of polypropylene with ketonic additives, were also degraded in pure oxygen atmosphere at three temperatures, namely, 90, 120, and 150°C. The experimental data of this work are summarized in Table III. The results of oxidation of the pure polymer are also shown in Figure 3. The dip in this figure at 90°C is caused by the

TABLE I
Thermal Oxidation in Air of Pure Polypropylene

Film thickness, mils	Temp, °C	Induction period, hr	Rate of oxidation, ml (at STP)/g of polymer-hr	A_{995}/A_{970} of polymer	Total oxygen absorbed, (at STP)/g of polymer	A_{CO}/A_{970} (oxidized)	A_{995}/A_{970} (oxidized)
—	118.6	30.0	3.76	0.883	31.6	0.342	0.992
—	120.3	24.0	—	0.870	52.1	0.615	1.01
0.43	118.7	30.5	—	0.890	38.4	0.371	1.00
0.34	119.4	18.0	4.02	0.865	52.5	0.667	0.998
0.35	118.4	24.0	3.72	0.895	25.5	0.349	0.984
0.68	119.4	18.0	3.83	0.875	24.3	0.223	0.980
	Average	24.1	3.85	0.880			

TABLE II
Thermal Oxidation in Air of Polypropylene Containing Ketonic Additives

Additive	Film thickness, mils	Temp, °C	Relative concentration of the additive A_{CO}/A_{970} (unoxidized)	Induction period, hr	Rate of oxidation, ml (at STP)/g of polymer-hr	A_{995}/A_{970} (unoxidized)	Total oxygen absorbed, ml (at STP)/g of polymer	A_{CO}/A_{970} (oxidized)	A_{995}/A_{970} (oxidized)
1-3-Diphenyl-2-propanone	—	119.6	2.44	<0.1	10.5	0.929	57.2	0.864	0.970
	—	119.2	0.717	<0.1	6.1	0.891	51.2	0.492	0.958
	0.34	118.9	0.318	0.5	7.6	0.875	72.9	0.915	1.02
	0.30	119.0	0[a]	3.0	—	0.865	62.7	0.885	1.00
	0.43	118.7	0[a]	3.0	6.0	0.875	61.6	0.680	1.00
p-Phenylaceto-phenone	0.57	118.9	2.18	85.0	1.43	0.894	—	0.421	1.02
	—	118.6	1.90	97.0	1.28	0.860	41.2	0.359	0.996
	0.33	118.8	0.900	42.0	1.50	0.916	50.5	0.483	0.994
	0.57	118.8	0.816	43.5	2.27	0.870	23.8	0.283	0.980
	0.32	119.0	0[a]	22.0	4.03	0.869	61.5	0.462	0.997
4-Phenylbenzo-phenone	0.50	119.4	1.39	70.0	1.35	0.914	—	0.589	1.03
	0.47	119.4	1.09	22.0	5.30	0.911	64.4	0.638	0.993
	0.70	118.8	1.08	42.0	—	0.911	61.6	0.576	1.03
	0.50	119.4	0.570	18.0	—	0.883	—	0	0.931
—							74.4	0.681	1.02

[a] This means that the ketonic additive is found in small concentration, undetectable by infrared spectroscopy.

TABLE III
Thermal Oxidation in Pure Oxygen Atmosphere of Polypropylene Systems

Polymer system	Film thickness, mils	Temp, °C	Relative concentration of the additive A_{CO}/A_{670} (unoxidized)	Induction period, hr	Rate of oxidation, ml (at STP)/ g of polymer-hr	A_{995}/A_{960} (unoxidized)	Total oxygen absorbed, ml (at STP)/g of polymer	A_{CO}/A_{970} (oxidized)	A_{995}/A_{970} (oxidized)
Pure polypropylene	0.6	149.8	—	<0.1	350	—	350	—	—
	0.6	119.3	—	1.8	38.8	—	146	—	—
	0.5	89.9	—	31	3.64	0.923	157	2.22	1.07
Polypropylene data from Chien and Boss[4]	2.0	150	—	6.5	107.3	—	—	—	—
Polypropylene + 1,3-diphenyl-2-propanone	0.40	149.9	0.493	<0.1	308	0.877	294	—	—
	0.50	120.0	0.466	2.25	33.5	0.874	228	2.52	1.05
	0.50	90.4	0.453	24	4.01	0.865	142	1.28	0.962
Polypropylene + *p*-phenylacetophenone	0.7	149.9	3.16	<0.1	282	0.894	288	—	—
	0.5	120.2	3.18	1.5	23.2	0.847	136	1.62	1.06
	0.5	90.2	3.21	35	2.82	0.841	66	0.222	0.972
Polypropylene + 4-phenylbenzophenone	0.4	149.8	1.08	<0.1	297	0.910	286	—	—
	0.5	119.7	0.964	3.50	11.1	0.918	136	1.42	1.03
	0.5	90.4	0.913	204	0.342	0.895	37.2	0.156	0.940

change in volume of the freshly added oxygen as it reaches the temperature of the apparatus. Under the severe oxidation conditions of pure oxygen atmosphere and higher temperatures (120 and 150°C), the effects of the ketones on the degradation of the polymer were very much less noticeable

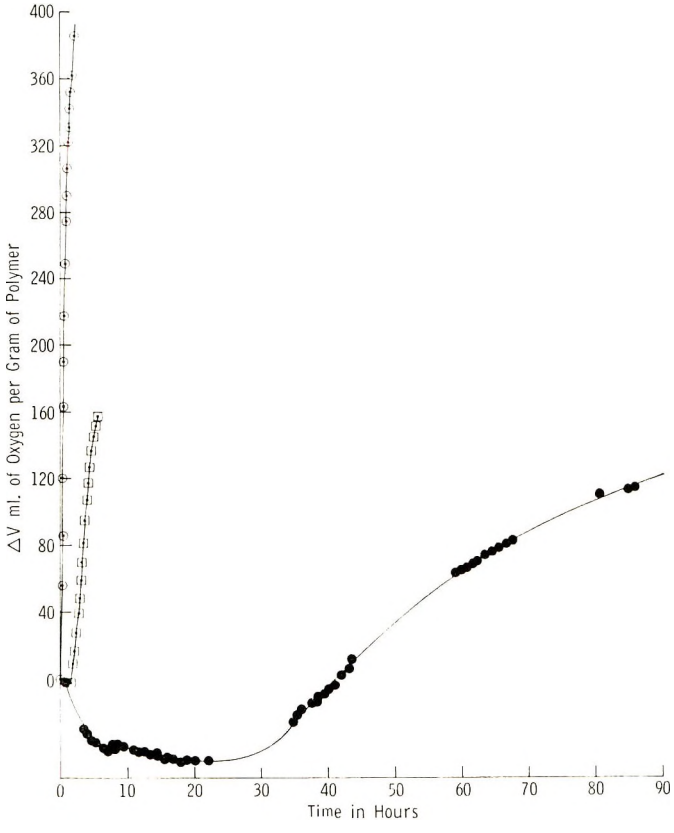

Fig. 3. Thermal degradation of pure polypropylene at (●) 90°C, (⊡) 120°C, and (○) 150°C and 1 atm pressure in oxygen.

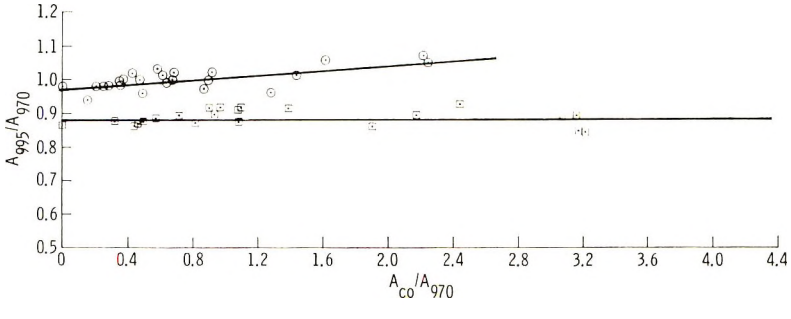

Fig. 4. Variation in the crystallinity band A_{995} with (⊡) concentration of added ketone and (○) degree of oxidation.

than when the oxidation was carried out at the lower temperature, 90°C, or when it was carried out in air.

Figure 4 shows the variation in the crystallinity band A_{995} with the amount of added ketone and with the degree of oxidation. The relative band height does not change with the amount of added ketone, but it increased linearly with the degree of oxidation.

DISCUSSION

The thermal oxidative degradation of isotactic polypropylene is most frequently measured by the length of the induction period and the rate of oxidation of the polymer. Three factors are known to influence the above two variables. These are: the temperature at which the oxidation is carried out, the oxygen pressure, and the film thickness of the sample. The effect of temperature as shown in Figure 3 is to shorten the duration of the induction period and to increase the rate of oxidation. A comparison of the results in Table I, where oxidation was carried out in an air atmosphere, and Table III, where pure oxygen was used, indicates that the oxygen pressure has a similar effect. There was no effect of film thickness on the oxidation of the polypropylene films studied in this work (0.3–0.8 mil). It is apparent that diffusion limitations are not applicable to thin films. For thicker films (2–75 mils), the works of Chien and Boss,[4] and Russell and Pascale[16] show that the oxidation of polypropylene is diffusion controlled. Both groups have established that thicker films are characterized by longer induction periods and lower rates of oxidation. A comparison of the results of oxidation of a film 2 mils thick obtained by Chien and Boss[4] to those obtained in this work (Table III) shows that at 150°C in a pure oxygen atmosphere the oxidation of the thinner film is much faster. It seems, therefore, that diffusion limitations are applicable in the range of thickness between 2 to 0.8 mils. The above authors[4] used a similar type of polypropylene to the one used in the present work.

The use of an additive, AH, with a polymer could enhance or inhibit the oxidation of the polymer depending on its rate of reaction as a chain initiator [eq. (1)]

$$\mathrm{AH} + \mathrm{O_2} \xrightarrow{k_1} \mathrm{HO_2}\cdot + \mathrm{A}\cdot \tag{1}$$

or a chain inhibitor [eq. (2)]

$$\mathrm{ROO}\cdot + \mathrm{AH} \xrightarrow{k_2} \text{inactive products} \tag{2}$$

On this basis the action of the three ketonic additives on the thermal stability of polypropylene could be explained. Whereas the 1,3-diphenyl-2-propanone with two $-\mathrm{CH_2}-$ groups situated between the carbonyl and the phenyl groups is expected to have a much higher k_1 than k_2, the other two ketones, *p*-phenylacetophenone and 4-phenylbenzophenone, can interact with the peroxy radical and produce resonance stabilized radicals.

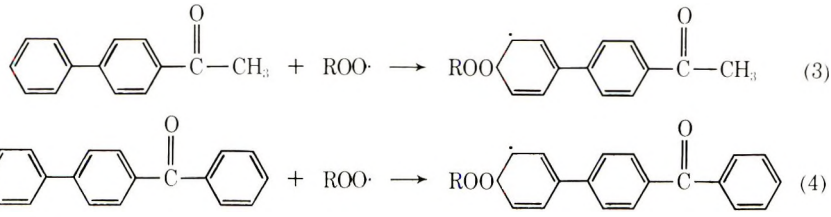

Since k_1 is more temperature-sensitive than k_2,[17] the rates of oxidation of the polypropylenes containing the three ketones are expected to be similar at the higher temperature. The individual effects of the additives are more noticeable at the lower temperatures (Table III).

The overall activation energy of the pure polypropylene was estimated from the variation of the rate of oxidation with temperature at a pressure of one atmosphere in oxygen. The value obtained is 22.5 kcal/mole as compared to 21.8 kcal/mole reported by Neimann.[17]

The use of thin films of polypropylene provided an excellent opportunity for the study of the variation of the infrared crystallinity band at 995 cm^{-1} with the degree of oxidation. Heinen[18] found that the degree of crystallinity of isotactic polypropylene is linearly related to the ratios of the bands at 1171 and 846 cm^{-1}, A_{1171}/A_{846}. Luongo,[19] however, found that it is more convenient to use the ratios of the band at 995 and 970 cm^{-1} to indicate the degree of crystallinity. The band at 970 cm^{-1} is a reference band and its intensity does not vary with the tacticity of the sample. Figure 4 shows the results of the infrared study of the polypropylene systems used in this work. In this figure the A_{CO}/A_{970} represents the concentration of ketones in the unoxidized samples, and the concentration of the nonvolatile carbonyl groups formed during oxidation in the oxidized samples. The ratio of the intensity of the peaks A_{970}/A_{995} remains constant with the concentration of the ketonic additive. This is rather surprising because disruption of some of the crystallinity is expected when an additive is placed in polypropylene. Density measurements by flotation method[20] were made on pure polypropylene and polypropylene with 10% (by weight) of added ketones. The results are shown in Table IV. It is apparent that no appreciable change in the density occurs when the additives are placed into the polymer.

TABLE IV
Densities of Unoxidized and Oxidized Polypropylene Samples

Polypropylene	Additive	Additive, wt-%	A_{CO}/A_{995}	Density, g/cc
Unoxidized	None	0	—	0.911
"	*p*-Phenylacetophenone	10	—	0.910
"	4-Phenylbenzophenone	10	—	0.896
"	1,3-diphenyl-2-propanone	10	—	0.909
Oxidized	None	—	0.156	0.920
"	None	—	1.42	0.943
"	None	—	2.22	0.961

Upon oxidation, the ratio of the peaks A_{995}/A_{970} increases linearly with the degree of oxidation (Fig. 4). A similar dependence is also observed for the change in density with the degree of oxidation (Table IV). Annealing has very little effect on the above two variables since unoxidized samples heated for long periods at lower oxygen pressures show density and A_{970}/A_{995} values similar to those of the unheated samples. Hence, the observed variations in the density and the infrared crystallinity values should be explained in terms of growth in the crystalline phase of the polymer upon oxidation due to the breaking of tie molecules.[14] The two lines in Figure 4 do not meet at zero A_{CO} because oxidation was already occurring during the induction period.[10] Infrared and oxygen absorption techniques cannot detect this low level of oxidation. It is well known, however, that some properties of polypropylene change drastically during the induction period.[14]

SUMMARY

In summary, the significance of this study is that the thermal degradation of polypropylene, for the first time, has been carried out in the absence of bulk or diffusion effects, through the use of thin films of the polymer. It clearly showed a linear relationship between the infrared crystallinity and the degree of oxidation of the polymer. The dual nature of a stabilizer as an oxidation inhibitor or initiator has been demonstrated by studying the effects of slightly stabilizing ketones on the degradation of polypropylene at three different temperatures.

References

1. S. S. Stivala and L. Reich, *Polym. Eng. Sci.*, **5**, 179 (1965).
2. W. L. Hawkins, W. Matreyek, and F. H. Winslow, *J. Polym. Sci.*, **41**, 1 (1959).
3. W. L. Hawkins, *Polym. Eng. Sci.*, **5**, 196 (1965).
4. C. R. Boss and J. C. W. Chien, *J. Polym. Sci. A-1*, **4**, 1543 (1966).
5. J. C. W. Chien and C. R. Boss, *J. Polym. Sci. A-1*, **5**, 1683 (1967).
6. J. C. W. Chien, E. J. Vandenberg, and H. Jabloner, *J. Polym. Sci. A-1*, **6**, 381 (1968).
7. J. C. W. Chien and H. Jabloner, *J. Polym. Sci. A-1*, **6**, 393 (1968).
8. J. C. W. Chien and C. R. Boss, *J. Polym. Sci. A-1*, **5**, 3091 (1967).
9. L. Reich and S. S. Stivala, *Revs. Macromol. Chem.*, **1**, 249 (1966).
10. S. S. Stivala, L. Reich, and P. G. Kelleher, *Makromol. Chem.*, **59**, 28 (1963).
11. S. S. Stivala and L. Reich, *Polym. Eng. Sci.*, **7**, 253 (1967).
12. M. G. Chan and W. L. Hawkins, *Polym. Eng. Sci.*, **7**, 264 (1967).
13. R. H. Hansen, C. A. Russell, T. DeBenedicts, W. M. Martin, and J. V. Pascale, *J. Polym. Sci. A*, **2**, 587 (1964).
14. H. J. Oswald and E. Turi, *Polym. Eng. Sci.*, **5**, 152 (1965).
15. D. A. Gordon and E. C. Rothstein, *Polym. Eng. Sci.*, **6**, 231 (1966).
16. C. A. Russell and J. V. Pascale, *J. Appl. Polym. Sci.*, **7**, 959 (1963).
17. M. B. Neimann, *Aging and Stabilization of Polymers*, Consultants Bureau, New York, 1965, pp. 4–37, 94–136.
18. W. Heinen, *J. Polym. Sci.*, **38**, 545 (1959).
19. J. P. Luongo, *J. Appl. Polym. Sci.*, **3**, 302 (1960).
20. I. Abu-Isa and M. Dole, *J. Phys. Chem.*, **69**, 2668 (1965).

Received August 4, 1969
Revised October 8, 1969

JOURNAL OF POLYMER SCIENCE: PART A-1 VOL. 8, 973-978 (1970)

Production of Organometallic Polymers by the Interfacial Technique. V. Partial Mechanistic Study of the Production of Poly[alkyl(aryl)oxysilanes]

CHARLES E. CARRAHER, JR.,* and GEORGE H. KLIMIUK,
Chemistry Department, University of South Dakota,
Vermillion, South Dakota 57069

Synopsis

A modified interfacial polymerization system capable of producing poly[alkyl(aryl)-oxysilanes] consisting of a dichlorosilane in an organic solvent as octane and a diol in 2,5-hexanedione is presented. It is believed that polymerization occurs near the interface in the dione phase. The products are low to intermediate in molecular weight. As the nature of silane is varied, the rate of polymer formation varies, the silane with the most electron-deficient silicon giving the greatest rate. Molecular weight is constant as diol is changed but varies when the silane is changed so that the silane with the most bulky substitutes will give polymer with the lowest molecular weight. The results are consistant with a S_N2 type reaction mechanism.

INTRODUCTION

For almost a quarter of a century the successful use of silicones in high- and low-temperature applications has prompted extensive research efforts to provide improved products through modifications of the polysiloxane chain. Curry, Byrd, et al.[1-3] have been most successful in the synthesis of poly(aryloxysilanes) employing the melt-polymerization technique condensing dianilinosilanes with aromatic diols.

Little has been reported on the production of organometallic polymers by the interfacial technique. Iskenderov et al.[4] in 1965 reported the first interfacial production of silicon-containing polymers by reacting sodium terephthalate in water with diethyldichlorosilane in benzene at room temperature. Zilkha et al.[5,6] reported the production of low molecular weight tin polyesters from the reaction of dialkyl(aryl)dichlorotin or tetraalkyl-(aryl)dichlorotin in an organic solvent with the sodium salt of bis[*o*-(carboxymethyl)phenyl] or bis[*p*-(carboxymethyl)phenyl]dimethylsilanes. (None of the above products are of the form reported in this paper.)

In the interfacial method, two fast-reacting monomers are dissolved in a pair of immiscible liquids, one of which is generally water. The water

* To whom communications should be directed.

phase contains a monomer such as a diol and any added alkali. The other phase consists of a monomer as a diacid halide and an organic liquid. Polymerization occurs at or near the liquid interface. It is found that in such a system with diol in water and silane in an organic solvent that the silane is preferentially hydrolized to give a product with a repeating backbone unit of —Si—O— and not the desired product with diol. Thus nonaqueous, two-phase systems were devised. Carraher[7–9] recently reported the first interfacial synthesis of poly(alkyloxysilanes) by a modified interfacial system. There has been no reported synthesis of polyaryloxysilanes by the interfacial technique. [A review of the synthesis and properties of polyalkyl(aryl)oxysilanes is given elsewhere.[7]] It is the purpose of this paper to report the synthesis of polyalkyl(aryl)oxysilanes by a new modified interfacial system.

The new modified interfacial system has, in place of the usual aqueous phase, 2,5-hexanedione containing diol, the dione acting to form an interface with the organic phase and as a solvent for the diol.

EXPERIMENTAL

Polymerizations were carried out in a 1-pt Kimax emulsifying jar placed on a Waring Blendor (Model 1001 or 1043) unless otherwise noted. The jar was vented by placing a glass tube, inserted in a cork stopper, through a hole in the jar cap. A second hole in the jar cap contained a separatory funnel secured in a cork stopper. The diol, base, and 2,5-hexanedione were added to the reaction jar. The lid was screwed on the jar. The organic hydrocarbon solvent containing dichlorosilane was poured into the separatory funnel. The blender was turned on and, after approximately $^1/_2$ min, the stopcock of the funnel was opened, allowing all the solution to enter the jar. After a set time the blender was turned off. The lid was removed and the reaction mixture was filtered by means of suction (to remove insoluble salt and base; the polymer is soluble in the dione phase). The liquid was then added to a separatory funnel and the phases separated. The dione phase is dark brown in color, while the hydrocarbon phase is colorless. The dione phase is added to ten times the volume of distilled water. The polymer precipitates as a viscous liquid. The polymer was evaporated to a solid at temperatures less than 60°C. Portions of acetone and ether were added to help evaporation of liquids from the polymer. The polymer is soluble in dipolar aprotic solvents but not in water.

Viscometry was performed at 30°C in acetone with a Cannon-Ubbelohde viscometer. Limiting viscosity numbers (LVN) were obtained by serial dilution of solutions of 1 g/100 ml and less.

Melting ranges (softening ranges) were determined on a Fisher-Johns melting point apparatus at an approximate heating rate of 2C°/min and were taken to be the temperature at which melting initially began to where melting was complete. Melting ranges obtained are given without claim to being a measure of the glass transition temperature or the crystalline melting point.

Infrared spectra were obtained by use of a Beckman IR-10 or Perkin-Elmer 237 with potassium bromide pellets. The spectra are in agreement with the structure I and with the spectra reported by Curry et al.[1-3]

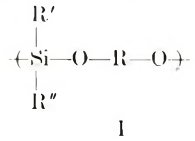

I

DISCUSSION AND RESULTS

The initial "modified" interfacial polycondensation system consisted of an organic solvent containing silane with the second phase consisting solely of liquid diol.[7,8] This system will be referred to as a M-1 system. The major disadvantage with this system is that it is limited to using diols which are liquid or which have low enough melting points so the temperature of the interfacial system can be raised above the melting point of the diol. The synthesis of polyaryloxysilanes by this method is excluded.

The water-replacing solvent in the system introduced in this paper is 2,5-hexanedione, which is immiscible with intermediate to long-chain hydrocarbon liquids such as octane and heptane and which dissolves both aliphatic and aromatic diols. This "modified" interfacial system is capable of producing polyalkyl(aryl)oxysilanes from the condensation of dihalosilanes and solid or liquid diols. This second, more general, system will be referred to as a M-2 system.

There are several differences between the M-1 and M-2 type systems. These are as follows: (a) the polymer produced in the M-1 type systems precipitates from the reaction system but it remains in the 2,5-hexanedione phase in the M-2 type systems; (b) in both systems, yield increases progressively with reaction time. The rate data for polymer formation for the M-1 system condensation of diphenyldichlorosilane with ethylene glycol conforms to a 5/3 order rate expression. The rate data for the M-2 system condensation of diphenyldichlorosilane with 2,2-bis(4-hydroxyphenylpropane) is found not to obey any simple rate expression. Yield

TABLE I
Physical Results as a Function of Stirring Time[a]

Stirring time, sec[b]	Yield, %	LVN, ml/g
15	67	4
30	73	6
60	77	4
120	81	4
240	86	4

[a] 0.021 mole diphenyldichlorosilane, 0.021 mole 2,2-bis(4-hydroxyphenyl)propane, 0.042 mole sodium hydroxide, 20 ml 2,5-hexanedione, 20 ml octane, and 25°C.

[b] Stirring time is the length of time the blender ran after the last of the organic solvent entered the reaction vessel from the separatory funnel.

TABLE II
Physical Results of Polymers as a Function of Comer Variation

Silane	Diol	Yield, % System A[a]	Yield, % System B[b]	LVN, ml/g System A	LVN, ml/g System B	Softening range °C System A	Softening range °C System B	Color
Diphenyl-dichlorosilane	2,2-Bis(4-hydroxy-phenyl)propane	60	81	6	4	145–155		Dk. brown
Methylphenyl-dichlorosilane	2,2-Bis(4-hydroxy-phenyl)propane	50	73	8	6	145–150		Dk. brown
Dimethyl-dichlorosilane	2.2-Bis(4-hydroxy-phenyl)propane	46	61	12	8	146–151		Dk. brown
Diphenyl-dichlorosilane	Ethylene glycol	63	55	6	4	134–144		Lt. tan
Methylphenyl-dichlorosilane	Ethylene glycol		36		6		116–129	Brown
Dimethyldi-chlorosilane	Ethylene glycol		7		7		87–98	Brown
Diphenyldi-chlorosilane	1,3-Dihydroxyacetone	51	53	6	4	147–154		Brown
Methylphenyl-dichlorosilane	1,3-Dihydroxyacetone		48		6		88–94	Brown
Dimethyl-dichlorosilane	1,3-Dihydroxyacetone		29		8		72–86	Brown
Diphenyl-dichlorosilane	Hydroquinone	53	56	5	4	101–112		Dk. brown
Diphenyl-dichlorosilane	1,3-Propanediol	60	50	6	4	45–57		Brown
Methylphenyl-dichlorosilane	1,3-Propanediol		29		7		52–62	Brown
Dimethyl-dichlorosilane	1,3-Propanediol		5		16		270–279	Lt. Brown

[a] System A: 0.018 mole silane, 0.018 mole diol, 0.040 mole sodium hydroxide, 20 ml 2,5-hexanedione, 20 ml octane, 2 min stirring time 25°C.
[b] System B: 0.021 mole silane, 0.021 mole diol, 0.042 mole sodium hydroxide, 20 ml 2,5-hexanedione, 20 ml octane, 2 min stirring time at 25°C.

increases rapidly to a stirring time of 15 sec and then only slowly increases with increased stirring time (Table I).

No noticeable variation of polymer molecular weight with time is observed (Table I). This is in agreement with a chain-type mechanism proposed for interfacial polymerizations.[10] This is also in agreement with the trend observed for the M-1 type systems[7,8] and with the findings of others.[11]

When the electronic and steric nature of the silane is changed there is a change in polymerization rate (yield at constant time) and molecular weight (Table II). The observed changes of polymerization rate can be explained by considering the electronic nature of the silanes. As the electron-withdrawing power of the substituents increases, polymerization rate increases [phenyl, Hammett σ (*meta*) 0.22,[12] Taft $\sigma^* = 0.60$;[13] *m*-methyl, σ (*meta*) $= -0.07$, $\sigma^* = 0.00$]. Since the phenyl group offers more bulk than the methyl group, it further suggests that steric conditions about the silicon atom are not critical in determining polymerization rate.

Whereas electronic arguments were used to explain the rate observations concerning change in the nature of the silane so that faster rates were found for systems containing diphenylsilane rather than dimethylsilane, just the opposite is observed for molecular weight. The dimethylsilane gives product with higher molecular weight than does diphenylsilane (Table I). An explanation is that the greater steric hindrance offered by the phenyl groups in diphenyldichlorosilane, while tending not to block the entrance of monomeric and oligomeric material, tends to block the approach of larger reactive molecules resulting in generally stepwise growth, i.e., addition of only small pieces to the chain at a given time. The dimethylsilane, by comparison, offers less steric hindrance and (relatively) does not block the approach of larger molecules making it possible for larger molecules to add increasing the molecular weight of the product.

The electronic and steric trends concerning silane are the same as those observed for the M-1 type system[7,8] and are consistent with an S_N2 type reaction mechanism.

The nucleophilic nature of the diols employed in the M-1 systems did not vary greatly (diols such as ethylene glycol and 1,3-propanediol) resulting in an apparent invariance of reaction rate with change of diol. In the present system the nucleophilicity of the diols was varied to a greater degree using greater nucleophilic diols as ethylene glycol and lesser nucleophilic diols as hydroquinone and 1,3-dihydroxyacetone [Hammett σ(*meta*) $= 0.22$,[12] and Taft $\sigma^* = 0.60$[13] for the phenyl group; σ(*meta*) $= -0.07$,[12] $\sigma^* = 0.00$[13] for the methyl group; σ(*meta*) $= -0.04$,[12] $\sigma^* = -0.10$[13] for the ethyl group; and σ(*meta*) $= 0.31$,[12] and $\sigma^* = 0.60$[13] for the CH_3CO group].

No simple trend is observed as the nucleophilic nature of the diol is varied. Since the number of systems studied is small generalized trends must be viewed with caution. With the exception of 2,2-bis(4-hydroxyphenyl)propane, the polymerization rates of diols with diphenyldichlorosilane are apparently invariant. With dimethylsilane and methylphenyl-

silane the situation is changed such that the lesser nucleophilic diols react faster with the silanes.

Variation of the diol has little effect on the molecular weight of the product (Table I), which is consistent with the findings reported for the M-1 type systems. More study is needed to discern more exactly and surely the influence of steric and electronic environments on the production of polyalkyl(aryl)oxysilanes.

In the system introduced in this paper, the polymer is soluble in the dione phase but insoluble in the organic hydrocarbon phase. It is thus possible that the reaction site is near the interface but in the dione phase. This is further substantiated by the fact that all the silanes employed in the study have solubilities in excess of 2.5 mole of silane per 100 ml of 2,5-hexanedione at 25°C and that the solubility of the diols in hydrocarbon solvents is low (the solubility of ethylene glycol is less than 0.02 mole/100 ml of octane at 25°C).

The correlation of molecular weight with viscosity and the presentation of polymerization rate and molecular weight results as a function of other variables will be presented in a subsequent article in this series.

A modified interfacial polymerization system capable of producing polyalkyl(aryl)oxysilanes is presented. The products are low to intermediate in molecular weight. The polymerization rate, as silane is varied, is the highest for the most electronegative silane. Molecular weight increases as the steric hindrance about the silicon atom decreases. The results are consistent with an S_N2 type reaction mechanism.

This work was supported by American Chemical Society Petroleum Research Fund Grant 1338-G13.

References

1. J. Curry and J. Byrd, *J. Appl. Polym. Sci.*, **9**, 295 (1959).

2. W. Dunnavant, R. Markle, P. Stickney, J. Curry, and J. Byrd, *J. Polym. Sci. A-1*, **5**, 707 (1967).

3. W. Dunnavant, R. Markle, R. Sinclair, P. Stickney, J. Curry, and J. Byrd, paper presented at American Chemical Society Meeting, 1967; *Polymer Preprints*, **8**, 1163 (1967); *Macromolecules*, **1**, 249 (1968).

4. M. Iskenderov, K. Plekhanova, and N. Adigezalova, *Uch. Zap. Azerb. Goz. Univ., Ser. Khim. Nauk*, **4**, 71 (1965).

5. S. Migdal, D. Gerther, and A. Zilkha, *J. Organometallic Chem.*, **11**, 441 (1968).

6. M. Frankel, D. Gerther, D. Wagner, and A. Zilkha, *J. Organometallic Chem.*, **9**, 83 (1967); *J. Appl. Polym. Sci.*, **9**, 3383 (1965).

7. C. Carraher, *J. Polym. Sci. A-1*, **7**,2351 (1969).

8. C. Carraher, paper presented at American Chemical Society Meeting, 1969; *Polymer Preprints*, **10**, 418 (1969).

9. C. Carraher, *J. Polym. Sci. A-1*, **7**, 2359 (1969).

10. P. W. Morgan, *Condensation Polymers: By Interfacial and Solution Methods*, Wiley, New York, 1965, pp. 20–30, 65, 68–75.

11. E. M. Hodnett and D. A. Holmer, *J. Polym. Sci.*, **58**, 1415 (1963).

12. H. H. Jaffe, *Chem. Revs.*, **53**, 191 (1953).

13. R. Taft, *J. Amer. Chem. Soc.*, **75**, 4231 (1953).

Received July 31, 1969
Revised October 8, 1969

JOURNAL OF POLYMER SCIENCE: PART A-1 VOL. 8, 979–990 (1970)

Polymerization by Transition Metal Derivatives. XII. Factors Controlling Activity and Stereospecificity in the 1,4 Polymerization of Butadiene by Monometallic Nickel Catalysts

J. P. DURAND, F. DAWANS, and PH. TEYSSIE,
Laboratoire de Chimie Macromoléculaire, Institut Francais du Pétrole, Rueil-Malmaison, France

Synopsis

In the course of investigations of polymerization of diolefins by transition metal derivatives, we have synthesized various monometallic nickel coordination catalysts. The complexes were prepared by reacting 2,6,10-dodecatriene-1,12-diyl nickel with protonic acids; they were shown to initiate the stereospecific polymerization of 1,3-butadiene. The study of these catalysts showed the strong influence of the nature of the counteranion used on the stereospecificity and the polymerization rate. Moreover, by adding various ligands, we were able to modify the behavior of the catalytic systems and to prepare either pure *cis*-1,4 or pure *trans*-1,4 or *cis–trans* equibinary polybutadienes, starting from the same complex and keeping a high 1,4 specificity. Some of these modifications were shown to be reversible.

INTRODUCTION

The important role of transition metal derivatives has been generally determined by the stereospecific polymerization of unsaturated hydrocarbons by means of Ziegler-Natta catalysts obtained from aluminum alkyls and transition metal compounds. In the polymerization of conjugated diolefins by these catalysts, it has been suggested that the polymer chain grows by insertion of the monomer into the π-allylic bond formed between the transition metal and the last polymerized unit. The importance of the transition metal was illustrated by the stereospecific polymerization of 1,3-butadiene in aqueous emulsion in the presence of rhodium salts and complexes.[1,2] Some examples of polymerization of butadiene by π-allyl derivatives of transition metals have already been reported: for instance, Wilke polymerized 1,3-butadiene by chromium and cobalt allyl derivatives;[3] studies on the polymerization of butadiene by π-allyl derivatives of nickel have also been published by various authors.[4,5]

In 1965, we investigated the synthesis of catalytic systems obtained by reacting various Ni (0) compounds with Lewis acids and their application for the polymerization of 1,3-butadiene. It proved possible to obtain

stereoregular 1,4-polybutadienes with different microstructures, depending on[6] the nature of the ligands bound to the nickel atom, as shown in Table I.

These results indicate that 2,6,10-dodecatriene-1,12-diyl nickel gives the more active catalytic system for the *cis*-1,4 polymerization of butadiene: this prompted us to study in more detail the systems obtained by reacting 2,6,10-dodecatriene-1,12-diyl nickel with various Lewis[6,7] and protonic[8–10] acids; monometallic nickel complexes of the π-allyl-Ni-X type were obtained, which are very efficient catalysts for the 1,4 polymerization of butadiene.

TABLE I
Polymerization of Butadiene in Presence of $Ni(L)_n$ and Acidic Cocatalysts

L_n in $Ni(L)_n$[a]	Structure of the polymers obtained[b]
DDTD ~ CDT ≫ $(COD)_2$ ≫ Cp_2 (decreasing activity)	*cis*-1,4-polybutadiene
$[(C_6H_5O)_3P]_4$	*trans*-1,4-polybutadiene
Cyclooctatetraene	*cis*/*trans*-1,4-polybutadiene
AN_2, Et_2diPyr	No polymers

[a] DDTD = 2,6,10-dodecatriene-1,12-diyl; CDT = 1,5,9-cyclododecatriene; $(COD)_2$ = bis-1,5-cyclooctadiene; AN_2 = bisacrylonitrile; Et_2diPyr = diethyl dipyridyl; Cp_2 = biscyclopentadiene.

[b] The vinyl content in these polymers is very low (<3%).

Moreover, by modifying the catalytic systems yielding *cis*-1,4-polybutadiene, we have synthesized[11] equibinary (*cis*-1,4–*trans*-1,4)-polybutadiene, i.e., a polybutadiene containing equimolecular amounts of *cis*-1,4 and *trans*-1,4 isomers. This new type of stereospecific polymerization, which does not take place with bimetallic catalytic systems, appears to be a general phenomenon; we have proposed[12] a preliminary tentative scheme of formation of these equibinary polydienes.

In this paper, we report a general survey of the results obtained with the use of 2,6,10-dodecatriene-1,12-diyl nickel in order to detail and complete previously published communications.

EXPERIMENTAL

Materials

Bis-1,5-cyclooctadiene nickel (0) was synthesized according to Wilke's procedure[13,14] by reduction of nickel acetylacetonate with triethylaluminum in the presence of 1,5-cyclooctadiene. This product was purified by crystallization from toluene at low temperature.

2,6,10-Dodecatriene-1,12-diyl nickel was prepared by reaction, between 0 and 20°C, of bis-1,5-cyclooctadiene nickel (0) with an excess of 1,3-butadiene in *n*-heptane and purified by elimination of excess butadiene, displaced 1,5-cyclooctadiene, and cyclododecatrienes. (Furthermore, we have shown that the addition of trans, trans, trans-cyclododecatriene to the polymeri-

zation medium does not modify the catalytic activity and the stereospecificity of the reaction.)

Benzene, toluene, chlorobenzene, *o*-dichlorobenzene, 1,2,4-trichlorobenzene, nitrobenzene, ethyl alcohol, and *n*-heptane used as reaction or polymerization solvents were anhydrous, purified products.

Gaseous butadiene was purified over potassium hydroxide pellets and dried successively on 4 Å molecular sieves and calcium hydride.

The acids were commercial products which were either distilled or recrystallized and dried before use.

Polymerization

All polymerizations were performed in Pyrex tubes, into which the reagents were transferred under an argon atmosphere by means of hypodermic syringes. The tubes were sealed with a torch and stirred in a thermostated water bath. The polymerizations were stopped by adding small amounts of a methanolic solution of aqueous hydrochloric acid containing an antioxidant and a chelating agent. The precipitated polymers were isolated by filtration, purified by successive dissolutions in benzene and precipitations in isopropyl alcohol and dried to constant weight under reduced pressure.

Properties of the Polymers

The polybutadiene microstructure was determined by infrared spectrophotometry according to the method of Morero et al.[15] in CS_2 solution.

The number-average molecular weight was determined with a Mechrolab 502 membrane osmometer on toluene solutions, and the weight-average molecular weight with a Sofica light-scattering photometer on cyclohexane solutions.

Differential thermal analyses were conducted on a CNRS model 2 microanalyser with 45×10^{-4} g of polymer rapidly cooled to $-140°C$ under helium atmosphere and then heated at a rate of about $2°C$/min.

EXPERIMENTAL RESULTS AND DISCUSSION

Catalyst Systems

It was reported by Wilke[16,17] that bis-1,5-cyclooctadiene nickel reacts with 1,3-butadiene to give 2,6,10-dodecatriene-1,12-diyl nickel (I), which in turn reacts with hydrogen chloride to give 2,6,10-dodecatriene-12-yl nickel chloride (II).

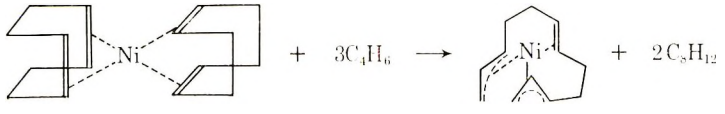

I

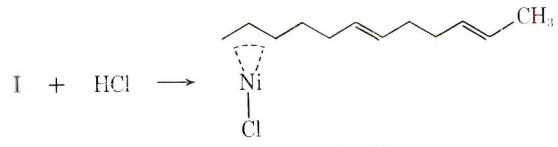

II

We reported previously[6,7] that monometallic catalytic systems, prepared by the reaction of bis-1,5-cyclooctadiene nickel with a protonic acid in the presence of butadiene are able to initiate stereospecific polymerization of butadiene and we have shown that, when hydrogen chloride is used, the active species is indeed 2,6,10-dodecatriene-12-yl nickel chloride (II).

$$\text{II} + n\ C_4H_6 \rightarrow \textit{cis}\text{-1,4-polybutadiene}$$

The NMR spectrum of the chloride complex performed in $CDCl_3$ solution at ambient temperature, as shown in Table II, reasonably accounts for the proposed structure, on the basis of relative absorption intensities and chemical shifts.

TABLE II

NMR Spectrum of 2,6,10-Dodecatriene-12-yl Nickel Chloride[a]

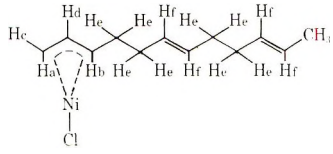

Chemical shift δ, ppm	Relative intensity	Attribution
1.25	2	H_a, H_b
1.62	3	H_{CH3}
2.10	8	H_e
2.85	1	H_c
5.05	1	H_d
5.50	4	H_f

[a] NMR study performed by Dr. H. Kawazura.

In the first step of this reaction, we have confirmed by quantitative vapor-phase chromatography that two moles of 1,5-cyclooctadiene were really liberated per mole of bis-1,5-cyclooctadiene nickel.

Using the same mode of synthesis, starting from various protonic acids, we obtained monometallic complexes which are efficient catalysts for 1,4 polymerization (Table III). These results show that the polymerization rate is maximum for an acid/nickel molar ratio equal to one, this observation confirming that the active species is a definite compound obtained by reacting one mole of nickel compound with one mole of protonic acid. However, in the case of picric acid, the maximum polymerization rate is obtained for an acid/Ni ratio of about 2; this particular behavior may be

TABLE III[a]

HX	Molar ratio HX/Ni	Reaction time, hr	PBD conversion, %	Microstructure		
				cis-1,4, %	*trans*-1,4, %	1,2, %
HCl	1	3	13	84	13	3
HBr	1	3	4	72	25	3
HI	1	6	30	0	100	0
CF_3COOH	1	3	90	91	4	5
CCl_3COOH	0.5	3	4	80	17	3
	1	3	30	91	6	3
	2	3	9	91	6	3
	4	3	1	83	12	5
$C_6H_2(NO_2)_3OH$	0.7	3	9	79	19	2
	1	3	8	87	10	3
	2	3	46	93	5	2
	4	3	11	90	7	3
$CHCl_2COOH$	1	20	60	90	7	3
$CH_2ClCOOH$	1	20	13	90	8	2
CH_3COOH	1	48	0	—	—	—
CH_3SO_3H	1	15	33	44	51	5
	4	15	17	51	44	5

[a] Conditions: $T = 55°C$; $[Ni] = 1.4 \times 10^{-2}$ mole/l.; $[C_4H_6]_0 = 3.4$ mole/l.

explained by the fact that a second mole of picric acid will act as a strong electron acceptor and thus increase the polymerization rate, as will be shown in the next part of this paper.

In the case of trifluoroacetic acid, we also reported previously the synthesis of a very active catalyst for the *cis*-1,4 polymerization of butadiene.[10] In the present paper, we did not isolate the complex after reacting I with trifluoroacetic acid, but we used the crude catalyst solution; this fact may explain the lower performances (activity and stereospecificity) obtained with this catalyst system.

Polymerization Results

With these catalytic systems, we have been able to show the strong influence of the structure of the acid and the nature of an additional ligand, not only on the stereospecificity of the reaction but also on the polymerization rate.

Influence of the Anion

Effect on Stereospecificity of the Reaction. As is apparent from Table III and as was previously reported,[9] the structure of the added acid strongly influences the stereospecific course of the reaction and consequently the microstructure of the polybutadiene formed. In fact, with HCl, HBr, and HI, the *trans*-1,4 content increases with decreasing electronegativity of the halide counterion used. Essentially *cis*-1,4-polybutadiene is obtained with HCl and crystalline *trans*-1,4-polybutadiene with HI; the

cis content is still higher when a more electron-withdrawing anion, like a trihaloacetate, is used.

We also reported previously[9] that results obtained with a very bulky counterion, i.e., formation of *cis*-1,4-polybutadiene with picric acid, seemed to indicate that the change of stereospecificity was probably not due entirely to a steric effect, but also to the inductive effect of the counterion; up to now however, this point could not be elucidated unequivocally, since it was shown that the presence of an electron-acceptor compound (e.g., an excess of picric acid) could promote the formation of pure *cis*-1,4-polybutadiene (see Table V); moreover, we have shown that 2,6,10-dodecatriene-1,2-diyl nickel when used in the presence of chloranil yields pure *cis*-1,4-polybutadiene while it yields small amounts of *trans*-1,4-polybutadiene when used alone.

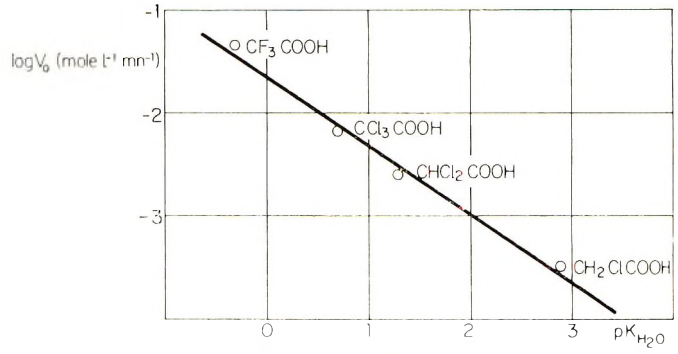

Fig. 1. Influence of the pK_{H_2O} of the acids $CH_{3-n}X_nCOOH$ on the initial polymerization rate. $[C_{12}H_{18}Ni] = [CH_{3-n}X_nCOOH] = 1.4 \times 10^{-2}$ mole/l.; $[C_4H_6]_0 = 3.4$ mole/l.; solvent = *n*-heptane; 55°C.

On the other hand, the NMR data obtained on 2,6,10-dodecatriene-12-yl nickel chloride (see Table II) might rule out the hypothesis that the *cis* or *trans* orientation would be due exclusively either to a change in the coordination of the first double bond in the growing chain to the nickel moiety, or to the *syn* or *anti* conformation of the terminal π-allyl group.[18]

Effect on Polymerization Rate. The activity of the catalytic systems described in this paper is strongly dependent on the structure of the acid (as shown in Table II) and increases sharply in the following order: $CH_3COOH < CH_2ClCOOH < CHCl_2COOH < CCl_3COOH < CF_3COOH$. Moreover, as illustrated by Figure 1, we observe a practically linear relationship between the logarithm of the initial polymerization rate and the pK of the corresponding acids, taken as a measure of the electron-withdrawing power of the counteranion present in the complex. A similar observation was made in the course of our investigations with π-allyl nickel haloacetates.[19]

These results confirm the tremendous influence of this parameter not only on the stereospecificity but still more on the polymerization rate.

Influence of the Ligands

In the introduction, we showed that both the activity and the stereospecificity of these catalytic systems are strongly dependent on the nature of the ligands bound to the nickel atom. The study of the influence of an additional ligand confirmed these results. It shows the ability of the same monometallic nickel complex to yield a *cis*-1,4, a *trans*-1,4, or an equibinary (*cis*-1,4–*trans*-1,4)-polybutadiene, according to the nature of the additional ligand used.

Trans-1,4-Polybutadiene. We reported previously the synthesis of *trans*-1,4-polybutadiene with 2,6,10-dodecatriene-12-yl nickel iodide. Now, we have found (Table IV) that, on using a catalytic system which gives *cis*-1,4-polybutadiene (for example, 2,6,10-dodecatriene-1,12-diyl nickel, CF_3COOH) when used alone, the addition of certain strongly electron-donating ligands, such as triphenylphosphite or alcohols, orients the reaction towards the formation of crystalline *trans*-1,4-polybutadiene. Other ligands such as phosphines deactivate the complexes completely.

TABLE IV[a]

Ligand (L)	Time, hr	Conversion, %	Microstructure			$[\eta]$ (toluene, 30°C)
			cis-1,4, %	*trans*-1,4, %	1,2, %	
None	3	90	91	4	5	0,57
$(C_6H_5)_3P$	20	0	—	—	—	—
$(C_6H_5O)_3P$	48	75	—	96	4	0,80
C_2H_5OH	24	3	—	96	4	—

[a] Conditions: $[C_{12}H_{18}Ni] = [CF_3COOH] = 1.4 \times 10^{-2}$ mole/l.; $[C_4H_6]_0 = 3.4$ mole/l.; 55°C in *n*-heptane; L/Ni = 1 except for C_2H_5OH, where L/Ni $\geq$ 2.

Equibinary (cis-1,4–trans-1,4)polybutadiene. We reported previously[11] the preparation of *cis–trans* equibinary polybutadiene by modifying a catalytic system giving, originally, *cis*-1,4-polybutadiene. In fact, with the catalytic system $C_{12}H_{18}Ni$–CF_3COOH, when the trifluoroacetic acid concentration is increased, we observe a very sharp decrease of the *cis*-1,4 content of the polymer obtained to a constant value of 50%, as it is shown in Figure 2. The same behavior is observed with difluorochloroacetic acid and again the 50/50 limiting value remains constant over a broad range of acid concentration.

The preparation of equibinary (*cis*-1,4–*trans*-1,4)-polybutadiene could be generalized by modifying the same catalytic system by addition of halogenated aromatic derivatives; in fact, if the butadiene polymerization is performed in pure chlorobenzene, *o*-dichlorobenzene, or 1,2,4-trichlorobenzene in place of *n*-heptane, benzene, or toluene an equibinary (*cis–trans*)-polybutadiene is also obtained. The results illustrated in Figure 2 suggest that the modification of the catalytic site is probably due not exclusively to the effect of the dielectric constant of the reaction medium

TABLE V[a]

Additive	Molar ratio, additive/Ni	Electron affinity, eV[b]	Conversion, %	Microstructure			[η] (toluene, 30°C)
				cis-1,4, %	*trans*-1,4, %	1,2, %	
			90	51	49	—	0.39
Nitrobenzene	1	0.5	1	90	6	4	
Iodine	1		11	93	4	3	0.31
1,3,5-Trinitrobenzene	1	0.7	28	96	2	2	0.43
Dichloronaphthoquinone	1	1.1	66	95	1	4	0.42
p-Chloranil	1	1.4	77	92	4	4	0.79
Ethanol	2	—	3[c]	—	96	4	
	10	—	9[c]	—	96	4	
	344	—	10[c]	—	96	4	
Triphenylphosphite	1	—	85[d]	—	96	4	1.53
		—	73[e]	—	96	4	0.80

[a] Conditions: $[C_{12}H_{18}Ni] = 1.4 \times 10^{-2}$ mole/l.; $[CF_3COOH] = 0.14$ mole/l.; $[C_4H_6] = 3.4$ mole/l.; $T = 30°C$; $t = 3^3/_4$ hr; solvent = toluene.

[b] Data of Briegleb.[20]

[c] $t = 24$ hr; $T = 55°C$.

[d] $t = 20$ hr.

[e] $t = 90$ min; $T = 55°C$.

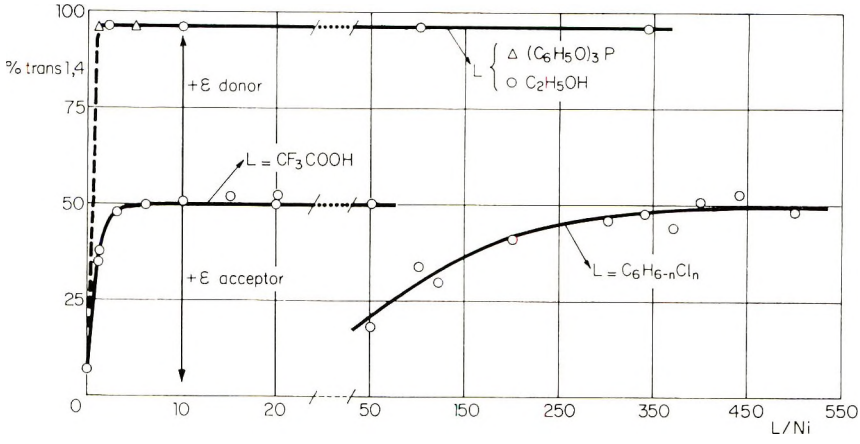

Fig. 2. Influence of additional ligands on the stereospecificity of the polymerization reaction. $[C_{12}H_{18}Ni] = [CF_3COOH] = 1.4 \times 10^{-2}$ mole/l.; $[C_4H_6]_0 = 3.4$ mole/l.; solvent = *n*-heptane; 55°C.

as was proposed previously,[9] but mostly to a coordination of solvent molecules on free positions of the complexes. In fact, the use of 1,2,4-trichlorobenzene ($\epsilon_{25} = 3{,}9$) or 1,2-dichlorobenzene ($\epsilon_{25} = 9{,}9$) as polymerization solvent, promotes, in both cases, the formation of equibinary poly(*cis*/*trans*)butadiene.

In addition to their high catalytic activity ($t_{1/2} < 20$ min at 55°C with $[C_4H_6]_0 = 3.4$ mole/l. and $[Ni] = 1.4 \times 10^{-2}$ mole/l.) a very interesting peculiarity of these various catalytic systems is the reversible character of the modifications described. The elimination, e.g. by evaporation, of the compound modifying the stereospecificity of the reaction (trifluoroacetic acid, chlorobenzene) results in a catalyst producing *cis*-1,4-polybutadiene. Moreover, even with catalyst systems yielding equibinary *cis*–*trans*-polybutadiene, it is possible, by adding electron-acceptor or electron-donor compounds, to obtain polybutadienes having respectively an all-*cis*-1,4 or crystalline all-*trans*-1,4 structure as shown in Figure 2.

Indeed the addition of electron-acceptor compounds, such as iodine, 1,3,5-trinitrobenzene, *p*-chloranil favors the formation of *cis*-1,4-polybutadiene, as is shown in Table V. Moreover, as reported previously[21,22] with others catalysts, the polymerization rate is strongly dependent on the electron affinity of the compound used. On the other hand, the addition of electron-donor compounds (for instance triphenylphosphite or alcohols) gives crystalline *trans*-1,4-polybutadiene; however, it is worthwhile to stress the good activity of the catalysts obtained and the high molecular weight of the polymers produced (Table V).

Polybutadiene Characteristics

With the same catalytic system by using different additional ligands we have shown that it is possible to synthesize at will, *cis*-1,4, *trans*-1,4 or

TABLE VI

Characteristics	*cis*-1,4 polymer		*trans*-1,4 polymer	Equibinary *cis*-1,4–*trans*-1,4 polymer
	Literature[10,23]	This work		
cis-1,4, %	>98	⩾91	—	50
trans-1,4, %			96	50
1,2, %			4	<1
[η] (toluene, 30°C)	2–3	0.5–0.7	0.8–1.6	0.2–0.6
$\bar{M}_w/\bar{M}_n$	3–4		8–10	4–5
Unsaturation, %	97–99	97–99		
Gel content, %	<1	<1	<1	<1
Glass transition temp, °C	−111	−111	(−96)	−105
Crystalline melting point, °C	−6	−8	91–105	—
Phase transition temp, °C			47–51	
Crystallinity (room temp), %			37–41	

equibinary *cis–trans*-polybutadienes. Characteristics of the polymers are summarized in Table VI. The stereospecificity of these catalysts is remarkable since they yield polybutadienes with a very high 1,4 content; the vinyl percentage, as determined from the absorption at 910 cm^{-1} is very low and sometimes undetectable, as for instance in the case of equibinary *cis–trans*-polybutadiene. Moreover, significant side reactions (i.e., cationic reactions) are excluded by the high unsaturation content of the polymers as well as the absence of gel.

We have shown previously[10] that these catalysts yield *cis*-1,4-polybutadiene having characteristics similar (see Table VI) to those of elastomeric polybutadiene samples obtained with Ziegler-Natta catalysts. With the catalytic system used in this work the activity, *cis*-1,4 content, and molecular weight are lower than those observed with isolated catalytic species,[10] although the products have a number of basic properties required for a *cis*-1,4 elastomer.

A *trans*-1,4-polybutadiene may be obtained with good activity ($t_{1/2} < 1$ hr at 55°C with $[C_4H_6]_0 = 3.4$ mole/l. and $[Ni] = 1.4 \times 10^{-2}$ mole/l.). Under certain conditions the molecular weight of the polybutadiene obtained is high ($\bar{M}_w$ around 300000); the polymer is crystalline (crystallinity around 40% as determined by x-ray spectroscopy, although the crystalline melting temperature was around 100°C). Moreover, this *trans*-1,4-polybutadiene shows a strong crystalline transition occurring about 50°C. Natta and Corradini[24] have reported a crystalline phase transition temperature at about 69°C and a melting point at about 135°C for a polybutadiene having a high *trans*-1,4 content. The lower melting and phase transition temperatures of *trans*-1,4-polybutadiene obtained in this work merely reflect a lower *trans*-1,4 content.

Equibinary *cis*-1,4–*trans*-1,4-polybutadienes, obtained with various catalysts described in this paper have in all cases low molecular weights

(around 30000); their physical properties appear to be different from those of pure *cis*-1,4- or *trans*-1,4-polybutadienes.

CONCLUSIONS

The study of the stereospecific polymerization of butadiene with monometallic nickel catalysts has shown that it is possible to control very closely both the catalytic activity and the geometrical isomerism of the polymers formed. In fact, with these catalysts, we have synthesized high-*cis*-1,4, high-*trans*-1,4, and equibinary *cis*-1,4–trans-1,4-polybutadienes.

The bulk of the results gathered in the course of this investigation suggests that the change from *cis* to *trans* orientation is due to the occupation of unshared coordination positions by the additional ligand. This hypothesis is supported by some cryometric measurements carried out in our laboratory, on π-allyl nickel trifluoroacetates.[25] The similar effect, observed with some anions, is presumably due also to the blocking or more precisely the "masking" of a coordination position caused by the anion volume or eventually by an inductive effect.

Concerning the formation of equibinary *cis–trans*-polybutadiene our results, according with the previously reported explanation,[11] are implying the alternative insertion of *cis*- and *trans*-1,4 units on two different coordination positions on the metal atom; a similar propagation scheme was previously proposed by Arlman and Cossee[26] for the formation of syndiotactic polyolefins. It may be interesting to point out that this scheme might be further supported by the very different behaviour of the two kinds of ligands added, the first one giving *trans*-1,4-polybutadiene and the other one equibinary (*cis*-1,4–*trans*-1,4)-polybutadiene; this result implies the existence of two different types of free coordination positions on the nickel complexes; this picture can fit very well with any kind of complex geometry where are found both apex and in-plane positions (octahedral, square pyramidal, or trigonal bipyramidal).

This work was done under contract with the Délégation Générale à la Recherche Scientifique et Technique (convention n. 66.00.459). The authors are indebted to Mr. J. C. Marinelli for his assistance with the experimental part of this work.

References

1. R. E. Rinehart, H. P. Smidt, H. S. Witt, and H. Romeyn, *J. Amer. Chem. Soc.*, **83**, 4864 (1961).

2. R. Dauby, F. Dawans, and Ph. Teyssie, in Macromolecular Chemistry, Prague 1965 (*J. Polym. Sci. C*, **16**), O. Wichterle and B. Sedlàček, Eds., Interscience, New York, 1967, p. 1989.

3. G. Wilke, B. Bogdanovic, P. Hardt, P. Heimbach, W. Keim, M. Kroner, W. Oberkirch, K. Tanaka, E. Steinrucke, D. Walter, and H. Zimmermann, *Angew. Chem.* (Intern. Ed.), **5**, 151 (1966).

4. L. Porri, G. Natta, and M. C. Gallazzi, *Chim. Ind.* (Milan), **46**, 428 (1964).

5. B. D. Babitskii, B. A. Dolgoplosk, V. A. Kormer, M. I. Lobach, E. I. Tinyakova, N. N. Chesnokova, and V. A. Yakovlev, *Vysokomol. Soedin.*, **6**, 2202 (1964).

6. F. Dawans and Ph. Teyssie, *C. R. Acad. Sci.* (Paris), **261C**, 497 (1965).
7. F. Dawans and Ph. Teyssie, *J. Polym. Sci. B*, **3**, 1045 (1965).
8. F. Dawans and Ph. Teyssie, *C. R. Acad. Sci.* (Paris), **263C**, 1512 (1966).
9. J. P. Durand, F. Dawans, and Ph. Teyssie, *J. Polym. Sci. B*, **5**, 785 (1967).
10. J. P. Durand, F. Dawans, and Ph. Teyssie, *J. Polym. Sci. B*, **6**, 757 (1968).
11. J. P. Durand and Ph. Teyssie, *J. Polym. Sci. B*, **6**, 299 (1968).
12. Ph. Teyssie, F. Dawans, and J. P. Durand, in *Macromolecular Chemistry, Brussels-Louvain 1967* (*J. Polym. Sci. C*, **22**), G. Smets, Ed., Interscience, New York, 1968, p. 221.
13. G. Wilke (to Studiengesellschaft Kohle), Fr. Pat. 1,320,729 (1964).
14. B. Bogdanovic, A. Kroner, and G. Wilke, *Ann. Chem.*, **699**, 1 (1966).
15. D. Morero, A. Santambrogio, L. Porri and F. Ciampelli, *Chim. Ind.* (Milan), **41**, 758 (1959).
16. G. Wilke, M. Kroner, and B. Bogdanovic, *Angew. Chem.*, **73**, 755 (1961).
17. G. Wilke (to Studiengesellschaft Kohle), Fr. Pat. 1,410,429 (1964).
18. T. Matsumoto and J. Furukawa, *J. Polym. Sci. B*, **5**, 935 (1967).
19. F. Dawans and Ph. Teyssie, *J. Polym. Sci. B*, **7**, 111 (1969).
20. G. Briegleb, *Angew. Chem.* (Intern. Ed.), **3**, 617 (1964).
21. O. K. Sharaev, A. W. Alferov, E. I. Tinyakova, B. A. Dolgoplosk, V. A. Kormer and B. D. Babitskii, *Dokl. Akad. Nauk SSSR*, **177**, 140 (1967).
22. G. Lugli, W. Marconi, A. Mazzei, and N. Palladino, *Inorg. Chim. Acta*, **3**, 151 (1969).
23. F. Dawans, J. P. Durand, and Ph. Teyssie (Institut Francais du Pétrole), Fr. Pat. 1,556,962 (1967).
24. G. Natta and P. Corradini, *Rubber Chem. Technol.*, **33**, 703 (1960).
25. J. C. Marechal, personal communication.
26. E. J. Arlman and P. Cossee, *J. Catal.*, **3**, 99 (1964).

Received October 13, 1969

JOURNAL OF POLYMER SCIENCE: PART A-1 VOL. 8, 991–1001 (1970)

Absorption and Fluorescence of a Nonionic Detergent in Aqueous Solution

SHOICHI IKEDA* and GERALD D. FASMAN, *Graduate Department of Biochemistry, Brandeis University, Waltham, Massachusetts 02154*

Synopsis

The absorption and fluorescence spectra of a detergent, polyoxyethylene octylphenyl ether, were measured in water at different concentrations. The absorption spectra had a peak at 275 mμ and a shoulder at 281 mμ. The spectra were independent of concentration below the critical micelle concentration, but the molar extinction coefficients of the peak and the shoulder increased with concentration above the critical micelle concentration. The critical micelle concentration value derived from the absorption data was in good agreement with those obtained by other methods. The fluorescence spectra of the detergent in water were independent of concentration in dilute solutions, if the intensities of the spectra were normalized at the peak at 302 mμ. At higher concentrations, a weak excimer band appeared at 345 mμ, whose intensity increased with concentration. The excimer band manifested itself at a concentration slightly lower than the critical micelle concentration. The main band decreased and the excimer band increased, as the temperature was raised. An excimer band was observed in the same region of the spectra for the pure detergent, either in the solid or liquid state. The equilibrium solid spectra exhibited a very strong excimer emission. It was concluded that the excimers were formed within micelles in the case of aqueous solutions.

INTRODUCTION

Detergent molecules form large aggregates in aqueous solution as the detergent concentration is increased. The micelle formation occurs at a well-defined concentration, the critical micelle concentration (CMC), above which both monomers and micelles exist. Various physical properties of a detergent solution suddenly change at this concentration, and their measurement as a function of concentration has provided useful methods for determining CMC.[1] Most of these properties are more or less concerned with the size of the solute species or their association equilibrium. However, other effects must be operative on detergent molecules when they are transferred from an aqueous to a micellar phase. The environment around a detergent molecule is consequently altered from a more polar to a less polar one, since the interior of a micelle is supposed to be similar to a liquid hydrocarbon. In addition, each detergent molecule is brought much closer to similar molecules in the micelle, while it is isolated from others in

* Present address: Department of Chemistry, Faculty of Sciences, Nagoya University, Nagoya, Japan.

solution. These two effects will influence the electronic structure of detergent molecules and consequently some observable changes in absorption or emission properties of detergent solutions are expected, if the molecule has a chromophoric or fluorophoric group in it.

A nonionic detergent, polyoxyethylene octylphenyl ether,

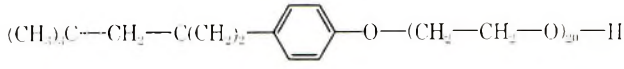

has been chosen to investigate the spectroscopic properties of a micelle. This detergent is indifferent to ionic association effects and has an aromatic group in it. Its micelle formation was previously studied by other methods.[2] The structure of the chromophore and fluorophore of the molecule is similar to that of anisole. In this connection, the present work constitutes an extension of a previous work[3] from this laboratory on phenol and its derivatives.

EXPERIMENTAL

Materials

Polyoxyethylene octylphenyl ether used in this study was the same sample as previously described.[2] It had 20 moles of ethylene oxide units per mole of detergent, and the molecular weight was assumed to be 1100. Aqueous solutions of the detergent were made up by dissolving the detergent in glass redistilled water. Methanol and dioxane were Matheson, Coleman and Bell spectrograde reagents.

Ultraviolet Absorption

The absorption spectra were measured on a Cary 14 spectrophotometer over the wavelength range 320–240 mμ at room temperature. A matched pair of cells was used, whose path length was either 1 cm or 1 mm. The temperature of solutions was varied by circulating water of constant temperature from a Haake thermostat through a temperature-regulating cell holder.

Fluorescence Emission

The fluorescence spectra were measured on a Zeiss MQZ-II spectrofluorometer at room temperature, with an Osram 450 W xenon lamp as light source. The excitation wavelength was 275 mμ, except where otherwise noted, and the slit width for the excitation was 0.5 mm. The slit width for the emission was fixed at 1 mm over the whole wavelength region examined. The emission spectra were recorded on a Sargent recorder. A cell with a square cross section of 1 cm in edge was put in a cell holder which was tilted in such a way as to observe the emission from the front surface. The temperature was altered by using a temperature-regulating cell holder, by circulating water from a Haake thermostat.

Fluorescence intensity was corrected for light source intensity and photomultiplier sensitivity, according to the calibration by Lehrer and Fasman.[3]

RESULTS

Absorption Spectra

Figure 1 shows the absorption spectra of the detergent in water at different concentrations. All the spectra have a peak around 275 mμ and a shoulder around 281 mμ. For most dilute solutions the spectra are independent of concentration, and the molar extinction coefficients at the peak and the shoulder are $\epsilon_{275} = 1330$ and $\epsilon_{281} = 1110$. At higher concentrations the absorption increases, and the splitting of the shoulder from the peak is more evident, together with a slight red shift of the spectra.

The molar extinction coefficients of the peak and the shoulder are plotted against concentration in Figure 2. The curves clearly indicate discontinuous changes of absorption at a certain definite concentration, which may be reasonably identified with the CMC of the detergent. The CMC, 0.077 g/dl or $7.0 \times 10^{-4}M$, thus obtained is in good agreement with the values, 0.075 and 0.078 g/dl, from sedimentation equilibrium and surface tension measurements, respectively.[2] The constant molar extinction coefficients

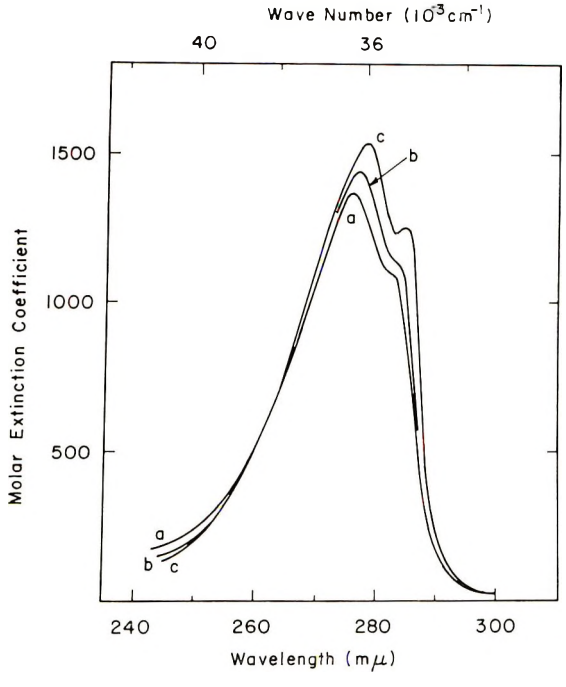

Fig. 1. Absorption spectra of the detergent in water at 23°C at different concentrations: (*a*) 0.0110–0.0771 g/dl; (*b*) 0.1121 g/dl; (*c*) 0.4914 g/dl.

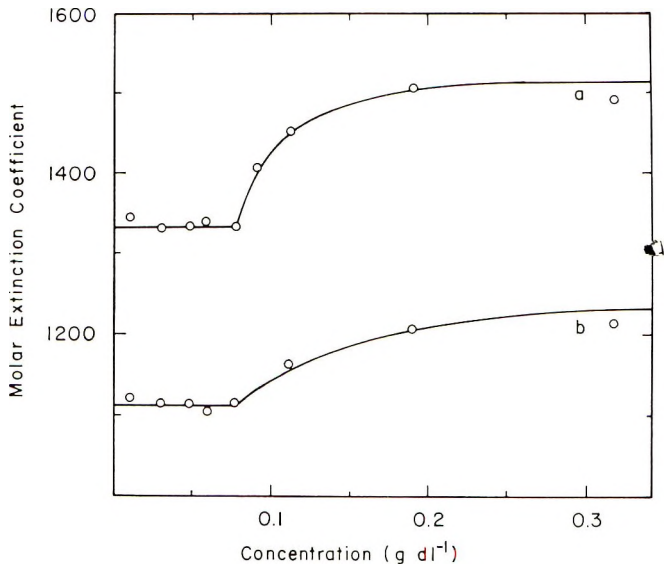

Fig. 2. Molar extinction coefficients of the absorption maxima as a function of detergent concentration at 23°C: (*a*) 275–278 mμ; (*b*) 281–284 mμ.

observed for dilute solutions are assigned to those of the detergent monomer in water, while the same coefficients of the detergent in a micelle can be obtained by extrapolating the ϵ values to higher concentrations. The limiting values are approximately equal to $\epsilon_{278} = 1540$ and $\epsilon_{281} = 1260$.

The detergent dissolved in methanol or dioxane gave spectra similar to those in water but were independent of concentration over the same concentration range. As compared with those in dilute aqueous solution, the spectra are characterized by stronger absorption and sharper splitting, together with a red shift of 2 mμ. At the peak and shoulder, $\epsilon_{277} = 1560$ and $\epsilon_{283} = 1300$ in methanol; $\epsilon_{277} = 1710$ and $\epsilon_{283} = 1460$ in dioxane.

These observations support the current view on micelle structure that detergent molecules in a micelle are held together with their nonpolar parts inside but with their polar heads on the surface in contact with water. The interior of each micelle is supposed to be like a liquid hydrocarbon. Thus a detergent molecule or, more specifically, each chromophore in the micelle is surrounded by a hydrocarbon environment or by a less polar medium than in water, and the absorption properties of the molecules in the micelle should resemble those in nonpolar solvents. The red shift, the increased absorption and the sharper splitting of fine structure have been observed for micelles as in organic solvents. However, the splitting of the two peaks is less distinct in the micelle and the molar extinction coefficients are not as high as in dioxane. These effects might be related to the location of the chromophore in the micelle: the chromophoric group is attached close to the polar end of the molecule so that it cannot be buried deeply inside the micelle where a hydrocarbon atmosphere would prevail.

The temperature effect on the absorption spectra is very subtle. The molar extinction coefficients at concentrations close to the CMC are altered at higher temperatures. This is because the CMC is lowered at higher temperatures, which is the behavior commonly observed for non-ionic detergents.[4–7]

Fluorescence Spectra

Aqueous solutions of the detergent exhibit fluorescence spectra with a maximum intensity around 300 mμ. Figure 3 shows the spectra at different detergent concentrations, all normalized at their peak position. The normalization has been carried out to obtain the emission spectra independent of the amount of light absorbed, since the recorded spectra are for solutions of different concentrations and, consequently, for different amounts of light absorbed. The amount of light absorbed cannot be evaluated from the absorption spectra, because of the extremely high concentrations of the detergent used and the geometry of the excitation and emission, i.e., front surface observations. Thus, the normalization will be suitable for com-

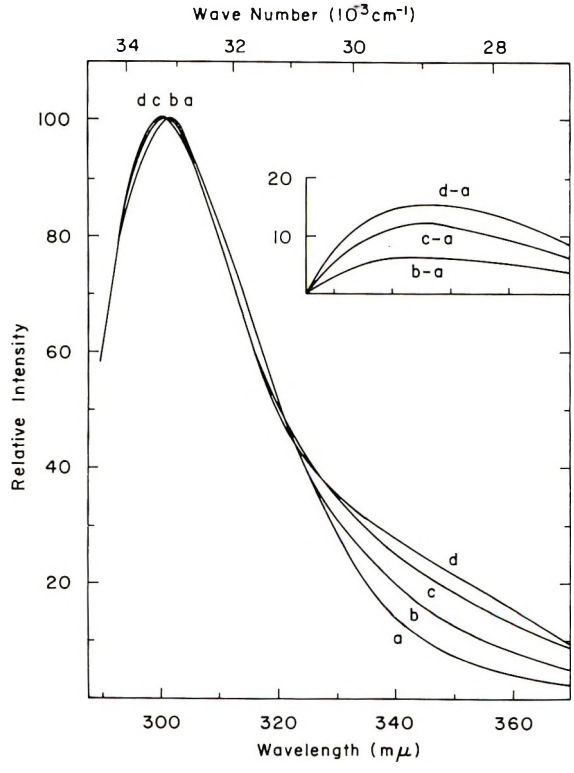

Fig. 3. Fluorescence spectra of the detergent in water at 23°C at different concentrations: (*a*) 0.0110–0.0600 g/dl; (*b*) 0.0771 g/dl; (*c*) 0.1121 g/dl; (*d*) 0.930 g/dl; isert: differences from *a*. Curves normalized at the peak position.

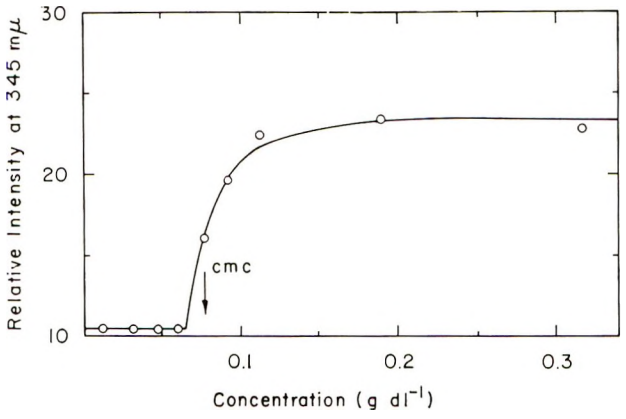

Fig. 4. Relative intensity of the emission peak at 345 mμ as a function of detergent concentration at 23°C.

parison of the emission properties of the detergent at different concentrations.

For dilute solutions the spectrum has a peak at 302 mμ and is independent of concentration. At higher concentrations, the peak position slightly shifts to the blue and a new shoulder appears around 345 mμ. The relative intensity of the shoulder increases with concentration, as shown in Figure 4, and the differences of the spectra from those obtained at low concentrations are inserted in Figure 3. The appearance of the new band is manifest above the CMC, but the intensity of the new band is appreciable at the CMC; that is, the band appears at a concentration slightly lower than the CMC. As the intensity of the new band is so weak that it does not contribute to the peak intensity of the main band, its origin may be attributed to the presence of micelles. However, the intensity of the new band seems to level off at high concentrations.

The emission spectra of the detergent in methanol and dioxane have a peak at 300 mμ, which is shifted to the blue by 2 mμ relative to that in dilute aqueous solutions. The spectra are independent of concentration and are superimposable on each other and to that in water at low concentrations, if they are normalized at the peak position.

These observations indicate that molecules in water emit at 302 mμ, while those in the micelle fluoresce at 300 mμ. The slight blue shift of the band can be attributed to the change in the environment of fluorophores from a polar to a nonpolar one. The appearance of the new band at 345 mμ, however, must come from some other effects, since the band is absent from the spectra in organic solvents. In the micelle the detergent molecules are situated in contact with one another and, except for the restriction that their polar ends are fixed on the micellar surface, they will be able to interact as strongly as in the liquid state. It is now known that many aromatic compounds can form dimers in the excited state, either in the liquid state[8,9] or in concentrated solutions[10–12]. Even in the crystalline

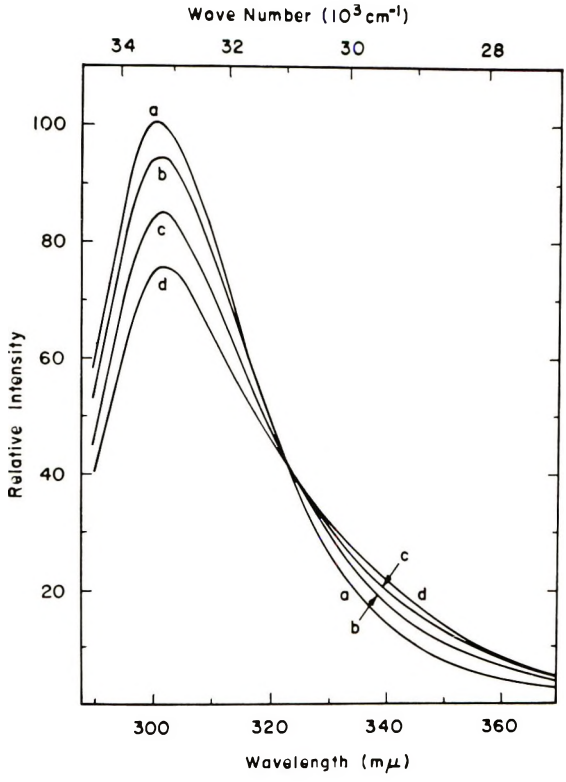

Fig. 5. Effect of temperature on the fluorescence spectra of the detergent in water at a concentration of 0.0600 g/dl: (*a*) 25°C; (*b*) 35°C; (*c*) 60°C; (*d*) 80°C.

state, they can form the excited dimers, if their aromatic rings are arranged in stacked pairs.[13] These excimers emit fluorescence at a longer wavelength than the normal monomer band, when they revert to two monomers in the ground state. Molecular interaction of a similar nature could occur for the detergent in a micelle, and the excimer could be formed when light was absorbed. The excimer band of the micelle is shifted to the red by 4300 cm^{-1} as compared with the monomer band. The red shift is of a magnitude comparable with that observed with liquid anisole.[3]

The effect of temperature on the fluorescence spectra is illustrated in Figure 5. The intensity of the monomer band decreases with increasing temperature, irrespective of concentration. This is the normal deactivation due to thermal agitation. However, the intensity of the excimer band changes with temperature in various ways, depending on the concentration. At very low concentrations no excimer band is present over the temperature range examined. For very concentrated solutions where the excimer band always exists, again its intensity remains unaltered by temperature. In contrast, at the intermediate concentrations or in the vicinity of the CMC, the intensity of the excimer band increases with temperature but

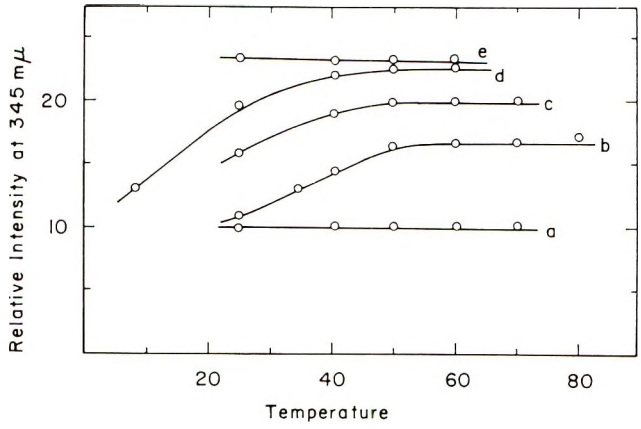

Fig. 6. Temperature dependence of the emission intensity of the excimer band at different concentrations: (*a*) 0.0307 g/dl; (*b*) 0.0600 g/dl; (*c*) 0.0771 g/dl; (*d*) 0.0913 g/dl; (*e*) 0.1898 g/dl. Spectra normalized for the peak intensity at 300 mμ at 25°C for each concentration.

ceases to increase at about 50°C. The intensity at 50°C. is again dependent on concentration. These temperature profiles of the excimer peak intensity are shown in Figure 6. The relative intensity has been normalized at the peak intensity at 300 mμ observed at 25°C.

The CMC is known to be lowered by temperature elevation.[4–7] Thus, at a fixed concentration, there will be more micelles formed upon raising the temperature, which would allow more excimers to be produced. The formation of excimers as well as micelles is favored at elevated temperatures where the hydrophobic interactions become more pronounced. However, at still higher temperatures, due to thermal agitation, excimers once formed would dissociate into monomers without excimer emission. Thus the intensity of the excimer band does not increase further above 50°C.

Fluorescence Spectra of Solid and Liquid States

Fluorescence spectra of the detergent, either in the solid or liquid state, exhibit two emission bands, as shown in Figure 7. At room temperature where the detergent is solid, a very strong excimer band is evident at 342 mμ besides the weaker monomer band at 302 mμ. Above 30°C, the detergent melts. Between 30 and 40°C the intensities of the two bands changed so slowly with time that the equilibrium spectra could not be obtained during the period of the experiments. The rate of intensity change with time was faster as the temperature was raised. General features of the spectra at different temperatures are shown in Figure 7; the monomer band is becoming more intense but the excimer band is weakening, as the temperature is raised and as the solutions stand for longer periods at elevated temperatures. At about 40°C, the equilibrium is now attained much more quickly, and the intensity relation of the two bands is now reversed

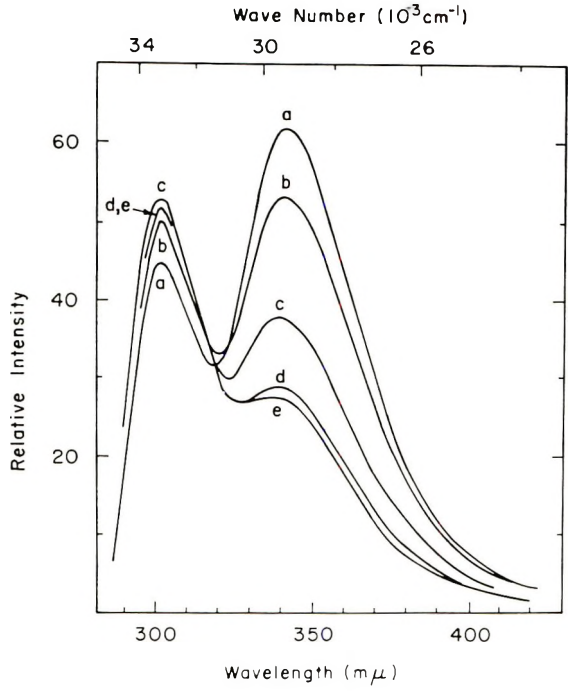

Fig. 7. Fluorescence spectra of the detergent in the solid and liquid states: (*a*) 25°C (*b*) 30°C; (*c*) 35°C; (*d*) 40°C; (*e*) 50 and 60°C. Spectra *b* and *c* were scanned from 275 mμ, 5 min after the temperature reached the specified values upon raising the temperature. Other spectra are for the equilibrium states.

as compared to that at room temperature; the main band is stronger than the excimer band. Further elevation of temperature up to 60°C did not influence the spectra very much. Once heated and melted, the detergent did not immediately recover its original spectrum at room temperature, after being cooled down to a temperature where the detergent solidified. After being kept for a few days at a low temperature, however, the original solid spectrum could be observed.

Cohesive forces of the detergent make favorable the parallel stacking arrangement of the aromatic rings, as the detergent solid is not crystalline but amorphous, and the strong excimer band is observed at 3900 cm^{-1} to the red of the main band. Upon melting, however, thermal motion disrupts some of the stacking of the aromatic rings and prevents the excimer formation, thus leading to the weaker excimer band. This effect of temperature has been generally observed for the excimer band of liquid aromatics.[3,8,9]

DISCUSSION

Changes in absorption properties when a detergent forms micelles had been expected by many workers, and the appearance of visible color of

alkylpyridinium iodide upon micelle formation was investigated spectroscopically by Harkins et al.[14] The spectral determination of CMC was subsequently applied by other workers[15,16] for the detergents of this particular series. The appearance of the new absorption band was attributed to the association effect of detergent cations with iodide upon micelle formation. The present detergent which is nonionic does not give any new absorption band when it forms micelles, but thereupon it shows a hyperchromic effect.

The fluorescence CMC, which may be defined by the concentration above which the excimer emission is observed, is found to be slightly lower than the absorption CMC. If the CMC in the excited state were different from that in the ground state and micelles in the excited state were formed at a concentration lower than the CMC in the ground state, the discrepancy could be readily explained. However, various evidence suggests that the excited state decays before the micelle–monomer re-equilibration takes place, so that the monomer–micelle equilibrium is not influenced by the electronic excitation.

According to the Ladenburg equation, the radiative lifetime of the excited state can be estimated from the intensity of the absorption band. The calculated lifetime is 3.4×10^{-8} sec for monomers in water and is slightly shorter for molecules in the micelle. During this time, an excited fluorophore must encounter another fluorophore to form an excimer. The following data will provide evidence that the excimer must be formed by an encounter of two molecules within a micelle and the micelle formation is not influenced by the light absorption. The rate of monomer–micelle conversion was recently measured by the temperature-jump method for dodecylpyridinium iodide,[17] which gave 5×10^{-2} sec for the half-period for a molecule to leave from a micelle. This is much slower than the fluorescence decay. Although other methods suggested the lifetime of a molecule staying in a micelle is shorter than 10^{-4} sec,[18,19] the lifetime of fluorescence decay would be much shorter than the time for monomer–micelle re-equilibration. The qualitative result derived for these detergents could be safely extended to the present detergent.[20] Thus, the association equilibrium of monomers and micelles will not be influenced by the electronic excitation but remains unaltered. This means that the excimer is formed within a micelle, but not with the interaction of a micelle with another or with a monomer in water.

It is known that small aggregates consisting of a few molecules are formed with some detergents in water, before the concentration reaches the CMC.[21] The formation of a small micelle, e.g., a "dimeric" one, would not influence the absorption properties of the detergent since the environment of each chromophore will not be very different from water. However, the emission properties of the detergent would be affected by the presence of such small micelles, since detergent molecules would be associated into stacked pairs even in a "dimeric" micelle, ready to form excimers. Without postulating the presence of such small micelles, however, the frequency of encounter of

two detergent molecules could be high enough to associate into a dimer in the excited state.

We would like to express our thanks to S. S. Lehrer for his helpful discussions. Publication No. 703 from the Graduate Department of Biochemistry, Brandeis University. Supported in part by research grants from the National Institutes of Health (No. GM-17533-09) and the National Science Foundation (No. GB-8642) and a research contract from the U. S. Army Medical Research and Development Command (No. DA-49-193-MD-2933).

References

1. J. E. W. McBain and E. Hutchinson, *Solubilization*, Academic Press, New York, 1955, Chap. 3.
2. S. Ikeda and K. Kakiuchi, *J. Colloid Interface Sci.*, **23**, 134 (1967).
3. S. S. Lehrer and G. D. Fasman, *J. Amer. Chem. Soc.*, **87**, 4687 (1965).
4. J. M. Corkill, J. F. Goodman, and R. H. Ottewill, *Trans. Faraday Soc.*, **57**, 1627 (1961).
5. K. Kuriyama, *Kolloid-Z. Z. Polym.*, **181**, 144 (1962).
6. M. J. Shick, *J. Phys. Chem.*, **67**, 190 (1963).
7. W. H. Herrmann, *J. Phys. Chem.*, **67**, 1796 (1963).
8. T. V. Iwanova, G. A. Mokeeva, and B. Y. Sveshnikov, *Optics and Spectroscopy*, **12**, 325 (1962).
9. J. B. Birks and J. B. Aladekomo, *Spectrochim. Acta*, **20**, 15 (1964).
10. T. Förster and K. Kasper, *Z. Elektrochem.*, **59**, 977 (1962).
11. E. Döller and T. Förster, *Z. Physik. Chem.*, (Frankfurt), **34**, 132 (1962).
12. J. B. Birks and L. G. Christophorou, *Proc. Roy. Soc.* (London), **A277**, 571 (1964).
13. B. Stephens, *Spectrochim. Acta*, **18**, 439 (1962).
14. W. D. Harkins, H. Krizek, and M. L. Corrins, *J. Colloid Sci.*, **6**, 576 (1951).
15. P. Mukerjee and A. Ray, *J. Phys. Chem.*, **67**, 190 (1963).
16. G. C. Kresheck, H. Schneider, and H. A. Scheraga, *J. Phys. Chem.*, **69**, 3132 (1966).
17. G. C. Kresheck, E. Hamori, G. Davenport, and H. A. Scheraga, *J. Amer. Chem. Soc.*, **88**, 246 (1966).
18. T. Nakagawa and K. Tori, *Kolloid-Z. Z. Polym.*, **194**, 143 (1964).
19. T. Nakagawa and H. Inoue, *Proc. 4th Intern. Congr. Surface Active Substances*, **2**, 569 (1964).
20. M. J. Jaycock and R. H. Ottewill, *Proc. 4th Intern Congr. Surface Active Substances*, preprint B/IV, 8 (1964).
21. P. Mukerjee, K. J. Mysels, and C. I. Dulin, *J. Phys. Chem.*, **62**, 1390 (1958).

Received July 29, 1969
Revised November 5, 1969

JOURNAL OF POLYMER SCIENCE: PART A-1 VOL. 8, 1003–1011 (1970)

Polytriazolines

P. M. HERGENROTHER and L. A. CARLSON,
Polymer Sciences Laboratory, Boeing Scientific Research Laboratories, Seattle, Washington 98124

Synopsis

Soluble polytriazolines of relatively high molecular weight ($\eta_{inh} \sim 0.6$ dl/g) have been prepared by the solution polymerization of 2,6-pyridinediyl dihydrazidine with three different aromatic dialdehydes. Thermogravimetric analysis of the polytriazolines showed weight losses in air and in nitrogen commencing at 280°C and 400°C, respectively. Several attempts to convert triazoline model compounds to the corresponding 1,2,4-triazoles and quantitatively to prepare methyl-substituted triazoline model compounds were unsuccessful.

INTRODUCTION

The versatility of dihydrazidines (diamidrazones) in polymer synthesis has been under investigation in our laboratories and elsewhere.[1–3] Our initial work concerned the preparation of soluble high molecular weight poly-*as*-triazines[4] and the synthesis of a high molecular weight precursor polymer, a poly-*N*-acylhydrazidine, which was preferentially cyclized to poly-1,2,4-triazole and/or poly-1,3,4-oxadiazole.[5] In this communication, preliminary work on the synthesis of poly([2,3-H]-1,2,4-triazolines) from the reaction of 2,6-pyridinediyl dihydrazidine with aromatic dialdehydes as shown in eq. (1) is presented.

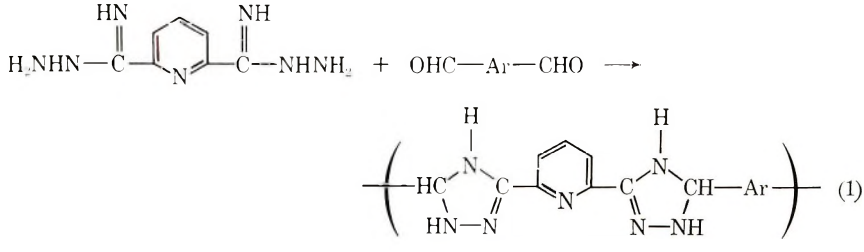

(1)

Polymer I, Ar = *m*-phenylene
Polymer II, Ar = *p*-phenylene
Polymer III, Ar = *p,p'*-oxydiphenylene

EXPERIMENTAL

Reactants

2-Pyridyl hydrazidine was prepared for model compound work by a known procedure[6] as white needles, mp 95–96°C (lit.[6] mp 95–96°C).

TABLE I
Characterization of Model Compounds

Model compound	Mp, °C	Crude yield, %	Formula	Elemental Analysis[a] C, %	H, %	N, %	Ultraviolet spectrum[b] λ_{max}, mμ	ε
3-Phenyl-5-(2-pyridyl)[2,3-H]-1,2,4-triazoline (I)	103.5–104.5	99	$C_{13}H_{12}N_4$	69.50 (69.62)	5.34 (5.39)	24.86 (24.98)	264 302	8,200 19,100
3,3′-(*m*-Phenylene)bis{5-(2-pyridyl)[2,3-H]-1,2,4-triazoline} (II)	145–146	97	$C_{20}H_{18}N_8$	64.78 (64.85)	4.96 (4.90)	30.46 (30.25)	258 290	29,900 18,100
5,5′-(2,6-Pyridinediyl)bis{3-phenyl-[2,3-H]-1,2,4-triazoline} (III)	186–187	97	$C_{21}H_{19}N_9$	68.37 (68.27)	5.01 (5.18)	26.58 (26.55)	240 306	14,700 42,100
3,3′-(*p*-Phenylene)bis{5-(2-pyridyl)-[2,3-H]-1,2,4-triazoline} (IV)	248–250	98	$C_{20}H_{18}N_8$	64.93 (64.85)	4.87 (4.90)	30.37 (30.25)	264 303 350	22,500 12,200 24,000
p,*p*′-Oxybis{3-(*p*-phenylene)-5-(2-pyridyl)[2,3-H]-1,2,4-triazoline} (V)	187.5–188.5	95	$C_{26}H_{22}N_8O$	67.76 (67.52)	4.73 (4.79)	24.50 (24.23)	263 366	25,500 49,500
3-Methyl-3-phenyl-5-(2-pyridyl)-[2-H]-1,2,4-triazoline (VI)	64.5–66	87	$C_{14}H_{14}N_4$	70.78 (70.57)	5.94 (5.92)	23.36 (23.51)	—	—
3,3′-(2,6-Pyridinediyl)bis {3-methyl-5-(2-pyridyl) [2-H]-1,2,4-triazoline} (VII)	189–190	65	$C_{21}H_{21}N_9$	63.36 (63.14)	5.36 (5.30)	31.70 (31.56)	—	—
Bis {3-(*p*-Phenylene)-3-methyl-5-(2-pyridyl) [2-H]-1,2,4-triazoline} (VIII)	241–243	81	$C_{28}H_{26}N_8$	70.52 (70.87)	5.57 (5.52)	23.29 (23.61)	—	—

[a] Theoretical values reported in parentheses.
[b] Measured in sulfuric acid.

2,6-Pyridinediyl dihydrazidine was obtained as pale yellow needles, mp 230–231°C (dec), by the same method as previously described.[4]

Oxybis(4-benzaldehyde) was synthesized via the Sommelet reaction starting with *p,p'*-bis(chloromethyl)diphenyl ether and hexamethylenetetramine to provide a pale green solid (65% yield), mp 63–65°C. Recrystallization from a mixture of *n*-hexane and benzene gave white plates, mp 65–66°C (lit.[7] mp 65–66°C).

p,p'-Diacetylbiphenyl was prepared by the Friedel-Crafts acetylation of biphenyl. Pale yellow platelets, mp 189–190°C (lit.[8] mp 190–191°C), were obtained after recrystallization from chloroform.

All other aromatic reactants were obtained commercially and purified in the appropriate manner by distillation or recrystallization. All solvents were reagent grade quality and used without further purification.

Model Compounds

Prior to polymer synthesis, a series of triazoline model compounds (I–V) as shown in Table I were prepared in quantitative yields by refluxing stoichiometric quantities of the two reactants in ethanol. The following procedure is representative of model compound preparation. Isophthalaldehyde (1.34 g, 0.01 mole) was added to a solution of 2-pyridyl hydrazidine (2.72 g, 0.02 mole) in ethanol (75 ml) at ambient temperature. The resulting yellow solution was heated at 78°C for 0.5 hr, followed by pouring onto ice to yield a pale yellow solid (3.65 g, 99% yield), mp 143–145°C. Recrystallization from a mixture of methanol (100 ml) and water (20 ml) gave yellow crystals (3.1 g, 85% recovery) of 3,3'-(*m*-phenylene) bis{5(2-pyridyl)[2,3-H]-1,2,4-triazoline} (II, Table I). The infrared spectrum as a Nujol mull is shown in Figure 1.

Methyl-substituted triazoline model compounds (VI–VIII) were prepared by the following representative procedure. A solution of 2-pyridyl hydrazidine (2.76 g, 0.02 mole) and acetophenone (2.40 g, 0.02 mole) in ethanol (60 ml) containing a catalytic amount of hydrogen chloride was refluxed for 18 hr. The resulting yellow solution was poured onto ice to

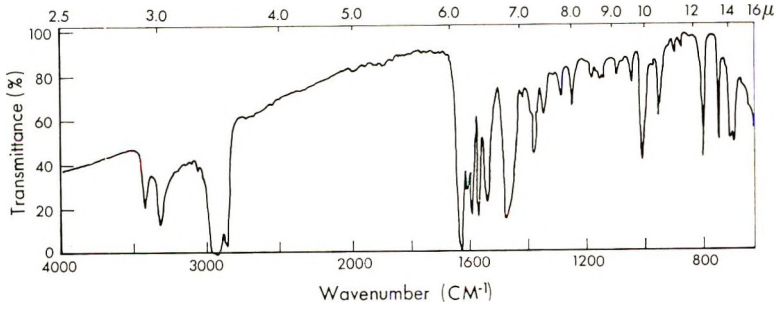

Fig. 1. Infrared spectrum (Nujol mull) of 3,3'-(*m*-phenylene)bis-[5-(2-pyridyl)-[2,3-H]-1,2,4-triazoline] (model compound II).

yield a yellow solid (2.1 g, 87% yield), mp 63–65.5°C. Recrystallization from *n*-hexane (80 ml) gave pale yellow plates (1.7 g, 81% recovery) of 3-methyl-3-phenyl-5-(2-pyridyl)[2-H]-1,2,4-triazoline (VI, Table I).

The preparation of 2-methylbenzimidazoline was attempted following a reported procedure.[9] A mixture of *o*-phenylenediamine (2.16 g, 0.02 mole) and acetophenone (2.40 g, 0.02 mole) in a polymerization tube under nitrogen was heated at 180°C for 18 hr. The dark reaction mixture was washed with diethyl ether to give a residual tan solid (0.62 g), mp 99–101°C. Partial concentration of the ether wash followed by dilution with *n*-hexane provided additional tan solid (0.71 g), mp 98–101°C. Mixed melting point with pure *o*-phenylenediamine was 98–101°C. The total recovery (1.33 g) of unreacted *o*-phenylenediamine was 62%. The reaction of 3,3′-diaminobenzidine with acetophenone at 180°C for 18 hr gave a 23% recovery of unreacted tetraamine.

Polymers

The polycondensations of 2,6-pyridinediyl dihydrazidine with aromatic dialdehydes were conducted by melt and solution methods. Melt condensation was performed in the following representative manner. A test tube containing an intimate mixture of 2,6-pyridinediyl dihydrazidine (1.932 g, 0.010 mole) and isophthalaldehyde (1.341 g, 0.010 mole) under an argon atmosphere was introduced into a preheated oil bath at 200°C. A partial yellow melt immediately formed with the evolution of volatiles. The temperature of the oil bath was raised to 250°C during 0.5 hr and maintained at 250°C for 1 hr. The resulting orange-brown product swelled but failed to dissolve completely in concentrated sulfuric acid. The infrared spectrum exhibited absorption of weak intensity at 4.45 μ (nitrile region) and at 5.9 μ (carbonyl region).

Solution polymerization was conducted in solvents such as *N*,*N*-dimethylacetamide, dimethyl sulfoxide, or *m*-cresol in the following manner. Isophthalaldehyde (1.341, 0.010 mole) was added to a solution of 2,6-pyridinediyl dihydrazidine (1.932 g, 0.010 mole) in *m*-cresol (28.5 ml) at 10°C. The yellow reaction mixture was stirred to ambient temperature during 0.5 hr to form a clear, slightly viscous, solution. Upon heating the solution to 100°C and maintaining at 100°C for 1 hr, a viscous colloidal solution formed. At 10% solids content, the colloidal solution failed to become clear even upon heating to 200°C. However, a clear yellow solution formed when the colloidal solution was diluted to ~3% solids content and heated.

The polymer was isolated from the viscous colloidal solution which had been heated to 100°C by dilution with methanol to provide a quantitative yield (2.9 g) of poly{3,3′-(*m*-phenylene)-5,5′-(2,6-pyridinediyl)di([2,3-H]-1,2,4-triazoline)} (polymer I) as a yellow solid. Characterization of the polymers prepared in this manner is presented in Table II.

TABLE II
Characterization of Polymers

Polymer	η_{inh}, dl/g[a]	Polymer softening temperature PST, °C[b]	Formula	Elemental analysis[c]			Ultraviolet spectrum[d]	
				C, %	H, %	N, %	λ_{max}, mμ	ε
I	0.51	280	$(C_{15}H_{13}N_7)_n$	61.73	4.60	33.29	240	32,000
				(61.83)	(4.51)	(33.66)	281	19,500
II	0.58	303	$(C_{15}H_{18}N_7)_n$	61.64	4.54	33.17	—	—
				(61.83)	(4.51)	(33.66)		
III	0.61	265	$(C_{21}H_{17}N_7O)_n$	65.29	4.58	25.13	—	—
				(65.78)	(4.47)	(25.58)		

[a] 0.5% dimethylsulfoxide, 25°C.
[b] Becomes transparent with little flow.
[c] Theoretical values reported in parentheses.
[d] Measured in sulfuric acid.

DISCUSSION

Prior to polymer synthesis, five triazoline model compounds were prepared to demonstrate the feasibility of this reaction for polymer formation and to obtain model compounds for use in polymer identification. As indicated in the experimental section, a number of model compounds (I–V) were prepared in quantitative yields by the solution cyclocondensation of hydrazidines with various aromatic aldehydes. Melt condensation of hydrazidines with aromatic aldehydes failed to provide quantitative yields of the desired model compounds. Representative model compound formation is shown in eq. (2).

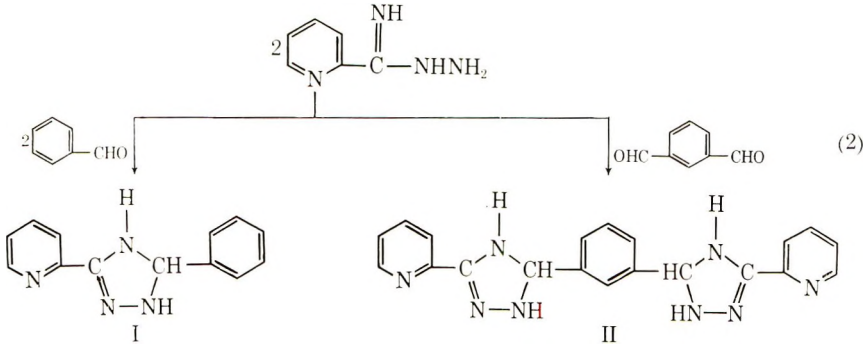

(2)

Polytriazolines of relatively high molecular weight ($\eta_{inh} \sim 0.6$ dl/g) were prepared by solution polymerization, whereas melt condensation failed to provide soluble polymers of high molecular weight. In the melt polymerization, problems were encountered in obtaining a homogeneous reaction medium which would permit the formation of a relatively high molecular weight polymer prior to becoming intractable. In an attempt to force the reaction to completion at higher temperature (250°C), partial decomposition occurred as indicated by an absorption at 4.45 μ(—C≡N) in the infrared spectrum of the product.

The polymers prepared by solution polymerization exhibited very limited solubility (~1%) at room temperature in solvents such as *m*-cresol, *N*,*N*-dimethylacetamide, or dimethyl sulfoxide. Tough, transparent, yellow films which exhibited good flexibility (finger-nail creaseable) were cast from formic or trifluoroacetic acid solutions. In addition, transparent yellow films of polymers I and III could be melt-pressed by sandwiching the yellow solids (isolated by quenching the viscous colloidal solution with methanol) between press platens preheated to 275°C under 200 psi for a few minutes.

It was thought that the polytriazolines could be converted to the more thermally stable triazole polymers by dehydrogenation. However, several attempts to convert model compounds I and II to the corresponding 1,2,4-triazoles as indicated in representative eq. (3)

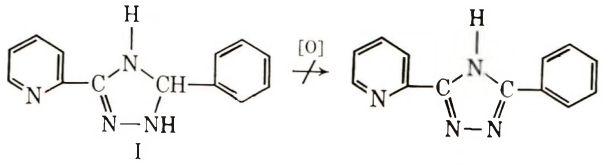

(3)

by treatment under various reaction conditions with sulfur, chloranil, ferric chloride, or dimethyl sulfoxide failed. In all cases where the starting model compound was not quantitatively recovered, partial oxidation had occurred as evidenced by the formation of dark blue to purple product. These materials were difficult to purify and characterize and such an effort was beyond the scope of this work.

In addition, the preparation of methyl substituted triazoline polymers from the reaction of 2,6-pyridinediyl dihydrazidine with aromatic diacetyl compounds such as *p*-diacetylbenzene or 2,6-diacetylpyridine was not attempted due to the results of model compound work. Quantitative yields of methyl substituted triazoline model compounds were not obtained even though reaction conditions were varied and solvents such as trifluoroacetic acid or *m*-cresol and catalysts such as *p*-toluenesulfonic acid or aluminum chloride were employed. This was surprising since the formation of relatively high molecular weight (η_{inh} = 0.6 dl/g) poly[2,2′-(*p*-phenylene)-5,5′-bibenzimidazole] from the reaction of 3,3′-diaminobenzidine with *p*-diacetylbenzene followed by the thermal elimination of methane from the precursor polymer has been described.[9] It was thought that the hydrazino portion of the hydrazidine would be more nucleophilic than an aromatic *o*-diamine and accordingly provide a higher yield of product when reacted with an aromatic acetyl compound such as acetophenone. This prompted a brief reinvestigation of the reaction of aromatic *o*-diamines with aromatic acetyl compounds. In our work, we were unable to obtain quantitative yields of benzimidazoline model compounds from the reaction of *o*-phenylenediamine or 3,3′-diaminobenzidine with acetophenone at 180°C as inferred in the literature.[9] In fact, a relatively high percentage (>20%) of unreacted amine was recovered in all attempts.

Thermal Stability

The thermal stability of the polytriazolines was determined by thermogravimetric analysis (TGA) using a Dupont 950 thermogravimetric analyzer. As anticipated for polymers with an incomplete aromatic structure, the triazoline polymers exhibited initial weight losses in air commencing about 280°C while in nitrogen, initial weight losses started about 400°C. The TGA curve for a typical polytriazoline (polymer I) is shown in Figure 2. Further evidence for the low thermal stability of triazoline polymers was indicated when the yellow polymers, isolated by diluting the colloidal solutions with methanol, were heated to 300°C under an argon atmosphere. The yellow solids, sintered, partially fused, and turned an orange color. Partial decomposition occurred as evidenced by weight losses (<10%)

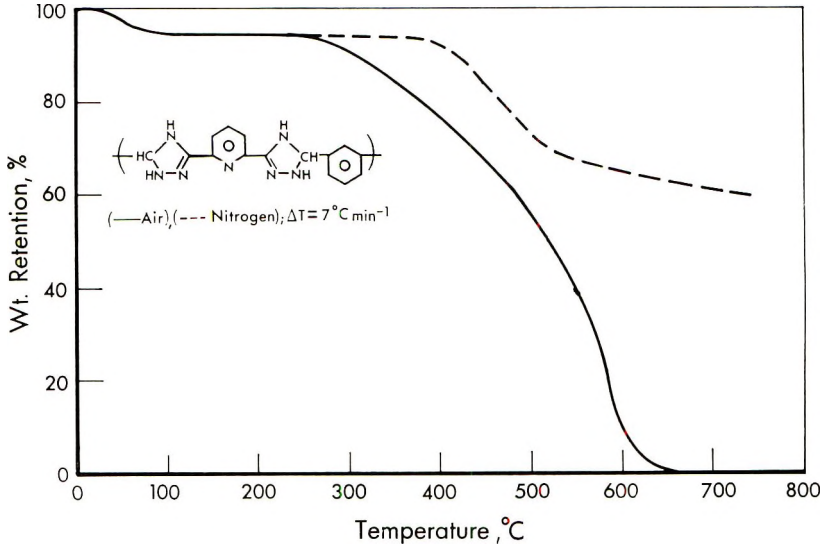

Fig. 2. Thermogravimetric analysis of polytriazoline (polymer I).

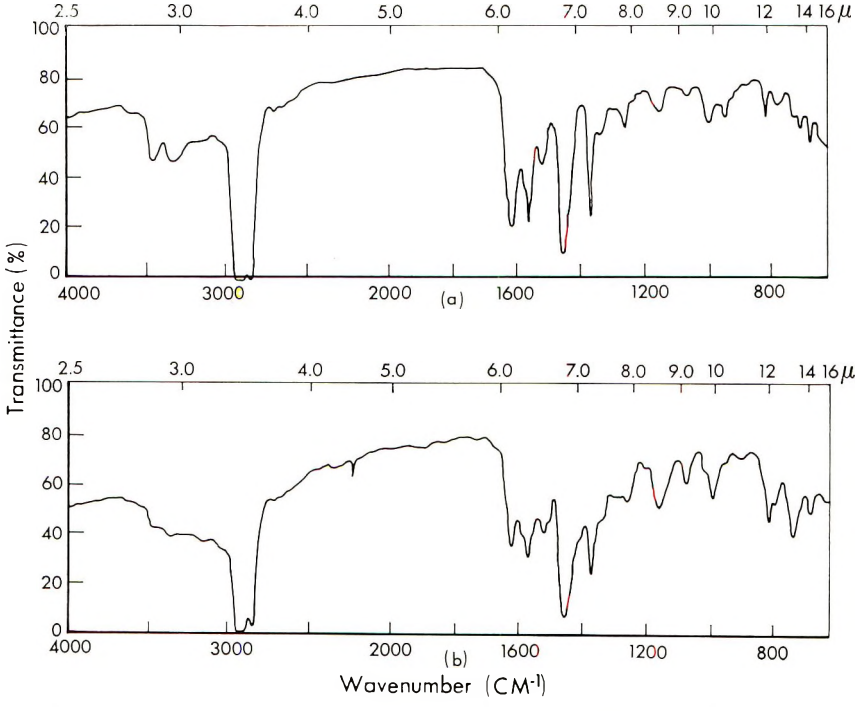

Fig. 3. Infrared spectra (nujol mulls) of poly [3,3′-(*m*-phenylene)-5,5′-(2,6-pyridinediyl) di([2,3-H]-1,2,4-triazoline)] (polymer I): (*a*) as isolated from solution; (*b*) after heating to 300°C (argon).

and the infrared spectra which showed several changes, one of which was the appearance of an absorption at 4.45 μ characteristic of —C≡N. The infrared spectra of polymer I before and after exposure to 300°C are shown in Figure 3.

References

1. M. Saga and T. Shono, *J. Polym. Sci. B*, **4**, 869 (1966).
2. V. V. Korshak, Ye S. Kronganz, and A. L. Rusanov, *Akad Nauk-SSSR Izv. Ser. Khim.* **1968**, 2663; *Chem. Abstr.*, **70**, 48415d (1969).
3. V. V. Korshak and A. L. Rusanov, *Akad. Nauk SSSR Izv. Ser. Khim.* **1968**, 2661; *Chem. Abstr.*, **70**, 78423e (1969).
4. P. M. Hergenrother, *J. Polym. Sci. A-1*, **7**, 945 (1968).
5. P. M. Hergenrother, *Macromolecules*, in press; *Polym. Reprints*, **10**, No. 2, 772 (1969).
6. F. H. Case, *J. Org. Chem.*, **30**, 931 (1965).
7. E. Gustak and A. Markovac-Prpic, *Archiv. Kam.*, **27**, 125 (1955); *Chem. Abstr.*, **50**, 10649g (1956).
8. C. V. Ferriss and E. E. Turner, *J. Chem. Soc.*, **1920**, 117, 1147.
9. D. N. Gray, L. L. Rouch, and E. L. Strauss, *Macromolecules*, **1**, 473 (1968).

Received September 10, 1969
Revised December 24, 1969

NOTES

A Comment on the Kinetics in a Heterogeneous Polymerization System

Studies on the catalytic polymerization have been furthered by recent advances in experimental techniques, and reasonable interpretations of the kinetics have been made (e.g., Kagiya et al.[1]), at least for polymerizations carried out in homogeneous systems. However, such kinetic treatments of homogeneous polymerization are not applicable to the polymerizations in a heterogeneous system where precipitation of the polymers takes place. For instance, Higashimura et al.[2] found that in the cationic polymerization of trioxane in nitrobenzene catalyzed by boron trifluoride etherate, the rate of polymerization was proportional to the second power of the residual monomer concentration when initial concentration of the monomer was high. Further, they pointed out that the initiation reaction, where the active species is considered to be $C_2H_5^+ \cdot (BF_3OC_2H_5)^-$, was complete at a very early stage of polymerization (occasionally after an induction period). These facts cannot be accounted for by the kinetic theory for a homogeneous system. The same authors[3] explained these peculiar phenomena in terms of the change in the dielectric constant of the system due to consumption of the monomer. However the reason seems to remain unsettled for the second power law found experimentally.

In this type of polymerization the fact that the resultant polymer precipitates in the homogeneous phase would be important, because the occlusion of the reactive chain end (or the loss of mobility of the growing chain) may well hinder the addition of the monomer molecules even if the resultant chain is "living" chemically. In fact such monomolecular termination was proposed for some polymerization reactions.[4]

In the kinetic studies of crystallization, the Avrami equation is widely used to account for the effect of the impingement of the growing crystallites. It is generally written[5] as

$$dX/dX' = 1 - (X/A) \tag{1}$$

where A is the fraction of the transformable mass in the system, X is the fraction actually transformed by the time t, and X' is the imaginary fraction transformed without any impingement of the crystallites. If the occlusion of the reactive chain end, i.e., physical termination, takes place just as the growth of the crystallites is interrupted by their mutual impingement, the application of the Avrami's equation to the polymerization kinetics will be useful. In this short note the kinetics of polymerization in a heterogeneous system will be examined along this line of argument.

Now let us assume a monomolecular reaction for the addition of monomer in a polymerizing system. The rate of the propagation of a chain is described by

$$dx_s^{\mathrm{L}}/dt = k(a - x) \tag{2}$$

for the living chain consisting of x_s^{L} monomer units and

$$dx_s^{\mathrm{D}}/dt = 0 \tag{3}$$

for the dead chain of x_s^{D} units, where a is the initial concentration of the monomer, $x = \Sigma x_s$, the total conversion at the time t, and k is the rate constant of the addition.

Further, the following points will be taken into account for the polymerization. At the beginning of the polymerization, the system is a homogeneous liquid of the solvent, the monomer, and a small amount of catalyst. The concentration of the last will be denoted by c_0. The activation of the catalyst takes place very rapidly, and the propaga-

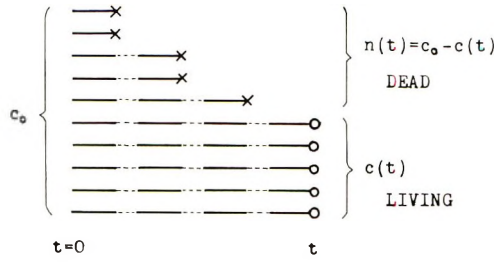

Fig. 1. Schematic illustration of the polymerization, in which all the initiation reactions takes place simultaneously at $t = 0$, followed by successive addition of the monomer; the number of reactive chain ends decreases with time due to the occlusion into the precipitate.

tion of all the chains commences simultaneously at the time $t = 0$. Neither transfer nor termination occurs chemically. However, the precipitation of the resultant polymer, which begins immediately after the initiation reaction, results in "physical" termination, i.e., occlusion of the growing chain ends. Thus the number of the dead chains $n(t)$ increases, and accordingly that of the living chains $c(t)$ decreases as the polymerization time t increases. This sort of reaction is illustrated schematically in Figure 1.

Under these conditions the apparent rate of polymerization is written by;

$$dx/dt = kc(t)(a - x) \tag{4}$$

In the case of the polymerization accompanying the precipitation of the resultant polymer, the phase change is considered a one-dimensional transformation of the growing units. In other words, the chain grows linearly during the polymerization and after the precipitation the polymer formed occupies a space which is approximately proportional to the mass of the polymer. This situation just corresponds to the one-dimensional growth of crystals, i.e., the growth of needlelike crystals. Therefore the Avrami equation, eq. (1), can be modified by using c_0 and $c(t)$ instead of dX'/dt and dX/dt, respectively.

$$c(t) = c_0[1 - (x/a)] \tag{5}$$

Thus, from eqs. (4) and (5), we obtain the expression (6) for the rate of polymerization:

$$dx/dt = kc_0a[1 - (x/a)]^2 \tag{6}$$

It can thus be derived that the rate of polymerization is proportional to the square of the residual monomer concentration. Equation (6) gives

$$a/(a - x) = kc_0t + 1 \tag{7}$$

or

$$x = a\{1 - [1/(kc_0t + 1)]\} \tag{7'}$$

Therefore, the time–conversion relationship should be similar to the usual second-order reactions.

We can also calculate the changes in the average molecular weights and the molecular weight distribution in the course of the polymerization.

The degree of polymerization of the chains which are "living" at time t or just occluded at time t, P^*, is equal to x_s^L for all of the $c(t)$ molecules. Integration of eq. (2) leads to;

$$P^* = \int (dx_s^L/dt)dt = (a/c_0) \ln (kc_0t + 1) \tag{8}$$

or

$$= (a/c_0) \ln [a/(a - x)] \tag{8'}$$

The sum of the chains which are already terminated by time t,

$$n(t) = c_0 - c(t)$$

may be written as a function of P^*

$$n = c_0(1 - e^{-(c_0/a)P^*}) \tag{9}$$

by using eqs. (5) and (8). Differentiation of eq. (9) leads to the increase dn in the number of chains whose ends are occluded when the polymer grows from the degree of polymerization P to $P + dP$;

$$dn = \frac{c_0^2}{a} e^{-(c_0/a)P} dP \tag{10}$$

Thus one can calculate the number-average molecular weight of the polymer which will be obtained by interrupting the polymerization at the time t, where the maximum molecular weight attained is P^*, as follows:

$$M_n = \frac{\int_0^{P^*} (mP)dn + mP^*c(t)}{n(t) + c(t)}$$

$$= (ma/c_0)(1 - e^{-(c_0/a)P^*}) \equiv mx/c_0 \tag{11}$$

where m is the molecular weight of the monomer unit. As can be seen, the number-average molecular weight is nothing but the ratio of the total mass polymerized to the concentration of the initial active site, the latter being the number of the chains included in the system. The total mass involves the mass of the living chains $mP^*c(t)$ and that of the dead chains (due to the occlusion) $\int_0^{P^*} (mP)dn$. Similarly the weight-average molecular weight may be written;

$$\bar{M}_w = \frac{\int_0^{P^*} (mP)^2 dn + (mP^*)^2 c(t)}{\int_0^{P^*} (mP)dn + mP^*c(t)}$$

$$= \frac{2m[(a/c_0)(1 - e^{-(c_0/a)P^*}) - P^*e^{-(c_0/a)P^*}]}{1 - e^{-(c_0/a)P^*}}$$

$$\equiv (2am/c_0)\{1 - \ln[a/(a - x)]^{(a-x)/x}\} \tag{12}$$

The weight-average molecular weight, when plotted against the conversion, deviates gradually from the number-average molecular weight and is twice the latter at 100% conversion (see Fig. 6).

As mentioned just before, the weights of the living and the dead polymer at any stage of the polymerization, W_L and W_D, respectively, are written:

$$W_L = mP^*c(t) = mc_0P^*e^{-(c_0/a)P^*} \tag{13}$$

$$W_D = \int_0^{P^*} (mP)dn = ma\{1 - [1 + (c_0/a)P^*]e^{-(c_0/a)P^*}\} \tag{14}$$

In Figure 2, the two quantities given by these equations, together with the total mass, are shown as a function of P^*. The mass of the dead fraction increases monotonously and finally coincides with the total mass, whereas the living fraction increases at first and then decreases as polymerization proceeds, having a maximum at $P^* = a/c_0$, and at

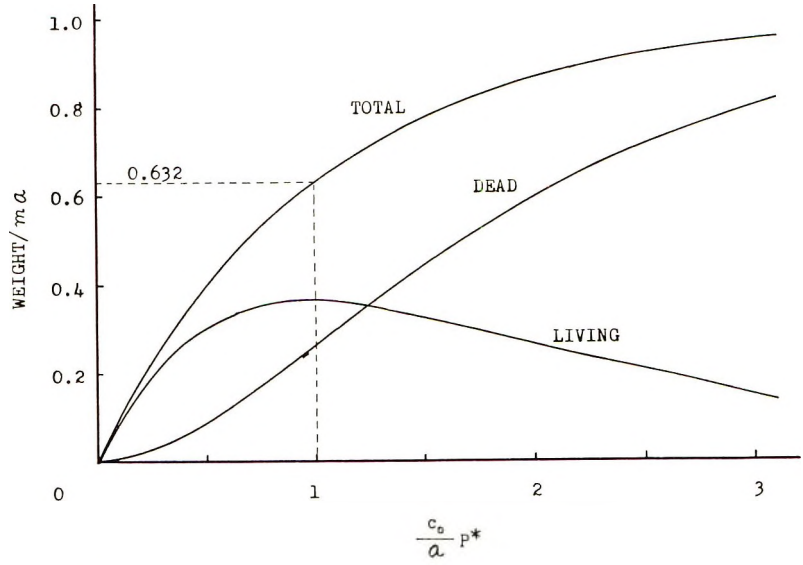

Fig. 2. Changes in the weight fractions of the living and the dead polymers as a function of the molecular weight of the living chain [calculated from eqs. (13) and (14), respectively]. The total of the two weight fractions is also shown.

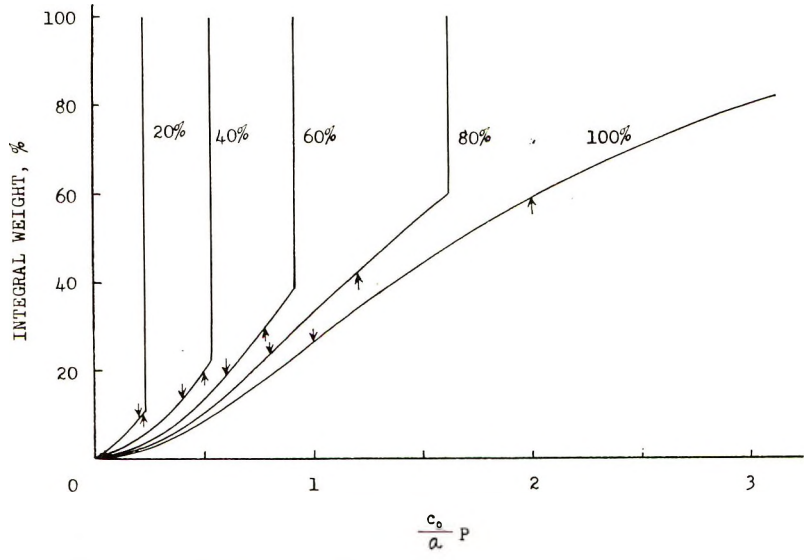

Fig. 3. Theoretical (integral weight) distribution curve for the polymers obtained by interrupting the polymerization at various conversions. The downward and upward arrows indicate the positions of the number-average and the weight-average molecular weights, respectively.

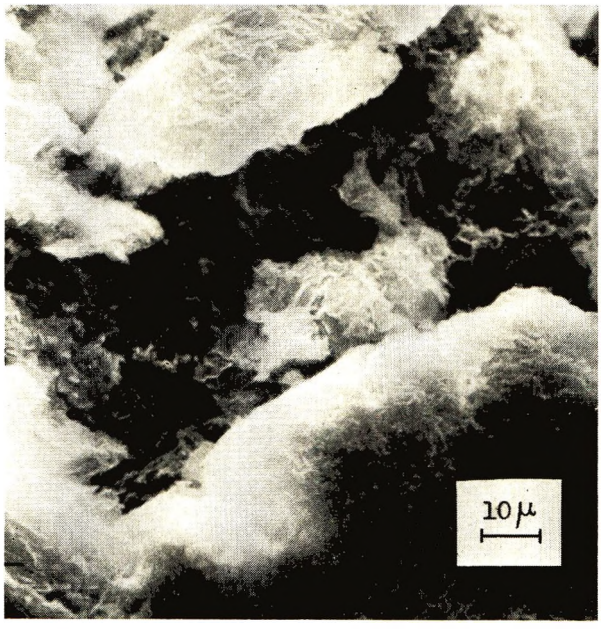

Fig. 4. Scanning-type electron micrograph of the crystalline aggregate of polyoxymethylene formed by the polymerization of trioxane in nitrobenzene.

63.2% conversion, irrespective of the various constants used in the above equations. From the curves in Figure 2, one can estimate the weight distribution of the polymers which will be obtained by interrupting the polymerization at various conversions. Figure 3 shows the integral weight distributions for five conversions, 20, 40, 60, 80, and 100%. The arrows pointing downwards and upwards in the figure indicate the positions of the number-average and weight-average molecular weights respectively.

We have repeated the experiment of Higashimura et al.[2] Our experimental conditions were: monomer, 3.3 mole/l.; catalyst, 1×10^{-3} mole/l.; temperature, 10°C. The reproducibility was good. The polymerization system became turbid on addition of the catalyst. After an induction period of a few minutes, the turbidity increased suddenly due to the precipitation induced by the polymerization, and finally the whole system apparently solidified. The precipitates observed with the use of optical and electron microscopes were made. In the very early stage of the polymerization, lamellar crystals of a size of the order of microns were suspended in the solution. However, soon after the induction period, random crystalline aggregates of the type shown in Figure 4 grew. In these stages the growing chain ends might have been buried in the crystalline aggregate so that propagation could not continue. The time–conversion plot obtained, as shown in Figure 5, is in very good agreement with the theoretical curve [eq. (7′)], for $kc_0 = 0.315$ and an induction time of 4 min. In fact, this polymerization is apparently a second-order reaction as was pointed out by Higashimura et al.[2] These authors discussed merely the relation between the relative viscosity of the polymer (at a given concentration) and the conversion. The average molecular weight was thus estimated from the intrinsic viscosity (measured in *p*-chlorophenol containing 2% α-pinene at 60°C) by using the equation of Kakiuchi et al.;[5]

$$[\eta] = 5.43\bar{M}_n^{0.66} \tag{15}$$

Average molecular weight is plotted against the conversion in Figure 6 in comparison with that obtained from the relative viscosity, measured by Higashimura et al.[2] under

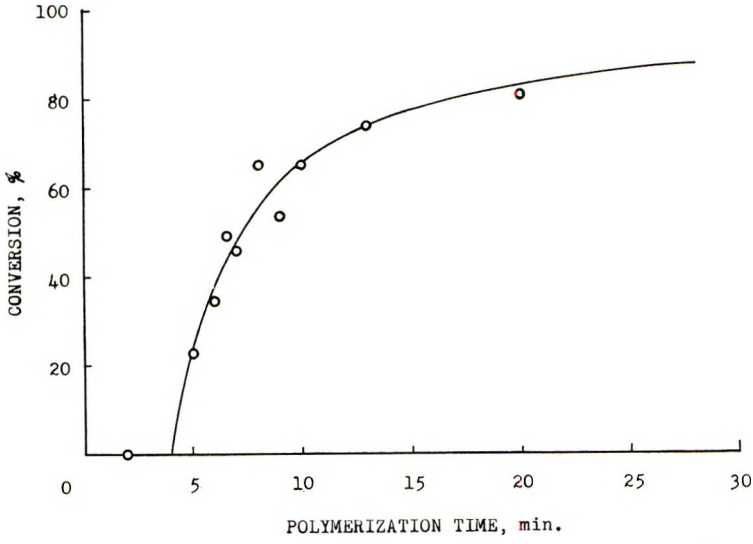

Fig. 5. Time–conversion plot for the polymerization of trioxane in nitrobenzene. Monomer, 3.3 mole/l.; catalyst, 1×10^{-3} mole/l.; temperature, 10°C. The curve is drawn by eq. (7′) for $kc_0 = 0.315$, induction time = 4 min.

the same conditions, assuming Huggins' constant $k' = 0.31$. In this figure are also included the corresponding curves calculated by eqs. (11) and (12) (for $C_0 = 1 \times 10^{-3}$ mole/l.). As can be seen, both types of plots lie approximately on a straight line and near the calulated M_n–conversion curve. Thus it may be said that the effectiveness of the catalyst was nearly 100% in this type of polymerization; i.e., no transfer reaction took place and the polymer chains propagated successively until they occluded.

As another example, the theory developed here will be applied to kinetic data obtained by Dimonie et al.[7] on the polymerization of epichlorohydrin. They carried out the polymerization in toluene at 30°C with triethylaluminum–water as catalyst and measured the rate of the polymerization by means of dilatometry. In this polymerization, the formation of the reactive sites is very fast and it is rather unlikely that new initiation or chain transfer reaction may occur during the subsequent propagation (at least when equimolar catalyst is used). Thus gellike polymers were obtained. Dimonie et al. analyzed their kinetic data on the following assumptions. Firstly there exist two types of reactive sites; one is stable throughout the polymerization; the other is unstable, so that their number diminishes as the polymerization proceeds. Secondly the addition of the monomer is a first-order reaction but the rate of the addition is different for the two kinds of the reactive sites. The kinetic data could be interpreted reasonably, but there is no direct evidence that these assumptions are valid.

In Figure 7 the reciprocal of the residual monomer fraction is plotted against the polymerization time for three different monomer concentrations. These plots were obtained from the data of Dimonie et al. (Fig. 6 in their paper[7]). As can be seen, a good linearity is obtained between the two quantities, which implies that the time–conversion relationship can be approximated by eq. (7). We have no information on the precipitation occurring in the course of the polymerization except the statement of that the polymer obtained was gellike in appearance ("had an aspect of gel"). In our experiment on the polymerization of epichlorohydrin in bulk with ferric chloride–propylene oxide as the catalyst, however, the resultant polymer was found to be a suspension of very fine precipitates of the polymer. In fact it was confirmed that the resultant polymer was insoluble in toluene and/or epichlorohydrin diluted with toluene. Therefore the poly-

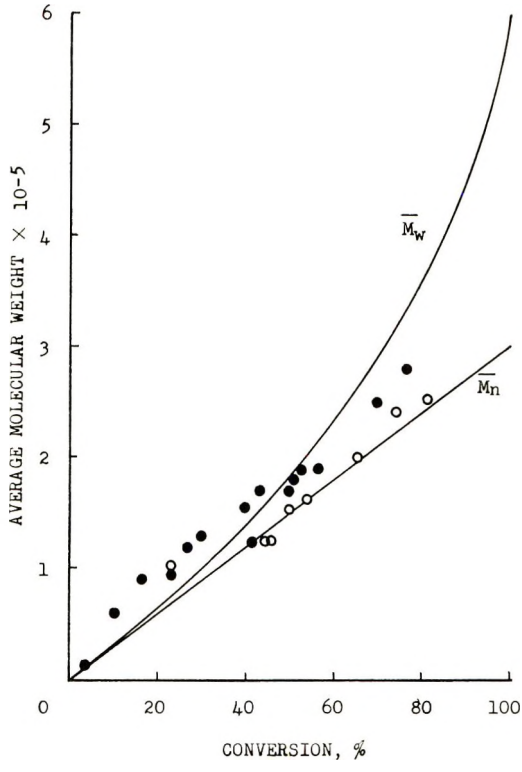

Fig. 6. Plot of the average molecular weights of the nascent polyoxymethylene against the conversion: (○) from the intrinsic viscosity, present experiment, (●) from the specific viscosity, data of Higashimura et al.[2] assuming a Huggins' constant of 0.31. The lower curve shown is the calculated $\overline{M}_n$–conversion relation; and the upper is the calculated $\overline{M}_w$–conversion relation.

merization mechanisms may be considered as follows: propagation of the chain takes place by "living" polymers, but the number of growing chains is decreased by the Avrami-type occlusion of the reactive ends into the precipitate.

The initial rate of the polymerization, i.e., the number of initial reactive sites multiplied by the addition constant, kc_0, obtained from the slope of the lines in Figure 6, is not proportional to the amount of the catalyst used, in contrast with the result of Dimonie et al.[7] However, this may not be unreasonable, because in this polymerization the catalyst is so ineffective (of the order of 10^{-2}–10^{-3}) that the quantitative discussion on the effect of its concentration is very difficult.

In this connection, the polymerization kinetics of *p*-xylylene, reported by Errede et al.[8] seems worth reconsidering. The essential points reported are as follows. The polymerization was carried out in toluene isothermally at −78°C. Initiation was caused by free radicals which were initially present in the monomer solution and no new site for the polymerization was created thereafter. Termination did not occur at this low temperature by chain-transfer reactions. Thus the propagation continued by successive addition of the monomer until the molecular weight of the linear chains reached values in excess of 2×10^6. Precipitation of the polymer was observed when the degree of polymerization exceeded about 20. The change of residual monomer concentration in the course of the polymerization was determined by a titration method.

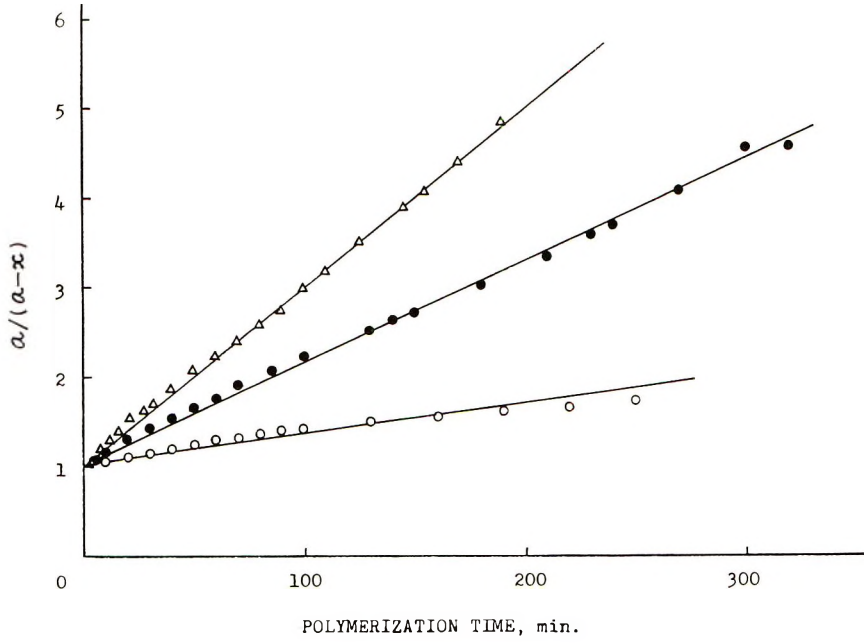

Fig. 7. Plot of the ratio of the initial monomer concentration to the residual monomer concentration against the time, for the polymerization of epichlorohydrin in toluene (data of Dimonie et al.[7]): and various catalyst concentrations: (△) 6 × 10^{-2} mole/l.; (●) 4.1 × 10^{-2} mole/l.; (○) 2 × 10 mole/l. Monomer concentration, 2 mole/l.

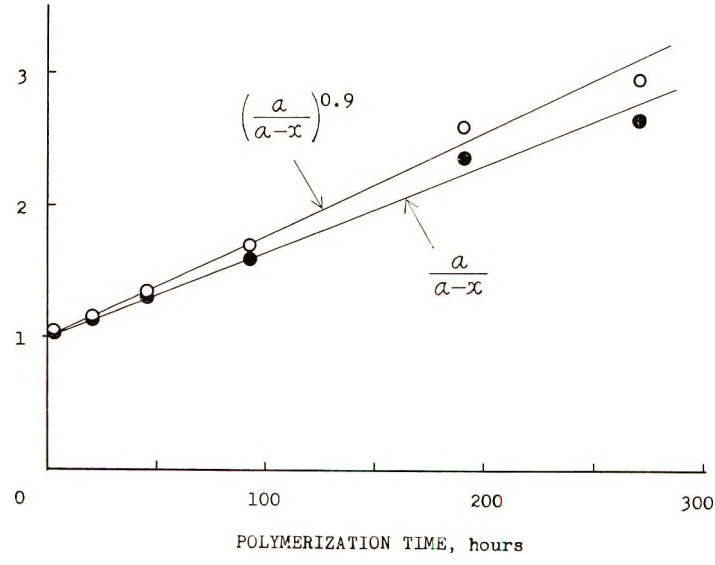

Fig. 8. Comparison of plots of (○) $[a/(a-x)]^{0.9}$ versus time and (●) $a/(a-x)$ versus time, for the polymerization of *p*-xylylene at −78°C. Data of Errede et al.[8]

In the first stage of the polymerization, which covers 10 hr, the number of sites for polymerization did not decrease appreciably, i.e., the polymerization was a first-order reaction with respect to the monomer concentration. When the polymerization proceeded further, however, deviation from first-order kinetic was found; the kinetics were described by eq. (16):

$$\left[\frac{a}{(a-x)}\right]^{2k/K} = 1 + 2Kc_0t \tag{16}$$

where K is a rate constant for the coupling between one insoluble free radical endgroup and another, which was considered to occur, despite the heterogeneous character of the system. The ratio $2K/k$ was determined experimentally as 0.9.

We do not know the details of the experiment of Errede et al., but it seems unlikely that coupling took place predominantly in the later stages of polymerization where the molecular chains should be occluded or immobilized in the precipitate. In fact this type of coupling is inconsistent with the Trommsdorf's effect[9] usually observed in bulk polymerization; the consumption of free radicals by coupling diminishes as polymerization proceeds due to the increase in the viscosity of the system. Furthermore, the coupling of the radical itself seems difficult because the mobility of the chain segments with a radical endgroup might be highly restricted at such a low temperature of polymerization, which is much lower than the glass transition temperature of the polymer (ca. 176–189°C). (This temperature was roughly estimated by taking $^2/_3$ of the melting point temperature of the polymer, 673–693°K[8], the effect of the solvent being considered to be very small at this low temperature.)

If the ratio $2K/k$ in eq. (16) were equal to 1 instead of 0.9, the equation would just coincide with eq. (7), implying that the Avrami-type occlusion of the reactive chain ends is the source of the decrease in the polymerization rate with time. As is shown in Figure 8, the linearity of plots of $[a/(a-x)]^{0.9}$ versus time obtained by Errede et al. still holds, even when the exponent was replaced by 1.

The author wishes to thank Professor T. Kawai of the Tokyo Institute of Technology and Drs. H. Kanetsuna, K. Tsuda, and H. Nakanishi of the Research Institute for Polymers and Textiles, for valuable discussions and advice.

References

1. T. Kagiya, M. Hatta, and K. Fukui, *Kobunshi Kagaku*, **20**, 730 (1963).
2. T. Higashimura, T. Miki, and S. Okamura, *Bull. Chem. Soc. Japan*, **39**, 25 (1966).
3. T. Miki, T. Higashimura, and S. Okamura, *Bull. Chem. Soc., Japan*, **39**, 41 (1966).
4. C. H. Bamford, A. D. Jenkins, M. C. R. Symmons, and M. G. Townsend, *J. Polym. Sci.*, **34**, 181 (1959).
5. M. Avrami, *J. Chem. Phys.*, **7**, 1103 (1939); *ibid.*, **8**, 212 (1940); *ibid.*, **9**, 117 (1941).
6. H. Kakiuchi and W. Fukuda, *Kogyo Kagaku Zasshi*, **66**, 964 (1963).
7. M. Dimonie and I. Gavăt, *Europ. Polym. J.*, **4**, 541 (1968).
8. L. A. Errede, R. S. Gregorian, and J. M. Hoyt, *J. Am. Chem. Soc.*, **82**, 5218 (1960).
9. E. Trommsdorf, H. Kohle, and P. Lagally, *Makromol. Chem.*, **1**, 169 (1948).

Masatoshi Iguchi

Research Institute for Polymers and Textiles*
4 Sawatari, Kanagawa-ku, Yokohama, Japan

Received August 14, 1969
Revised October 17, 1969

* Present address: University of Essex, Department of Chemistry, Colchester, Essex, England.

Photosensitization of Polyacetylenes

A previous communication[1] disclosed the discovery of a new class of photosensitive polymers. These polymers were made by the oxidative coupling of the bispropargyl ethers of various biphenols. Although these polymers were light-sensitive, they required moderately long exposure times for insolubilization. The introduction of a carbonyl moiety shortened the exposure time necessary for insolubilizing the polymer.

We examined a large number of light absorbing additives to one of the polymers. The base polymer chosen was the most easily available polymer, that from the bispropargyl ether of bisphenol-A (I). This polymer (BPA) was readily soluble in common

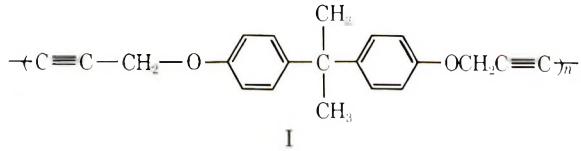

I

solvents and had a sufficiently long crosslinking time so that major improvements would be easily noticed.

The additives listed in Table I were dissolved in a 5% polymer solution, the solution placed on glass slides and the solvent evaporated. After exposure of the film to a GE-AH4 100-W medium-pressure mercury arc at a distance of 10 cm for the selected time, the slide was developed in toluene for 2 min. The insolubilization of the polymer film was determined by its adherence to the glass slide. These results are shown in Table I.

TABLE I
Sensitizers Added to BPA Polymer

Sensitizer (10% of polymer)	Crosslink time, sec
None	120
Azobenzene	60
Anthracene	50
Maleic anhydride	40
p-Benzoquinone	40
p-Diiodobenzene	30
Acetophenone	30
Rose Bengal	25
p-Diethynylbenzene	25

A wide variety of light-absorbing species increases the speed of the crosslinking (insolubilization). Unexpectedly, one of the better sensitizers is *p*-diethynylbenzene,[2] and a copolymer of this material and the BPA bispropargyl ether was made.

One copolymer was made containing 3 wt-% of the *p*-diethynylbenzene. This copolymer was extremely sensitive to light. Under comparable conditions it crosslinks in under 1 sec, compared to the unsensitized homopolymer time of 120 sec. The ultraviolet spectrum of the copolymer is shown in Figure 1 with the spectrum of the unsensitized polymer shown for comparison. The intense absorptions at 312 mμ (ϵ = 69,000) and 334 mμ (ϵ = 111,000) are due to the bisacetylene linkage II. The rapid crosslinking

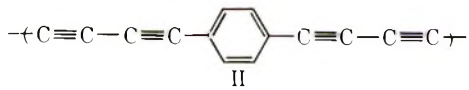

II

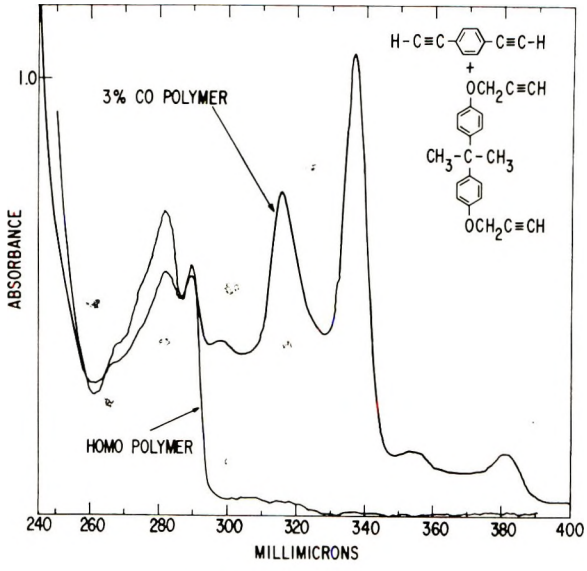

Fig. 1. Ultraviolet spectra.

of this polymer is believed to be due to the efficiency of utilization of incident light rather than due to a change in mechanism but, until the mechanism of crosslinking is known, this is speculation.

A detailed study of this chromophore is in progress.

References

1. A. S. Hay, D. A. Bolon, K. R. Leimer, and R. F. Clark, *J. Polym. Sci. B*, in press.
2. A. S. Hay, *J. Org. Chem.*, **25**, 637 (1960).

A. S. Hay
D. A. Bolon
K. R. Leimer

General Electric Research and Development Center
Schenectady, New York

Received September 30, 1969
Revised November 12, 1969

The *Journal of Polymer Science* publishes results of fundamental research in all areas of high polymer chemistry and physics. The *Journal* is selective in accepting contributions on the basis of merit and originality. It is not intended as a repository for unevaluated data. Preference is given to contributions that offer new or more comprehensive concepts, interpretations, experimental approaches, and results. Part A-1 *Polymer Chemistry* is devoted to studies in general polymer chemistry and physical organic chemistry. Contributions in physics and physical chemistry appear in Part A-2 *Polymer Physics*. Contributions may be submitted as full-length papers or as "Notes." Notes are ordinarily to be considered as complete publications of limited scope.

Three copies of every manuscript are required. They may be submitted directly to the editor: For Part A-1, to C. G. Overberger, Department of Chemistry, University of Michigan, Ann Arbor, Michigan 48104; and for Part A-2, to T. G Fox, Mellon Institute, Pittsburgh, Pennsylvania 15213. Three copies of a short but comprehensive synopsis are required with every paper; no synopsis is needed for notes. Books for review may also be sent to the appropriate editor. Alternatively, manuscripts may be submitted through the Editorial Office, c/o H. Mark, Polytechnic Institute of Brooklyn, 333 Jay Street, Brooklyn, New York 11201. All other correspondence is to be addressed to Periodicals Division, Interscience Publishers, a Division of John Wiley & Sons, Inc., 605 Third Avenue, New York, New York 10016.

Detailed instructions in preparation of manuscripts are given frequently in Parts A-1 and A-2 and may also be obtained from the publisher.